

**Peptide-conjugated fluorophores with
aggregation-induced emission properties for
specific protein recognition**

Dissertation

for

the doctoral degree of

Dr. rer. nat.

from the Faculty of Biology

University of Duisburg-Essen

Germany

Submitted by

Daniel Seifert

born in Haan

August 2021

DuEPublico

Duisburg-Essen Publications online

UNIVERSITÄT
DUISBURG
ESSEN

Offen im Denken

ub | universitäts
bibliothek

Diese Dissertation wird via DuEPublico, dem Dokumenten- und Publikationsserver der Universität Duisburg-Essen, zur Verfügung gestellt und liegt auch als Print-Version vor.

DOI: 10.17185/duepublico/74993

URN: urn:nbn:de:hbz:465-20231030-144733-1

Alle Rechte vorbehalten.

The experiments underlying the present work were conducted in the Group of Structural and Medicinal Biochemistry at the Center of Medical Biotechnology (ZMB) at the University of Duisburg-Essen.

1. Examiner: Prof. Dr. Peter Bayer
2. Examiner: Jun.-Prof. Dr. Jens Voskuhl
3. Examiner: Prof. Dr. Markus Kaiser

Chair of the Board of Examiners: Prof. Dr. Perihan Nalbant

Date of the oral examination: 28. October 2021

*"People say nothing is impossible, but I do nothing
every day."*

Winnie-the-Pooh

Contents

List of Figures	V
List of Tables	VII
List of Equations	VIII
List of Abbreviations	IX
1 Abstract	1
2 Zusammenfassung	2
3 Introduction	4
3.1 Fluorescence - A Form of Luminescence	4
3.2 Aggregation-Induced Emission (AIE)	5
3.2.1 Mechanisms of AIE	5
3.2.2 Technical applications for AIEgens	6
3.2.3 Chemical applications for AIEgens	7
3.2.4 Biological applications for AIEgens	8
3.3 Peptidyl Prolyl <i>cis/trans</i> Isomerases (PPIases)	12
3.4 Parvulins	12
3.5 The human Parvulin Pin1	15
3.5.1 <i>hPin1</i> related diseases	15
3.5.2 Regulation of <i>hPin1</i> - Multiple ways to control <i>hPin1</i> activity . . .	16
3.5.3 Structure of <i>hPin1</i>	17
3.5.4 Inhibition of <i>hPin1</i> - Natural and synthetic inhibitors	20
3.6 Aims	20
4 Materials & Methods	22
4.1 Materials	22
4.1.1 Chemicals	22
4.1.2 Consumables	22
4.1.3 Devises	23
4.1.4 Buffer and Solutions	24
4.1.5 Nutritional media	25
4.1.6 Plasmids	26
4.1.7 Bacterial strains	26
4.1.8 Software	27
4.2 Molecular biology methods	27
4.2.1 Transformation of plasmid DNA	27
4.2.2 Protein expression	27

4.3	Biochemical methods	28
4.3.1	Protein purification	28
4.3.2	Determination of protein concentration	29
4.3.3	SDS-Polyacrylamide gel electrophoresis (SDS-PAGE)	29
4.4	Chemical synthesis	30
4.4.1	Peptide synthesis	30
4.4.2	Peptide compounds	32
4.4.3	Copper(I)-catalyzed azide-alkyne cycloaddition (CuAAC)	36
4.4.4	Chemical characterization of peptide-coupled fluorophores	38
4.4.5	High-performance liquid chromatography (HPLC)	49
4.4.6	Ion exchange of peptide-coupled fluorophores	49
4.4.7	Liquid chromatography linked mass spectrometry (LC-MS)	49
4.4.8	High resolution mass spectrometry (HR-MS)	50
4.5	UV-VIS spectroscopy	50
4.6	Fluorescence spectroscopy	50
4.6.1	Sample preparation	51
4.6.2	Determination of autofluorescence	51
4.6.3	Binding study of fluorophores with <i>hPin1</i> and <i>hPin1-WW</i>	51
4.7	NMR Spectroscopy	52
4.7.1	Sample preparation	52
4.7.2	Data acquisition and processing	52
4.7.3	TFA detection by ^{19}F NMR spectroscopy	53
4.7.4	^{15}N -HSQC binding experiments with the <i>hPin1-WW</i> domain	53
4.8	NMR structure calculation	54
4.8.1	Ligand parametrization for CYANA	54
4.8.2	Structure calculation of fluorophore F10 with CYANA	54
4.8.3	Dihedral angle prediction via TALOS+	55
4.8.4	Calculation of the complex structure with UNIO	55
5	Results	57
5.1	Expression and purification of <i>hPin1</i> and <i>hPin1-WW</i>	57
5.2	Chemical synthesis	58
5.2.1	Peptide synthesis	58
5.2.2	Copper(I)-catalyzed alkyne-azide cycloaddition (CuAAC)	60
5.3	Characterization of peptide-conjugated fluorophores	63
5.3.1	UV-VIS spectroscopy - Solubility and extinction coefficients of peptide-coupled fluorophores	63
5.3.2	Fluorescence properties of peptide-coupled fluorophores	64
5.4	Specific recognition of the <i>hPin1-WW</i> domain	67
5.4.1	NMR titration experiments	67
5.4.2	Fluorescence titration experiments	70

5.4.3	Influence of a peptide linker on protein binding and its fluorescence properties	71
5.4.4	Comparison of fluorescence intensity for fluorophores with one or two binding sites	75
5.5	Effect of protein size on fluorescence increase	78
5.6	Structural analysis of fluorophore F10	79
5.6.1	Parametrization and peak assignment of the AIE-core ring system	79
5.6.2	Assignment of amino acids	81
5.6.3	NMR structure of fluorophore F10	82
5.7	Analysis of the complex structure of <i>hPin1</i> -WW with fluorophore F10 . .	84
5.7.1	Assignment of intermolecular and intramolecular contacts	85
5.7.2	Calculation of the NMR complex structure of <i>hPin1</i> -WW and F10	86
6	Discussion	90
6.1	Synthesis of peptide-coupled TPN derivatives	90
6.2	The new <i>hPin1</i> -WW specific fluorophores form a well-defined structure with enhanced solubility and good AIEE properties	91
6.3	The newly designed AIEgens bind specifically to the <i>hPin1</i> -WW domain	94
6.3.1	A short peptide exhibits better binding properties	95
6.3.2	The asymmetric and single peptide-conjugated fluorophore F10 is less emissive upon protein binding	95
6.4	The fluorophore F10 binds on top of the <i>hPin1</i> -WW domain	96
7	Outlook	100
8	Appendix	101
8.1	NMR spectroscopy	101
8.1.1	Acquisition parameter of NMR spectra	101
8.1.2	¹ H-NMR spectra	102
8.1.3	¹ H, ¹⁵ N-HSQC titration experiments	108
8.2	Fluorescence titrations of fluorophores F2-4 with <i>hPin1</i> -WW	112
8.3	Liquid chromatography-mass spectroscopy (LC-MS)	115
	References	122
	Danksagung	154
	Lebenslauf	156
	Eidesstattliche Erklärungen	157

included on the attached CD:

- PDF file of this work
- Library files of the non-natural amino acids
- *UPL* and *LOL* files of the protein complex structure
- Hydrogen bonds of the *hPin1-WW* domain
- Assignment of the cross-peaks of the isolated fluorophore

List of Figures

1	Jablonski diagram	4
2	Chemical structures of the AIEgens TPE, HPS and THBA	5
3	Fluorescence of HPS in a THF/H ₂ O mixture	6
4	Specific turn-on detection of CN ⁻ in solution	7
5	AIEgens for specific thiol detection	9
6	Detection and discrimination of the expression level of LAPTM4B protein in different cells	10
7	Phthalocyanine derivatives with AIE properties	11
8	Phylogenetic tree of parvulins	14
9	Structure of <i>hPin1</i> and the single WW domain	19
10	Vector map of the modified pET41b vector	26
11	Chemical structure of AIE-active core molecules used for synthesis	30
12	Reaction mechanism of the copper (I)-catalyzed azide-alkyne cycload- dition (CuAAC)	37
13	Protein purification of <i>hPin1</i> -WW and <i>hPin1</i>	58
14	Schematic representation of the SPPS	59
15	Illustration of the CuAAC reaction for fluorophore F1	61
16	Excitation (dotted) and emission spectra (solid) of fluorophore F1 in aqueous solution	65
17	Autofluorescence properties of peptide-conjugated fluorophores	66
18	Specific binding of fluorophore F1 to the <i>hPin1</i> -WW domain	68
19	Specific recognition of fluorophore F1 (50 μM) with the <i>hPin1</i> -WW domain	70
20	Fluorescence titrations of fluorophores F1-F4 at 50 μM with the <i>hPin1</i> - WW domain	72
21	Concentration dependency of fluorophore F1	73
22	Concentration dependency of fluorophore F10	76
23	Comparison of the maximum change of fluorescence upon protein binding	77
24	Fluorescence measurement of fluorophore F1 with <i>hPin1</i> -FL	78
25	Numbering and assignment of the AIE-core ring system	80
26	Assignment of <i>cis</i> and <i>trans</i> amino acids	82
27	Structure of the isolated fluorophore F10	83
28	Rotations of the AIE-core in the F10 structure	84
29	Superposition of the 2D-x2NOESY (red) and 2D-x2TOCSY (green) spectra	86
30	NMR solution structure of <i>hPin1</i> in complex with fluorophore F10	88
31	Contacts between the fluorophore F10 and <i>hPin1</i> -WW domain	89
32	Model of the fluorophore F1	93
33	Comparison of <i>hPin1</i> -WW complex structures and ligand binding	97
34	Protein changes upon fluorophore binding	98
A1	¹ H-NMR spectrum of fluorophore F0	102

A2	¹ H-NMR spectrum of fluorophore F1	102
A3	¹ H-NMR spectrum of fluorophore F2	103
A4	¹ H-NMR spectrum of fluorophore F3	103
A5	¹ H-NMR spectrum of fluorophore F4	104
A6	¹ H-NMR spectrum of fluorophore F5	104
A7	¹ H-NMR spectrum of fluorophore F6	105
A8	¹ H-NMR spectrum of fluorophore F7	105
A9	¹ H-NMR spectrum of fluorophore F8	106
A10	¹ H-NMR spectrum of fluorophore F9	106
A11	¹ H-NMR spectrum of fluorophore F10	107
A12	¹ H, ¹⁵ N-HSQC titration spectra of <i>hPin1</i> -WW domain with fluorophore F2	108
A13	¹ H, ¹⁵ N-HSQC titration spectra of <i>hPin1</i> -WW domain with fluorophore F3	109
A14	¹ H, ¹⁵ N-HSQC titration spectra of <i>hPin1</i> -WW domain with fluorophore F4	110
A15	¹ H, ¹⁵ N-HSQC titration spectra of <i>hPin1</i> -WW domain with fluorophore F10	111
A16	Concentration dependency of fluorophore F2	112
A17	Concentration dependency of fluorophore F3	113
A18	Concentration dependency of fluorophore F4	114
A19	LC-MS spectra of peptide P0	115
A20	LC-MS spectra of peptide P1	115
A21	LC-MS spectra of peptide P2	115
A22	LC-MS spectra of peptide P3	116
A23	LC-MS spectra of peptide P4	116
A24	LC-MS spectra of peptide P5	116
A25	LC-MS spectra of peptide P6	117
A26	LC-MS spectra of peptide P7	117
A27	LC-MS spectra of peptide P8	117
A28	LC-MS spectra of peptide P9	118
A29	LC-MS spectra of fluorophore F0	118
A30	LC-MS spectra of fluorophore F1	118
A31	LC-MS spectra of fluorophore F2	119
A32	LC-MS spectra of fluorophore F3	119
A33	LC-MS spectra of fluorophore F4	119
A34	LC-MS spectra of fluorophore F5	120
A35	LC-MS spectra of fluorophore F6	120
A36	LC-MS spectra of fluorophore F7	120
A37	LC-MS spectra of fluorophore F8	121
A38	LC-MS spectra of fluorophore F9	121
A39	LC-MS spectra of fluorophore F10	121

List of Tables

1	Bacterial strains for protein expression and DNA isolation	26
2	Conditions for the expression of <i>hPin1</i> , <i>hPin1</i> -WW and isotope labeled <i>hPin1</i> -WW domain	28
3	Program for the purification of <i>hPin1</i> and <i>hPin1</i> -WW by a GSH column .	29
4	Composition of used SDS gels	30
5	Peptide sequences synthesized with SPPS in 3 letter code	31
6	Setups for optimization of CuAAC reaction	37
7	Linear gradient used for LC-MS	49
8	Parameters for HR-MS	50
9	Fluorophore concentrations used for fluorescence binding studies . . .	51
10	Parameters for F10 structure calculation with CYANA	54
11	Parameters for complex structure calculation with UNIO	56
12	Systematic representation of all synthesized peptides	60
13	Optimization of the CuAAC for fluorophore F1	62
14	Systematic representation of all synthesized fluorophores	62
15	Solubility of peptide-coupled fluorophores	63
16	Extinction coefficients of peptide-coupled fluorophores	64
17	Dissociation constants of selected amino acids at fluorophore binding .	69
18	Stoichiometric factor n for symmetric fluorophores F1-F4 at various concentrations	74
19	Dissociation constants of symmetric fluorophores F1-F4 at various concentrations	74
20	Statistics of the NMR complex structure calculated by UNIO	87
A1	Acquisition parameter of NMR spectra	101

List of Equations

1	Calculation of binding constant K_D and stoichiometry factor n	52
2	Total chemical shift perturbation calculation	53
3	CYANA target function	55

List of Abbreviations

% (w/v)	Percentage weight per volume
% (v/v)	Percentage volume per volume
¹³ C	Isotope labelled carbon
¹⁵ N	Isotope labelled nitrogen
¹⁹ F	Isotope labelled fluorine
A β	Amyloid beta
ACN	Acetonitrile
ACQ	Aggregation induced emission
AD	Alzheimer's disease
AML	Acute myeloid leukemia
AIE	Aggregation induced emission
AIEE	Aggregation induced emission enhancement
AIEgen	Fluorophore with AIE properties
APP	Amyloid precursor protein
ATP	Adenosine triphosphate
BMRB ID	Biological magnetic resonance data bank identifier
BSA	Bovine serum albumin
CLSM	Confocal laser scanning microscopy
COSY	Correlation spectroscopy
CTD	Carboxyl-terminal domain
C-terminus	Carboxyl-terminus
CuAAC	Copper(I)-catalyzed azide-alkyne cycloaddition
CV	Column volume
CYPs	Cyclophilins
d	Doublet (NMR)
δ	Chemical shift (NMR)
Da	Dalton
DAPK1	Death-associated protein kinase 1
DCM	Dichloromethane
DIC	Diisopropylcarbodiimide
DIPEA	N,N-Diisopropylethylamine
DNA	Deoxyribonucleic acid
DMF	Dimethylformamide
DMSO-d ₆	Deuterated dimethylsulfoxid
DTM	Dipentamethylene thiuram monosulfide
EDTA	Ethylenediaminetetraacetic acid
<i>E. coli</i>	<i>Escherichia coli</i>
ESI	Electrospray ionization

FA	Formic acid
FHA	Forkhead-associated domain
FKBP	FK506 binding protein
Fmoc	Fluorenylmethoxycarbonyl protecting group
FPLC	Fast protein liquid chromatography
GFP	Green fluorescent protein
GSH	Glutathione
GST	Glutathione S-transferase
h	hour
HBTU	Hexafluorophosphate Benzotriazole Tetramethyl Uronium
HD	Huntington's disease
HEPES	4-(2-Hydroxyethyl)-1-piperazineethanesulfonic acid
HOBt	Hydroxybenzotriazole
HPLC	High-performance liquid chromatography
HPS	Hexaphenylsilole
HPTFAA	Heptylphenyltrifluoroacetamide
HR-MS	High resolution mass spectroscopy
HSA	Human serum albumin
HSP	Heat shock protein
HSQC	Heteronuclear single quantum correlation
Hz	Hertz
IPTG	Isopropyl β -d-1-thiogalactopyranoside
K_D	Dissociation constant
LAPTM4B	Lysosomal-associated transmembrane protein 4B
LC	Liquid crystal
LC-MS	Liquid chromatography mass spectroscopy
m	Multiplet (NMR)
min	Minute
MLK3	Mixed-lineage kinase 3
MP	Monopartite
MTS	Mitochondrial targeting sequence
m/z	Mass-to-charge ratio
(NF)- κ B	Nuclear factor kappa-light-chain-enhancer of activated B cells
NIMA	Never in mitosis gene A
NLS	Nuclear localization signal
NMP	N-Methyl-2-pyrrolidone
NMR	Nuclear magnetic resonance
NOESY	Nuclear Overhauser effect spectroscopy
N-terminus	Amino-terminus
OD ₆₀₀	Optical density at 600 nm

OLED	Organic light-emitting diode
OFET	Organic field-effect transistors
PAGE	Polyacrylamide gel electrophoresis
PBS	Phosphate buffered saline
PEG	Polyethylene glycol
PD	Parkinson's disease
PDB	Protein data bank
PKA	Protein kinase A
PLK1	Polo-like kinase
PML	Promyelocytic leukemia protein
PMT	Photomultiplier tube
PTM	Post-translational modification
PP2A	Protein phosphatase 2
PPase	Peptidyl prolyl cis/trans isomerase
ppm	Part per million
pRb	Retinoblastoma protein
PTPA	Protein-pSer/pThr-phosphatase2A activator
qui	Quintet (NMR)
RIM	Restriction of intramolecular motions
RIR	Restriction of intramolecular rotations
RIV	Restriction of intramolecular vibrations
RMSD	Root mean square deviation
RNA	Ribonucleic acid
RNAP II	RNA Polymerase II
ROS	Reactive oxygen species
rpm	Revolutions per minute
RSK2	Ribosomal protein S6 kinase 2
RT	Room temperature
s	Second; Singlet (NMR)
SDS	Sodium dodecyl sulfate
SMILES	Simplified molecular input entry specification
SPPS	Solid phase peptide synthesis
t	Time; Triplet (NMR)
t _R	Retention time
TAR	Triazole ring
TFA	Trifluoroacetic acid
TFAA	Trifluoroacetyl amino
THBA	10,10',11, 11'-Tetrahydro-5,5-bidibenzo[a,d][7]-annulenylidene
THF	Tetrahydrofuran
TIPS	Triisopropyl silane

TLC	Thin-layer chromatography
TMA	Trimethylamine
TOCSY	Total-correlation spectroscopy
TPE	Tetraphenylethene
TPN	Thiophthalonitrile
UTR	Untranslated region
UV	Ultraviolet light
VIS	Visible light
xNOESY	Filtered-edited NOESY spectra
x2NOESY	Double filtered NOESY spectra

Amino acid code table

Alanine	Ala	A
Arginine	Arg	R
Asparagine	Asn	N
Aspartic acid	Asp	D
Cysteine	Cys	C
Glutamine	Gln	Q
Glutamic acid	Glu	E
Glycine	Gly	G
Histidine	His	H
Isoleucine	Ile	I
Leucine	Leu	L
Lysine	Lys	K
Methionine	Met	M
Phenylalanine	Phe	F
Proline	Pro	P
Serine	Ser	S
Threonine	Thr	T
Tryptophan	Trp	W
Tyrosine	Tyr	Y
Valine	Val	V
Azidohomoalanine	Aha	-
Phospho-serine	pSer	pS
Phospho-threonine	pThr	pT
Any amino acid	Xaa	-

1 Abstract

The phenomenon of aggregation-induced emission (AIE) has become increasingly popular in recent years and a wide range of fluorophores exhibiting AIE properties (AIEgens) were synthesized for the specific recognition of small biogenic molecules and biological macromolecules [109, 161]. Upon protein binding the molecular motions of the fluorophores are restricted, which induces an increase in fluorescence signal, which can be used as a direct read-out option for binding analysis. However, the AIEgens were only used for qualitative recognition. In contrast, the new fluorophores in this work were used for quantitative analysis of protein binding using fluorescence.

This new and unique class of luminophores is based on aromatic thioethers bearing nitrile groups in *ortho*-position and were successfully modified with peptides for the specific recognition of the *hPin1*-WW domain. Therefore, peptides containing the *hPin1* specific pThr-Pro binding motif were synthesized by solid phase peptide synthesis (SPPS) and coupled to the AIE-core by copper(I)-catalyzed alkyne-azide cycloaddition (CuAAC). *hPin1* is a well described protein and the WW-domain, known as the substrate binding module, was used as a model protein to build a fluorescence-based assay for protein binding with direct read-out from fluorescence intensity.

Biochemical characterization of the new fluorophores showed an increased solubility in aqueous solutions and enhanced salt tolerance compared to previously described thioterephthalonitrile (TPN) derivatives [97]. Dissolved in an aqueous solution, the fluorophores exhibited low autofluorescence induced by the fluorophore structure, showing the peptide being helically twisted over the AIE-core and bound on top of the aromatic rings. Upon protein binding the fluorescence signal increased significantly and proves the excellent aggregation-induced emission enhancement (AIEE) properties of the fluorophores. Specificity against the *hPin1*-WW domain was demonstrated by both NMR- and fluorescence titration experiments and all fluorophores exhibited good binding constants in a low μM range.

By adding amino acids between the aromatic AIE-core and the *hPin1* specific pThr-Pro binding motif, the influence of a linker and its length was investigated. At low fluorophore concentrations ($\leq 25 \mu\text{M}$) the protein binding was similar for all linker lengths, but at higher fluorophore concentrations ($\geq 25 \mu\text{M}$) the binding curves could not be fitted with the expected binding model of two proteins binding a single fluorophore molecule. The effect was enhanced at greater linker lengths and was also increased at higher fluorophore concentrations, making the AIEgen suitable for protein detection and binding analysis only at low concentrations.

Finally, the NMR structure of a fluorophore bearing a single peptide-arm was solved alone and in complex with the *hPin1*-WW domain and showed the fluorophore-protein interaction and rotational restrictions at a structural level. The *hPin1*-WW domain exhibited the typical three-stranded antiparallel β -sheet with the fluorophore bound on top. The coupled peptide is recognized first and the aromatic AIE-core makes addi-

tional contacts with the WW-domain.

In summary, the specific protein recognition and the quantitative analysis of protein binding was demonstrated for peptide-coupled TPN fluorophores in a fluorescence-based assay with direct read-out. In addition, the binding was shown by the protein-fluorophore complex structure.

2 Zusammenfassung

Das Phänomen der aggregationsinduzierten Emission (AIE) ist in den letzten Jahren immer beliebter geworden und viele Fluorophore mit AIE-Eigenschaften (AIEgens) wurden für die spezifische Erkennung von kleinen biogenen Molekülen und biologischen Makromolekülen synthetisiert [109, 161]. Allerdings wurden diese nur für den qualitativen Nachweis verwendet. Im Gegensatz dazu wurden die neuen Fluorophore in dieser Arbeit für die quantitative Untersuchung von Protein-Ligand-Bindungen verwendet.

Diese neue Klasse an Luminophoren basiert auf aromatischen Thioethern mit zusätzlichen Nitrilgruppen in *ortho*-Position und wurde hier erfolgreich für die spezifische Erkennung der *hPin1*-WW-Domäne modifiziert. Dazu wurden Peptide mit dem *hPin1*-spezifischen pThr-Pro-Bindungsmotiv durch Festphasen-Peptidsynthese (SPPS) hergestellt und mit Hilfe der Kupfer(I)-katalysierten Alkin-Azid-Cycloaddition (CuAAC) an den aromatischen AIE-Kern gekoppelt. *hPin1* ist ein hervorragend untersuchtes Protein und die WW-Domäne, beschrieben als das Substratbindungsmodul, wurde deshalb als Modellprotein für einen fluoreszenzbasierten Assay verwendet. Die Protein-Ligand Bindung kann durch die AIEgens direkt über die Fluoreszenzintensität verfolgt und ausgelesen werden.

Die biochemische Charakterisierung der neuen AIEgens zeigte eine erhöhte Löslichkeit in wässrigen Lösungen und eine deutlich verbesserte Salztoleranz im Vergleich zu den bisher beschriebenen Thioterephthalonitril (TPN)-Derivaten [97]. Die AIEgens wiesen zudem eine geringe Autofluoreszenz auf, die durch die Struktur des Fluorophors erklärt werden kann. Der Fluorophor bildet einen C-förmigen aromatischen AIE-Kern mit dem Peptid helikal nach oben gedreht und auf den aromatischen Ringen gebunden. Durch Proteinbindung nimmt die induzierte Fluoreszenz deutlich zu und beweist so die hervorragenden aggregationsinduzierten emissionsverstärkenden (AIEE)-Eigenschaften. Die Spezifität für die *hPin1*-WW-Domäne wurde sowohl durch NMR- als auch durch Fluoreszenz-Titrationsexperimente nachgewiesen und ergab gute Bindungskonstanten in einem niedrigen μM -Bereich für alle Fluorophore.

Durch das Einfügen von Aminosäuren zwischen den aromatischen AIE-Kern und dem pThr-Pro-Bindungsmotiv wurde der Einfluss eines Linkers und dessen Länge untersucht. Bei niedriger Fluorophorkonzentration ($\leq 25 \mu\text{M}$) konnten keine Unterschiede in der Proteinbindung der Fluorophore in Abhängigkeit der Linkerlänge festgestellt wer-

den. Bei höheren Fluorophorkonzentrationen ($\geq 25 \mu\text{M}$) jedoch konnten die Bindungskurven nicht mit dem erwarteten Bindungsmodell (2 Proteine : 1 Fluorophor) analysiert werden. Dieser Effekt verstärkt sich mit höheren Fluorophorkonzentrationen und ist bei größeren Linkern ausgeprägter, weshalb die AIEgens nur bei niedrigen Konzentrationen verwendet werden können.

Abschließend wurde die NMR-Struktur eines Fluorophors im Komplex mit der hPin1-WW-Domäne gelöst. Die Komplexstruktur besteht aus dem bekannten dreisträngigen antiparallelen β -Faltblatt der WW-Domäne und dem oberhalb gebundenen Fluorophor. Das gekoppelte Peptid wird dabei von der WW-Domäne spezifisch erkannt. Durch die zusätzlichen Kontakte der WW-Domäne zum aromatischen AIE-Kern können die Rotationsbeschränkungen des Fluorophors sichtbar gemacht werden.

Somit wurde die spezifische Proteinerkennung und die quantitative Analyse der Proteinbindung für peptidgekoppelte TPN-Fluorophore in einem fluoreszenzbasierten Assay mit direktem *read-out* nachgewiesen und die Bindung anhand der Struktur des Protein-Fluorophor-Komplexes veranschaulicht.

3 Introduction

3.1 Fluorescence - A Form of Luminescence

The phenomenon of luminescence is the spontaneous emission of light from a molecule shortly after electronic excitation, triggered by light. Luminescence can be divided into the two categories of phosphorescence and fluorescence. Phosphorescence is described as the emission of light from an excited triplet state to the ground state. Due to the same spin orientation in both states, the transition is forbidden and rather slow. A typical transition takes 10^{-3} to 10^0 s, but also longer phosphorescence durations up to minutes has been described. In contrast, fluorescence is the transition from an excited singlet to ground state. Here, the electrons are paired and the typical fluorescence lifetime of 10^{-8} s is much shorter than for phosphorescence [132]. Fluorescence is typically a phenomenon of aromatic molecules and often occurs in nature, such as for quinine and the green fluorescent protein (GFP) [244]. The process of absorption and emission can be illustrated with the Jablonski diagram (figure 1) [113].

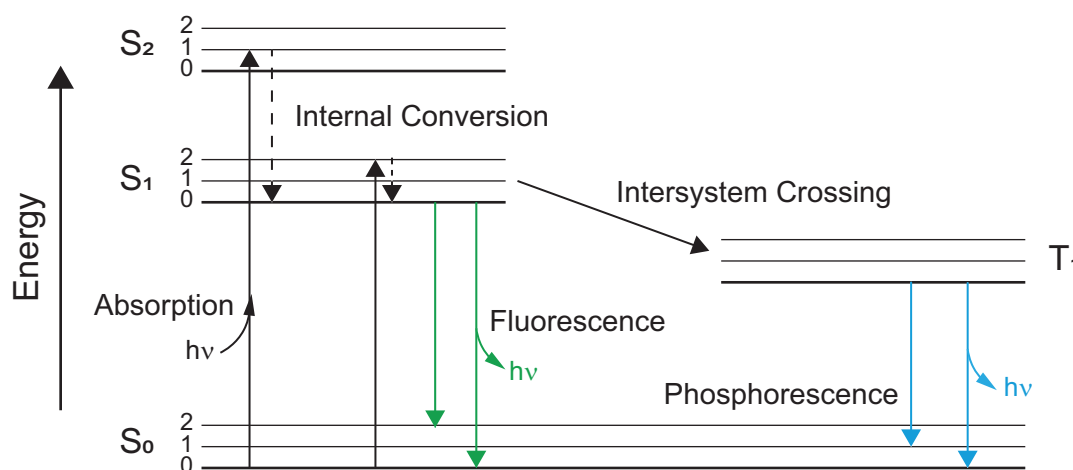


Figure 1: Jablonski diagram [132].

The Jablonski diagram shows the principle of luminescence, in which the electron from the ground state (S_0) gets excited to a higher electronic singlet state (S_1 or S_2). The smaller energy differences are defined as vibrational states (0,1,2,...). After excitation with light of a specific wavelength λ_{Ex} , the electron first relaxes into the lowest vibrational state of S_1 . This process is called internal conversion and the energy is released in the form of heat. Due to the loss of energy, the emission of light in the next step (transition to ground state) is slightly red-shifted and thus less energetic [76]. This difference between the excitation and emission wavelength is called Stokes shift and is an important factor in the utilization of fluorescence spectroscopy [132].

3.2 Aggregation-Induced Emission (AIE)

Nowadays there is a wide range of luminophores with different fluorescence properties and almost endless applications. But luminophores often suffer from a phenomenon known as aggregation-caused quenching (ACQ) [69]. ACQ describes the reduced or completely diminished fluorescence signal of commonly used luminophores or natural occurring luminescent molecules and has been known for several decades [69]. The ACQ effect is described as the non-radiative relaxation of excited states through π - π stacking interactions of adjacent molecules.

In contrast, aggregation-induced emission (AIE) describes the opposite phenomenon and was the first time mentioned by the group of Ben Zhong Tang in 2001 [171]. These luminophores do not show emission in solution, but feature strong emission when clustered, aggregated, bound and in a solid state. Molecules featuring the AIE effect are called AIEgens and some of the most frequently used AIEgens are hexaphenylsilole (HPS) [171, 256, 316] and tetraphenylethene (TPE) [247, 279, 317]. In addition to the traditional AIEgens, there is a group of fluorophores with low fluorescence in solution whose signal strength is enhanced by aggregation. These are described as aggregation-induced emission enhancement (AIEE) fluorophores and complete the class of AIEgens.

3.2.1 Mechanisms of AIE

HPS- and TPE conjugates are perfect examples to describe and visualize the mechanism of molecular restrictions which lead to the emission of light (figure 2) [243]. In total, there are three main hypotheses to describe the phenomenon of AIE: restriction of intramolecular rotations (RIR), restriction of intramolecular vibrations (RIV) and restriction of intramolecular motions (RIM), which involves a combination of RIR and RIV.

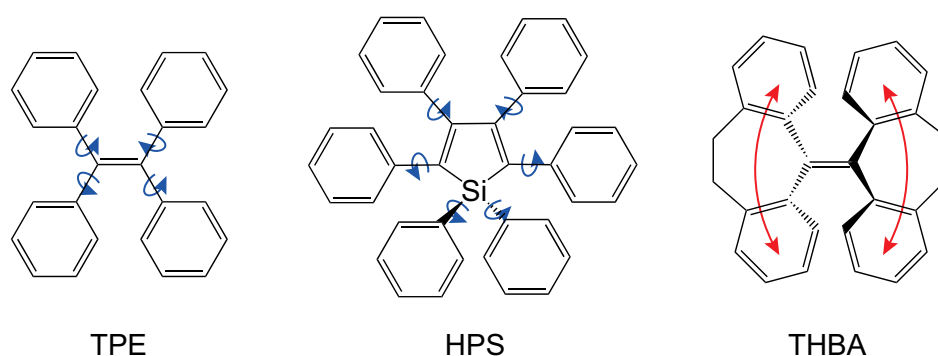


Figure 2: Chemical structures of the AIEgens TPE, HPS and THBA. The molecular structures of TPE and HPS show the rotational axes (blue) connecting the central ethene or silole to the outer phenyl rings [243]. THBA shows the vibrational motions (red) that lead to the radiation-free relaxation of the molecule [98].

HPS, the first described AIEgen [171], consists of a silacyclopenta-2,4-diene core with six phenyl rings in a propeller-shaped conformation. When dissolved in a proper solvent like THF or acetonitrile, the phenyl rings can rotate around the single bond axes and excited states can decay without radiation. However, at a higher aqueous fraction around 80%, HPS tends to aggregate and fluorescence is induced (figure 3) [35, 181]. The same process can be observed for TPE [180, 243, 279]. Both molecules show a twisted molecular structure that prevents π - π stacking, which would diminish the RIR-induced fluorescence [141, 309].

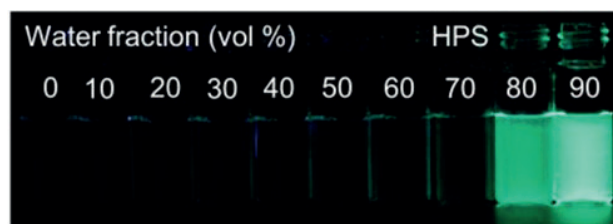


Figure 3: Fluorescence of HPS in a THF/H₂O mixture. Photograph of glass vials with 20 μ M HPS in solution or as suspension. The solvent mixture changes from 100% THF to 10% THF and 90% H₂O and shows the AIE effect of HPS. Reprinted with permission from [181]. Copyright 2015, American Chemical Society.

RIRs alone cannot describe the AIE effect of all AIEgens. Molecules like the 10,10',11,11'-tetrahydro-5,5-bidibenzo[*a,d*][7]-annulenyliene (THBA) [141, 170] (figure 3), do not have rotatable axes, but still show the AIE effect. For these molecules, vibrational motions are responsible for the AIE effect. In the case of THBA the connected phenyl rings do not rotate, but vibrate as shown in figure 3 and thus consume the absorbed energy without radiation. Also, the vibration of connected nitrile groups can contribute to RIV and induce fluorescence. In summary, molecules subject to either restriction system must be AIEgens. When both systems (RIR and RIV) are involved, the restrictions are grouped under the term motions (RIM).

3.2.2 Technical applications for AIEgens

With the steadily increasing number of AIEgens and the growing interest in AIE technology, more and more applications are being developed and researched. AIEgens are easy to synthesize and can be a cost-efficient alternative for currently available materials. For example, they are used in various optoelectronic systems, like e.g. organic light-emitting diodes (OLEDs) [317], organic field-effect transistors (OFETs) [6, 159], liquid crystals (LCs) [127] and photovoltaics [181].

OLEDs are utilized to build up optical displays which are then used in electronic devices such as tablets, mobile phones or televisions screens. A huge area of research is the development of new molecules to build up thin layers of OLEDs that are cheaper and more effective compared to commercially available OLEDs or traditional inorganic

LEDs. By polymerization of the AIEgen TPE and varying the connections between the TPE building blocks, new OLEDs have been created that offer good alternatives covering the entire visible spectrum of light [146, 315, 317].

Photovoltaics is the direct conversion of light energy into electrical energy using solar cells and is an important and promising renewable energy source for environmentally friendly energy policies [9]. An AIEgen in the form of a TPE paired up with a malononitrile has been reported as a luminogenic material in photovoltaic cells and to increase their power output [144].

3.2.3 Chemical applications for AIEgens

Sensing is a major field in the chemical industry and is of great importance for environmental control such as water treatment. However, it can be very extensive due to the high number of cations and anions. In recent years several AIEgens have been designed for the specific detection of a wide range of ions [37].

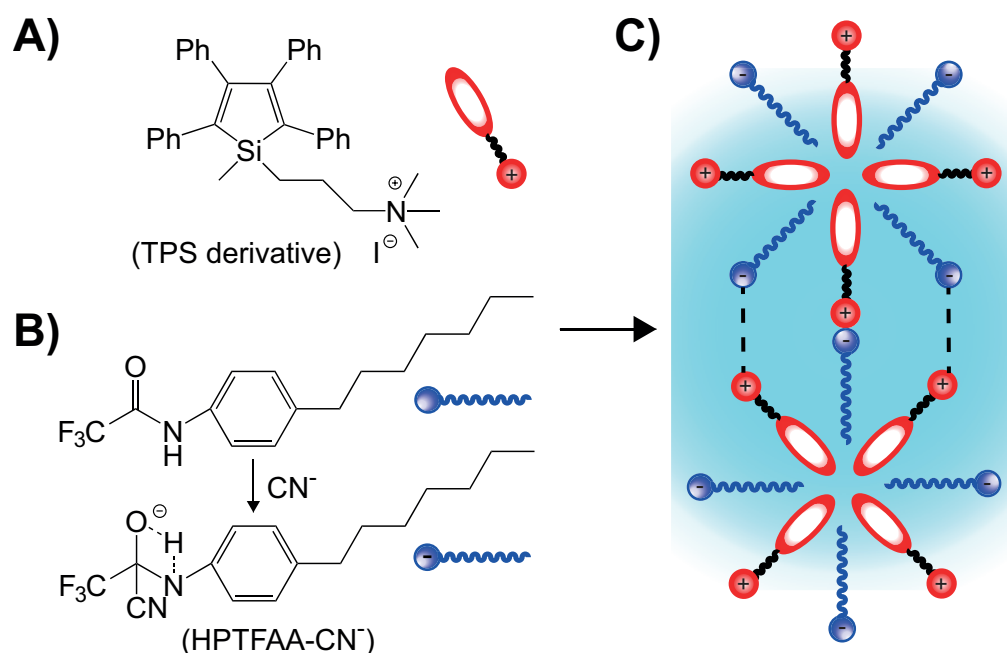


Figure 4: Specific turn-on detection of CN^- in solution. (A) chemical structure of the TPS derivative with the positively charged ammonium group. (B) Chemical structure of heptylphenyltrifluoroacetamide (HPTFAA) and its reaction with CN^- . (C) Assembly of both compounds yield the fluorescence turn-on signal. Adapted with permission from [207]. Copyright 2009, American Chemical Society.

One of the interesting target ions is cyanide (CN^-), a highly toxic and potentially lethal ion for humans [44, 52]. The functional trifluoroacetamino (TFAA) group is an excellent receptor for cyanides and has been used by several groups for its detection. CN^- binds to TFAA through nucleophilic addition, changing the molecule's charge and electrostatic properties. Zhang's group designed a heptylphenyltrifluoroacetamide (HPTFAA), which showed low fluorescence when paired up with an ammonium decorated

TPS derivative, but a strong turn-on signal when treated with CN^- . The CN^- converts HPTFAA into an amphiphilic molecule, which then induces the formation of heteroaggregates between the positive TPS derivative and HPTFAA- CN^- [278] (figure 4).

Kumar *et al.* showed another application for TFAA groups in AIEgens. The TFAA group was added twice to a hexaphenylbenzene-based receptor, which showed a stronger fluorescence signal at CN^- detection and also a large bathochromic signal shift of 105 nm [211].

In addition to the here described AIEgens for the sensing of CN^- , there are multiple AIEgens specified for other ions such as Ag^+ [166, 293], Hg^{2+} [275], Cu^{2+} [175], Al^{3+} [145, 297], Fe^{3+} [17], Zn^{2+} [274, 283], F^- [185], ClO^- [272, 294] and many more.

Beside the ion-specific AIEgens, several TPE derivatives and other AIEgens have also been designed as specific sensors for pH [281], gases [28, 259] and peroxides [106, 156]. H_2O_2 , a member of the peroxides and reactive oxygen species (ROS), is a strong oxidizer and can be harmful for organisms. ROS are highly reactive and connected to aging [153], oxidative stress [108, 235] and cancer development [3, 212]. The group of Zhang *et al.* reported a TPE-based AIEgen for the specific recognition of H_2O_2 . In the reaction, H_2O_2 oxidized the included ester and the following hydrolysis resulted in the hydrophobic *p*-pyridine-substituted TPE [106]. The resulting TPE derivative is highly hydrophobic and tends to aggregate in aqueous solution.

3.2.4 Biological applications for AIEgens

The system of AIE also has become a powerful tool in life science with a steadily increasing number of applications in the field of biological sensing. Here, the range of AIE targets extends from small biogenic molecules (e.g. monosaccharides, ATP, thiols and HSA) [88, 158, 161, 314] and biological macromolecules (e.g. proteins, DNA and enzymes) [162, 277, 320] to complete organelles and cells (e.g. endoplasmic reticulum, HeLa/HEK-293 cells and viruses) [122]. Some of these achievements are described in detail below to give a brief overview about the possibilities for AIE-based sensing.

Biothiols, as an example for small biogenic molecules, represent a major group of antioxidants. As cysteine (Cys), Homocysteine (Hcy) or glutathione (GSH), they play an important role against ROS and related diseases [218, 264]. They are involved in many biological and physiological processes and can be detected by a variety of methods, such as chromatography [38, 286] or electrochemical assays [280]. Also, AIEgens were specifically designed for their detection, using thiol chemistry. Adding a maleimide group to the TPE-core (TPE-MI) diminished the fluorescence both in solution and the aggregated state, but it was restored after alkene hydrothiolation (figure 5 A). The TPE-MI molecule was successfully used to detect Cys in the presence of other non-thiol amino acids on TLC plates, which then could be used as TPE-MI coated test strips (figure 5 B) [103, 160]. However, the maleimide group does not discriminate between different thiols. Therefore, Tang's group created a TPE derivative (TPE-DCV), which

was even able to detect GSH in the presence of other thiols [161]. A different approach for thiol detection was used by Zhang *et al.*, in which a peptide containing five carboxyl groups was fused to the AIE-core (TPE-SS-D₅) via a disulfide linkage. Afterwards this linkage could be cleaved by thiols in solution, resulting in a hydrophobic TPE derivative and the formation of fluorescent aggregates (figure 5,C) [311].

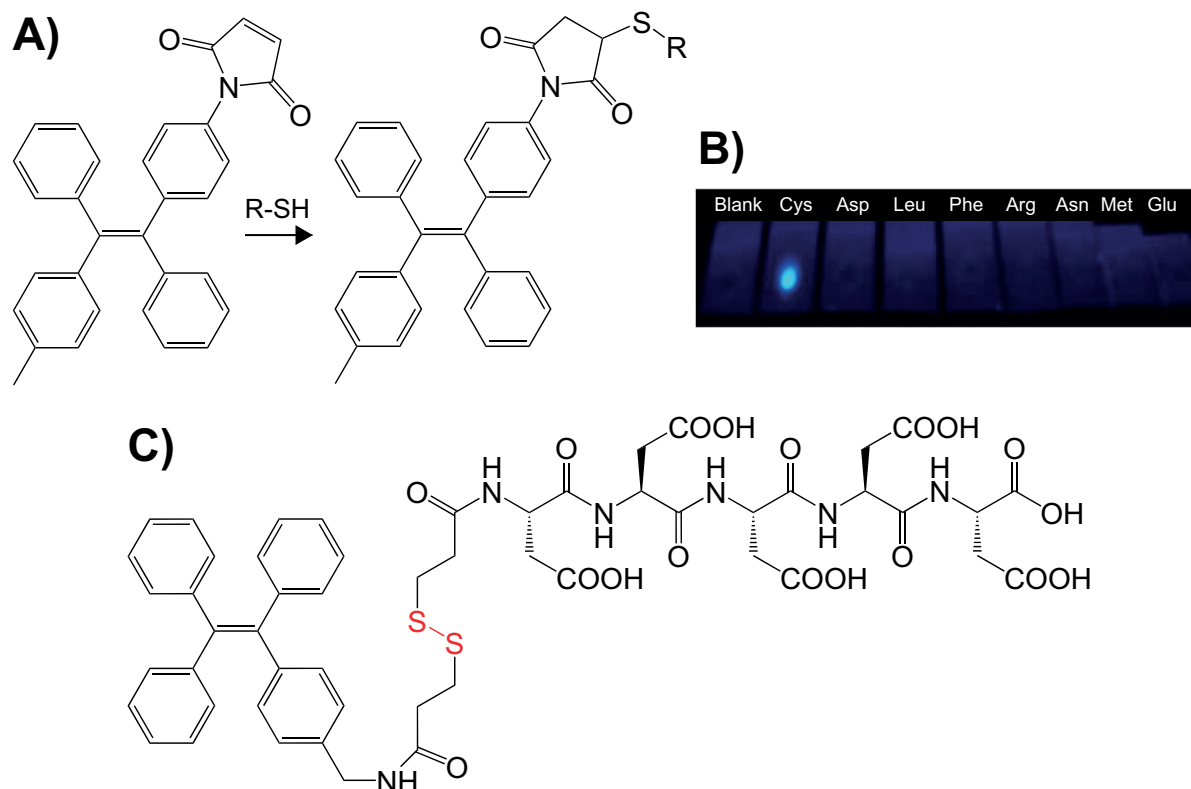


Figure 5: AIEgens for specific thiol detection. (A) Chemical structure of TPE-MI and its reaction with thiols, based on alkene hydrothiolation [160]. (B) Photograph of the turn-on detection of Cys from other amino acids on TLC plates. Figure adapted from [103]. (C) Chemical structure of TPE-SS-D₅ and the cleavable disulfide linkage highlighted in red. Adapted with permission from [311]. Copyright 2014, American Chemical Society.

In addition, the specific detection of macromolecules, especially of single proteins *in vitro* and *in vivo*, is of great interest in pharmaceuticals and the diagnosis and treatment of diseases. Still, it remains challenging to design effective probes, but in recent years fluorescence became a major factor in protein sensing and identification [318]. Due to the low fluorescence background of biological samples, fluorescence-based probes offer a high signal-to-noise ratio and are ideal candidates for the detection of biological macromolecules. Many groups designed turn-on AIEgens to detect a wide range of proteins including membrane proteins and multiple enzymes. They were used for the qualitative detection in SDS-PAGE [307], localization in cells [152, 174], detection of protein folding and aggregation [104, 252] and detection of enzymatic activity [148, 273]. While addressing enzymatic activity *in vitro* is relatively easy by creating AIE-based

substrates, which then can be bound or cleaved, the specific protein detection inside cells is far more complex.

For instance, Zhang *et al.* synthesized a novel AIE probe for the specific detection of the lysosomal-associated transmembrane protein 4B (LAPTM4B) protein in different types of cells [109]. The AIEgens consisted of the TPE-core, decorated with the decapeptide IHGHHIISVG (referred to as AP2H) and bound specifically to the extracellular loop 2 (EL2, PYRDDVMSVN) of the LAPTM4B protein. The protein is widely overexpressed in many tumors, including breast cancer [292], liver cancer [240, 302], ovarian cancer [305] and cervical cancer [183] and therefore is considered as a strong biomarker for cancer cells.

As shown by Zhang *et al.*, the AIEgen is almost non-emissive in normal Chang liver cells, but fluorescence turns on strongly when incubated with human liver cancer cells HepG2, human hepatoma cells BEL 7402 or HeLa cells (figure 6) [109]. The AIEgen was successfully used at neutral (pH 7.4) and acidic (pH 5.5) conditions and showed a slightly stronger fluorescence at lower pH.

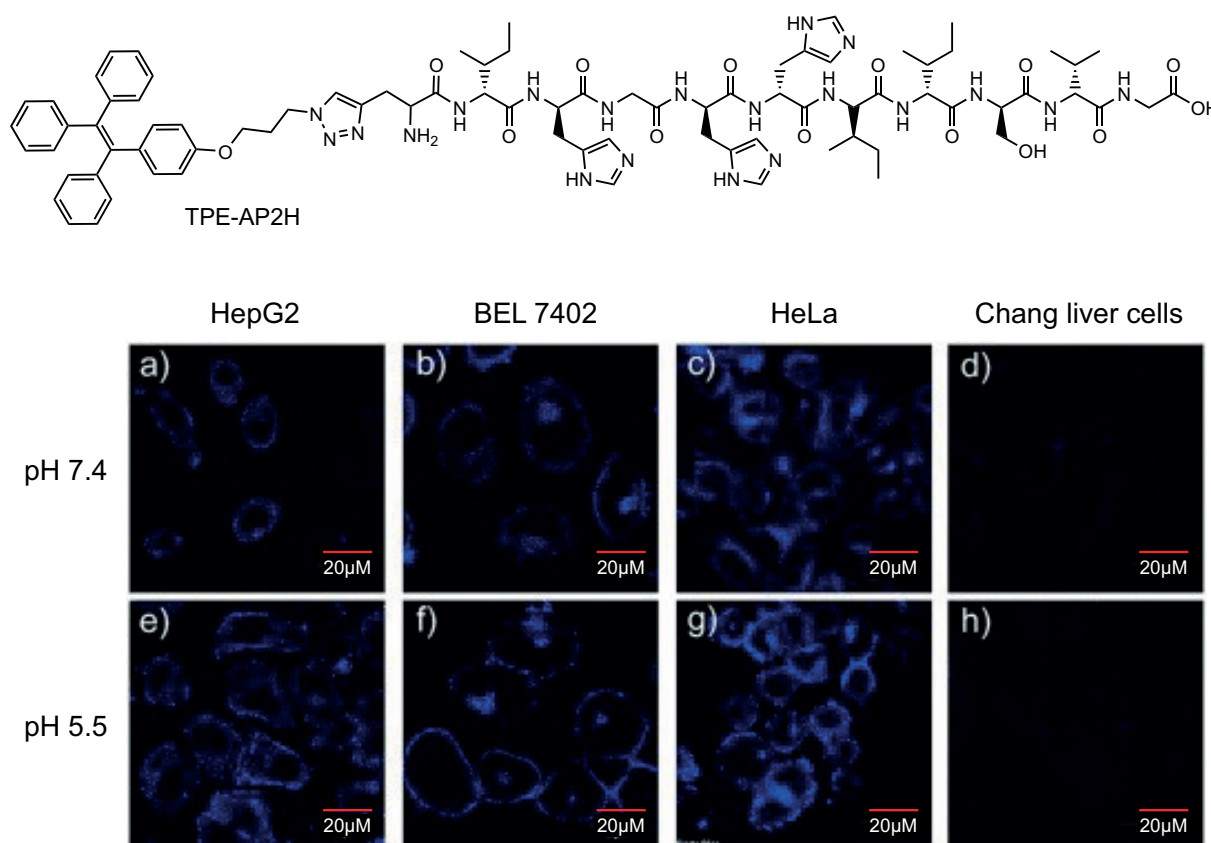


Figure 6: Detection and discrimination of the expression level of LAPTM4B protein in different cells. On top the chemical structure of TPE-AP2H. Confocal laser scanning microscopy (CLSM) images of HEPG2 cell (A,E), BEL7402 cells (B,F), HeLa cell (C,G) and Chang liver cells (D,H) at neutral and acidic pH. Scaling bars: 20 μm. Reprinted with permission from ref [109]. Copyright 2014 Wiley-VCH Verlag GmbH & Co. KGaA.

A new unique class of luminophores with AIE properties were synthesized by the group of J. Voskuhl [221]. Thioterephthalonitriles (TPNs) are composed of aromatic thioethers and were varied in their substitution pattern, resulting in promising AIEgens with tunable excitation and emission wavelengths (figure 7, B). Additional advantages are the short and efficient synthetic route and the broad range of functional groups, which can be added for specific modification [221]. Due to their aromatic core structure, coupled with thioethers, the AIEgens provide an increased flexibility paired up with good photophysical properties and a luminescence quantum yield up to 23.1% as solid compound [220].

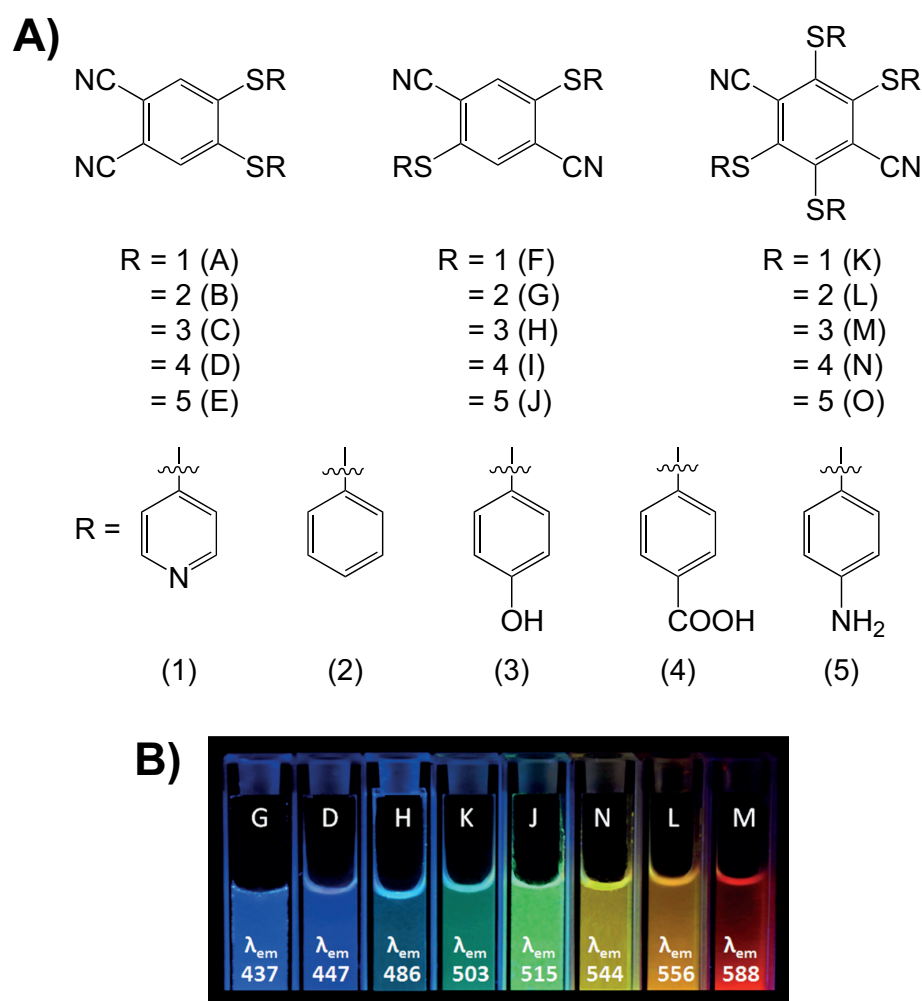


Figure 7: Phthalocyanine derivatives with AIE properties. (A) Chemical structures of multiple AIE active phthalocyanine derivatives. (B) Fluorescence images of selected fluorophores under UV light (365 nm). The fluorophores were prepared in 99% H₂O/1% DMF at a concentration of 100 μ M. Reprinted with permission from Ref [221]. Copyright 2017 Wiley-VCH Verlag GmbH & Co. KGaA.

With all the possible targets in biological systems the number of AIEgens and applications during the last 20 years has increased enormously and have been summarized in multiple reviews over the years [27, 61, 181].

3.3 Peptidyl Prolyl *cis/trans* Isomerases (PPlases)

Cellular processes are under strict control and regulated by various mechanisms including protein-protein and protein-DNA interactions [131,208]. The interactions are based on the specific recognition of peptide sequences or structural motifs and can be divided into permanent and transient. [41] While permanent interactions are characterized by a strong binding affinity and a long binding duration, transient interactions are weak and short-term [1,208]. Regulation of these interactions is often controlled by post-translational modifications [271] like methylation [135,205], acetylation [47,291], sulfation or phosphorylation [125,210]. Phosphorylation of proteins and peptides is a reversible process in eukaryotes and occurs principally on the side chains of serine, threonine and tyrosine residues [210]. Here, kinases catalyze the phosphoryl transfer from a donor, usually ATP, to the side chain hydroxyl group of the receptor substrate [31]. Apart from being regulated by these PTMs, the interactions are strongly dependent on the structural arrangement and thus on the correct protein folding [117]. While protein folding is generally a spontaneous process controlled by several groups of proteins, e.g. chaperones such as heat shock proteins (HSPs) and protein disulfide isomerases, the peptidyl-prolyl bond does not spontaneously adopt the intended conformation [20,87,147]. Due to steric hindrance caused by the side chains, the *cis* conformation only accounts for 0.1-1% [234,310] of the peptide bonds. In contrast, 5-30% of peptidyl prolyl bonds exhibit the *cis* conformation depending on peptide or protein length [114,192]. Because of the thermodynamically slow *cis/trans* isomerization of peptidyl prolyl bonds, which takes place in tens to hundreds of seconds and requires an activation energy of about 80 kJ/mol, this can lead to a rate limiting step during protein refolding or *de novo* synthesis [23,59,65,80].

In this case, peptidyl prolyl *cis/trans* isomerases (PPlases; EC 5.2.1.8) can help accelerate the relatively slow *cis/trans* isomerization of peptidyl prolyl bonds and act as a molecular switch for conformational changes in proteins [7,66]. Given the importance of the PPlase superfamily, members are present ubiquitously in eukaryotic and prokaryotic organisms and are expressed in low levels in almost all tissues [241]. They have been detected in the cytosol, mitochondria [25], the golgi apparatus and associated with membranes and can be further divided into three subfamilies: cyclosporin A binding proteins, also known as cyclophilins (CYPs), FK506 binding proteins (FKBPs) and non-immunosuppressive binding parvulins [67,94,214,215,245].

3.4 Parvulins

The subfamily of parvulin, was initially discovered and isolated by the group of Gunther Fischer in 1994 [214,215]. The first identified member was the cytosolic protein Par10 from *Escherichia coli* (*E. coli*), whose PPlase domain showed no similarity in sequence to other PPlases. It was shown that Par10 was not inhibited by cyclosporin

A or FK-506. Due to its small molecular weight of 10.1 kDa the new subfamily was named parvulin (*parvus*= tiny; very small) [214,215]. On the basis of sequence homology further prokaryotic proteins were identified and added to the parvulin family. SurA from *E. coli* is a periplasmic multi-domain protein involved in the folding and maturation of porins in the outer membrane. With its chaperone-like activity for outer membrane proteins, SurA is necessary for the survival and growth of *E. coli* in the stationary phase [134,261]. SurA deletion mutants in *E. coli* can be compensated for by another periplasmic parvulin named PpiD [46]. Other prokaryotic members of the parvulin family are the PmpA from *Lactococcus lactis* [48], NifM from *Azotobacter vinelandii* [116] and PrsA from *Bacillus subtilis* [130].

The first eukaryotic protein discovered and added to the family of parvulins was Ess1 from *Saccharomyces cerevisiae* [92, 93]. Ess1 was found to be essential for the growth of yeast, regulating the structure and function of the eukaryotic RNA polymerase II [75, 92, 191]. By binding to the carboxyl-terminal domain (CTD) of Rpb1 and changing its conformational state, Ess1 controls the initiation of transcription and termination as well as RNA processing [91, 176, 246]. Shortly after the discovery of Ess1, the homologous and still best studied parvulin, *human* Pin1 (*hPin1*), was discovered and described for the first time [163]. *hPin1* and its numerous homologs in e.g. *Arabidopsis thaliana* (*AtPin1*) [133] and *Malus domestica* (*MdPin1*) [303] are phospho-specific PPLases and form the biggest of the three parvulin subfamilies (see figure 8). Besides *hPin1*, *hPar14* and *hPar17* were identified and complete the class of human parvulins [193,262]. *hPar14* and *hPar17* were found to be single domain proteins with an unstructured and mainly basic N-terminal extension [195,238]. Due to alternative transcriptional initiation, *hPar17* contains a 25 amino acid extension compared to *hPar14*. Both proteins show no preference for phosphorylated substrates [194,258,262]. Along with *EcPar10* they form the second class of parvulins, the class of non-phosphospecific parvulins. The function and localization of *hPar14* depends strongly on its phosphorylation state at various positions within the N-terminal extension. Here phosphorylation of Ser⁷, Ser⁹ and Ser¹⁹ is of special interest. While the phosphorylations at Ser⁷ and Ser⁹ in combination with the 14-3-3-protein are necessary for the transport to the cytosol, the phosphorylation of Ser¹⁹ is needed for the import into the nucleus and its function there [193,219]. Phosphorylation at Ser¹⁹ also suppresses DNA binding, which normally takes places at AT-rich regions of double-stranded DNA (dsDNA) [219,254]. In contrast, the dephosphorylated *hPar14* can associate with chromatin and pre-ribosomal ribonucleoprotein (pre-rRNP) complexes inside the cellular nucleus [71, 232]. In combination with the highest expression level in the S and G2/M phase of mitosis, *hPar14* is most likely associated with DNA replication, DNA repair, chromatin remodeling, and ribosome biogenesis [70, 71, 232].

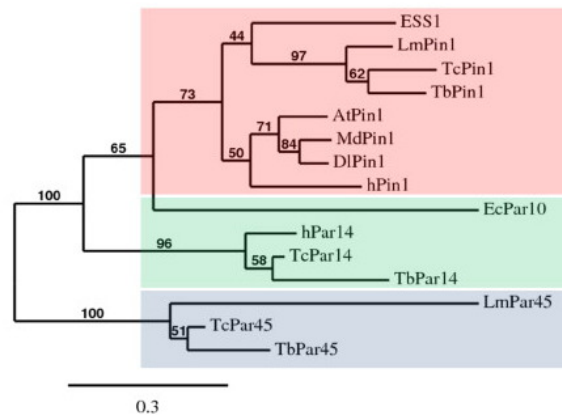


Figure 8: Phylogenetic tree of eukaryotic parvulins. Parvulins are divided into three subfamilies: Pin1-type or phosphorylation dependent parvulins (in red), parvulins with a non-specific substrate (in green) and Par45 related parvulins (in blue). Shown are ESS1 from *Saccharomyces cerevisiae*, LmPin1 and LmPar45 from *Leishmania major*, TcPin1, TcPar14 and TcPar45 from *Trypanosoma cruzi*, TbPin1, TbPar14 and TbPar45 from *Trypanosoma brucei*, AtPin1 from *Arabidopsis thaliana*, MdPin1 from *Malus domestica*, DIPin1 from *Digitalis lanata*, hPin1 and hPar14 from humans and EcPar10 from *Escherichia coli*. Reprinted with permission from Ref [54]. Copyright 2010, Elsevier B.V.

Most results described and published in the literature do not discriminate between hPar14 and hPar17. Therefore, functions may overlap or may have been incorrectly assigned to hPar14 and need to be further investigated. Unlike hPar14 and its homologs, which were found in all metazoans, hPar17 was shown to be present exclusively in the mitochondria of *Hominidae* [124, 219]. Here the extended N-terminus is suggested to act as a mitochondrial targeting sequence (MTS) and guide the protein into the mitochondria. In addition, *in vitro* experiments involving hPar17 showed DNA binding, tubulin polymerization [194, 258], and a 5 times higher affinity towards actin binding compared to hPar14 [78].

The third and final class of parvulins comprises Par45 and Par45-like proteins. These parvulins are unique to unicellular eukaryotes and were first discovered in 2005 in *Dictyostelium discoideum* and *Chlamydomonas reinhardtii* [53, 267]. Later homologs were also found in the parasites *Trypanosoma* and *Leishmania* [54, 79]. Par45 is a much bigger protein than the already described parvulin members, containing the characteristic C-terminal PPIase domain and a N-terminal forkhead-associated (FHA) domain [49, 50]. However, other than the localization inside the nucleus and the isomerase activity of TcPar45 towards Arg-Pro containing peptides, no specific activity or function could be proven [54, 79].

3.5 The human Parvulin Pin1

Originally found in a yeast two-hybrid system, *hPin1* was described as an interacting partner for the NIMA (never in mitosis gene A) kinase from *Aspergillus nidulans* and is still the best characterized parvulin today [163]. The NIMA kinase is essential for cells to enter mitosis and leads to cell resting when overexpressed [204]. *hPin1* was therefore suspected to be involved in cell division. This assumption was later proven by deletion studies of Pin1/Ess1 in mutagenic yeast cells and the stop of mitosis in the G2 phase during overexpression of Pin1 in HeLa cells [13, 163]. Here the deletion led to a disruption of mitosis followed by apoptosis, which finally labeled *hPin1* as a regulator for mitosis [241, 298]. The first evidence indicating the specificity of *hPin1* against phosphorylated substrates was found in the crystal structure (PDB: 1PIN). In the structure the bound sulfate ion mimics the phosphoryl group (figure 9), and shortly after the phosphate specificity was proven by a binding assay using various model substrates [60, 222, 300].

In addition, the specificity was also obtained for the first cellular targets Cdc25 [45, 241, 300, 319], the hyper-phosphorylated tau protein (p-tau) [164, 287, 319] and the C-terminal domain (CTD) of the RNA Polymerase II (RNAP II) [5, 298]. P-tau plays a crucial role in neurodegenerative diseases and Cdc25, a Cdc2-directed phosphatase, controls cell cycle transitions (G1 to S phase and G2 to M phase) [74, 102, 121, 186]. Regulation of the activating factor Cdc25 is catalyzed by the Pin1-dependent and *trans* specific protein phosphatase 2 (PP2A). Thus, *hPin1* mediates the *cis/trans* conversion of PP2A targeted proteins and enables their dephosphorylation [319]. Additionally, *hPin1* regulates function of RNAP II via binding to the CTD of its largest subunit and regulating the phosphorylation state [298]. RNAP II is active in multiple pre-mRNA events and is critical for its transcription and processing, through which *hPin1* is involved in the cell cycle [299].

3.5.1 *hPin1* related diseases

Other than the regulation of cell cycle progression [163], *hPin1* is involved in multiple processes such as differentiation [112, 197], senescence [36, 260] and apoptosis [14, 209]. Due to its wide participation in cellular processes *hPin1* is involved in various diseases and dysfunctions, including viral infections [105, 151, 199], metabolic syndrome [90, 173, 198], immune response [55, 56, 228], tumorigenesis [126, 142, 226, 304] and degenerative disorders [57, 63, 77, 96, 229, 276].

With today's increasing life expectancy, neurodegenerative diseases such as Parkinson's disease (PD), Alzheimer's disease (AD) and Huntington's disease (HD) are becoming increasingly important in medical healthcare and research. Biochemically, AD is characterized by plaque accumulation caused by protein misfolding [68, 73, 95]. Two proteins involved in accumulation of plaques, Amyloid-beta ($A\beta$) and p-tau, are regu-

lated by *hPin1* [81, 118, 154, 196]. Whereas p-tau is regulated by its phosphorylation state [72, 129, 164], *hPin1* controls the production of $A\beta$ [4, 206], but is deficient and less active in neurodegenerative diseases [26]. Through oxidation inside the catalytic domain, the isomerization efficiency of *hPin1* is decreased and dephosphorylation of p-tau is downregulated [33, 251, 276]. Therefore, the isomerization rate of p-tau from *cis* to *trans* is decreased and hyper-phosphorylated tau in *cis* conformation can pair up as helical filaments and further aggregate into neurofibrillary tangles [11, 19, 178]. Additionally, *hPin1* slows down the production of $A\beta$, a polypeptide of the amyloid precursor protein (APP) and the main component of senile plaques [89, 111, 206]. The $A\beta$ polypeptide is produced by APP proteolysis and induced by oxidative stress [187]. Another emerging field of *hPin1* research is tumorigenesis and cancer, the leading cause of death worldwide [253]. In contrast to neurodegenerative diseases, in cancer cells *hPin1* is highly expressed [39]. It inhibits about 20 tumor suppressors and up-regulates more than 50 oncogenes [39, 223]. Therefore, it is correlated with multiple forms of human cancers [289, 295, 306, 321]. Tumor suppressors, such as the promyelocytic leukemia protein (PML) [82, 230] or the retinoblastoma protein (pRb) [223, 268], try to inhibit and prevent cancerization by suppressing cell growth of damaged cells. Cancer cells in return use a wide range of mechanisms to overcome these suppressions and promote proliferation. In prostate cancer for example, *hPin1* destabilizes the PML, a powerful suppressor, by inducing its ubiquitination and thus inactivating it [150]. Additionally, *hPin1* can regulate the pathway of the nuclear factor (NF)- κ B and thus induce cancer cell proliferation. The NF- κ B pathway is involved in various cancers, such as endometrial carcinoma and acute myeloid leukemia (AML) and is activated by the increased accumulation of RelA, c-Rel and v-Rel [58, 228, 231].

3.5.2 Regulation of *hPin1* - Multiple ways to control *hPin1* activity

Expression and activity of *hPin1* is directly regulated by multiple mechanisms including transcriptional, post-transcriptional and post-translational regulations. The first level of control is the transcriptional regulation by transcription factors, such as the E2F family, Notch1 and other proteins [225, 227]. Members of the E2F family bind to a specific E2F binding site inside the promoter and stimulate *PIN1* transcription. Furthermore, this promoter activity can be enhanced by the oncogenic proteins *Neu* and *Ras*, which takes places in breast cancer, for example [227, 289]. Notch1 also binds to the promoter of *PIN1* and directly induces transcription. In this case, *hPin1* can bind to the phosphorylated Notch1, isomerize it and increase its cleavage by γ -secretase. This leads to a vicious cycle of binding and cleavage [225].

After transcriptional regulation of the *PIN1* gene, mRNA stability and protein translation are essential for expression. Here multiple micro-RNAs (miRNAs), which are small, non-coding RNAs, have been identified to control *hPin1* expression. MiR-200c [172], miR-200b [312] and miR-296-5p [136] were discovered to bind specific consensus se-

quences at the 3'-untranslated region (UTR) of *hPin1* mRNA, inhibiting its translation. With downregulation of these factors in tumors, *hPin1* is overexpressed and therefore promotes cell cycle progression. Additionally, miR-874-3p [140] and miR-140-5p [301] were found to interact with mRNA and negatively influence *hPin1* expression. Other mechanisms for cells to control protein activity are post-translational modifications. The PTMs control and regulate protein stability, substrate binding ability, catalytic activity and protein localization.

For *hPin1*, phosphorylation [40,165], ubiquitination [51], oxidation [33,251] and SUMOylation [32] have been reported [34]. Phosphorylation, the most prominent of all known PTMs, takes place at multiple serine residues and is present in both domains. For instance, Ser¹⁶, located inside the WW-domain, is phosphorylated by the protein kinase A (PKA), leading to a diminished substrate binding ability [165]. The phosphorylation of Ser¹⁶ is notable, because multiple effects can occur depending on the kinase interacting with *hPin1*. While the phosphorylation by PKA and aurora kinase A shows a negative effect on substrate binding and thus suppresses *hPin1* function [139, 165], the modification by the ribosomal protein S6 kinase 2 (RSK2) supports the cell transformation [40]. The other phosphorylation sites at Ser⁶⁵, Ser⁷¹ and Ser¹³⁸ are inside the catalytically active PPIase domain. Ser⁶⁵, phosphorylated by the polo-like kinase (PLK1), prevents ubiquitination and proteasomal degradation by stabilizing the protein [51]. In addition, it triggers the transition from the G2- to M-phase. In contrast, Ser¹³⁸, phosphorylated by the mixed-lineage kinase 3 (MLK3), activates the catalytic function and thereby promotes nuclear translocation [217]. The death-associated protein kinase 1 (DAPK1), a tumor suppressor and known for its ability to bind *hPin1*, adds a phosphoryl-group to Ser⁷¹ that also inhibits catalytic activity, preventing nuclear translocation [137]. Oxidation at Cys¹¹³, inside the catalytically active PPIase domain, abolishes the activity completely but does not affect substrate binding [33]. Finally, SUMOylation at Lys⁶ and Lys⁶³ results in a lower protein stability with a highly reduced ability to bind substrates.

3.5.3 Structure of *hPin1*

Many structures have been solved to this day and give a detailed view into the structural arrangement of the full-length *hPin1* protein as well as the isolated domains. The first insight into the structure were achieved by Ranganathan *et al.* in 1997 through co-crystallization with an Ala-Pro dipeptide [216]. *hPin1* consists of 163 amino acids and is divided into two domains, connected by a flexible linker of 16 amino acids (Pro³⁷-Pro⁵²). The C-terminal PPIase domain exhibits the typical parvulin order of secondary structure elements $\beta_1\alpha_1\alpha_2h\beta_2\alpha_4\beta_3\beta_4$ (h: short helix or a helical turn of 4 amino acids) with an extended loop between β_1 and α_1 . The catalytically active PPIase domain is built up of a core of 4 antiparallel β -sheets surrounded by 3 α -helices. The catalytic cleft is sheltered by the extended β_1 - α_1 loop and occupied by a sulfate ion and an

Ala-Pro dipeptide in the crystal structure [216]. The sulfate ion mimics the phosphoryl group of substrates and is coordinated by the basic amino acids Lys⁶³, Arg⁶⁸ and Arg⁶⁹ of the β_1 - α_1 loop. Additionally, the crystal structure contains 2 polyethylene glycols (PEGs), one located between the two domains and the other at a hydrophobic patch (Ile⁹⁶, Phe¹⁰³, Met¹⁴⁶ and Leu¹⁶⁰) at the opposite side of the catalytic cleft. The PEG400 sandwiched between the two domains is most likely a crystal packing artefact, the PEG400 molecule on the backside covers a possible patch for protein-protein interactions.

The N-terminal WW domain, a type IV WW domain, consists of a three-stranded antiparallel β -sheet and acts as a binding module against pThr/Ser-Pro containing polypeptides. The substrate, bound in the *trans* configuration, is held in place by the side chains of amino acids Ser¹⁶, Arg¹⁷, Tyr²³ and Trp³⁴. Here the positively charged side chain of Arg¹⁷ contacts with the phosphate group [233], while Trp³⁴ and Tyr²³ interact with the proline by π - π ring stacking interaction. The WW domain is mainly responsible for substrate selectivity. It binds the substrate in the proper orientation and delivers it to the catalytically active PPlase domain. Studies from Innes *et al.* additionally showed a preferential binding of hPin1 towards Xaa-Pro-Pro motifs [110].

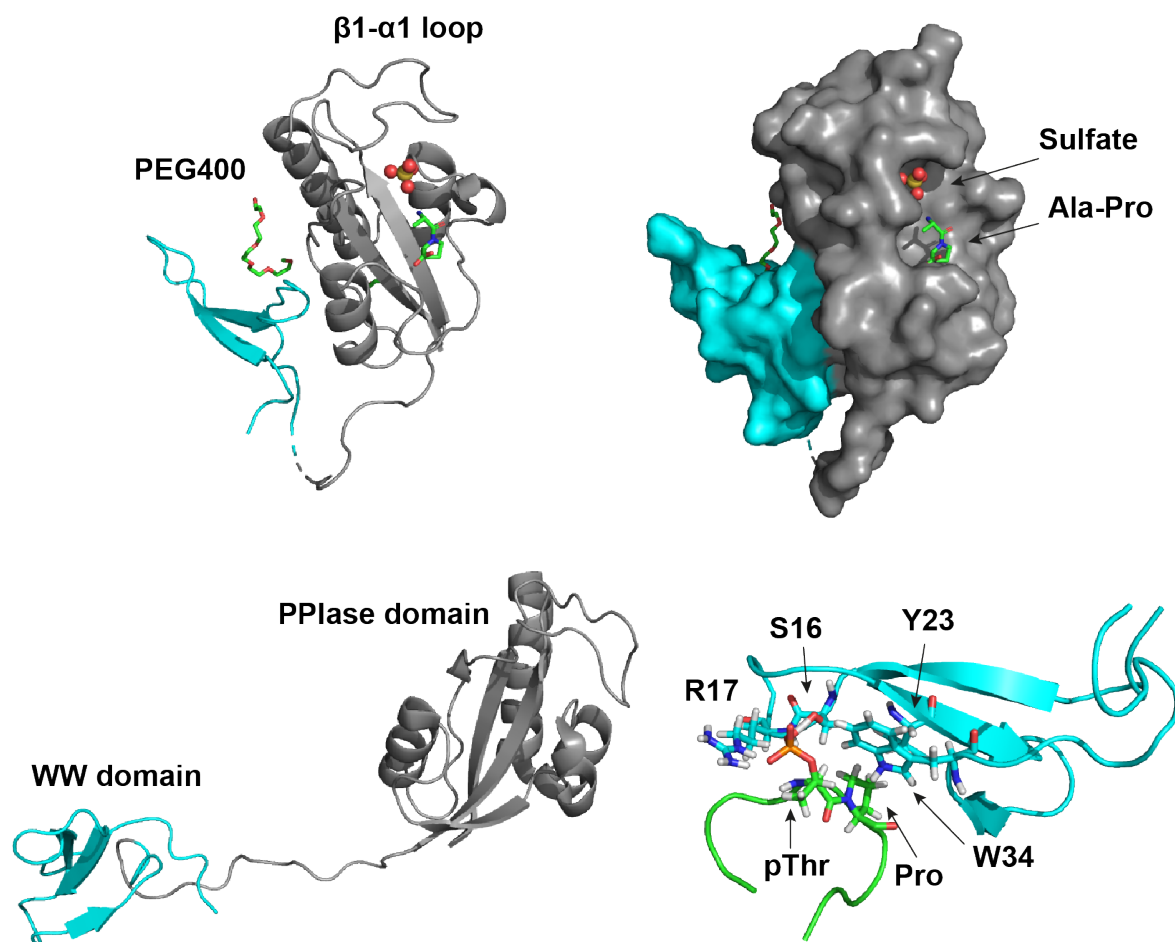


Figure 9: Structure of *hPin1* and the isolated WW domain. Shown at the top is the first crystal structure by Ranganathan *et al.* in complex with an Ala-Pro dipeptide. Top left: Cartoon representation with sulfate ion as spheres and the Ala-Pro dipeptide and PEG molecule highlighted as sticks. Additionally labeled is the specific β_1 - α_1 loop. Top right: Surface view of *hPin1* with the dipeptide and sulfate ion inside the catalytic cleft. The PPlase domain is shown in grey and the WW domain in light blue (PDB: 1PIN) [216]. Bottom left: The NMR structure of *hPin1* (PDB: 1NMV) with its flexible linker [12]. In contrast to the crystal structure, the NMR structure shows only weak domain interactions. Bottom right: NMR structure of the isolated WW domain (PDB: 1I8G) with a phosphorylated peptide sequence from CDC25 (green) [287]. Highlighted as sticks are the pThr-Pro motif and the amino acids Ser¹⁶, Arg¹⁷, Tyr²³ and Trp³⁴, responsible for substrate binding.

While crystal structures are very rigid and show only a single conformational state, the solution structure of *hPin1* by NMR shows highly dynamic interactions. Here the linker shows its flexibility, and the WW domain is seen as a substrate binding module which relocates the substrate towards the catalytic center. In addition, the separated domains no longer form an interface at the opposite of the substrate binding area, which promotes the importance of the flexible linker for substrate binding [12, 115].

3.5.4 Inhibition of *hPin1* - Natural and synthetic inhibitors

As described above *hPin1* is overexpressed in most cancers, which makes the protein a perfect target for therapy and drug design. Many patients would benefit from a synthetic or natural regulator/inhibitor. Several molecules, with varying mechanisms, have already been described as potent inhibitors. The first and most prominent one, named juglone, binds covalently to the Cys¹¹³ of *hPin1* and thus blocks the catalytic center [99]. Juglone was used successfully in *in-vitro* experiments [30] and cellular studies [43, 107, 120], but is not selective against *hPin1* in a cellular environment. Due to its 1,4-naphthoquinone core, juglone and its derivatives irreversibly modify all accessible cysteines and are therefore not suitable for specific inhibition [29, 99].

The second group of inhibitors are competitive binding small molecules, like the rationally designed tetraoxobenzo-phenanthroline [263] and dipentamethylene thiuram monosulfide (DTM) [257]. DTM competitively binds to *hPin1* and inhibits cell cycle progression. In addition, epigallocatechin gallate, a natural antioxidant found in large quantities in dried tea leaves, was found to block the substrate binding site at both domains and prevent growth of tumor cells [265, 290].

Moreover, in the last two decades peptidic inhibitors and substrate analogs of *hPin1* were discovered. Based on a combinatorial library, peptides were tested for their ability to inhibit *hPin1* function. These peptides, built up of five to eight amino acids and containing non-proteogenic amino acids, were shown to block cell cycle progression [285, 313]. In subsequent experiments, the inhibitory effect of these peptide inhibitors was shown to increase as a result of cyclization [15, 157]. The conformational lock of peptidic substrates by the group of Etzkorn favored *cis* over *trans* by a factor of 20, which makes phosphorylated cyclized *cis* peptides the most potent inhibitors to date [282, 296].

3.6 Aims

The detection, monitoring and characterization of proteins or other biological macromolecules has become increasingly important and fluorescence is a useful tool to study these interactions. Target proteins, for example, can be co-expressed with fluorescent proteins such as GFP or expressed separately and labeled with commonly used fluorophores such as the Alexa Fluor series and fluorescein [119, 128].

In recent years, however, the phenomenon of AIE has become increasingly popular and a number of AIEgens for specific detection of biomolecules were synthesized and published [61, 155, 181]. In contrast to regular fluorophores, AIEgens offer advantages such as the resistance against photobleaching and a direct read-out option from fluorescence intensity. However, most of them are synthesized using a long and inefficient synthetic route or are hard to specifically modify.

In this work the new TPN derivatives by the group of J. Voskuhl are based on aromatic

thioethers connected in *para*-position and can be synthesized in a short synthetic route with high yields of 90-95% [221]. The thioethers provide the AIEgens with high structural flexibility around the rotational axis. Consequently, the AIEgens show high potential for molecular restrictions upon protein binding. Using AIEgens we will be able to create soluble, specific and durable fluorescence markers for selected targeting of specific proteins. In combination with the *hPin1*-WW domain, a well described protein, the AIEgens will be used to establish a model system that proves the principle of peptide-conjugated TPN derivatives targeting a specific protein. The AIEgens are expected to give a unique turn-on signal upon protein binding that can be monitored directly by fluorescence spectroscopy.

First, the new AIEgens will be designed and synthesized for the specific recognition of the *hPin1*-WW domain. Therefore, peptides containing the *hPin1* specific pThr-Pro binding motif are coupled to the aromatic AIE-core via copper(I)-catalyzed azide-alkyne cycloaddition (CuAAC) and tested for their solubility and fluorescence properties. The AIEgens should exhibit good solubility and in addition low autofluorescence for a high signal-to-noise ratio. Afterwards the conditions for protein binding and determination of binding constants will be optimized for stable and reproducible fluorescence measurements.

In the next step, the influence of a peptide linker between the aromatic AIE-core and the *hPin1* specific pThr-Pro binding motif and the influence of its length on protein binding and fluorescence intensity will be analyzed. Likewise, the influence of the number of coupled peptide arms on the fluorescence properties upon binding will be tested. In addition to the biochemical characterization by fluorescence spectroscopy, the molecular structure of an AIEgen in solution is of great interest to fully understand the fluorescence behavior. While structures of small chemical molecules such as the DSA of the group of J. Voskuhl [97] are mainly solved as crystal structures, the new AIEgens will be solved by NMR spectroscopy. Unlike crystal structures, an NMR structure displays the actual conformation of the AIEgen in an aqueous solution as used in the assay, rather than the solid or crystalline state. Finally, an NMR complex structure of the best AIEgen bound to the *hPin1*-WW domain will be calculated to demonstrate the protein-ligand interactions and show molecular contacts that can explain the AIEE effect.

4 Materials & Methods

4.1 Materials

4.1.1 Chemicals

Chemicals not listed were bought from Carl Roth, Sigma Aldrich, AppliChem, Fischer Scientific, Fluka, Bernd Kraft, SERVA, Merck, Novabiochem and used without further purification.

¹⁵ N-Ammonium chloride, 99-atom% ¹⁵ N (¹⁵ N-NH ₄ Cl)	Cortecnet
Biotin	AppliChem Panreac
Cobalt(III) chloride (CoCl ₃)	Fluka
Cyanocobalamin	Sigma Aldrich
Deuterium oxide (D ₂ O)	EURISO-TOP GmbH
Fmoc-Azidohomoalanine (Fmoc-L-Aha-OH)	Iris Biotech GmbH
N-alpha-(9-Fluorenylmethyloxycarbonyl)-O-benzyl-L-phosphothreonine (Fmoc-Thr(PO(OBzl)OH)-OH)	ABCR GmbH
Folic acid	Sigma Aldrich
¹³ C-D-Glucose, 99-atom% ¹³ C	Cortecnet
Iron(III) chloride (Fe(III)Cl ₃)	Sigma Aldrich
Kanamycin sulfate	MP Biomedicals GmbH
2-Mercaptoethanol	Carl Roth GmbH
Nicotinamide	AppliChem Panreac
Pantothenic acid hemicalcium salt	Sigma Aldrich
Riboflavin	Sigma Aldrich
Rink Amide resin (100-200 mesh)	Merck
N,N,N,N-Tetramethyl-O-(1H-benzotriazole-1-yl)uronium hexafluorophosphate (HBTU)	Carbolution
Thiamine hydrochloride (Vitamin B ₁)	Carl Roth GmbH
Triisopropyl silane (TIPS)	TCI Chemicals
Zinc sulfate (ZnSO ₄)	Carl Roth GmbH

4.1.2 Consumables

Consumable	Description	Manufacturer
Centrifugation concentrator	Vivaspin 15R	Sartorius
Fluorescence cuvette	Ultra-micro cuvette	Hellma Analytics
Gel filtration column	HiLoad 16/600 Superdex 75 pg	GE Healthcare
Glutathione Sepharose	4 Fast Flow	GE Healthcare
ESI Chip	HD_ESI_Chip_5.5µm	Fisher Scientific

NMR tubes	3 mM tube	Deutero GmbH
	5 mm Shigemi tube	Shigemi Inc.
Plasmid Miniprep kit	NucleoSpin TM Plasmid	Macherey-Nagel
Protein ladder	PageRuler TM Plus Prestained	Thermo Scientific
Sterile filter	0.22 μm	Millipore
UV cuvettes	Micro cuvette	Hellma Analytics

4.1.3 Devices

Devise	Description	Manufacturer
Balances and scales	ABJ 83	Kern
	EG	Kern
Centrifuges	Avanti JE, JLA 9.100	Beckmann
Electrophoresis chambers	Mini-PROTEAN Tetra System	BioRad
Fluorescence spectrometer	FP-8300	JASCO
FPLC	NGC Chromatography system	BioRad
	Azura [®]	Knauer
Heat block	Thermomixer comfort	Eppendorf
HPLC	Prominence UFLC system	Shimadzu
HPLC rp-column	Luna [®] 5 μm C18(2), 100x21.20 mm	Phenomenex
HR-MS system	Orbitrap: Exactive Plus TM	Thermo Scientific
	Triversa NanoMate [®]	Advion
Incubator shaker	Multitron HT	Infors
LC-MS system	UV Detector: Accela TM	Thermo Scientific
	Column: Eclipse XDB-C18 5 μm	Agilent
	Mass spectrometer: LCQ Fleet TM ESI-MS	Thermo Scientific
NMR spectrometer	Bruker Ultrashield 700,MHz	Bruker BioSpin
	Bruker Avance Neo II 500 MHz	Bruker Biospin
pH Meter	SevenCompact	Mettler Toledo
	pH-Meter-766 Calimatic	Knick
pH Sensor	InLab Micro	Mettler Toledo
	InLab Routine	Mettler Toledo
Power Supplies	PowerPac Basic	BioRad
Rotors ultracentrifuge	Ti 45	Beckmann
Synthesis robot	Syro I	MultiSynTech
Table centrifuges	Centrifuge 5415 R	Eppendorf
	Centrifuge 5810 R	Eppendorf
Ultrasonic devise	Sonopuls	Bandelin

UV-VIS spectrometer	Cary 100Bio	Varian
---------------------	-------------	--------

4.1.4 Buffer and Solutions

Coomassie staining solution	0.25% (w/v) Coomassie brilliant blue G-250 50% (v/v) Ethanol 10% (v/v) Acetic acid
Elution buffer	1x PBS; pH 7.5 20 mM Glutathione red.
Fluorescence buffer	20 mM HEPES; pH 7.0
Gel filtration buffer	50 mM KPi; pH 7.4 150 mM NaCl
High salt buffer	1x PBS; pH 7.4 500 mM NaCl
M9 salts (10x)	337 mM Na ₂ HPO ₄ 220 mM KH ₂ PO ₄ 85.5 mM NaCl
NMR buffer	50 mM KPi; pH 7.0
PBS-buffer	10 mM Na ₂ HPO ₄ ; pH 7.0 1.8 mM KH ₂ PO ₄ 2.7 mM KCl 137 mM NaCl
SDS electrophoresis buffer	25 mM Tris; pH 8.3 0.1% (w/v) SDS 250 mM Glycin
SDS sample buffer (5x)	250 mM Tris-HCl; pH 6.8 50% (v/v) Glycerol 10% (w/v) SDS 14 mM 2-Mercaptoethanol 0.004% (w/v) Bromophenol blue
Separating gel buffer	1.5 M Tris, pH 8.8

Stacking gel buffer	0.5 M Tris; pH 6.8
Trace metals	53.7 mM Na ₂ EDTA 61.8 mM Fe(III)Cl ₃ 34 mM CaCl ₂ 626 μM ZnSO ₄ 641 μM CuSO ₄ 710 μM MnSO ₄ 757 μM CoCl ₂
Vitamin stock	81.9 μM Biotin 45.3 μM Folic acid 148,2 μM Thiamine 209.8 μM Pantothenic acid 0.7 μM Cyanocobalamine 409.4 μM Nicotinamide 132.9 μM Riboflavin

4.1.5 Nutritional media

LB medium pH 7.0	10 g/L Tryptone 5 g/L Yeast 10 g/L NaCl
2xYT medium pH 7.0	16 g/L Tryptone 10 g/L Yeast 5 g/L NaCl
M9 minimal medium pH 7.4	1x M9 salts 1.0 mL Trace metals 1.5 mL Vitamin stock 0.1 mM CaCl ₂ 2 mM MgSO ₄ 4 g/L D-Glucose or 3 g/L ¹³ C-D-Glucose 0.7 g/L NH ₄ Cl or ¹⁵ NH ₄ Cl

4.1.6 Plasmids

Plasmids used were previously made internally and are based on a modified pET41b vector. It contains the target protein (*hPin1* or *hPin1-WW*) fused to an N-terminal GST-tag and an additional HRV 3C site (PreScission site).

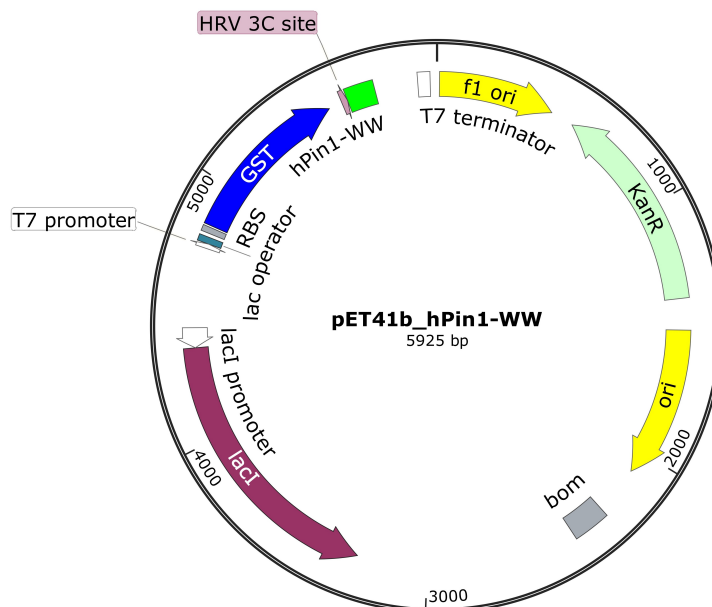


Figure 10: Vector map of the modified pET41b vector, here for the expression of the *hPin1-WW*. The plasmid contains the kanamycin resistance cassette (mint), the replication origins (yellow), the *lacI* cassette (purple) with *lacI* promoter (white), the GST tag (blue), the *hPin1-WW* domain (green) and the PreScission protease cleavage site (HRV 3C site).

4.1.7 Bacterial strains

For the expression of *hPin1* and *hPin1-WW* the bacterial strain *Escherichia coli* BL21 (DE3)-T1^R was used, and for the preparative isolation of plasmid DNA the *E. coli* strain DH5 α was used.

Table 1: Bacterial strains for protein expression and DNA isolation

Bacterial strain	Genotype
<i>E. coli</i> BL21(DE3)-T1 ^R	F ⁻ <i>ompT hsdS_B (r_B⁻m_B⁻) gal dcm λ(DE3) tonA</i>
<i>E. coli</i> NEB5 α	<i>fhuA2</i> Δ (argF-lacZ)U169 <i>phoA glnV44 Φ80 Δ(lacZ)M15 gyrA96 recA1 relA1 endA1 thi-1 hsdR17</i>

4.1.8 Software

NMR data acquisition / processing	Topspin 3.5 (Bruker)
NMR data analysis	Cara (Wüthrich lab) (www.cara.nmr.ch) [123]
NMR structure calculation	Cyana 2.1 (Güntert lab) (www.cyana.org) [83–86, 101, 236] UNIO (Dr. Torsten Herrmann; www.unio-nmr.fr)
Peak picking	SPARKY (Goddard <i>et al.</i>) [255]
Dihedral angle prediction	Talos (NMRPipe package) [42]
Model building	Pymol 2.3 (www.pymol.org)
Structure visualization	Pymol 2.3 (www.pymol.org)
Statistics and data analysis	GraphPad Prism (GraphPad Software)
Analysis of mass spectrometry	Xcalibur (ThermoFischer) MestReNova (Mestrelab Research)
Online smiles translator	Cactus (https://cactus.nci.nih.gov/translate)
Draw molecules	ChemDraw (Perkin Elmer)

4.2 Molecular biology methods

4.2.1 Transformation of plasmid DNA

For the transformation of plasmid DNA into *E. coli* BL21(DE3)-T1^R or *E. coli* DH5 α , 50 μ L of cells were thawed on ice and incubated with 100 ng of DNA for 20 min. Afterwards the transformation is achieved by heat shock at 42 °C for 30 s, followed by another incubation on ice for 2 min. Finally 200 μ L of preheated LB media was added and the cells recovered for 1 h at 37 °C and 500 rpm in a thermal mixer. For the final selection of the *E. coli* cells, 50 μ L were plated on a LB-agar-plate with 50 μ g/mL ampicillin and incubated overnight at 37 °C.

4.2.2 Protein expression

The heterologous expression of *hPin1* and *hPin1*-WW domain was performed in *E. coli* BL21(DE3)-T1^R cells. For this, an overnight culture was grown and 25 mL was used to inoculate the main culture. The proteins were expressed in a 5 L flask with 1 L of media and 50 μ g/mL kanamycin. First the main culture was grown at 37 °C and 160 rpm to an OD₆₀₀ of 0.6 – 0.8, before the expression was induced by adding 200 μ M IPTG. The expression parameters for *hPin1* and *hPin1*-WW domain are summarized in Table 2. After expression the *E. coli* cells were harvested by centrifugation and the cell pellet was flash-frozen in liquid nitrogen. The cell pellet was stored at -20 °C.

Table 2: Conditions for the expression of *hPin1*, *hPin1-WW* and isotope labeled *hPin1-WW* domain

Parameters	<i>hPin1</i>	<i>hPin1-WW</i>	¹⁵ N <i>hPin1-WW</i> & ¹⁵ N, ¹³ C <i>hPin1-WW</i>
Temperature	30 °C	30 °C	30 °C
Time	5 h	overnight	overnight
Media	2xYT	LB	M9

4.3 Biochemical methods

4.3.1 Protein purification

Cell lysis

The frozen bacterial cells were thawed at room temperature (RT) and the pellet of a 1 L cell pellet was resuspended in 25 mL PBS buffer. All following purification steps were performed at 4 °C. The cell suspension was mixed with 5 mg lysozyme and 0.5 mM PMSF and incubated for 1 h. The cells were then sonicated using 10 cycles of 30 sec with 60% amplitude. After cell disruption, membranes and other insoluble cell components were separated by ultracentrifugation (1 h at 125,000 g). The supernatant was filtered using a sterile membrane (0.22 μm) and further purified by affinity chromatography.

GSH affinity chromatography

Here the filtered supernatant was loaded onto a Glutathion (GSH) column with a column volume (CV) of 20 mL and the proteins were purified by the protocol in table 3. The purification was performed at 1 mL/min and the elution was monitored by the absorbance at 280 nm. The elution was collected in 2 mL fractions and further analyzed by SDS-PAGE (section 4.3.3). The protein-containing fractions were pooled and concentrated to 50-60 mg/mL.

Table 3: Program for the purification of *hPin1* and *hPin1*-WW by a GSH column

Purification steps	Buffer	Volume
Wash	PBS pH 7.5	2.5 CV
High salt elution	High salt buffer	4 CV
Wash	PBS pH 7.5	2.5 CV
Elution	Elution buffer	5 CV

Size exclusion chromatography

The final protein purification was performed by size exclusion chromatography. For this, 100 mg GST fusion protein was mixed with 0.8 mg PreScission protease and incubated in a 2 mL sample loop for 6 to 8 h. The protein mix was then applied to a gel filtration column (HiLoad 26/600 Superdex 75 pg) and purified with gel filtration buffer at 1.5 mL/min. The elution was again monitored by the absorbance at 280 nm and collected in 2.5 mL fractions. The purified protein was finally dialyzed against fluorescence- or KPi buffer using a centrifugal concentrator with a molecular weight cutoff of 3 kDa.

4.3.2 Determination of protein concentration

The protein concentration was calculated by using either a Bradford protein assay [21] or measuring the absorbance at 280 nm using NanoDrop2000 and calculating the concentration with the Beer-Lambert law. For calculation with the Beer-Lambert law the following extinction coefficients were used: $\epsilon(hPin1) = 21095 \text{ M}^{-1} \text{ cm}^{-1}$ and $\epsilon(hPin1\text{-WW}) = 13980 \text{ M}^{-1} \text{ cm}^{-1}$.

For the Bradford protein assay 999 μL of Bradford reagent was mixed with 1 μL protein in a semi-microcuvette and incubated at RT. The absorbance after 5 min was measured at 595 nm and the protein concentration calculated relative to a BSA standard.

4.3.3 SDS-Polyacrylamide gel electrophoresis (SDS-PAGE)

The analytical separation of proteins was performed by their molecular weight using SDS-polyacrylamide gel electrophoresis (SDS-PAGE). Here a 5% stacking gel was used followed by a 12.5% or a 15% separation gel. The gels used have been prepared in accordance with table 4.

Prior to analysis the samples were mixed with SDS sample buffer (5x) and heated to 90 °C. The separation was carried out at 50 mA per connected gel. Afterwards the gels were stained for 15 min in Coomassie staining solution and then destained with water.

Table 4: Composition of used SDS gels

Chemicals	Stacking gel	Separation gel
Acrylamide	5% (w/v)	15% (w/v) or 12.5% (w/v)
Tris	41 mM	330 mM
SDS	0.08% (w/v)	0.10% (w/v)
APS	0.08% (w/v)	0.10% (w/v)
TEMED	0.17% (v/v)	0.08% (v/v)

4.4 Chemical synthesis

The AIE-active thioethers (figure 11) used for the following synthesis were synthesized by Steffen Riebe and Matthias Hayduck (Group of J. Voskuhl).

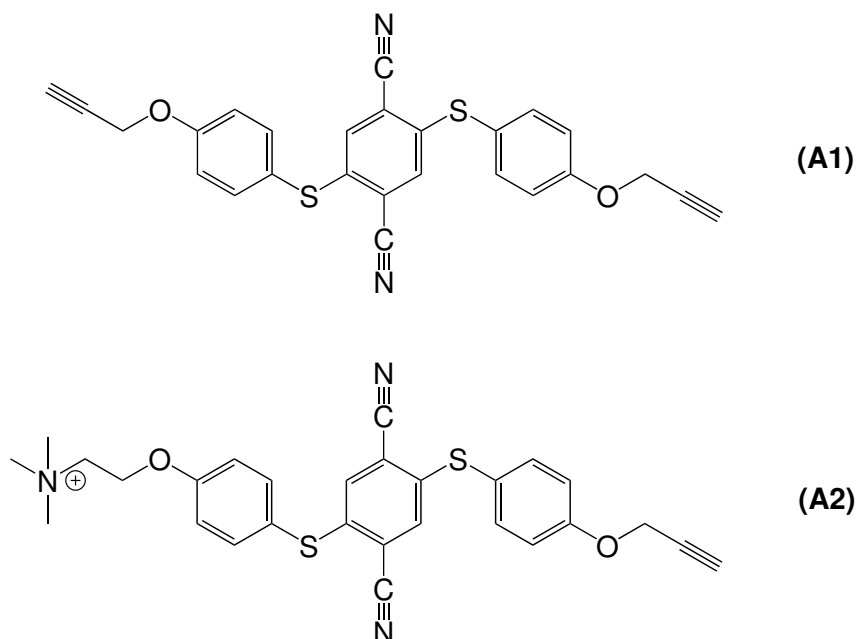


Figure 11: Chemical structure of AIE-active core molecules used for conjugation with specific peptide sequences. The symmetric fluorophores 1-9 were synthesized with AIE-core **A1** and the asymmetric fluorophore 10 with AIE-core **A2**.

4.4.1 Peptide synthesis

The peptides were synthesized using solid phase peptide synthesis (SPPS) with standard Fmoc chemistry. The coupling of amino acids was performed in double coupling using DIC and HBTU as coupling reagent. As resin a rink amide was used to get an amidated C-terminus. First 200 mg resin was swollen in DCM and washed twice with 1.2 mL DMF for 30 min. Then the resin was deprotected, washed and the amino acid

was coupled. These steps were repeated until the final peptide sequence was completed. The individual steps are described in more detail below and the synthesized peptide sequences are listed in table 5.

Table 5: Peptide sequences synthesized with SPPS in 3 letter code

Name	Peptide sequence (N → C)
Peptide 1	Aha-pThr-Pro-Ala-NH ₂
Peptide 2	Aha-Ala-pThr-Pro-Ala-NH ₂
Peptide 3	Aha-Ala-Gly-pThr-Pro-Ala-NH ₂
Peptide 4	Aha-Ala-Gly-Ala-Gly-pThr-Pro-Ala-NH ₂
Peptide 5	Aha-Ala-Gly-Ala-Gly-Ala-Gly-pThr-Pro-Ala-NH ₂
Peptide 6	Aha-pThr-Gly-Ala-NH ₂
Peptide 7	Aha-Thr-Pro-Ala-NH ₂
Peptide 8	Aha-Thr-Gly-Ala-NH ₂
Peptide 9	Aha-Thr-Phe-Ala-NH ₂
Peptide 0	Aha-pThr-Arg-Ala-NH ₂

with Aha: L-Azidohomoalanine

Fmoc deprotection

For Fmoc deprotection the washed resin was incubated for 3 min with 1.2 mL piperidine (40%) in DMF. After solvent removal, the deprotection was repeated with 20% piperidine for 12 min. Finally, the resin got washed 6 times for 1 min with 1.3 mL DMF.

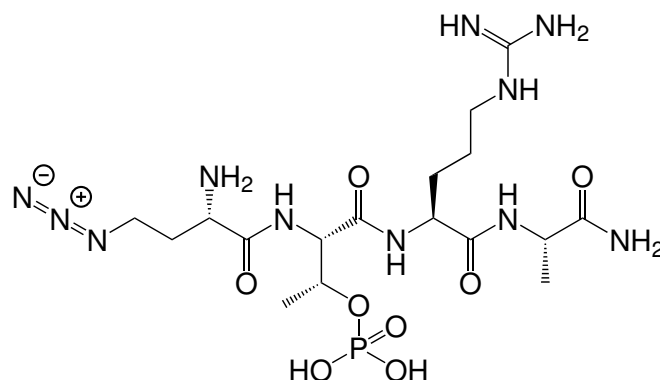
Amino acid coupling

For coupling, the amino acids (4 eq) were dissolved with 0.1 M HOBt in DMF. The resin was then mixed with the amino acid solution, HBTU (4 eq) in DMF and DIPEA (4 eq) in NMP (final volume: 2.04 mL). The solution was shaken for 40 min followed by a washing step containing 3 wash cycles with 2.1 mL DMF for 1 min. For double coupling the steps were repeated with DIC (4 eq) in DMF instead of HBTU.

Peptide cleavage from resin

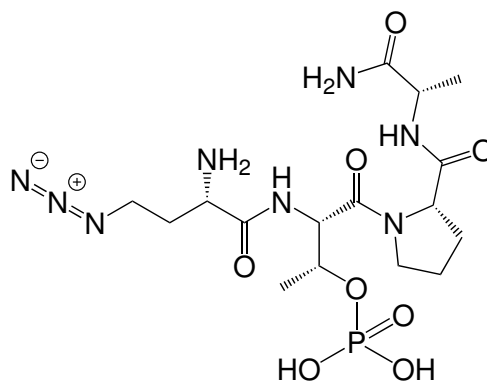
For cleavage and final deprotection, the resin was mixed with 5 mL 95% | 2.5% | 2.5% of TFA | TIPS | H₂O and the reaction was carried out at RT for 3 h. Afterwards the peptides were precipitated in 45 mL ice cold diethyl ether and separated by centrifugation. The peptides were dissolved in 20% ACN/80% H₂O and finally purified by rp-HPLC (4.4.5).

4.4.2 Peptide compounds

L- γ -Azidohomoalanine-O-Phospho-L-Threonine-L-Arginine-L-Alanine-Amide**Peptide 0 (P0)**

The peptide **P0** was synthesized by standard SPPS and after HPLC purification a total yield of 75.8 mg (137.4 μ mol, 98%) could be isolated as a white solid.

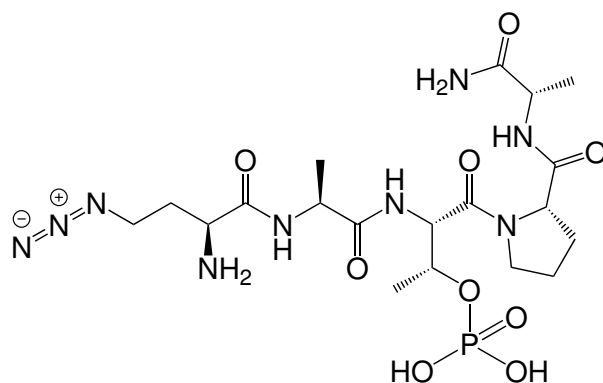
LC-MS (ESI): t_R = 1.42 min; m/z = 552.10 [M + H]⁺, 1103.01 [2M + H]⁺, 1654.87 [3M + H]⁺, calculated for C₁₇H₃₄N₁₁O₈P: 551.50.

L- γ -Azidohomoalanine-O-Phospho-L-Threonine-L-Proline-L-Alanine-Amide**Peptide 1 (P1)**

The peptide **P1** was synthesized by standard SPPS and after HPLC purification a total yield of 65.3 mg (132.6 μ mol, 94%) could be isolated as a white solid.

LC-MS (ESI): t_R = 1.69 min; m/z = 492.95 [M + H]⁺, 984.82 [2M + H]⁺, 1476.72 [3M + H]⁺, calculated for C₁₆H₂₉N₈O₈P: 492.43.

L- γ -Azidohomoalanine-L-Alanine-O-Phospho-L-Threonine-L-Proline-L-Alanine-Amide

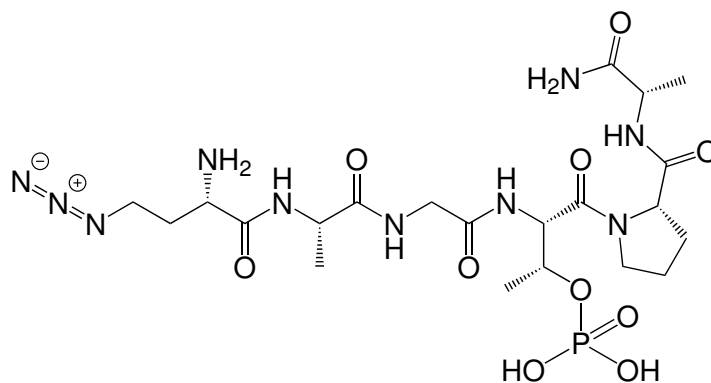


Peptide 2 (P2)

The peptide **P2** was synthesized by standard SPPS and after HPLC purification a total yield of 77.0 mg (136.6 μ mol, 98%) could be isolated as a white solid.

LC-MS (ESI): t_R = 2.12 min; m/z = 565.08 [M + H]⁺, 1128.91 [2M + H]⁺, 1693.08 [3M + H]⁺, calculated for C₁₉H₃₄N₉O₉P: 563.51.

L- γ -Azidohomoalanine-L-Alanine-Glycine-O-Phospho-L-Threonine-L-Proline-L-Alanine-Amide

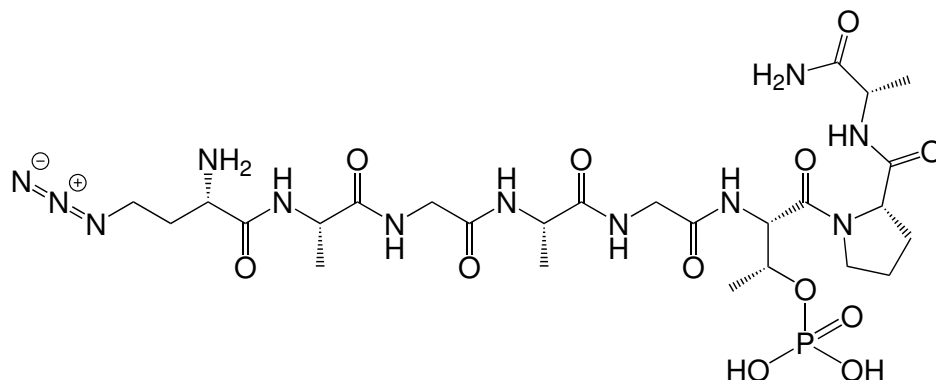


Peptide 3 (P3)

The peptide **P3** was synthesized by standard SPPS and after HPLC purification a total yield of 82.5 mg (132.9 μ mol, 92.9%) could be isolated as a white solid.

LC-MS (ESI): t_R = 1.76 min; m/z = 621.09 [M + H]⁺, 1240.77 [2M + H]⁺, 1860.48 [3M + H]⁺, calculated for C₂₁H₃₇N₁₀O₁₀P: 620.56.

L- γ -Azidohomoalanine-L-Alanine-Glycine-L-Alanine-Glycine-O-Phospho-L-Threonine-L-Proline-L-Alanine-Amide

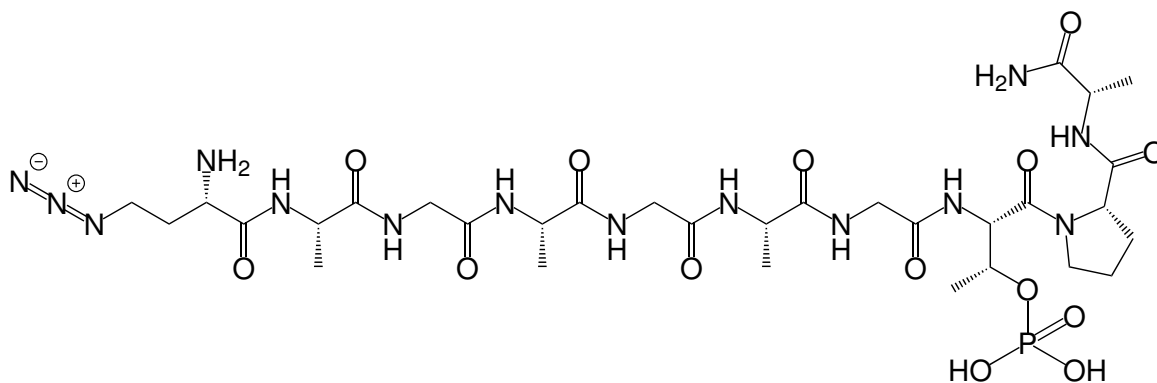


Peptide 4 (P4)

The peptide **P4** was synthesized by standard SPPS and after HPLC purification a total yield of 103.1 mg (137.6 μ mol, 88%) could be isolated as a white solid.

LC-MS (ESI): t_R = 1.82 min; m/z = 375.17 [M + 2H]²⁺, 749.22 [M + H]⁺, 1497.08 [2M + H]⁺, calculated for C₂₆H₄₅N₁₂O₁₂P: 748.69.

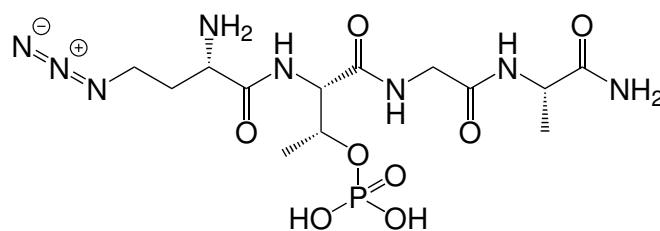
L- γ -Azidohomoalanine-L-Alanine-Glycine-L-Alanine-Glycine-L-Alanine-Glycine-O-Phospho-L-Threonine-L-Proline-L-Alanine-Amide



Peptide 5 (P5)

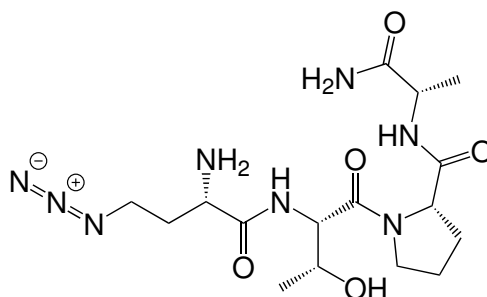
The peptide **P5** was synthesized by standard SPPS and after HPLC purification a total yield of 107.0 mg (122.0 μ mol, 87%) could be isolated as a white solid.

LC-MS (ESI): t_R = 1.91 min; m/z = 439.42 [M + 2H]²⁺, 877.18 [M + H]⁺, 1753.72 [3M + H]⁺, calculated for C₃₁H₅₃N₁₄O₁₄P: 876.82.

L- γ -Azidohomoalanine-O-Phospho-L-Threonine-Glycine-L-Alanine-Amide**Peptide 6 (P6)**

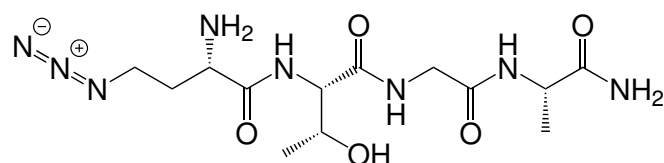
The peptide **P6** was synthesized by standard SPPS and after HPLC purification a total yield of 63.1 mg (139.5 μ mol, 95.5%) could be isolated as a white solid.

LC-MS (ESI): t_R = 1.53 min; m/z = 453.03 [M + H]⁺, 904.91 [2M + H]⁺, 1357.52 [3M + H]⁺, calculated for C₁₃H₂₅N₈O₈P: 452.36.

L- γ -Azidohomoalanine-L-Threonine-L-Proline-L-Alanine-Amide**Peptide 7 (P7)**

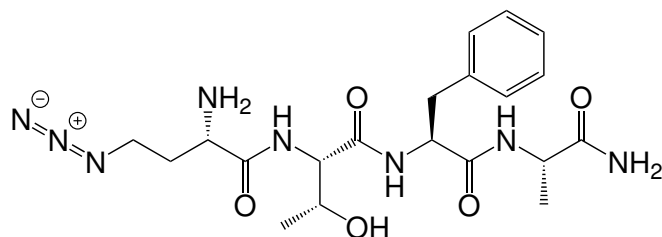
The peptide **P7** was synthesized by standard SPPS and after HPLC purification a total yield of 69.6 mg (168.7 μ mol, 99.2%) could be isolated as a white solid.

LC-MS (ESI): t_R = 2.03 min; m/z = 413.94 [M + H]⁺, 826.68 [2M + H]⁺, calculated for C₁₆H₂₈N₈O₅: 412.45.

L- γ -Azidohomoalanine-L-Threonine-Glycine-L-Alanine-Amide**Peptide 8 (P8)**

The peptide **P8** was synthesized by standard SPPS and after HPLC purification a total yield of 49.2 mg (131.6 μ mol, 94.0%) could be isolated as a white solid.

LC-MS (ESI): t_R = 1.91 min; m/z = 373.97 [M + H]⁺, 746.67 [2M + H]⁺,
calculated for C₁₃H₂₄N₈O₅: 372.39.

L- γ -Azidohomoalanine-L-Threonine-L-Phenylalanine-L-Alanine-Amide**Peptide 9 (P9)**

The peptide **P9** was synthesized by standard SPPS and after HPLC purification a total yield of 21 mg (45.4 μ mol, 35%) could be isolated as a white solid.

LC-MS (ESI): t_R = 4.81 min; m/z = 464.04 [M + H]⁺, 926.70 [2M + H]⁺,
calculated for C₂₀H₃₀N₈O₅: 462.51.

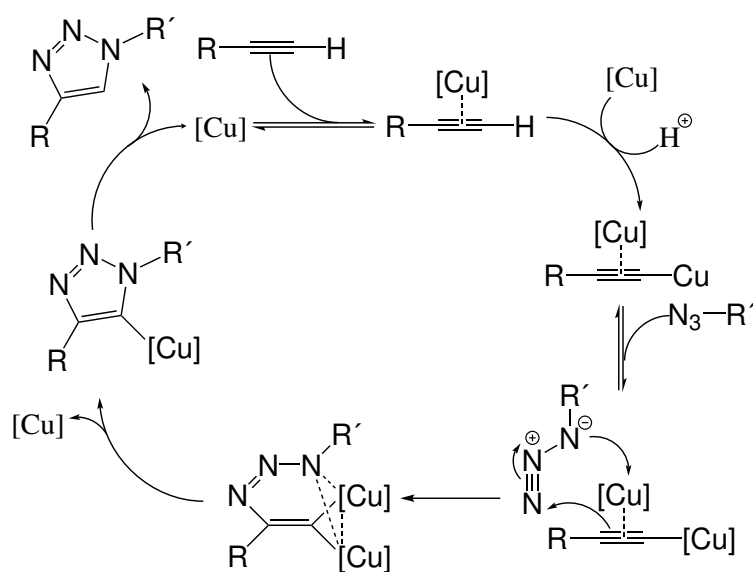
4.4.3 Copper(I)-catalyzed azide-alkyne cycloaddition (CuAAC)

The purified peptides were fused to the AIE-active core (figure 11) by a copper(I) catalyzed azide-alkyne cycloaddition. For this the AIE-active core was mixed with the copper catalyst and the peptide. The starting materials were then degassed, dissolved in completely degassed solvent and mixed at RT for 3 to 5 days. To optimize the yield of the CuAAC, parameters like the organic solvent (DMF or 2:1 THF in H₂O) and the copper catalyst (CuI or CuSO₄) were varied (table 6).

Table 6: Setups for optimization of CuAAC reaction

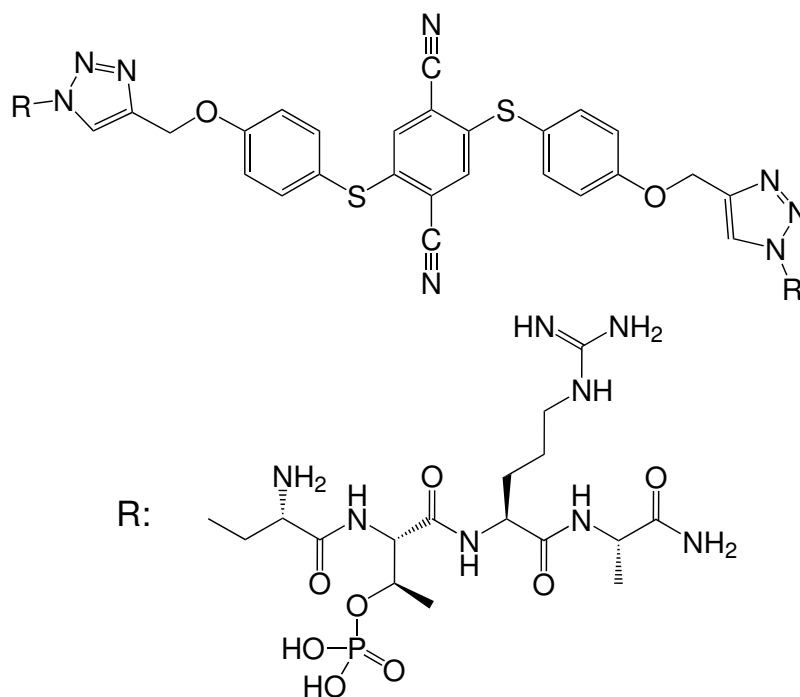
Parameter	Reaction 1	Reaction 2	Reaction 3	Reaction 4
AIE-core	8-10 mg	8-10 mg	8-10 mg	8-10 mg
Peptide	2.4 eq	2.4 eq	2.4 eq	2.4 eq
Solvent	THF/H ₂ O	THF/H ₂ O	DMF	DMF
CuSO ₄	0.6 eq	0.6 eq	0.6 eq	-
CuI	-	-	-	4 eq
Na-ascorbate	1.3 eq	1.3 eq	1.3 eq	-
Volume	5 mL	9 mL	9 mL	9 mL

The detailed reaction mechanism for CuAAC is shown in figure 12. The copper(I) catalyst, in the form of CuI or CuSO₄ reduced by sodium ascorbate, binds to the triple bond of the alkyne, forming a π -complex. Thereby, the terminal hydrogen becomes deprotonated, resulting in the σ -bound Cu-acetylide intermediate. By coordination of a second π bound copper(I) to the triple bond, the active complex is formed. In the next step, the azide gets coordinated to the alkyne by both copper atoms. The so created six-membered copper metal cycle is stabilized by the second copper atom. After ring contraction and elimination of a copper atom, a triazolyl-copper derivative is gained. Finally the derivative gets protonated, resulting in the triazole product and the release of a copper atom for another catalytic cycle [182,288].

**Figure 12: Reaction mechanism of the copper (I)-catalyzed azide-alkyne cycloaddition (CuAAC). [288]**

4.4.4 Chemical characterization of peptide-coupled fluorophores

Di-(L-Homoalanine-O-Phospho-L-Threonine-L-Arginine-L-Alanine-Amide)-conjugated *para*-phenolthiophthalonitrile



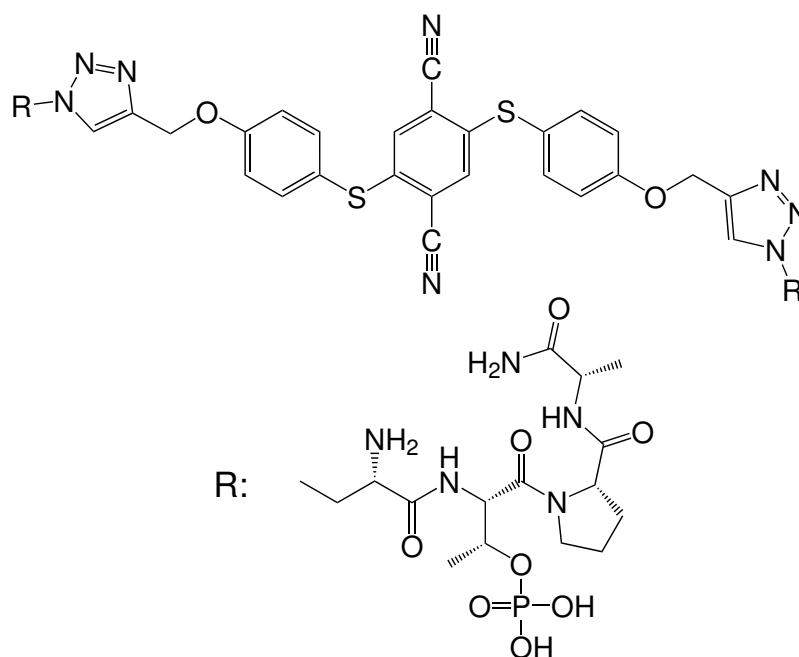
Fluorophore 0 (F0)

Fluorophore **F0** was synthesized with compounds **A1** and **P0** using CuAAC under oxygen-free conditions (table 6, reaction 2). Finally a total yield of 2.4 mg (1.1 mmol, 17.7%) could be isolated as a yellow solid.

^1H NMR (700 MHz, DMSO- d_6): δ 9.19 (s, 2H), 8.34 (s, 4H), 8.10 (s, 2H), 7.57 (s, 2H), 7.54 (d, J = 8.9 Hz, 2H), 7.31 (s, 2H), 7.20 (d, J = 9.2 Hz, 4H), 6.97 (s, 2H), 5.24 (s, 6H), 4.54 (t, J = 8.1 Hz, 6H), 4.50-4.47 (m, 2H), 4.44 (m, 2H), 4.24-4.22 (m, 2H), 4.14 (qui, J = 7.5 Hz, 2H), 2.43-2.40 (m, 2H), 2.37-2.29 (m, 6H), 1.77-1.73 (m, 2H), 1.62-1.56 (m, 10H), 1.26 (s, 4H), 1.22 (d, J = 6.5 Hz, 6H), 1.19 (d, J = 7.4 Hz, 6H).

LC-MS (ESI): t_R = 5.56 min; m/z = 389.78 $[\text{M} + 4\text{H}]^{4+}$, 519.40 $[\text{M} + 3\text{H}]^{3+}$, 778.54 $[\text{M} + 2\text{H}]^{2+}$, 1555.21 $[\text{M} + \text{H}]^+$, calculated for $\text{C}_{60}\text{H}_{84}\text{N}_{24}\text{O}_{18}\text{P}_2\text{S}_2$: 1555.55.

Di-(L-Homoalanine-O-Phospho-L-Threonine-L-Proline-L-Alanine-Amide)-conjugated *para*-phenolthioterephthalonitrile



Fluorophore 1 (F1)

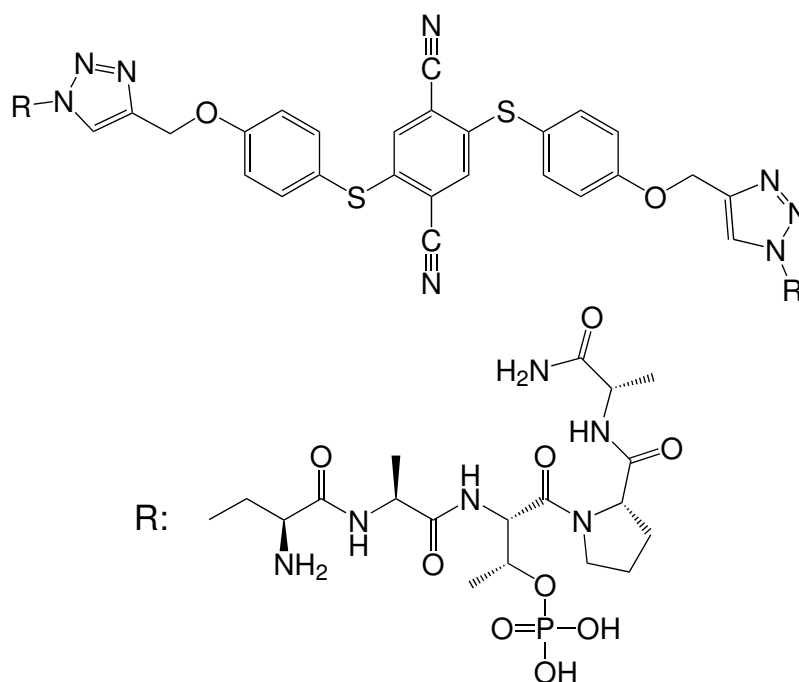
Fluorophore **F1** was synthesized with compounds **A1** and **P1** using CuAAC under oxygen-free conditions (table 6, reaction 2). Finally a total yield of 12.8 mg (8.9 mmol, 49.6%) could be isolated as a yellow solid.

$^1\text{H NMR}$ (700 MHz, 10% $\text{D}_2\text{O}/\text{H}_2\text{O}$): δ 8.95 (s, 2H), 8.73 (s, 2H *cis*), 8.51 (s, 2H *cis*), 8.27 (s, 2H), 8.07 (s, 2H *cis*), 8.01 (s, 2H), 7.48 (s, 2H), 7.28 (s, 4H), 7.01 (s, 2H), 6.98 (s, 2H), 6.89 (s, 4H), 4.54 (s, 4H), 4.39-4.34 (m, 2H, 2H *cis*), 4.23-4.19 (m, 4H, 2H *cis*), 3.79 (s, 2H), 3.73 (s, 2H), 3.44 (m, 2H *cis*), 3.39 (m, 2H *cis*), 2.51 (s, 4H), 2.36 (s, 2H *cis*), 2.16 (s, 2H), 2.05 (m, 2H *cis*), 1.95 (s, 2H), 1.82 (s, 4H), 1.75 (s, 2H *cis*), 1.66 (s, 2H *cis*), 1.40 (d, $J = 7.4$ Hz, 6H *cis*), 1.35 (d, $J = 5.2$ Hz, 6H), 1.28 (d, $J = 6.4$ Hz, 6H), 1.24 (d, $J = 5.6$ Hz, 6H *cis*).

LC-MS (ESI): $t_R = 6.00$ min; $m/z = 479.96$ $[\text{M} + 3\text{H}]^{3+}$, 719.52 $[\text{M} + 2\text{H}]^{2+}$, 1437.14 $[\text{M} + \text{H}]^+$, calculated for $\text{C}_{58}\text{H}_{74}\text{N}_{18}\text{O}_{18}\text{P}_2\text{S}_2$: 1437.41.

HR-MS:	m/z calculated	m/z measured	Δ [ppm]
$[\text{M} + 2\text{H}]^{2+}$	719.2245	719.2232	1.81
$[\text{M} + 2\text{H}]^{2+}$	719.7262	719.7253	1.25
$[\text{M} + 2\text{H}]^{2+}$	720.2279	720.2245	4.72

Di-(L-Homoalanine-L-Alanine-O-Phospho-L-Threonine-L-Proline-L-Alanine-Amide)-conjugated *para*-phenolthioterephthalonitrile



Fluorophore 2 (F2)

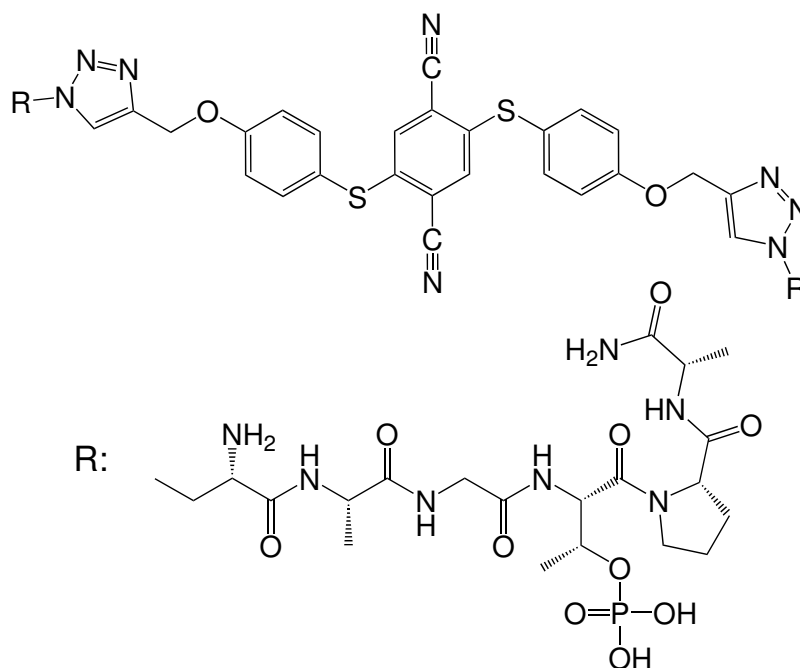
Fluorophore **F2** was synthesized with compounds **A1** and **P2** using CuAAC under oxygen-free conditions (table 6, reaction 2). Finally a total yield of 8.3 mg (5.3 mmol, 32.4%) could be isolated as a yellow solid.

^1H NMR (700 MHz, 10% $\text{D}_2\text{O}/\text{H}_2\text{O}$): δ 8.98 (s, 2H), 8.89 (s, 2H *cis*), 8.63 (s, 2H), 8.51 (s, 2H *cis*), 8.31 (s, 2H), 8.19 (s, 2H *cis*), 8.17 (s, 2H *cis*), 8.08 (s, 2H), 7.50 (s, 2H), 7.44 (s, 2H *cis*), 7.29 (s, 4H), 7.02 (s, 2H), 6.94 (s, 2H *cis*), 6.97 (s, 2H), 6.90 (s, 4H), 4.44 (s, 2H), 4.37 (s, 2H), 4.29 (s, 2H), 4.23 (t, $J = 6.6$ Hz, 2H), 4.17 (s, 2H), 3.77 (s, 2H), 3.54 (s, 2H), 2.58 (s, 2H), 2.50 (s, 2H), 2.12 (s, 2H), 1.82 (s, 2H), 1.73 (m, 4H), 1.36-1.33 (m, 12H), 1.29 (s, 6H).

LC-MS (ESI): $t_R = 6.04$ min; $m/z = 527.37$ [$M + 3\text{H}$] $^{3+}$, 790.58 [$M + 2\text{H}$] $^{2+}$, 1579.09 [$M + \text{H}$] $^+$, calculated for $\text{C}_{64}\text{H}_{84}\text{N}_{20}\text{O}_{20}\text{P}_2\text{S}_2$: 1579.56.

HR-MS:	m/z calculated	m/z measured	Δ [ppm]
[$M+2\text{H}$] $^{2+}$	790.2616	790.2594	2.78
[$M+2\text{H}$] $^{2+}$	790.7633	790.7621	1.52
[$M+2\text{H}$] $^{2+}$	791.265	791.2616	4.30

Di-(L-Homoalanine-L-Alanine-Glycin-O-Phospho-L-Threonine-L-Proline-L-Alanine-Amide)-conjugated *para*-phenolthioterephthalonitrile



Fluorophore 3 (F3)

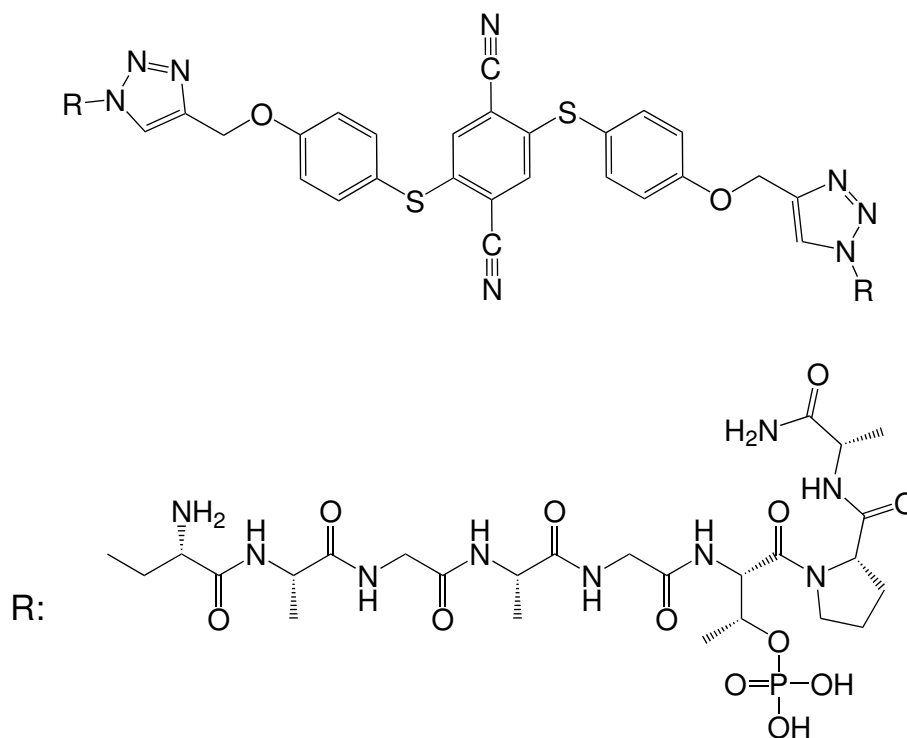
Fluorophore **F3** was synthesized with compounds **A1** and **P3** using CuAAC under oxygen-free conditions (table 6, reaction 2). Finally a total yield of 22.8 mg (13.5 mmol, 55.3%) could be isolated as a yellow solid.

^1H NMR (700 MHz, 10% $\text{D}_2\text{O}/\text{H}_2\text{O}$): δ 8.86 (s, 2H), 8.48 (s, 2H), 8.45 (s, 2H), 8.08 (s, 2H), 7.51 (s, 2H), 7.28 (s, 4H), 7.04 (s, 2H), 7.00 (s, 2H), 6.89 (s, 4H), 4.56 (s, 2H β pThr), 4.39-4.37 (m, 2H), 4.32-4.30 (m, 2H), 4.25 (t, J = 6.7 Hz, H), 4.12 (s, 2H), 3.94 (s, 4H), 3.79-3.72 (m, 2H), 3.67-3.61 (m, 2H), 2.54 (s, 4H), 2.21 (s, 2H), 1.95 (s, 2H), 1.82 (s, 4H), 1.39-.136 (m, 12H), 1.25-1.23 (m, 6H).

LC-MS (ESI): t_R = 5.98 min; m/z = 565.45 $[\text{M} + 3\text{H}]^{3+}$, 848.03 $[\text{M} + 2\text{H}]^{2+}$, 1694.14 $[\text{M} + \text{H}]^+$, calculated for $\text{C}_{68}\text{H}_{90}\text{N}_{22}\text{O}_{22}\text{P}_2\text{S}_2$: 1693.67.

HR-MS:	m/z calculated	m/z measured	Δ [ppm]
$[\text{M}+2\text{H}]^{2+}$	847.2831	847.2815	1.89
$[\text{M}+2\text{H}]^{2+}$	847.7848	847.7840	0.94
$[\text{M}+2\text{H}]^{2+}$	848.2865	848.2827	4.48

Di-(L-Homoalanine-L-Alanine-Glycin-L-Alanine-Glycin-O-Phospho-L-Threonine-L-Proline-L-Alanine-Amide)-conjugated *para*-phenolthioterephthalonitrile



Fluorophore 4 (F4)

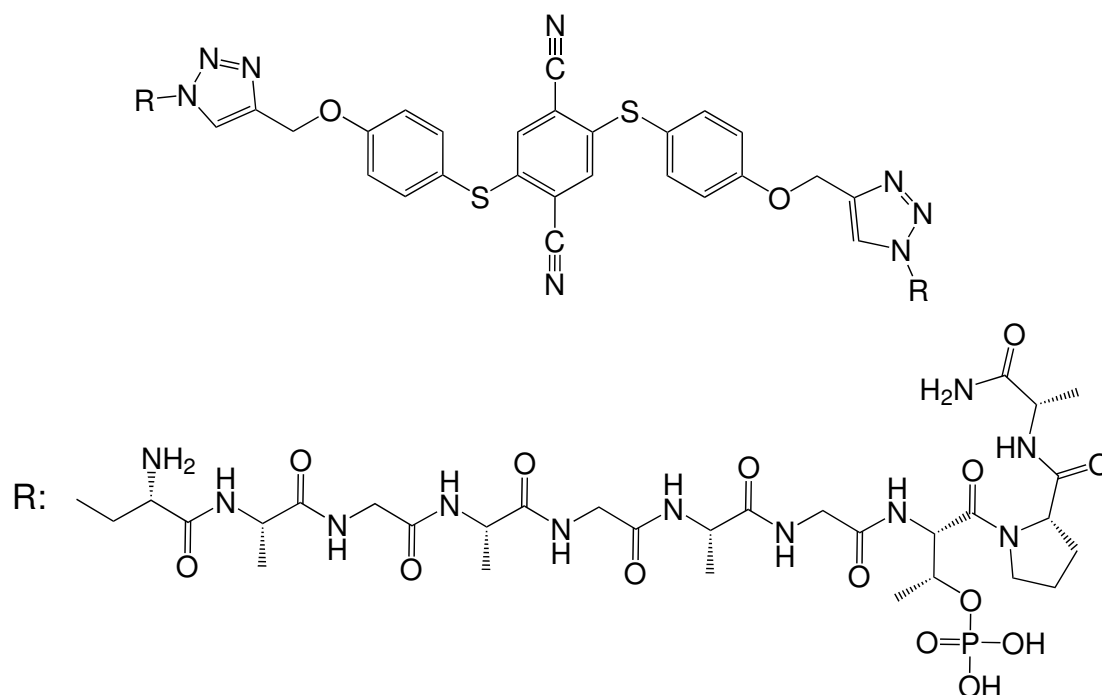
Fluorophore **F4** was synthesized with compounds **A1** and **P4** using CuAAC under oxygen-free conditions (table 6, reaction 2). Finally a total yield of 13.7 mg (7.0 mmol, 54.8%) could be isolated as a yellow solid.

$^1\text{H NMR}$ (700 MHz, 10% $\text{D}_2\text{O}/\text{H}_2\text{O}$): δ 8.89 (s, 2H), 8.51 (s, 2H), 8.42 (d, $J = 5.9$ Hz, 2H), 8.33 (t, $J = 6.0$ Hz, 2H), 8.19 (d, $J = 6.0$ Hz, 2H), 8.15 (d, $J = 5.1$ Hz, 2H), 8.09 (s, 2H), 7.56 (s, 2H *cis*), 7.52 (s, 2H), 7.29 (s, 4H), 7.05 (s, 2H), 7.02 (s, 2H), 6.91 (s, 4H), 4.52 (m, 2H), 4.39-4.32 (m, 6H), 4.27-4.23 (m, 2H), 4.13 (s, 2H), 3.92 (s, 8H), 3.82 (s, 2H), 3.70 (d, $J = 8.5$ Hz, 2H), 2.55 (s, 2H), 2.51 (s, 2H), 2.27-2.23 (m, 2H), 2.02-1.97 (m, 2H), 1.91-1.85 (m, 4H), 1.39-1.37 (m, 18H), 1.32-1.30 (m, 6H).

LC-MS (ESI): $t_R = 5.86$ min; $m/z = 975.79$ [$M + 2H$] $^{2+}$, 1950.23 [$M + H$] $^+$,
calculated for $\text{C}_{78}\text{H}_{106}\text{N}_{26}\text{O}_{26}\text{P}_2\text{S}_2$: 1949.93.

HR-MS:	m/z calculated	m/z measured	Δ [ppm]
[$M+2H$] $^{2+}$	975.3417	975.3380	3.79
[$M+2H$] $^{2+}$	975.8434	975.8378	5.74
[$M+2H$] $^{2+}$	976.3450	976.3360	9.22

Di-(L-Homoalanine-L-Alanine-Glycin-L-Alanine-Glycin-L-Alanine-Glycin-O-Phospho-L-Threonine-L-Proline-L-Alanine-Amide)-conjugated *para*-phenol-thioterephthalonitrile



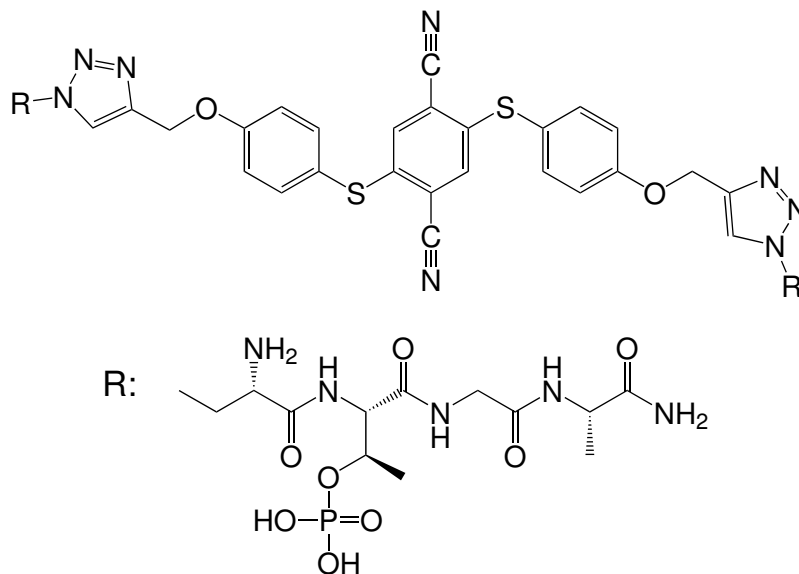
Fluorophore 5 (F5)

Fluorophore **F5** was synthesized with compounds **A1** and **P5** using CuAAC under oxygen-free conditions (table 6, reaction 2). Finally a total yield of 8.0 mg (3.6 mmol, 16.5%) could be isolated as a yellow solid.

$^1\text{H NMR}$ (700 MHz, DMSO-d_6): δ 8.86 (d, $J = 7.3$ Hz, 2H), 8.44 (s, 4H), 8.35 (t, $J = 5.5$ Hz, 2H), 8.24 (t, $J = 6.1$ Hz, 2H), 8.20-8.18 (m, 2H), 8.10-8.04 (m, 4H), 7.58 (d, $J = 9.0$ Hz, 4H), 7.43 (s, 2H), 7.24 (d, $J = 9.0$ Hz, 4H), 5.26 (s, 4H), 4.67-4.54 (m, 6H), 4.44-4.39 (m, 2H), 4.35-4.27 (m, 4H), 4.23-4.16 (m, 2H), 3.47 (s, 2H), 2.38-2.34 (m, 4H), 2.13-2.07 (m, 2H), 1.95-1.90 (m, 2H), 1.89-1.83 (m, 4H), 1.34-1.23 (m, 30H).

LC-MS (ESI): $t_R = 5.79$ min; $m/z = 736.29$ $[\text{M} + 3\text{H}]^{3+}$, 1103.81 $[\text{M} + 2\text{H}]^{2+}$,
calculated for $\text{C}_{88}\text{H}_{122}\text{N}_{30}\text{O}_{30}\text{P}_2\text{S}_2$: 2206.19.

Di-(L-Homoalanine-O-Phospho-L-Threonine-Glycine-L-Alanine-Amide)-conjugated *para*-phenolthioterephthalonitrile

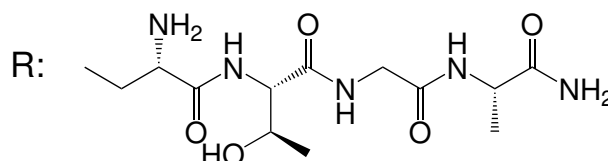
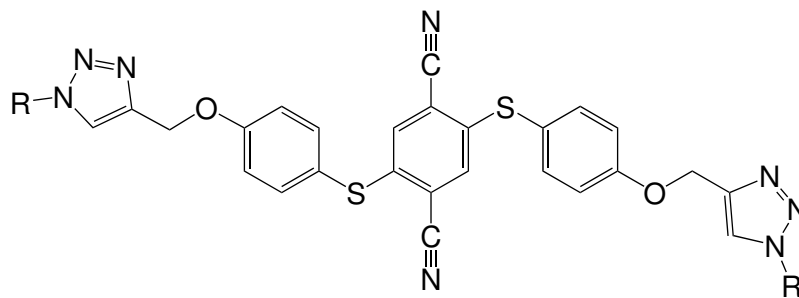


Fluorophore 6 (F6)

Fluorophore **F6** was synthesized with compounds **A1** and **P6** using CuAAC under oxygen-free conditions (table 6, reaction 2). Finally a total yield of 7.2 mg (5.3 mmol, 31.6%) could be isolated as a yellow solid.

^1H NMR (700 MHz, DMSO- d_6): δ 8.52 (s, 2H), 8.30 (s, 2H), 8.14 (d, J = 8.1 Hz, 2H), 7.54 (d, J = 9.0 Hz, 4H), 7.20 (d, J = 9.2 Hz, 4H), 7.02 (s, 2H), 5.23 (s, 6H), 4.56-4.50 (m, 6H), 4.44 (s, 2H), 4.21 (qui, J = 7.4 Hz, 2H), 4.07-4.03 (m, 2H), 3.80-3.78 (m, 2H), 2.37-2.30 (m, 6H), 1.28-1.26 (m, 14H), 1.22 (d, J = 7.3 Hz, 10H).

LC-MS (ESI): t_R = 5.91 min; m/z = 679.36 $[\text{M} + 2\text{H}]^{2+}$, 1357.01 $[\text{M} + \text{H}]^+$,
calculated for $\text{C}_{52}\text{H}_{66}\text{N}_{18}\text{O}_{18}\text{P}_2\text{S}_2$: 1357.28.

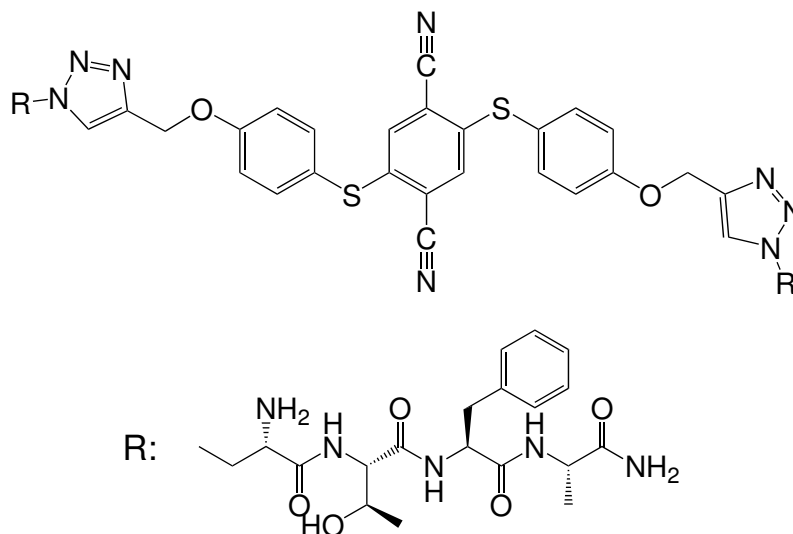
Di-(L-Homoalanine-L-Threonine-Glycine-L-Alanine-Amide)-conjugated *para*-phenolthioterephthalonitrile**Fluorophore 8 (F8)**

Fluorophore **F8** was synthesized with compounds **A1** and **P8** using CuAAC under oxygen-free conditions (table 6, reaction 2). Finally a total yield of 5.5 mg (4.6 mmol, 18.9%) could be isolated as a yellow solid.

^1H NMR (700 MHz, 10% $\text{D}_2\text{O}/\text{H}_2\text{O}$): δ 8.74 (s, 2H), 8.41 (s, 2H), 7.89 (s, 2H), 7.75 (s, 2H), 7.14 (s, 4H), 6.89 (s, 2H), 6.73 (s, 4H), 4.30 (s, 2H), 4.15 (s, 2H), 4.09 (t, $J=5.3$ Hz, 2H), 4.00 (t, $J=7.1$ Hz, 4H), 3.84-3.78 (m, 6H), 2.42 (s, 4H), 1.10 (s, 6H), 1.09 (s, 6H).

LC-MS (ESI): $t_R=6.10$ min; $m/z=599.47$ [$M+2\text{H}$] $^{2+}$, 1197.21 [$M+\text{H}$] $^+$,
calculated for $\text{C}_{52}\text{H}_{64}\text{N}_{18}\text{O}_{12}\text{S}_2$: 1197.32.

**Di-(L-Homoalanine-L-Threonine-L-Phenylalanine-L-Alanine-Amide)-conjugated
para-phenolthioterephthalonitrile**



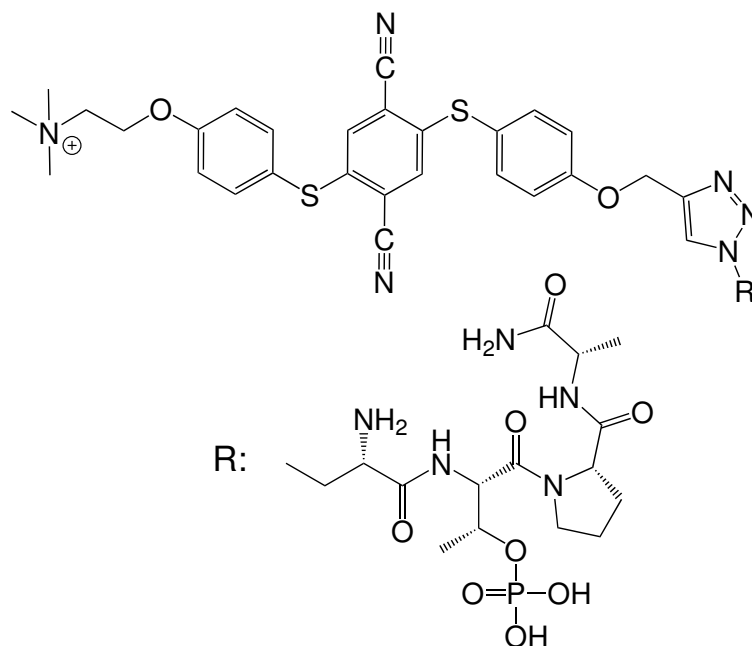
Fluorophore 9 (F9)

Fluorophore **F9** was synthesized with compounds **A1** and **P9** using CuAAC under oxygen-free conditions (table 6, reaction 2). Finally a total yield of 3.4 mg (2.5 mmol, 17.0%) could be isolated as a yellow solid.

$^1\text{H NMR}$ (700 MHz, DMSO-d_6): δ 8.45 (d, $J = 8.2$ Hz, 2H), 8.36 (d, $J = 7.5$ Hz, 2H), 8.22 (m, 2H, 2H *cis*), 8.13-8.07 (m, 4H), 7.57 (d, $J = 9.0$ Hz, 4H), 7.44 (s, 2H), 7.27-7.22 (m, 8H), 7.20-7.17 (m, 6H), 7.10-7.07 (m, 2H), 5.25 (s, 4H), 4.63-4.57 (m, 2H), 4.50-4.41 (m, 6H), 4.29-4.26 (m, 2H), 4.22-4.18 (qui, 2H), 4.04-4.00 (m, 2H), 2.84-2.78 (m, 2H), 2.27-2.16 (m, 6H), 1.29 (d, $J = 7.5$ Hz, 6H), 1.26 (s, 2H), 1.22 (d, $J = 7.3$ Hz, 2H), 1.05 (d, $J = 6.6$ Hz, 6H).

LC-MS (ESI): $t_R = 6.44$ min; $m/z = 689.61$ [$M + 2H$] $^{2+}$, 1377.33 [$M + H$] $^+$,
calculated for $\text{C}_{66}\text{H}_{76}\text{N}_{18}\text{O}_{12}\text{P}_2\text{S}_2$: 1377.57.

**L-Homoalanine-O-Phospho-L-Threonine-L-Proline-L-Alanine-Amide-conjugated
para-phenolthioterephthalonitrile**



Fluorophore 10 (F10)

Fluorophore **F10** was synthesized with compounds **A2** and **P1** using CuAAC under oxygen-free conditions (table 6, reaction 2). Finally a total yield of 9.6 mg (9.7 μmol , 49.7%) could be isolated as a yellow solid.

^1H NMR (700 MHz, 10% $\text{D}_2\text{O}/\text{H}_2\text{O}$): δ 8.97 (d, $J=6.4$ Hz, 2H), 8.71 (d, $J= 8.9$ Hz, 2H *cis*), 8.59 (d, $J 5.4$ Hz, 2H *cis*), 8.39 (d, $J= 6.1$ Hz, 2H), 8.13 (s, 1H *cis*), 8.12 (s, 1H), 7.51 (s, 2H), 7.49 (s, 2H *cis*), 7.45 (d, $J= 8.9$ Hz, 2H), 7.43 (d, $J= 8.9$ Hz, 2H), 7.28 (s, 1H), 7.26 (s, 1H), 7.07 (d, $J= 9.4$ Hz, 2H), 7.06 (d, $J= 10.7$ Hz, 2H), 6.96 (s, 1H), 6.90 (s, 1H *cis*), 5.20 (s, 1H), 5.18 (s, 1H), 4.57 (d, $J= 8.4$ Hz, 1H), 4.53-4.50 (m, 3H), 4.40-4.38 (m, 1H; 1H *cis*), 4.24 (m, 1H), 4.19-4.16 (m, 2H; 1H *cis*), 3.86-3.82 (m, 3H), 3.77-3.74 (m, 1H), 3.52-3.47 (m, 2H *cis*), 3.25 (s, 9H), 2.53 (dd, $J= 7.0$ Hz, 2H), 2.48-2.43 (m, 1H *cis*), 2.28-2.24 (m, 1H), 2.14-2.10 (m, 1H *cis*), 2.04-2.00 (m, 1H), 1.95-1.86 (m, 2H), 1.80-1.76 (m, 1H *cis*), 1.44 (d, $J= 7.5$ Hz, 3H *cis*), 1.37 (d, $J= 6.2$ Hz, 3H), 1.34 (d, $J= 7.3$ Hz, 3H), 1.28 (d, $J= 6.0$ Hz, 3H *cis*).

LC-MS (ESI): $t_R= 6.01$ min; $m/z= 496.76$ $[\text{M} + \text{H}]^{2+}$, 992.11 $[\text{M}]^+$,
calculated for $\text{C}_{44}\text{H}_{55}\text{N}_{11}\text{O}_{10}\text{PS}_2^+$: 993.08.

HR-MS:	<i>m/z</i> calculated	<i>m/z</i> measured	Δ [ppm]
[M] ⁺	992.3307	992.3278	2.92
[M] ⁺	993.3340	993.3321	1.91
[M] ⁺	994.3374	994.3335	3.92
[M+H] ²⁺	496.6690	496.6676	2.82
[M+H] ²⁺	497.1707	497.1689	3.62
[M+H] ²⁺	497.6723	497.6702	4.22

4.4.5 High-performance liquid chromatography (HPLC)

The final purification step of peptides and peptide modified fluorophores was a preparative rp-HPLC (column: Luna® 5 μ m C18 (2) 100x21.20 mm). A linear gradient of ACN in water with 0.1% TFA was used at a flow rate of 20 mL/min. Detection was carried out at 210 nm and 254 nm. Peaks were collected manually.

4.4.6 Ion exchange of peptide-coupled fluorophores

The fluorophores were purified by HPLC using TFA as an additive for better separation. Due to its toxicity TFA is not compatible with all proteins or possible cell experiments and needs to be removed. Therefore the lyophilized final fluorophores were dissolved in 100 mM HCl and incubated at RT for 1 min. Afterwards the fluorophores were lyophilized again. This process was repeated 3 times. To remove excess HCl and get a desirable consistency this process was repeated 2 more times with H₂O. The complete exchange of TFA by chloride was checked with ¹⁹F-NMR spectroscopy.

4.4.7 Liquid chromatography linked mass spectrometry (LC-MS)

Analysis of intermediates and final fluorophores was performed by a LC-MS system from Thermo Fisher Scientific. The system consists of the UV detector Thermo Scientific AccelaTM with the chromatographic column Eclipse XDB-C18 5 μ m from Agilent and the mass spectrometer Thermo Scientific LCQ FleetTM ESI-MS. Here a linear gradient of ACN and H₂O with 0.1% formic acid (FA) was used at a flow rate of 1 mL/min.

Table 7: Linear gradient used for LC-MS

Volume	Solvent
0-1 mL	10% ACN + 0.1% FA
1-10 mL	10% ACN + 0.1% FA → 90% ACN + 0.1% FA
10-12 mL	90% ACN + 0.1% FA

4.4.8 High resolution mass spectrometry (HR-MS)

For high resolution mass spectrometry an in-house standard method was used and performed by David Podlesainski (group of Prof. M. Kaiser). The sample was prepared in a mixture of ACN and H₂O (1:1) with 0.1% FA. An ExactiveTM Plus Orbitrap mass spectrometer in combination with a TriVersa NanoMate and an ESI Chip®5.5 μM was used. Measurement was performed in positive mode and parameters are listed in table 8.

Table 8: Parameter for HR-MS

Parameter	Value
Resolution	140000
Spray voltage	1500 V
Capillary temp.	250 °C
S-lens RF level	50
AGC target	3e6

4.5 UV-VIS spectroscopy

The solubility in water and the tolerance towards salts of newly designed and synthesized fluorophores is a critical step for the usage in *in-vivo* and *in-vitro* experiments. To show the solubility in aqueous solution, the fluorophores were dissolved in pure water up to a concentration of 20 mM and then diluted to 10 μM. These experiments were repeated in fluorescence buffer and PBS buffer. Here the turbidity at RT at λ₆₀₀ was measured and plotted against the fluorophore concentration.

In addition to the solubility test at 600 nm the absorption of soluble fluorophores at λ₄₀₀ was recorded to calculate an extinction coefficient ε₄₀₀ and get a method for concentration determination besides weighing in and dissolving.

For this, the fluorophores were dissolved in H₂O to a concentration of 1 mM and the absorption measured at 400 nm. The following measurement points (800 μM, 600 μM ... 10 μM) were generated from a serial dilution. In total, the experiments were carried out in triplicate with separate weights.

4.6 Fluorescence spectroscopy

Fluorescence spectroscopy is a sensitive method for qualitative and quantitative analysis. With the aggregation-induced emission properties of the new fluorophores, fluorescence spectroscopy provides a direct readout for binding studies without any modifications of proteins or peptides.

Here the fluorophores were tested for autofluorescence, the maximum change in fluorescence induced by protein binding and the dissociation constant (K_D). The fluorophores were then compared to each other, and the differences caused by linker lengths were analyzed.

4.6.1 Sample preparation

To avoid solubility effects during fluorescence spectroscopy, the samples were dissolved and diluted to the final working concentration 24 h before measurement. The fluorophores were always dissolved in H₂O to a concentration of 1 mM. For titration experiments the fluorophores were then diluted in fluorescence buffer.

4.6.2 Determination of autofluorescence

To determine the working concentration for titration experiments, the fluorophores were tested for autofluorescence in H₂O, fluorescence buffer and PBS buffer at various concentrations (10 μ M to 1 mM). The fluorescence intensity was plotted against the fluorophore concentration afterwards.

4.6.3 Binding study of fluorophores with *hPin1* and *hPin1-WW*

To characterize the binding of *hPin1* and *hPin1-WW* to the peptide-coupled fluorophores, the proteins were titrated to the fluorophores and the change in fluorescence signal was detected with $\lambda_{ex} = 399$ nm and $\lambda_{em} = 489$ nm. The measurements were performed with 60 μ L fluorophore at various concentrations and therefore the PMT voltage (450 V - 700 V) had to be adjusted (table 9). Temperature was set to 25 °C, emission and excitation slits to 5 nm and 10 measurements were averaged for each titration point. To avoid dilution effects, the fluorophore was added to the protein stock in fluorescence buffer (20 mM HEPES pH 7.0). Fluorescence titrations were performed at least in triple determination.

Table 9: Fluorophore concentrations used for fluorescence binding studies

Parameter	Concentration with corresponding PMT					
Concentration	10 μ M	25 μ M	50 μ M	100 μ M	150 μ M	200 μ M
PMT	750 V	650 V	600 V	550 V	500 V	450 V

Finally the fluorescence signal was plotted against the protein concentration and the binding curve was fitted with equation 1. Here the dissociation constant K_D as well as the stoichiometric factor n were calculated. For calculation, the autofluorescence was

subtracted from each titration, the change in signal averaged and the fit forced through the origin (0/0).

Equation 1: Calculation of binding constant K_D and stoichiometry factor n

$$Y = A_0 + A_{max} \cdot \frac{\left((F + n \cdot K_D) - \sqrt{(F + n \cdot x + K_D)^2 - (4 \cdot F \cdot n \cdot x)} \right)}{2 \cdot F} \quad (1)$$

In addition to the dissociation constant K_D and stoichiometry factor n , the equation contains the fluorophore concentration F , the fluorescence offset A_0 and the maximum fluorescence signal A_{max} .

4.7 NMR Spectroscopy

4.7.1 Sample preparation

For HSQC titration experiments, the buffer of the *hPin1*-WW domain (expressed and purified as ^{15}N labeled protein) was changed to NMR buffer. Then a sample of 250 μL with a concentration of 400 μM was used in a 3 mM NMR tube. Additionally the fluorophore was dissolved in H_2O to 2 mM.

For structural analysis by NMR spectroscopy, the fluorophores F1 and F10 were dissolved in 10% D_2O /90% H_2O . For data acquisition a 200 μL sample with a concentration of 1 mM was used in a 3 mm NMR tube. Due to the reuse of fluorophores for fluorescence spectroscopy afterwards, the addition of DSS was avoided.

For calculation of the NMR complex structure of *hPin1*-WW with fluorophore F10, the protein was expressed and purified double labeled (sec.4.3.1, sec.4.2.2). After separate buffer exchange of the protein and fluorophore into NMR buffer, they were dried by lyophilization and dissolved afterwards in 100% D_2O . Then the protein was mixed with the fluorophore to a final sample of 1 mM $^{13}\text{C},^{15}\text{N}$ -*hPin1*-WW domain with 1 mM fluorophore F10 in NMR buffer and 100% D_2O . For data acquisition a 5 mm Shigemi NMR tube with a sample volume of 350 μL was used.

4.7.2 Data acquisition and processing

The NMR measurements were acquired with a Bruker Ultrashield 700-NMR (Bruker BioSpin, Fällanden) at a proton frequency of 700.22 MHz. The NMR spectrometer (700 MHz) was equipped with a triple resonance cryo probe (700 MHz). The temperature was set to 25 °C and controlled by a BVT3000 control unit (Bruker BioSpin, Fällanden). Pulse programs were mainly taken from the Bruker standard library or were provided by Dr. Kristian Schweimer (University of Bayreuth). Set up of the acquisition parameters as well as data processing were performed with the program TopSpin 3.5

(Bruker BioSpin, Fällanden). Detailed settings are described in the corresponding sections or in the appendix. 1D data were processed with the command *efp*, while 2D data were processed with *xfb* and 3D data with *tf3 n*, *tf2 n*, *tf1 n*. After processing, the automatic polynomial baseline correction for 2D spectra was executed with *abs1* and the automatic water correction performed with *abs2.water*. For 3D spectra the correction was done accordingly with *tabs3*, *tabs2* and *tabs1*.

4.7.3 TFA detection by ^{19}F NMR spectroscopy

To check the final fluorophores for complete ion exchange, methods like ion chromatography [62] or ^{19}F NMR spectroscopy [213] can be used. In this work the fluorophores were tested for remaining TFA by recording a ^{19}F -NMR spectrum. The samples were analyzed for a TFA signal at -79.83 ppm. A TFA dilution series in D_2O was taken as standard and positive control. The experiments were carried out by Dr. Jürgen Linders (group of Prof. C. Mayer) on a 500 MHz Bruker Avance Neo II equipped with a DiffBBI probe head.

4.7.4 ^{15}N -HSQC binding experiments with the *hPin1-WW* domain

To show the specific binding of peptide-conjugated fluorophores (fluorophores 1-4, 10) to the binding pocket of *hPin1-WW*, ^1H , ^{15}N -HSQC titration experiments were performed. For this the buffer of purified ^{15}N -labeled protein was changed to NMR buffer, the protein diluted to 400 μM and a total volume of 250 μL was used for a single experiment. The fluorophores were dissolved in H_2O to 2 mM. After each titration step a ^1H , ^{15}N -HSQC spectrum was recorded. After binding the fluorophore, the chemical environment for the protein had changed. This results in a change of chemical shifts of the amino acids involved in the binding process. These shifts were measured and the total shift perturbation for both dimensions calculated using equation 2 [10]. Due to a larger shift range of ^{15}N compared to ^1H an additional weighting factor of 0.154 was used [10].

Equation 2: Total chemical shift perturbation calculation

$$\Delta\delta_{total} = \sqrt{(\Delta\delta_N \cdot 0.154)^2 + (\Delta\delta_H)^2} \quad (2)$$

The total shifts of each amino acid were plotted against the fluorophore concentration and finally fitted with equation 1. Analogous to the fluorescence analysis, the dissociation constant K_D and the stoichiometric factor n were calculated.

4.8 NMR structure calculation

4.8.1 Ligand parametrization for CYANA

CYANA is a script-based program for automated structure calculation of biological macromolecules. It uses automated nuclear Overhauser effect spectroscopy (NOESY) assignments with a fast torsion angle dynamics algorithm. For normal structure calculation a standard residue library file is used. To calculate the 3D NMR structure of fluorophore F10 additional library files for the amidated C-terminus, the phosphorylated threonine and the AIE-core had to be created. Thereby the AIE-core was defined as side chain addition to the homoalanine.

At the beginning the chemical structures were drawn with the program ChemDraw and saved as molecular data file (.mol). Afterwards the file was translated into a simplified molecular input entry specification (SMILES) code (.smi), which then was converted into a PDB file with 3D coordinates. The final cyana library file (.lib) was then created manually by defining angles, bonds, using the 3D coordinates and adding pseudo atoms. The new atom numbering is illustrated in figures 25 A.

4.8.2 Structure calculation of fluorophore F10 with CYANA

Structure calculation of the isolated fluorophore F10 was carried out by the program CYANA. For this, distance information from the $^1\text{H}, ^1\text{H}$ -NOESY spectrum was used. The chemical shifts were assigned manually and saved as a *shifts.prot* file. The assignment for the coupled amino acids was done using a 2D-COSY and 2D-TOCSY experiment, while the assignment of the AIE-core ring system required additional data from a 2D-NOESY spectrum. Likewise, cross-peaks were picked and assigned manually and exported as *NOESY.peaks* using the program SPARKY. Finally the NOESY peaklist *NOESY.peaks* was used together with the input files *shifts.prot* and *init.cya* for structure calculation. The *init.cya* file includes commands to read the cyana standard library, the manually defined libraries and ligand sequence.

Table 10: Parameters for F10 structure calculation with CYANA

Parameter	
Number of shifts (<i>shifts.prot</i>)	31
Number of peaks (<i>NOESY.peaks</i>)	195
Shift tolerance ($^1\text{H}, ^1\text{H}'$)	0.03, 0.03
Number of torsion angle dynamics steps	10000
randomseed	434726

In total 7 cycles with 100 structures were calculated, sorted by the target function (equation 3) and the 30 best structures summarized, averaged and displayed in the output files (.upl, .pdb, .noa and .ovw).

Equation 3: CYANA target function. The function compares the calculated structures with experimental data and is defined as zero if all experimental distance restraints and torsion angle restraints are fulfilled. Included are the upper and lower bounds $b_{\alpha\beta}$, for the distances $d_{\alpha\beta}$ between two atoms α and β and restraints on individual torsion angles θ_i with the allowed intervals $[\theta_i^{min}, \theta_i^{max}]$. I_U , I_l and I_V are considered as atom pairs (α, β) with violated upper, lower or van der Waals distance bounds. I_a is the set of restrained torsion angles. w_U , w_l , w_V and w_a are overall weighting factors for the corresponding restraint and $w_{\alpha\beta}^c$ and w_i individual weighing factors. The term $\Gamma_i = \pi - (\theta_i^{max} - \theta_i^{min})/2$ marks the half-width of the forbidden torsion angle range. Δ_i displays the size of torsion angle restraint violation [84, 86].

$$V = \sum_{c=U,l,v} w_c \sum_{(\alpha,\beta) \in I_c} w_{\alpha\beta}^c (d_{\alpha\beta} - b_{\alpha\beta})^2 + w_a \sum_{i \in I_a} w_i \left[1 - \frac{1}{2} \left(\frac{\Delta_i}{\Gamma_i} \right)^2 \right] \Delta_i^2 \quad (3)$$

4.8.3 Dihedral angle prediction via TALOS+

TALOS+ is a program for the prediction of protein backbone torsion angles ϕ and ψ . Therefore information of chemical shift assignments from $^1\text{H}^N$, $^1\text{H}^\alpha$, $^{13}\text{C}^\alpha$, $^{13}\text{C}^\beta$, $^{13}\text{C}^O$ and ^{15}N for any residue is combined with the protein sequence. For this the proteins are divided into tripeptides, which are then compared to a data bank of about 200 high resolution crystal protein structures. Additionally, TALOS+ includes an artificial neural network (ANN), analyzing chemical shifts and protein sequence to predict the secondary structure for a given residue. In the prediction process, each residue receives an average value of the 10 most suitable predictions, which were then taken and rated as good, ambiguous or bad. For structure calculation only good angle predictions are selected [42, 242].

For backbone torsion angle prediction of the *hPin1*-WW domain in complex with the fluorophore F10, the protein sequence in combination with the chemical shifts were exported as a *Talos.tab* file by the program CARA. In this work the shifts were imported from an apo solution structure (BMRB 19258) [169]. Finally, the TALOS+ file was converted by the shell script *talos2dyana.com* into a CYANA suitable format and the output file *angle.aco* was taken as angle restraint file for the structure calculation.

4.8.4 Calculation of the complex structure with UNIO

The structure of *hPin1*-WW in complex with the fluorophore F10 was calculated in cooperation with Dr. Torsten Herrmann. The initial structure, the final structure as well as adjustments and changes in the program UNIO for non-natural amino acids

were performed by Dr. Torsten Herrmann. The NMR spectra acquisition, peak picking (*.peaks* files), prediction of angle restrictions (*angle.aco*), adjustments and optimization of distance constraint files (*.upl*) were performed by myself.

In total 5 NOESY spectra were used for the calculation. The normal aromatic and aliphatic 3D ^{13}C -NOESY experiments were used as complete spectra with automatic peak picking and assignment by UNIO. The aliphatic and aromatic filtered-edited ^{13}C 3D-NOESY spectra (3D-xNOESY) [24, 138, 322] and the double filtered 2D-NOESY spectrum (2D-x2NOESY) [284] were finally used as optimized upper limit files (*.upl*). For this the cross-peaks were assigned manually and the upper distance limits were adapted during the optimization process.

To keep the core structure of a three-stranded antiparallel β -sheet, additional limits for the corresponding hydrogen bonds were set. The lower limits *hbonds.lol* and upper limits *hbonds.upl* were manually defined and added to the calculation. Additionally, the predicted dihedral angle restraints *angle.aco* from TALOS+, the molecule sequence *molecule.seq* file and the non-natural CYANA library files were added. To calculate a complex structure, a single *molecule.seq* file is necessary. For this the ligand is connected to the protein by a defined linker. In total 40 structures were calculated in 7 cycles and the best 20 were summarized and displayed in the statistics.

Table 11: Parameters for complex structure calculation with UNIO

Parameter	
Number of shifts (<i>hPin1-WW.prot</i>)	404
Number of peaks	558 (3D aliphatic ^{13}C -NOESY) 140 (3D aromatic ^{13}C -NOESY)
Number of distance limits (<i>.upl</i>)	20 (2D double filtered-NOESY) 24 (3D filtered-edited aliphatic ^{13}C -NOESY) 11 (3D filtered-edited aromatic ^{13}C -NOESY)
<i>angle.aco</i>	50
Number of H-bonds (<i>.upl</i> and <i>.lol</i>)	20
Number of torsion angle	8000
dynamics steps	
seed	4371

5 Results

In recent years the AIE effect has been studied for a wide range of fluorophores including the new thioterephthalonitriles (TPNs). The more flexible and tunable new TPN-AIEgens are composed of aromatic thioethers and were successfully tested with small biomolecules such as spermine [97]. In this work the TPN derivatives are specifically modified to recognize the *hPin1*-WW domain and prove the principle of protein binding for TPNs, which then can be used to characterize protein-ligand binding.

5.1 Expression and purification of *hPin1* and *hPin1*-WW

To characterize the specific binding between proteins and the peptide-coupled fluorophores, the human peptidyl-prolyl *cis/trans* isomerase 1 (*hPin1*) as well as the isolated *hPin1*-WW domain were expressed (section 4.2.2) and purified (section 4.3.1) as GST tagged fusion proteins. In addition to the unlabeled proteins, ^{15}N - and $^{15}\text{N},^{13}\text{C}$ labeled *hPin1*-WW were expressed and purified for NMR experiments (section 4.7).

The chromatograms and SDS gels of the GSH affinity chromatography (figure 13 A,C) show a typical purification step of a GST tagged protein and are similar for both proteins. The elution profiles of both show a flow through peak (FT) followed by a high salt wash peak (HS) and a GSH induced elution peak of GST fusion protein (E). The fractions containing GST fusion protein were collected, pooled and concentrated. Afterwards the GST tag was removed by PreScission protease. In a subsequent size exclusion chromatography (figure 13 B,D) the GST tag as well as the PreScission protease (G) were separated from the target proteins (P). Finally, the expression and purification of both proteins was successful and yielded high amounts of pure protein.

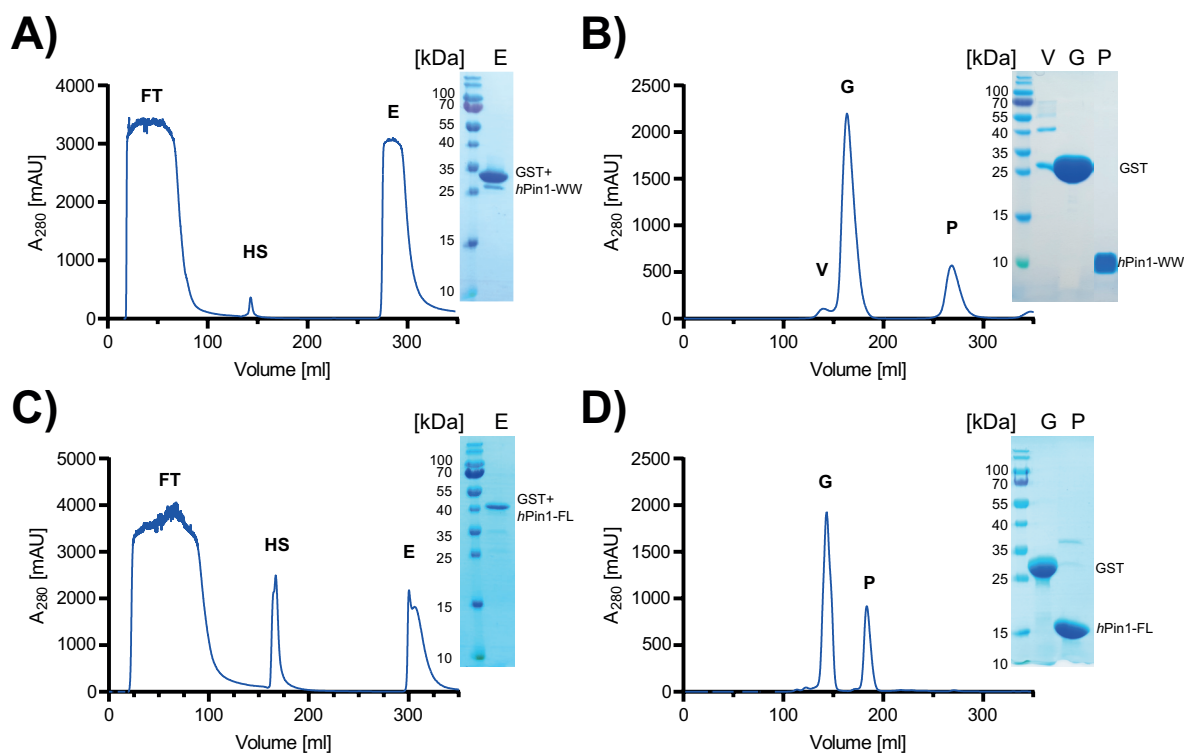


Figure 13: Protein purification of *hPin1-WW* and *hPin1*. Shown are the chromatograms and SDS gels of the GSH affinity chromatography of *hPin1-WW* (A) and *hPin1* (C). The flow through (FT) contains *E. coli* proteins which did not bind to the GSH column. After a washing step unspecific bound proteins were eluted (HS) by using high salt buffer which reduces electrostatic interactions between proteins. As shown in the SDS gel the elution peak (E) contains GST and GST fusion protein. The chromatograms and SDS gels of the size exclusion chromatography of *hPin1-WW* (B) and *hPin1* (D) show the separation of unknown proteins in the void volume (V), cleaved GST and PreScission protease (G) from the target proteins *hPin1-WW* and *hPin1* (P).

5.2 Chemical synthesis

5.2.1 Peptide synthesis

To specifically modify the AIE-core (figure 11) for selective protein recognition, peptides containing an N-terminal azidohomoalanine were synthesized by solid phase peptide synthesis (SPPS) (figure 14). The SPPS consists of two phases, the solid phase of an insoluble polymer with a linker molecule and a liquid phase for the addition and removal of reagents and reactants. The synthesis is carried out from the C-terminus to the N-terminus and the first step is the Fmoc deprotection of the linker molecule. In the following step, the carboxylic acid of the next amino acid is deprotected and can be coupled to the free amino group of the linker. The peptide coupling is performed again with a different coupling reagent. Then the amino protection group is cleaved off and the next amino acid can be coupled. The reaction cycle is repeated until the final peptide sequence is obtained. Finally, the peptide is cleaved from the resin and all protecting groups are removed.

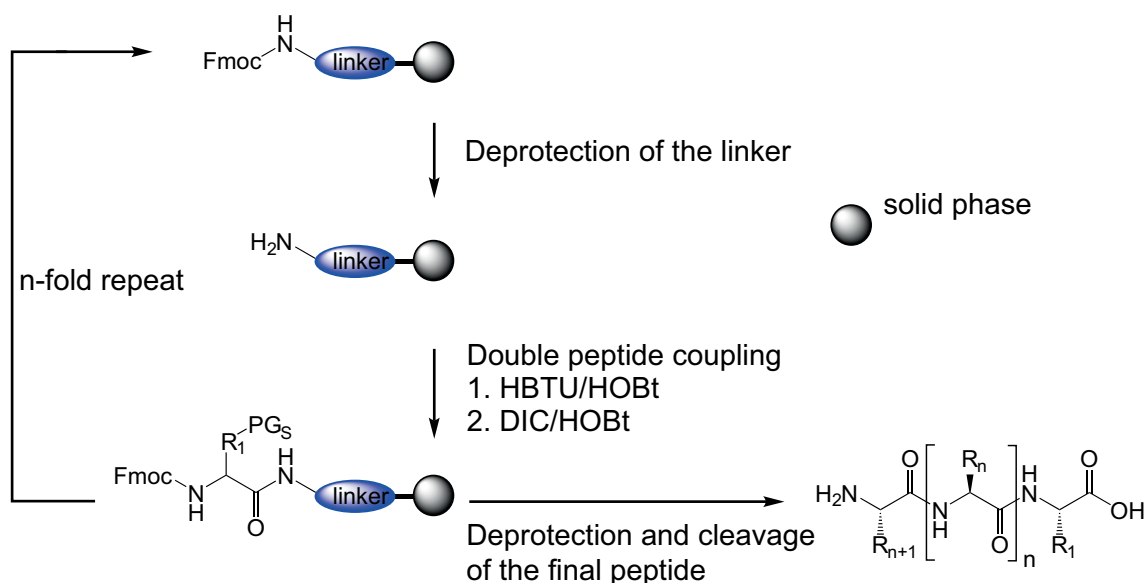


Figure 14: Schematic representation of the SPPS. PG_S: protection group of the side chain. Adapted from ref [239].

The included azido-group could be used after the synthesis to couple the peptide onto the AIE-molecules A1 and A2 (section 4.4, figure 11) using CuAAC. The protein specificity against the *hPin1*-WW domain was achieved by including the pThr-Pro motif into the peptide sequence.

The analysis of the correct peptide synthesis was performed by LC-MS and ¹H-NMR spectra with assignment of resonances in the corresponding spectra. Due to the proline in most of the peptides, additional peaks could be observed in the ¹H-NMR characterization. These peaks represent signals of peptides with a peptidyl-prolyl bond in *cis* conformation which made the peak integration inaccurate. For a more accurate ¹H-NMR assignment, experiments like a ¹H,¹H-COSY, a ¹H,¹H-TOCSY or a ¹H,¹H-NOESY are needed and were performed exclusively with the final fluorophores. Peptide synthesis was efficient (87% to 99%) for almost all peptides, except P9 (35%). Purification by diethyl ether precipitation followed by rp-HPLC was sufficient for further synthesis. In addition to the set of peptides for protein recognition (P1-P5), another set of peptides with a slightly modified binding motif (peptides 0, 6-9) was synthesized. Here, the Xaa-pThr-Pro-Xaa motif was eliminated by replacing the phospho-threonine with a normal threonine (peptides 7+8+9) and/or proline with another amino acid. Here, the approach was to prevent specific binding by removing the proline in exchange for a non-binding glycine (peptide 6+8) or a larger amino acid like phenylalanine (peptide 9) and arginine (peptide 0) which then could cause steric hindrance. All peptides used in this work, with their respective sequences and yields, are summarized below (table 12).

Table 12: Systematic representation of all synthesized peptides

Peptide	Sequence (N → C)	Yield
P0	N ₃ —●—●—●—●—NH ₂	98%
P1	N ₃ —●—●—●—●—NH ₂	94%
P2	N ₃ —●—●—●—●—●—NH ₂	98%
P3	N ₃ —●—●—●—●—●—●—NH ₂	93%
P4	N ₃ —●—●—●—●—●—●—●—●—NH ₂	88%
P5	N ₃ —●—●—●—●—●—●—●—●—●—NH ₂	87%
P6	N ₃ —●—●—●—●—NH ₂	96%
P7	N ₃ —●—●—●—●—NH ₂	99%
P8	N ₃ —●—●—●—●—NH ₂	94%
P9	N ₃ —●—●—●—●—NH ₂	35%

● Homoalanine ● Ala ● pThr ● Pro ● Gly ● Arg ● Thr ● Phe

5.2.2 Copper(I)-catalyzed alkyne-azide cycloaddition (CuAAC)

To add the azide-bearing peptides to the AIE-core molecules (A1 and A2) obtained from the group of J. Voskuhl, the CuAAC was used. The reaction is shown as an example for fluorophore F1 in figure 15.

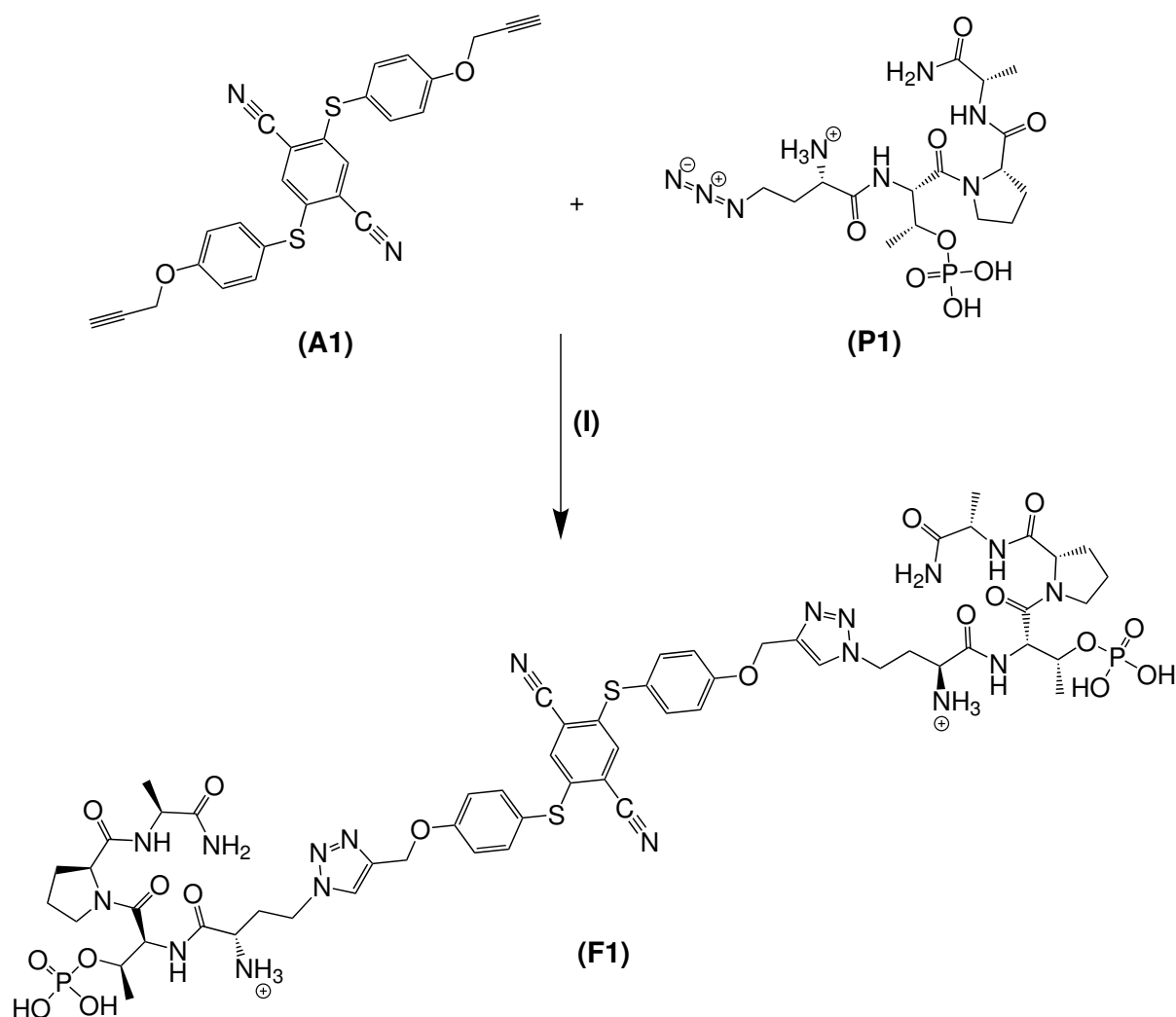


Figure 15: Illustration of the CuAAC reaction for fluorophore F1. (I): 0.6 eq CuSO_4 , 1.3 eq. Sodium ascorbate, THF/ H_2O (2:1), 5 days.

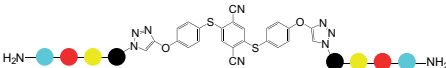
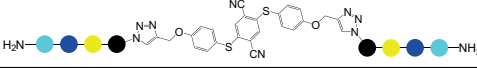
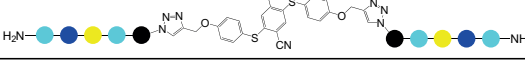
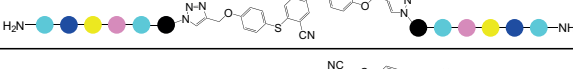
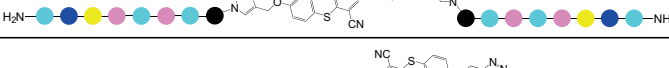
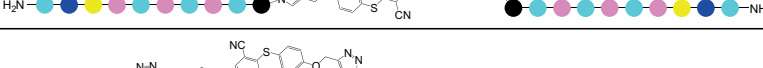
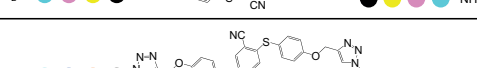
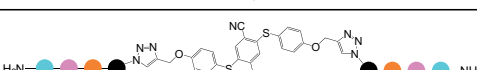
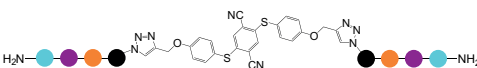
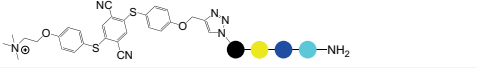

Starting the optimization with a solvent mix of THF/ H_2O and an AIE-core concentration of 2 mg/mL, a yield of 5-10% was achieved. To increase the reaction efficiency, solvent, reaction volume and copper catalyst were varied (table 13).


After the CuAAC, the fluorophores were purified by filtration and standard rp-HPLC (section 4.4.5). The optimization results showed a significant increase in yield by adjusting the reaction volume from 5 mL to 9 mL due to the concomitant increase of reactant solubility. Based on the sufficient yield of ~50%, all following syntheses were carried out according to reaction 2 and fluorophores are summarized in table 14.

Table 13: Optimization of the CuAAC for fluorophore F1

	Parameter	Yield
Reaction 1	THF/H ₂ O (5 mL) CuSO ₄	5-10%
Reaction 2	THF/H ₂ O (9 mL) CuSO ₄	50%
Reaction 3	DMF (9 mL) CuSO ₄	28%
Reaction 4	DMF (9 mL) CuI	46%

Table 14: Systematic representation of all synthesized fluorophores

Fluorophore	Sequence (N → C)	Yield
F0		17.7%
F1		49.6%
F2		32.4%
F3		55.4%
F4		54.8%
F5		16.5%
F6		31.6%
F7		50.0%
F8		18.9%
F9		17.0%
F10		49.7%



5.3 Characterization of peptide-conjugated fluorophores

5.3.1 UV-VIS spectroscopy - Solubility and extinction coefficients of peptide-coupled fluorophores

Solubility of peptide-coupled fluorophores

The solubility of small molecules and tolerance to salts are crucial for the experimental use in biological systems. Due to the hydrophobicity of the AIE-core and the intolerance of the disulfonate-conjugated fluorophore (referred to DSA) to ionic buffers, the new AIE fluorophores were tested for their solubility properties (table 15). The already described DSA [97] showed a good solubility in H₂O and buffer with low ionic strength, but was completely insoluble at isotonic conditions (PBS buffer).

Table 15: Solubility of peptide-coupled fluorophores in H₂O and buffers

Fluorophore	H ₂ O (pH 3-4)	Fluorescence buffer (pH 7)	PBS buffer (pH 7)
DSA	≈ 2 mM	≈ 2 mM	not soluble
F0	not soluble	not soluble	not soluble
F1	> 20 mM	> 20 mM	> 20 mM
F2	≈ 5 mM	> 20 mM	> 20 mM
F3	≈ 5 mM	≈ 10 mM	≈ 10 mM
F4	> 20 mM	≈ 20 mM	≈ 5 mM
F5	not soluble	not soluble	not soluble
F6	not soluble	not soluble	not soluble
F7	> 20 mM	> 20 mM	> 20 mM
F8	> 20 mM	> 20 mM	> 20 mM
F9	not soluble	not soluble	not soluble
F10	> 20 mM	≈ 10 mM	≈ 3 mM

The new fluorophores with specific binding motifs (F1-4, F10) showed an increased solubility and salt tolerance compared to the previous fluorophores such as DSA. Small differences in solubility were just detectable by turbidity measurements at 600 nm. With the exception of F10, where solubility decreases with increasing ionic strength, no tendency could be observed in the concentration range up to 20 mM. The fluorophores with interrupted binding motifs F0, F6 and F9 were neither soluble in H₂O nor in buffer. Here the exchange of proline to either an arginine (F0), a glycine (F6) or a phenylalanine (F9) led to the aggregation in aqueous solution. The solubility was tested down to a concentration of 25 μM and aggregation could be seen by the naked eye. In comparison, fluorophores F7 and F8 were soluble up to at least 20 mM. Interestingly F8 differs

from F6 just by the missing phosphoryl group, which in general is a positive factor for solubility of peptides, proteins or other molecules. Nevertheless both non-binding fluorophores were further tested towards their autofluorescence and ability to act as a soluble addition for a one-site binding fluorophore.

Extinction coefficients of peptide-coupled fluorophores

The concentrations of reactants in a biological binding assay are also of essential importance for its correct analysis. Protein concentration can either be determined by a Bradford protein assay or with Lambert Beer's law (section 4.3.2). Nowadays, the extinction coefficient of peptides and proteins can be calculated with online tools, but not for small molecules such as the aromatic core of the synthesized fluorophores. To simplify the concentration determination for upcoming experiments, the extinction coefficients of all fluorophores were determined experimentally at λ_{400} (section 4.5). The results of the serial dilution showed just minor differences in the extinction coefficients between the fluorophores.

Table 16: Extinction coefficients of peptide-coupled fluorophores

Fluorophore	ϵ_{400} [$M^{-1}cm^{-1}$]
F1	3411 ± 21
F2	3167 ± 26
F3	3779 ± 28
F4	3472 ± 21
F7	3384 ± 12
F8	3248 ± 36
F10	3469 ± 27

5.3.2 Fluorescence properties of peptide-coupled fluorophores

The effect of aggregation-induced emission can be described as a turn-on signal and was shown for DSA upon spermine binding [97]. In contrast, the fluorophores synthesized in this work showed autofluorescence in aqueous solutions without a binding partner. For the specific recognition of the *hPin1*-WW and the quantitative analysis of the binding, soluble fluorophores with minimal autofluorescence are needed to obtain a maximum fluorescence increase upon protein binding. To get the best possible conditions for upcoming binding experiments the fluorophores were tested for differences in their fluorescence properties such as autofluorescence, excitation and emission wavelengths.

The excitation and emission spectra were identical for all new peptide-coupled fluorophores and were also similar to DSA. The excitation maximum was red-shifted by 14 nm compared to DSA and displayed a wide plateau around 393-402 nm with a maximum at 399 nm. The emission spectra, however, exhibited the same maximum at 489 nm with an additional secondary maximum at 530 nm (figure 16) [97].

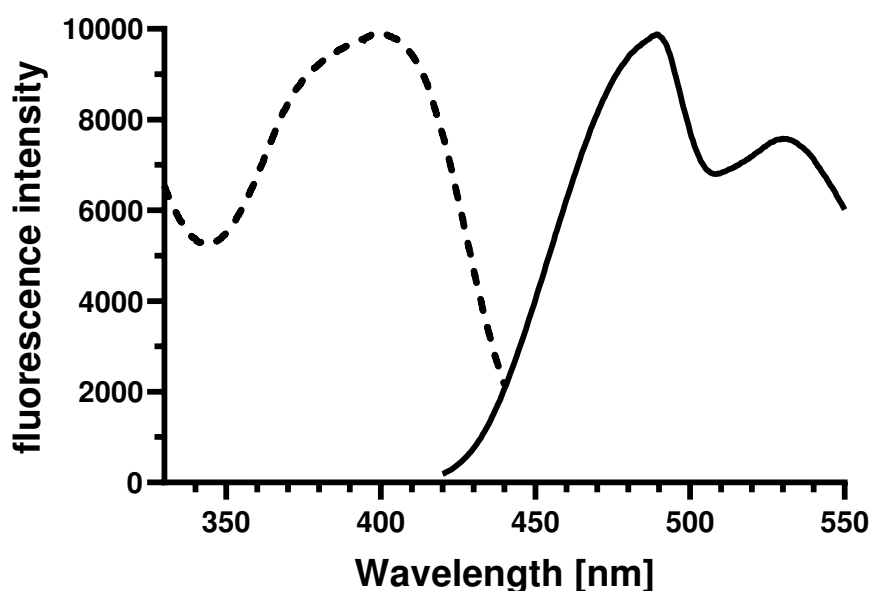


Figure 16: Excitation (dotted) and emission spectra (solid) of fluorophore F1 in aqueous solution.

The autofluorescence was shown to be concentration dependent and almost not visible at low concentrations ($\leq 50 \mu\text{M}$) (figure 17 B). While at low concentrations no differences between the fluorophores were observed, increasing concentrations induced significantly higher autofluorescence for the *hPin1*-WW specific fluorophores F1-F4, than for the non-binding fluorophores F7+F8 or the asymmetric F10. At higher concentrations the fluorescence curve for water-solubilized F1-F4 flattened out. At the same concentrations F1 was shown to form soluble aggregates, which then slowly sank to the bottom. The autofluorescence properties in H_2O showed promising results for low concentrations (figure 17 A,B), but for further protein-based assays the fluorophores had to be checked at physiological pH and with buffer including salt. Therefore the experiment was repeated in 20 mM HEPES pH 7.0 and PBS-buffer pH 7.0 (figure 17 C).

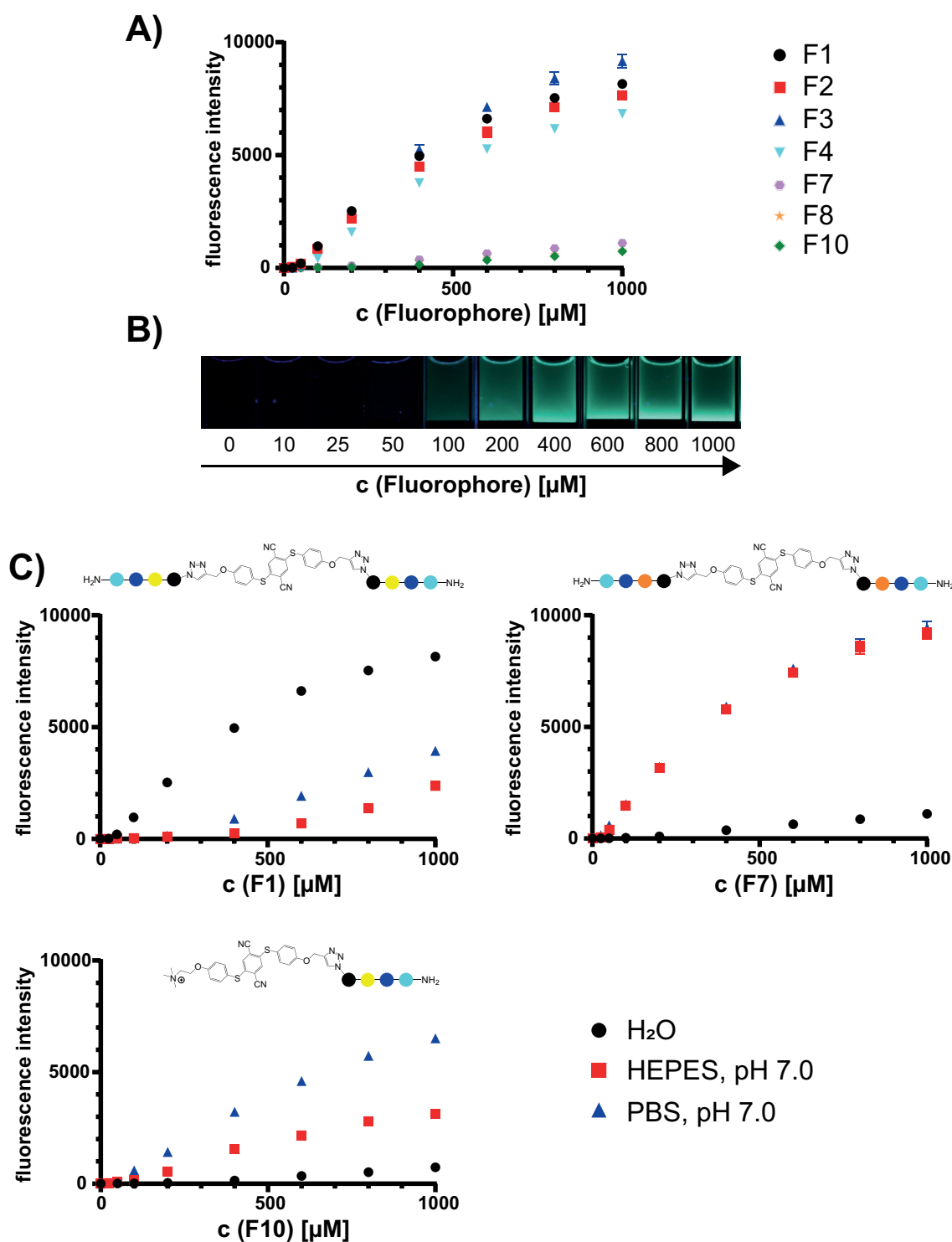


Figure 17: Autofluorescence properties of peptide-conjugated fluorophores. (A) Concentration dependent change in autofluorescence of all fluorophores in H₂O. **(B)** Photograph of cuvettes containing water-solubilized F1 at increasing concentrations up to 1 mM. **(C)** Influence of pH (HEPES) and salts (PBS) on autofluorescence, shown as an example for the symmetric fluorophore F1, the non-binding F7 and the asymmetric F10. Fluorescence measurements were performed at 25 °C with a PMT of 400 V.

Dissolving the fluorophores in 20 mM HEPES buffer pH 7.0 significantly reduced the autofluorescence of F1. The effect could be observed for all binding-specific fluorophores (F1-F4), but was less intense for F4. The additional ionic strength in PBS-

buffer only slightly increased the signal at higher concentrations. In contrast, the non-binding fluorophores F7 and F8 exhibited low autofluorescence in H₂O, but an increased signal when dissolved in 20 mM HEPES pH 7.0 or PBS-buffer pH 7.0. Similar to F7 and F8, the asymmetric F10 showed a higher autofluorescence signal at neutral pH, but also an increased fluorescence under isotonic conditions (PBS).

In conclusion, all binding specific fluorophores showed a similar autofluorescence at low concentrations indicating no or low aggregation and therefore provide good original conditions for further protein binding experiments. Due to the large buffer and salt tolerance of *hPin1*-WW and to avoid even small differences in autofluorescence, 20 mM HEPES pH 7.0 was chosen as the buffer for fluorescence spectroscopy.

5.4 Specific recognition of the *hPin1*-WW domain

The WW domain acts as a substrate binding module for the PPlase domain of *hPin1* towards phosphorylated Thr/Ser-Pro motifs in target peptides and proteins. This binding motif was included in the new fluorophores and should be recognized by the *hPin1*-WW domain. To show the specific recognition and binding of the fluorophores by the protein, methods such as NMR titration experiments and fluorescence titrations were used. In the following subsections the results for the new fluorophores are summarized.

5.4.1 NMR titration experiments

To prove the specific binding of the fluorophores by the *hPin1*-WW domain, an NMR titration experiment was performed. The ¹H,¹⁵N- heteronuclear single quantum coherence (HSQC) spectrum provides information of directly coupled ¹H and ¹⁵N nuclei in a two-dimensional spectrum. The spectrum displays the chemical shifts for ¹H in the direct dimension (X-axis) and the shifts for ¹⁵N in the indirect dimension (Y-axis). Due to differences in the chemical environment, the spectrum exhibits a unique signal for every amide N_H and side chain amide N_H except for proline and the free N-terminal NH₃⁺. Therefore the ¹H,¹⁵N-HSQC spectrum is a powerful tool to map interaction of protein-ligand complexes, as residues involved in binding are found in a different chemical environment resulting in chemical shift perturbation. For weak interactions the exchange between *k_{on}* and *k_{off}* is fast enough to observe chemical shifts as an average of free and bound protein [177]. By superimposing multiple HSQC spectra at different titration points, the fast exchange allows the measurement of chemical shift perturbation, which for a single binding event can be seen as signals moving in a straight line. For analysis of the titration of *hPin1*-WW with the fluorophores, the protein assignment was imported from the biomedical magnetic resonance data bank (BMRB; ID 19258, [168]) and adjusted to the recorded signals of the *hPin1*-WW apo spectrum. The superposition of ¹H,¹⁵N-HSQC spectra at increasing fluorophore concentrations showed a high number of residues undergoing chemical shift perturbation (figure 18, A).

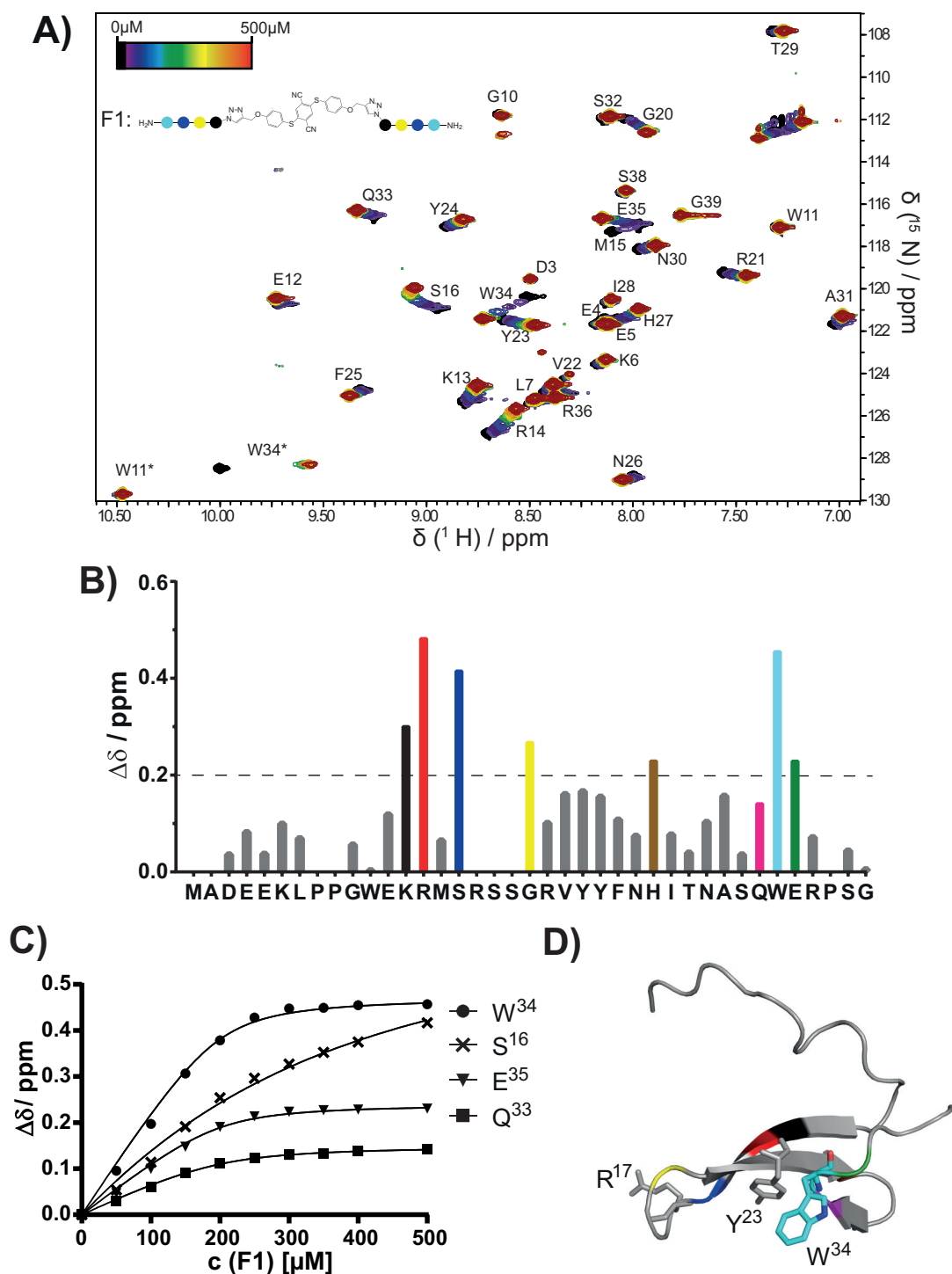


Figure 18: Specific binding of fluorophore F1 to the *hPin1*-WW domain. (A) $^1\text{H},^{15}\text{N}$ -HSQC spectra from *hPin1*-WW domain (400 μM) with different color-coded concentrations (0-500 μM) of fluorophore F1. The side chain amides of W¹¹ and W³⁴ are labelled with an additional star (*). Residues M¹⁵ and W³⁴ showed line broadening, which leads to a loss of signal at intermediate fluorophore concentrations. Residue S¹⁶ showed a secondary chemical shift at high fluorophore concentrations, which can indicate soluble aggregates or unspecific binding. (B) Total chemical shift perturbation for every amino acid after the addition of 500 μM F1. Amino acids with a total shift of 0.2 and Q³³ as a direct neighbor of W³⁴ are colored. (C) Binding curves of selected amino acids S³⁴, Q³³, W³⁴ and E³⁵. (D) NMR Structure of the *hPin1*-WW domain (PDB: 2M8I, [168]) with shifting amino acids colored. Additionally, the amino acids R¹⁷, Y²³ and W³⁴ directly involved in binding are shown as sticks [233].

As seen for the stepwise addition of fluorophore F1 (figure 18, A), ligand binding induced changes in chemical shifts in both the ^1H and ^{15}N dimensions. The superposition of HSQC spectra showed similar shift perturbations to other titration experiments with *hPin1* specific peptides and peptide-coupled nanoparticles [224]. In all titration experiments significant shifts were observed for the amino acids S^{16} , Q^{33} , W^{34} and Q^{35} , which were described to be essential for specific recognition of the pT-P motif [233]. The chemical shifts were plotted against fluorophore concentration and binding curves were fitted (figure 18, C). Due to the fluorophore structure of F1-F4 with two identical binding sites, a stoichiometric factor $n=2$ was added.

Additionally, residues M^{15} and W^{34} showed loss of signal at intermediate fluorophore concentrations up to complete disappearance. For $\text{H}\epsilon$ of W^{34} the signal reappeared at higher concentrations, where the protein is saturated with ligand. For these amino acids or side chains the chemical shift perturbation could not be traced to determine a K_D . Plotting total chemical shift perturbations for all amino acids against the protein sequences showed additional significant shifts for amino acids K^{13} and R^{14} , which are part of first β -sheet (figure 18, B). Mapping all of these significant shifts onto the NMR solution structure of the *hPin1*-WW domain (figure 18, D) displayed the binding site for the WW-domain [8, 287].

Dissociation constants of about 20-50 μM were calculated from binding curves of the selected amino acids S^{16} , Q^{33} , W^{34} and E^{35} . These were similar to binding constants obtained for free peptides containing the pT-P motif [224, 269]. Signals of S^{16} displayed a secondary shift at high fluorophore concentrations resulting in an insufficient fit for F1 and slightly higher binding constants of 30-95 μM for fluorophores F2-F4. For fluorophore F1 the amino acid S^{16} was excluded from analysis.

Table 17: Dissociation constants of selected amino acids at fluorophore binding

	S^{16}	Q^{33}	W^{34}	E^{35}
F1	-	$39.3 \pm 7.9 \mu\text{M}$	$19.3 \pm 6.8 \mu\text{M}$	$24.0 \pm 8.6 \mu\text{M}$
F2	$84.6 \pm 15.0 \mu\text{M}$	$55.9 \pm 3.0 \mu\text{M}$	$37.2 \pm 1.8 \mu\text{M}$	$31.9 \pm 2.8 \mu\text{M}$
F3	$45.6 \pm 8.2 \mu\text{M}$	$32.4 \pm 3.8 \mu\text{M}$	$30.9 \pm 5.9 \mu\text{M}$	$25.9 \pm 6.8 \mu\text{M}$
F4	$95.3 \pm 18.4 \mu\text{M}$	$17.6 \pm 2.2 \mu\text{M}$	$21.9 \pm 3.0 \mu\text{M}$	$19.6 \pm 3.1 \mu\text{M}$
F10	$30.8 \pm 14.7 \mu\text{M}$	$38.2 \pm 6.5 \mu\text{M}$	$22.7 \pm 5.6 \mu\text{M}$	$18.9 \pm 5.0 \mu\text{M}$

In summary, the NMR titration experiments showed specific binding of all tested fluorophores (F1-F4, F10) by the *hPin1*-WW domain. The calculated K_D s were as expected and most importantly comparable to previously tested peptides [224, 269]. In the next steps the fluorophores will be characterized for their fluorescence properties upon protein binding to demonstrate their usability in fluorescence titration experiments.

5.4.2 Fluorescence titration experiments

In addition to NMR spectroscopy, fluorescence spectroscopy is often used to visualize protein-protein or protein-ligand interactions and characterize them. The method usually used is called fluorescence anisotropy and typically requires fluorescence labeling of the smaller binding partner. Ideally, the fluorophores are stable, small, bright and do not interfere with components of the biological system. But often the selection of a suitable fluorophore is problematic due to unspecific binding or steric hindrance. Here the new fluorophores offer new possibilities for a fluorescence-based method with direct read out. Instead of detecting the anisotropy, for fluorophores the total change in fluorescence signal can be used to detect protein-ligand binding. Upon addition of protein the fluorophores are bound and molecular movements like rotations are restricted, inducing the AIEE effect.

To further characterize the fluorophore, its protein binding properties and change in fluorescence intensity were investigated. Fluorescence titration experiments of fluorophores F1-F4 and F10 with *hPin1*-WW were performed. As an example a titration with 50 μM F1 and the *hPin1*-WW domain is shown in figure 19 A. The fluorescence signal plotted against the protein concentration showed a typical binding curve and was fitted with a stoichiometry of 1:2 (ligand:protein).

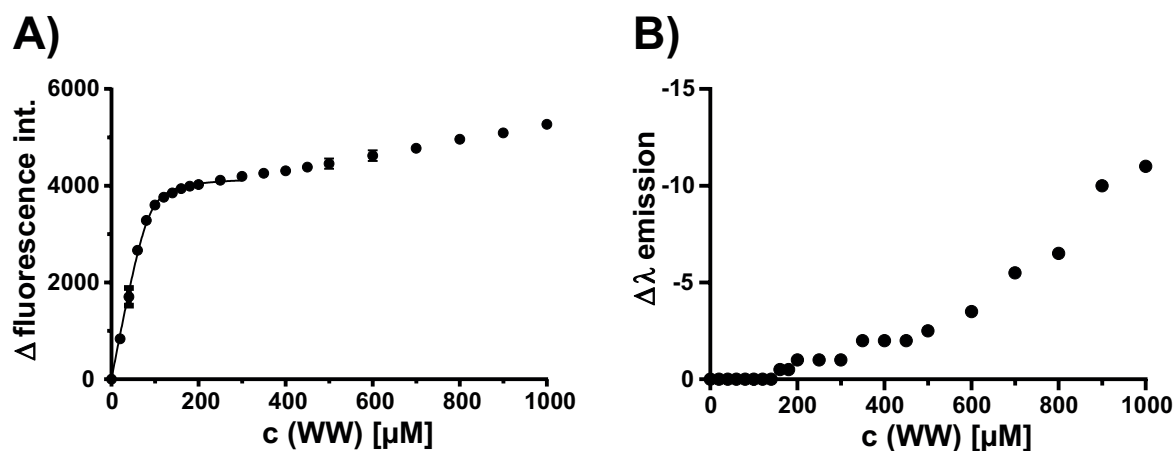


Figure 19: Fluorescence titration of fluorophore F1 (50 μM) with the *hPin1*-WW domain. (A) Binding curve and non-linear fit for the titration of F1 with *hPin1*-WW. (B) Hypsochromic shift of F1 with increasing protein concentration.

With protein excess (at approximately 200 μM *hPin1*-WW domain), the fluorescence signal reached saturation, but with six times excess the fluorescence signal increased again. Simultaneously the emission maximum shifted hypsochromically from 489 nm to 478 nm indicating additional non-specific binding or possibly formation of higher soluble aggregates (figure 19 B).

In total, the fluorescence titration experiment was performed at least three times and confirmed the specific recognition of the *hPin1*-WW domain. Protein binding induced a

concentration-dependent increase in fluorescence intensity making fluorescence titration a suitable method to determine binding constants with TPN-based AIEgens.

5.4.3 Influence of a peptide linker on protein binding and its fluorescence properties

Next, the influence of the peptide linker on fluorescence properties during protein binding was investigated. With increasing linker length, the distance between the aromatic AIE-core and bound protein changes and could influence the induced fluorescence signal. While fluorophore F1, which does not contain an additional linker sequence, was shown to be specifically bound by the *hPin1*-WW domain, a long linker could affect the degree of molecular restriction upon protein binding. One may hypothesize that with a too long linker sequence the protein would possibly be bound too far from the AIE-core and the rotation may not be restricted to induce a sufficient AIE effect. Based on the first successful titration with F1 (figure 19), the same titration experiment was also performed for fluorophores F2-F4 with equal fluorophore concentration of 50 μM and PMT of 600 V to check the influence of different linker lengths.

For all symmetric fluorophores (F1-F4) the typical shape of a binding curve was obtained (figure 20) and no significant differences or trends in the maximum fluorescence signal were observed. For fluorophores F1 and F2 the data points could be fitted perfectly with the assumed 1:2 binding model ($n=0.5$), resulting in binding constants of $K_D=2.7 \pm 0.7 \mu\text{M}$ (F1) and $K_D=4.5 \pm 0.4 \mu\text{M}$ (F2). For F3 and F4 however, the binding model did not fit the experimental data (black fit) and had to be adjusted. To represent the experimental data, the stoichiometric factor n was changed to a variable factor and was fitted together with the K_D (red fit). The adjusted fitting model resulted in stoichiometric factors of $n=0.73$ (F3) and $n=1.09$ (F4) with $K_D=5.1 \pm 1.8 \mu\text{M}$ (F3) and $K_D=23.3 \pm 4.9 \mu\text{M}$ (F4).

The fluorophores exhibit autofluorescence at all tested concentrations with linear increasing intensity (figure 17). This autofluorescence may be a result of soluble aggregates. To check the influence of possible soluble aggregates on the binding affinity and the stoichiometry factor n , the fluorescence titrations were repeated at multiple fluorophore concentrations (10-200 μM). The fluorescence titrations and fitted binding curves are shown as an example for F1 in figure 21 and were similar for the other symmetric fluorophores F2-F4 (appendix figures A16, A17, A18). Statistics are summarized in tables 18 and 19.

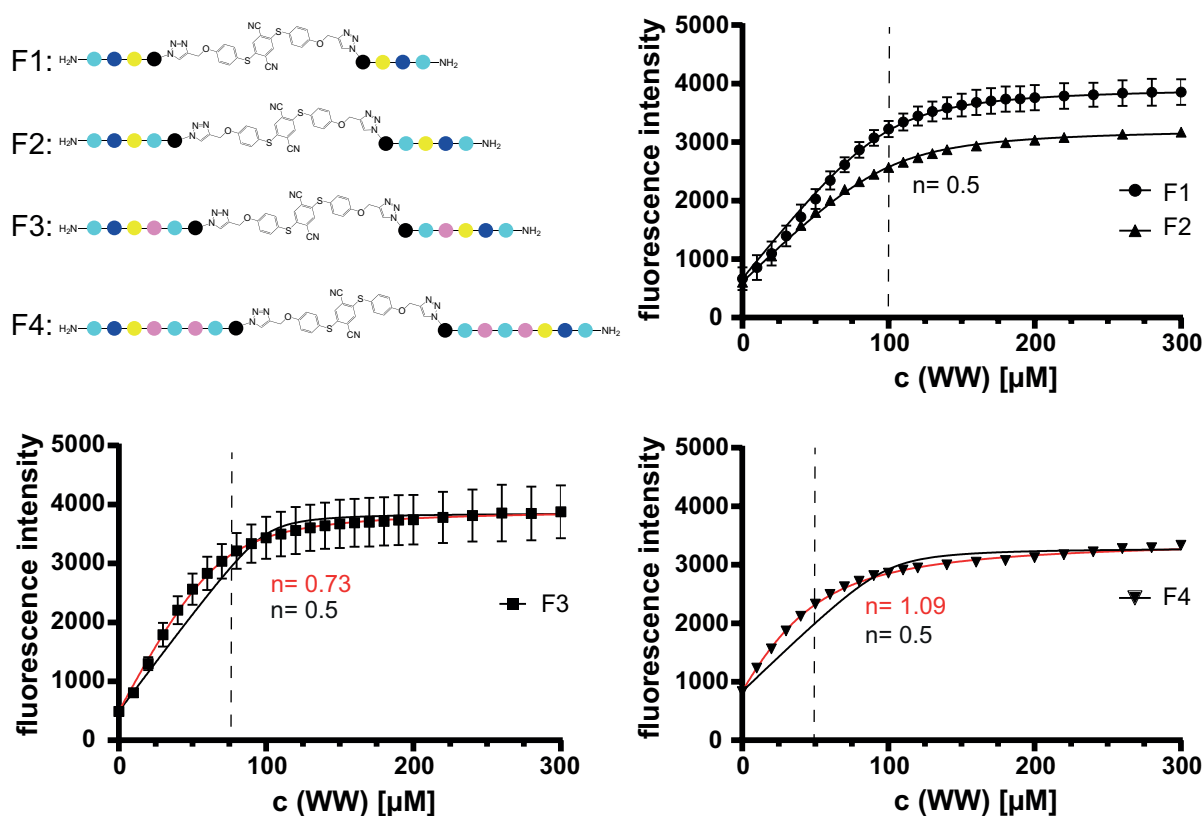


Figure 20: Fluorescence titration of fluorophores F1-F4 at 50 μM with the *hPin1*-WW domain. On top the fluorescence titrations for F1 and F2 fitted with the assumed binding model of two proteins binding to a single fluorophore molecule with two binding sites. Bottom shows the binding curves for fluorophores F3 and F4. The data were fitted with a 2:1 binding model ($n = 0.5$) and with a variable stoichiometry factor resulting in value of $n = 0.73$ (F3) and $n = 1.09$ (F4). The equivalence point for each fluorescence titration is marked with dotted lines.

The specific binding of the *hPin1*-WW domain to the symmetric fluorophores F1-F4 was successfully proven at various concentrations. Even at lower concentrations in the range of the binding constant, the change in fluorescence signal was sufficient to fit a binding curve and calculate binding constants. At lower concentrations of 10 μM and 25 μM the non-linear fits could be fitted with the 1:2 binding model for all fluorophores. However, at higher concentrations ($\geq 100 \mu\text{M}$), no calculation fitted the experimental data (black fit) and the stoichiometric factor was again set as a variable factor (red fit). The change in stoichiometric factor increased with increasing fluorophore concentration and was most pronounced for the larger F3 and F4 (table 18).

The results showed a tendency that fluorophores containing a larger peptide linker were affected more strongly and at lower concentrations. However, with an increasing stoichiometric factor n , increased K_D s could be observed (table 19). While small stoichiometric changes did not affect the K_D as much, stoichiometric factors around $n = 1$ increased the calculated K_D values by a factor of three to ten. At low fluorophore concentrations the calculated K_D s were in a low μM range from 1.6-8.0 μM and increased up to 57.6 μM for a higher stoichiometry.

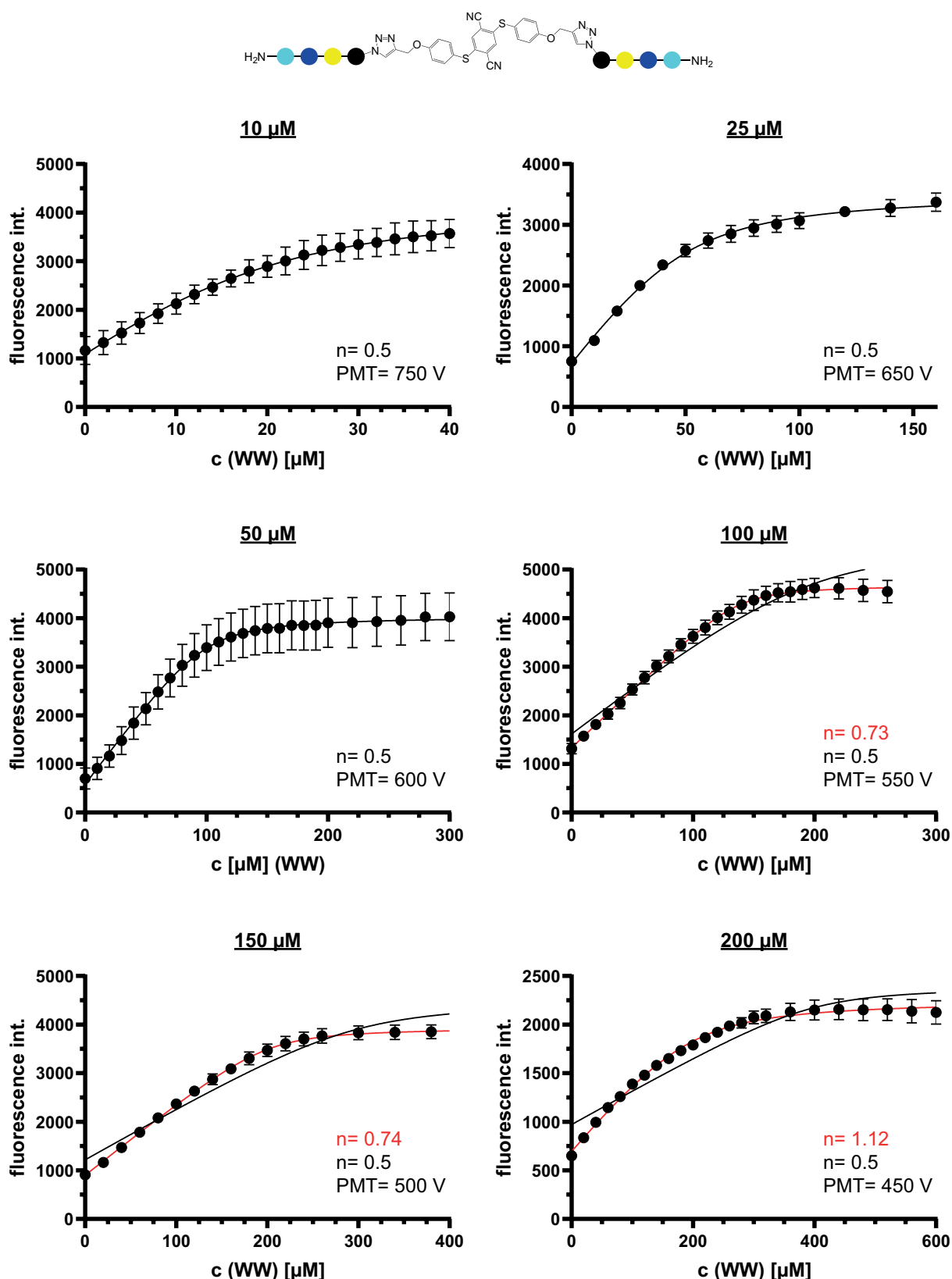


Figure 21: Concentration dependency of fluorophore F1. Fluorescence titrations with various concentrations of F1 (10-200 μM). Shown are non-linear fits with a set stoichiometry factor n of 0.5 (black) and a variable factor (red). With increasing fluorophore concentration the assumed binding ratio of 2:1 (protein:fluorophore) did not fit. With increasing fluorophore concentration the PMT was adjusted to detect intensities of bound and unbound fluorophore (see section 4.6.3 table 9).

Table 18: Stoichiometric factor for symmetric fluorophores F1-F4 at various concentrations. The factor was fixed at $n=0.5$ for low fluorophore concentrations. For larger fluorophore concentrations n was fitted.

c (F)	F1	F2	F3	F4
10 μM	0.5	0.5	0.5	0.5
25 μM	0.5	0.5	0.5	0.5
50 μM	0.5	0.5	0.73 ± 0.05	1.09 ± 0.10
100 μM	0.73 ± 0.01	0.72 ± 0.03	1.27 ± 0.09	0.93 ± 0.08
150 μM	0.74 ± 0.01	0.82 ± 0.02	1.72 ± 0.06	1.34 ± 0.06
200 μM	1.12 ± 0.06	0.92 ± 0.04	2.67 ± 0.30	1.78 ± 0.14

Table 19: Dissociation constants of symmetric fluorophores F1-F4 at various concentrations. The K_D s were fitted with n values from table 18.

c (F)	F1	F2	F3	F4
10 μM	$4.0 \pm 0.8 \mu\text{M}$	$6.9 \pm 0.7 \mu\text{M}$	$5.8 \pm 0.7 \mu\text{M}$	$4.4 \pm 0.5 \mu\text{M}$
25 μM	$4.8 \pm 0.9 \mu\text{M}$	$8.0 \pm 0.8 \mu\text{M}$	$1.6 \pm 0.4 \mu\text{M}$	$2.7 \pm 0.7 \mu\text{M}$
50 μM	$2.7 \pm 0.7 \mu\text{M}$	$4.5 \pm 0.4 \mu\text{M}$	$5.1 \pm 1.8 \mu\text{M}$	$23.3 \pm 4.9 \mu\text{M}$
100 μM	$2.0 \pm 0.6 \mu\text{M}$	$8.5 \pm 2.1 \mu\text{M}$	$6.1 \pm 3.8 \mu\text{M}$	$19.0 \pm 8.4 \mu\text{M}$
150 μM	$3.9 \pm 1.3 \mu\text{M}$	$12.0 \pm 2.6 \mu\text{M}$	$35.9 \pm 4.6 \mu\text{M}$	$15.6 \pm 3.9 \mu\text{M}$
200 μM	$30.5 \pm 8.2 \mu\text{M}$	$16.7 \pm 5.0 \mu\text{M}$	$49.6 \pm 20.0 \mu\text{M}$	$57.6 \pm 16.0 \mu\text{M}$

Overall the symmetric fluorophores F1-F4 were tested successfully for the specific recognition of the *hPin1*-WW domain. All tested linker lengths at all tested fluorophore concentration resulted in saturated binding curves. However, the binding curves revealed additional unspecific interactions at higher concentrations, probably caused by the formation of soluble fluorophore aggregates. These interactions are increased for fluorophores with an increased linker length and additionally influences K_D calculation at lower concentrations. For this, small fluorophore concentrations ($\sim 25 \mu\text{M}$) are ideal for K_D determination at all linker lengths, while the binding curve at high fluorophore concentrations cannot be fitted with the assumed binding model of 2:1 (protein: fluorophore). Due to the following adaptation of the stoichiometric factor the K_D calculation got influenced negatively. Hence the fluorophore F1, containing the smallest peptide, is the best derivative with two binding sites synthesized in this work to specifically target the *hPin1*-WW domain and characterize its binding.

5.4.4 Comparison of fluorescence intensity for fluorophores with one or two binding sites

After demonstrating the binding specificity for the symmetric fluorophores F1-F4 and the calculation of the corresponding binding constants, the number of binding sites (one or two) and their influence was investigated. While proteins bound to two binding sites can restrict molecular rotations from both sides, the restriction upon a single protein bound to the fluorophore might not result in a sufficient restriction. Therefore, the focus using fluorophores with one binding site was on the maximum fluorescence and the change in fluorescence upon protein binding compared to the symmetric fluorophores F1-F4 with two binding sites.

Two approaches were pursued to synthesize fluorophores with one binding site. The attempt with F0, F6-F9 did not result in fluorophores that are soluble and have low autofluorescence, and therefore the asymmetric fluorophore F10 with a soluble TMA group was synthesized. This fluorophore showed a sufficient solubility and just slightly higher autofluorescence in buffer at neutral pH compared to being solubilized in H₂O. The effect was negligible at concentrations lower than 200 μM (figure 17 C). Thus, fluorophore F10 shows good solubility and autofluorescence properties, which are also comparable to fluorophores F1-F4. Hence, the fluorophore F10 is a good candidate to compare the fluorescence properties of fluorophores bearing one or two binding sites. The fluorescence titration experiments with F10 and the *hPin1*-WW domain were performed in accordance with the titrations of F1-F4, in a fluorophore concentration range of 10-200 μM and at PMT values between 750 V (10 μM) and 450 V (200 μM).

At low fluorophore concentration (10 μM), the change of fluorescence intensity induced by protein binding was very low and indistinguishable from noise (figure 22). However, at concentrations between 25 μM and 100 μM and corresponding PMT values of 550-650 V the signal-to-noise ratio was sufficient to fit the experimental data and calculate the K_D s. In this concentration range the calculated K_D s were similar to those of the symmetric fluorophores: $11.5 \pm 4.3 \mu\text{M}$ (@ 25 μM F10), $7.0 \pm 3.9 \mu\text{M}$ (@ 50 μM F10) and $2.3 \pm 1.5 \mu\text{M}$ (@ 100 μM F10). But with increasing fluorophore concentration, the binding curves changed again. At 150 μM and higher, the autofluorescence was greater than the protein induced fluorescence. Analysis of the experimental data resulted in negative binding curves (figure 22), indicating less molecular restrictions. Here, the protein may interact with the soluble aggregated fluorophore and affects the aggregation equilibrium.

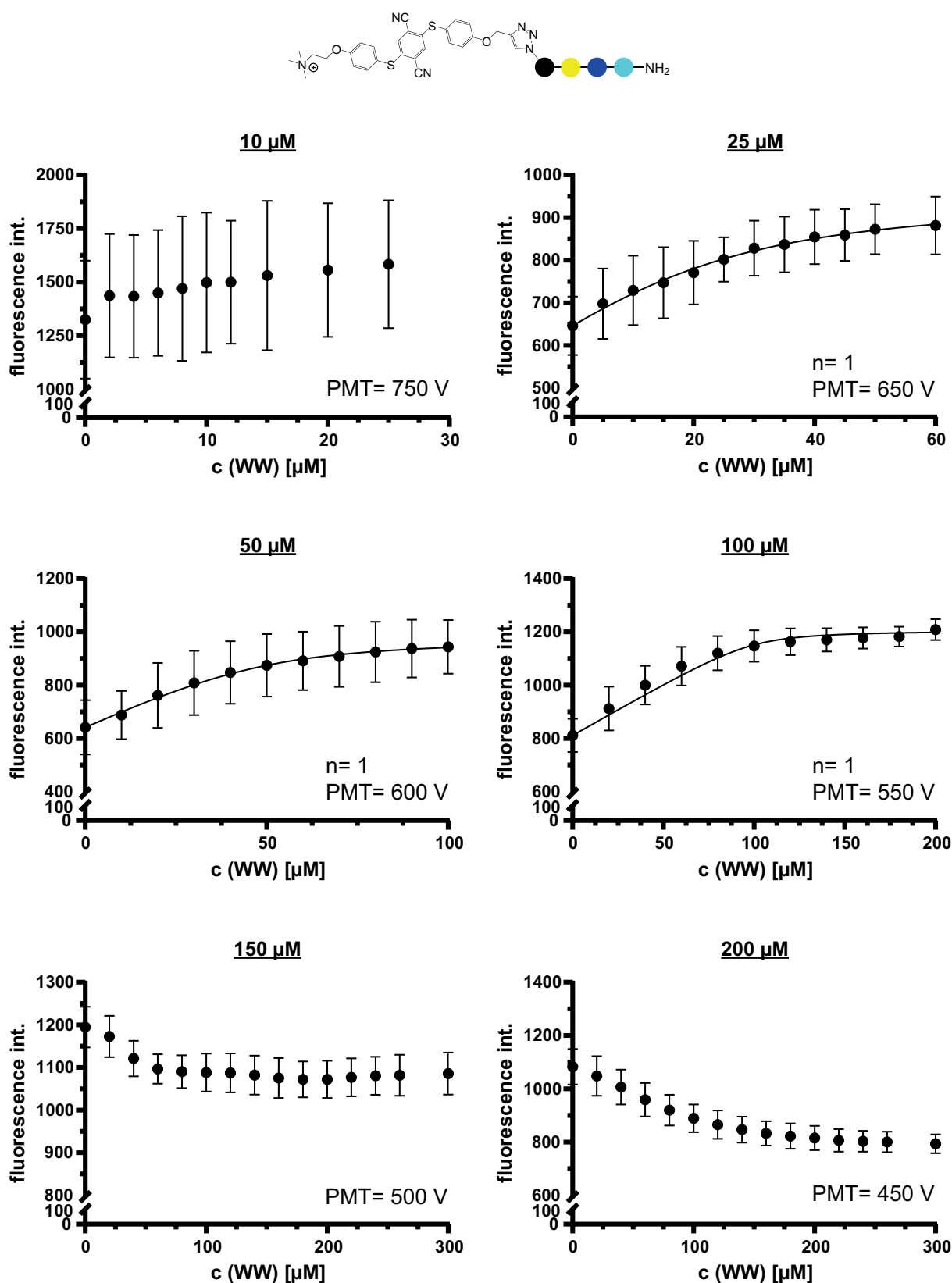


Figure 22: Concentration dependency of fluorophore F10. Shown are the fluorescence titrations of fluorophore F10 with the *hPin1*-WW domain at multiple fluorophore concentrations between 10 and 200 μM . Binding curves were fitted with a 1:1 binding model ($n=1$; equation 1). At higher fluorophore concentrations (150-200 μM), the fluorescence intensity decreased upon protein binding. The PMT was adjusted according to the experiments shown in figure 21.

While similar K_D s in the low μM range were observed for the binding of all fluorophores (F1-F4 and F10) to the *hPin1*-WW domain, the total fluorescence intensities and especially the change of fluorescence intensity upon protein binding was significantly different for F10 (figure 23) at all concentrations, compared to fluorophores F1-F4 bearing two binding sites.

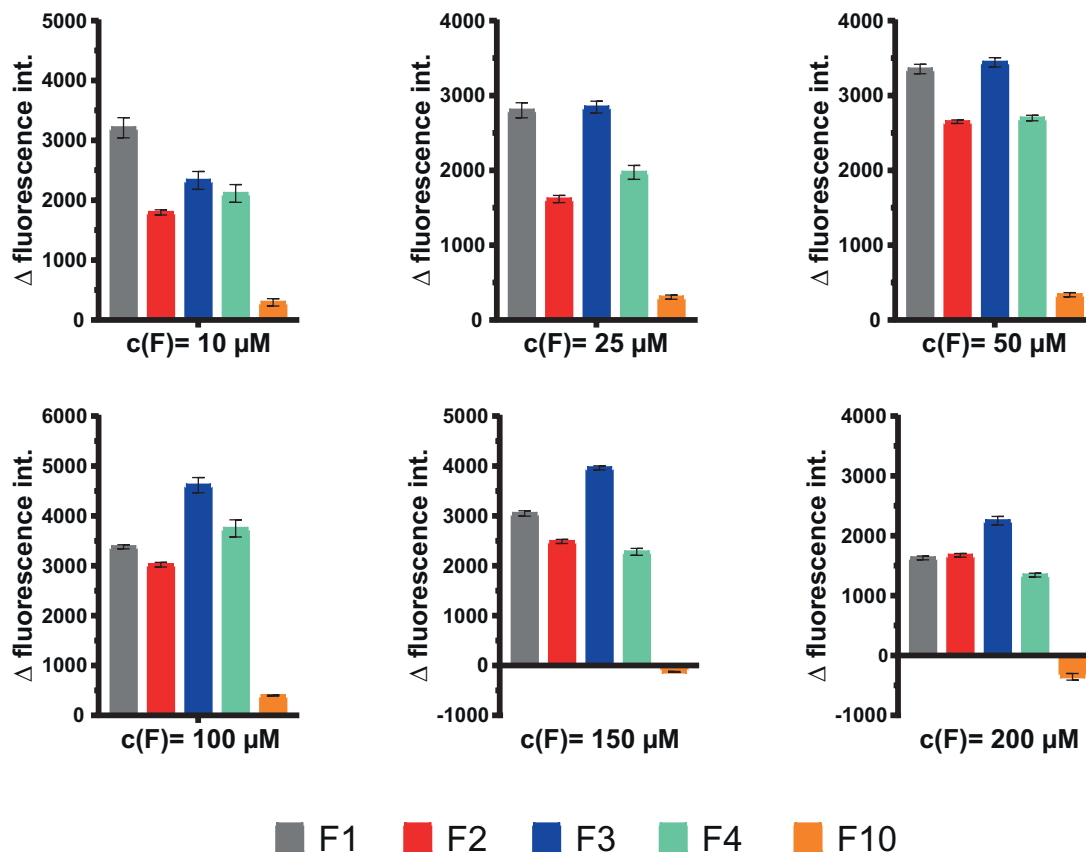


Figure 23: Comparison of the maximum change of fluorescence upon protein binding. The change of fluorescence intensity for the fluorophores F1-F4+F10 at all tested fluorophore concentrations (10-200 μM). Fluorescence titrations were performed at PMT voltages of 750 V (10 μM), 650 V (25 μM), 600 V (50 μM), 550 V (100 μM), 500 V (150 μM) and 450 V (200 μM).

For the symmetric fluorophores the increase in fluorescence signal was significantly higher than for the fluorophore F10. In total, the fluorescence intensity of F10 increased by 20-50% or even decreased upon binding the *hPin1*-WW domain. In contrast, the symmetric fluorophores showed a better signal-to-noise ratio and an increasing fluorescence signal up to 600% upon protein binding.

In conclusion the fluorophore F10 can be used for fluorescence titration experiments with the *hPin1*-WW domain in a defined intermediate concentration range of 25-100 μM , but suffers from a low signal-to-noise ratio. The calculated K_D s (2.3-11.5 μM) are comparable to the K_D s calculated for F1-F4 (1.6-8.5 μM), but due to the significant higher increase of fluorescence signal for fluorophores with two binding sites (F1-F4),

F10 seems not to be an alternative to fluorophore F1, which earlier was described as the best candidate for *hPin1*-WW recognition (see section 5.4.3). The results show a greater increase of fluorescence signal upon protein binding for F1-F4 indicating better rotational restriction when bound to two proteins.

5.5 Effect of protein size on fluorescence increase

After the successful recognition of the *hPin1*-WW domain, binding was also tested for the *hPin1* full-length protein (*hPin1*-FL), consisting of the WW-domain and a catalytic PPlase domain. The full-length protein has a molecular weight four times greater than the isolated WW-domain and was expected to restrict molecular motions even more. The higher level of restriction should then result in a greater fluorescence signal compared to the binding of the WW-domain. To test this assumption, fluorescence titration experiments with *hPin1*-FL were carried out, based on the results with the *hPin1*-WW domain. A fluorophore concentration of $50\ \mu\text{M}$ and a PMT of 600 V was used, but titration data did not result in a saturated binding curve (not shown). Therefore, a time resolved fluorescence measurement of the binding event was recorded to test if protein binding results in a time-invariant fluorescence signal (figure 24, A).

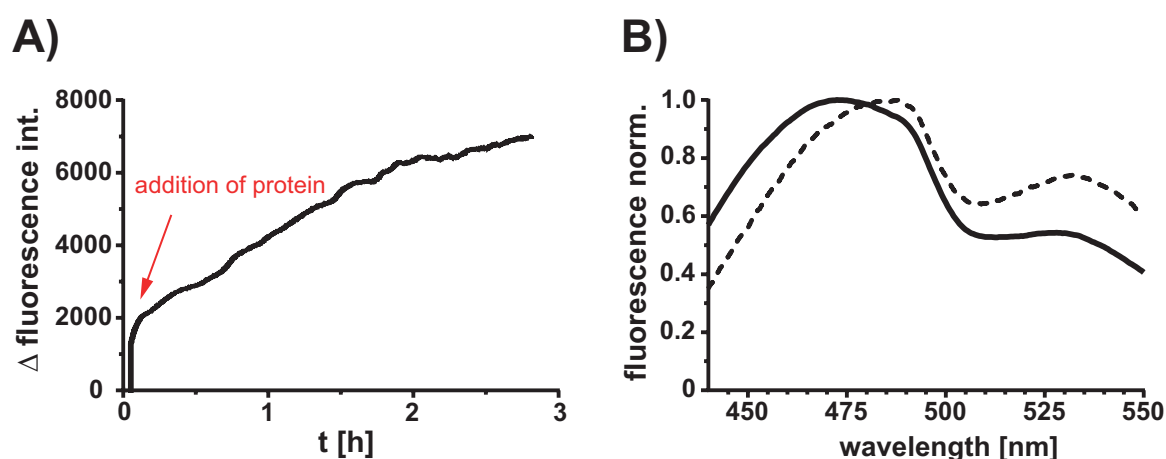


Figure 24: Fluorescence measurement of fluorophore F1 with *hPin1*-FL. (A) Time dependent fluorescence signal of F1 with full length *hPin1* protein. The initial auto fluorescence was set to 0 and after the addition of $10\ \mu\text{M}$ protein (3 min) no more protein was added and the fluorescence signal was monitored over time. **(B)** Normalized emission spectra directly after protein addition (dotted) and after 3 h (solid). The maximum shifted from 489 nm to 472 nm.

After the addition of $10\ \mu\text{M}$ *hPin1*-FL protein the fluorescence signal increased significantly (~ 1300 int.), suggesting fast and specific protein binding. Thereafter, however, the signal increased linearly without further addition of protein. The increase in fluorescence indicates further unknown molecular restrictions. This phenomenon was observed for all binding specific fluorophores. Furthermore, a shift of the emission maximum to 472 nm was induced over time (figure 24, B). In summary, the steadily

increasing fluorescence signal interfered with the expected fluorescence signal and made it impossible to fit and analyze the experimental data. Therefore, the fluorophores are not suitable for the quantitative analysis of the *hPin1*-FL protein.

5.6 Structural analysis of fluorophore F10

The structure of small chemical molecules are often solved with crystallography, including the disulfonate derivative DSA by the group of J. Voskuhl [97]. The crystal structure of DSA revealed a stretched linear structure with twisted aromatic rings [97]. Adding short unstructured peptide sequences to the AIE-core molecules (A1 and A2, figure 11), a similar ring structure with flexible and unstructured peptides at both ends was expected for the new peptide-conjugated fluorophores. In this work, however, the chemical characterization by 2D NMR spectra of this new fluorophores showed a high number of cross-peaks in the 2D-NOESY spectrum, indicated the presence of a defined structure, rather than a flexible random-coil behavior of the peptide arms. Based on this, the structure of the asymmetric F10 should be calculated by NMR spectroscopy. The NMR solution structure will show the structural arrangement of the conjugated peptide relative to the AIE-core and will help to understand the AIEE properties of the fluorophore on a structural level.

5.6.1 Parametrization and peak assignment of the AIE-core ring system

The structure calculation was carried out using the program CYANA. CYANA uses library files to describe the configuration and geometry of amino acids and dihedral angles. For the calculation of fluorophore F10, library files for the AIE-core, the amidated C-terminus and the phosphorylated threonine had to be created. While the phosphoryl group and amide group were just small additions to the file, the AIE-core molecule had to be parametrized completely from scratch. It was defined as a side chain addition to the homoalanine, which is a nonstandard amino acid and had to be parametrized as well. The newly created library files are shown in the electronic appendix (CD/Appendix/library_files) and atom numbering of the AIE-core ring system is shown in figure 25 A. Hydrogens were numbered in accordance with covalently bound carbon atoms.

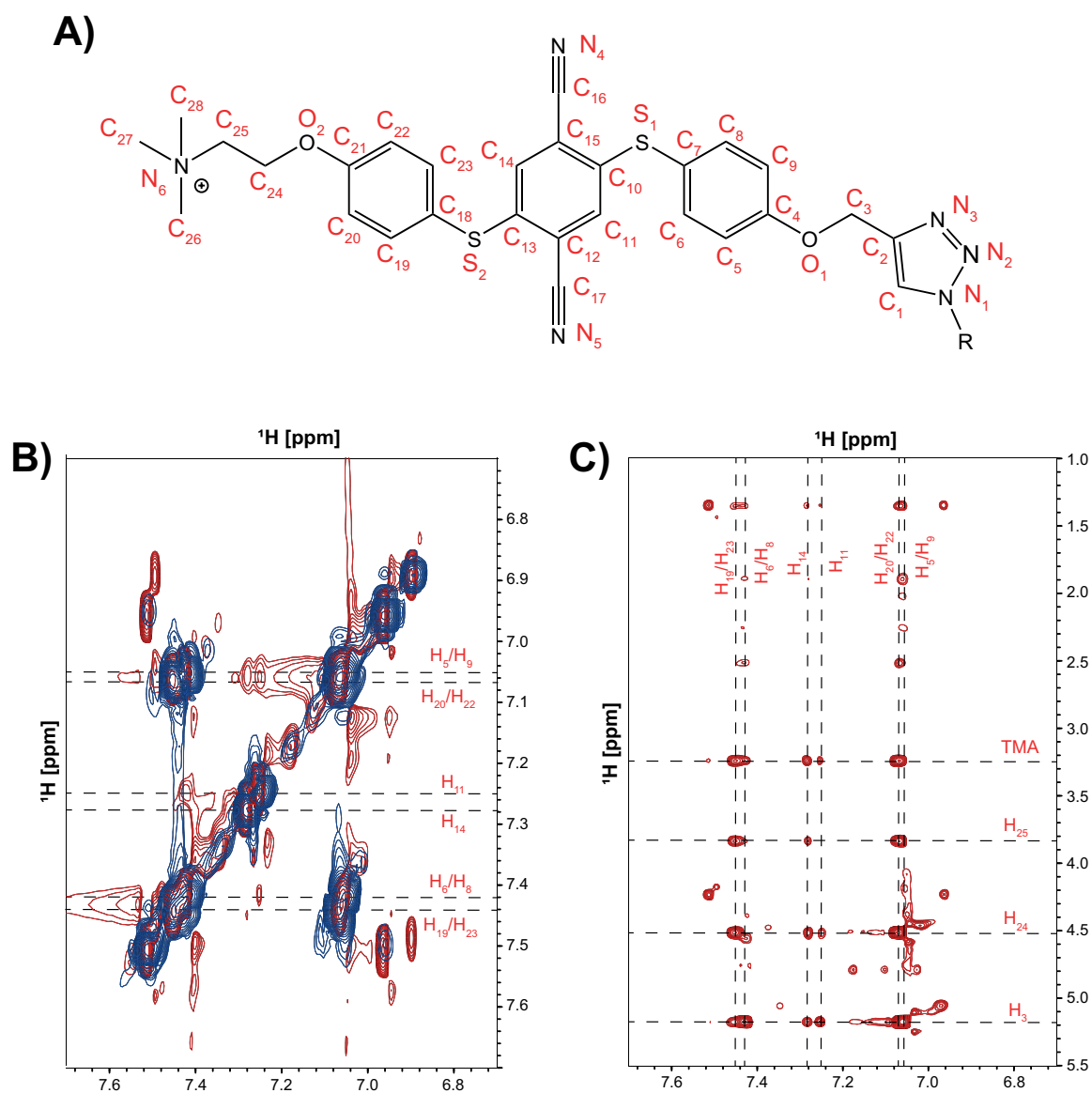


Figure 25: Numbering and assignment of the AIE-core ring system. (A) Chemical structure and heavy atom numbering of the parametrized AIE-core. H-atoms were numbered according to the numbering of their covalently bound C-atom. (B) Superposition of the COSY (blue) and NOESY spectra (red) from the H_{aro} - H_{aro} region. Hydrogens of the three different rings could be distinguished. (C) The expansion shows the signals from the H_{aro} - H_{ali} region of the NOESY spectrum of F10. With the cross-peaks from H_3 , H_{24} , H_{25} and triethylamine (TMA), the phenylene rings could be assigned.

For the assignment of all cross-peaks of the fluorophore F10 all 2D-spectra (2D-COSY, 2D-TOCSY and 2D-NOESY) had to be used. In the following part only the assignment of the aromatic hydrogens (H_{aro}) with the help of the 2D-NOESY and 2D-COSY spectra are described. The $^1H, ^1H$ -COSY spectrum provides information about spins connected within three bonds. Based on the resulting COSY peak pattern, the two hydrogens of the middle aromatic ring (H_{11} and H_{14}) could be distinguished from those of the outer rings. Atoms H_{11} and H_{14} are single hydrogens with no additional spin system directly connected and therefore should display a single diagonal peak with no cross-

peaks in a COSY spectrum. This pattern for a H_{aro} was only found for the peaks at 7.25 ppm and 7.28 ppm (figure 25 B). With additional NOESY cross-peaks to the outer phenylene rings and their intensity differences, the peaks could be assigned to H_{11} (7.25 ppm) and H_{14} (7.28 ppm). The NOESY spectrum provides information of spins through space and within a distance of 6 Å. As a result, the NOESY spectrum contains distance information between protons, which are represented by the peak intensities. Short distances around 1.8-3 Å display more intense cross-peaks than longer distances of 3-6 Å.

The outer phenylene groups are connected to the central ring via a thioether and consist of an additional ether bond in the *para*-position. These bonds form rotational axes, which are mainly responsible for the AIEE properties of this molecule. Here, the rotations around these axes were also the reason for chemically equivalent Hs which appeared as a single signal in NMR spectra. The chemically equivalent hydrogen pairs were H_5/H_9 , H_6/H_8 , H_{19}/H_{23} and H_{20}/H_{22} , which were defined and used as pseudoatoms (Q) for the CYANA calculation. The COSY spectrum showed eight peaks in the aromatic area of 6.7-7.7 ppm. With the help of an additional NOESY spectrum the peaks could be assigned.

The four diagonal peaks at 7.06 ppm, 7.07 ppm, 7.43 ppm and 7.45 ppm were assigned to the Hs of the outer phenylene rings. With the help of the NOESY cross-peaks at 5.18 ppm (H_3), 4.52 ppm (H_{24}), 3.84 ppm (H_{25}) and 3.25 ppm (TMA) the peaks could be assigned (figure 25,C) to the left and right outer phenylene ring. While the shifts at 7.06 ppm and 7.43 ppm displayed a more intense peak to H_3 and lower intensities to H_{24} , H_{25} and TMA, the shifts at 7.07 ppm and 7.45 ppm showed opposite intensities. With these cross-peaks and the primary structure (figure 25,A) the peaks were assigned as follows: H_5/H_9 (Q_4): 7.06 ppm, H_6/H_8 (Q_5): 7.43 ppm, H_{19}/H_{23} (Q_6): 7.45 ppm and H_{20}/H_{22} (Q_7): 7.07 ppm.

5.6.2 Assignment of amino acids

Assignment of amino acids in NMR spectroscopy is a standard method and can be done for small peptides based on the peak pattern of the superimposed COSY and TOCSY spectrum if all amino acids are unique (figure 26). In contrast to the COSY spectrum with cross-peaks showing couplings over up to three bonds, the TOCSY spectrum provides couplings of each H atom with all other Hs within the complete spin system (amino acid). Here all Hs show cross-peaks to each other and therefore can be grouped and assigned to a matching amino acid.

The conjugated peptide contained four amino acids, of which only the Ala and pThr were visible in the amide area of the spectra (\approx 6.5-9.5 ppm). The homoalanine forms the N-terminal end and therefore contains a free amino group (NH_3), which quickly exchanges protons with water and therefore no signal can be detected. The other amino acid not observable in the amide region was proline, which does not contain an amide

proton due to its ring closure. Another unique feature of peptidyl prolyl bonds is their *cis/trans* distribution. Due to the high percentage of *cis* conformation, the neighboring amino acids appeared as both, *cis* and *trans* conformers. They were distinguished by intensity differences and only *trans* peaks were used for structure calculation.

The TOCSY spectrum contains shift information of a complete spin system (amino acid) and could be used to assign the pThr and Ala. In comparison to Ala, pThr contains an additional CH group and could thus be distinguished from pThr. The final assignment for amide protons was pThr(*trans*): 8.98 ppm, pThr(*cis*): 8.71 ppm, Ala(*trans*): 8.39 ppm and Ala(*cis*): 8.59 ppm.

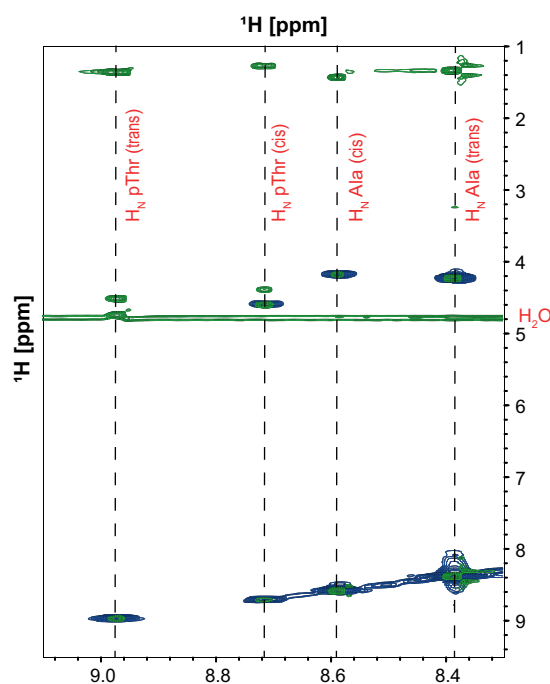


Figure 26: Assignment of *cis* and *trans* amino acids. Superposition of COSY (blue) and TOCSY (green) spectra. The expansion shows the amide region with the *cis* and *trans* peaks of pThr and Ala.

A list of all assignments can be found in the electronic appendix (CD/Assignment_F10).

5.6.3 NMR structure of fluorophore F10

The structure of fluorophore F10 was calculated only with proton distance information. All chemical shifts could be assigned and in total 195 manually assigned NOESY peaks were included in the calculation. Due to the small molecule size, a total of 100 structures were calculated and sorted by their target function value (equation 3). The values of the best 30 target functions were summarized and averaged to a final target function value of $0.65 \pm 0.11 \text{ \AA}^2$ with an average backbone RMSD of $0.39 \pm 0.07 \text{ \AA}$.

The structure was calculated using the AIE-core as side chain addition of homoalanine. The stick representation shows the fluorophore from the side (left) and rotated from the top (right) (figure 27). The phenylene rings are folded to the same side and form a

cage-like core structure that forms hydrophobic interactions with the proline above it. The peptide is helically twisted over the directly linked outer phenylene ring and at the same time the TMA group is directed downwards in the opposite direction (figure 27). The view from top side of the molecule clearly shows the proline interaction with the left phenylene ring. The phosphoryl group, part of the binding motif, is directed to the top, where it is freely accessible and can be recognized by the *hPin1*-WW domain.

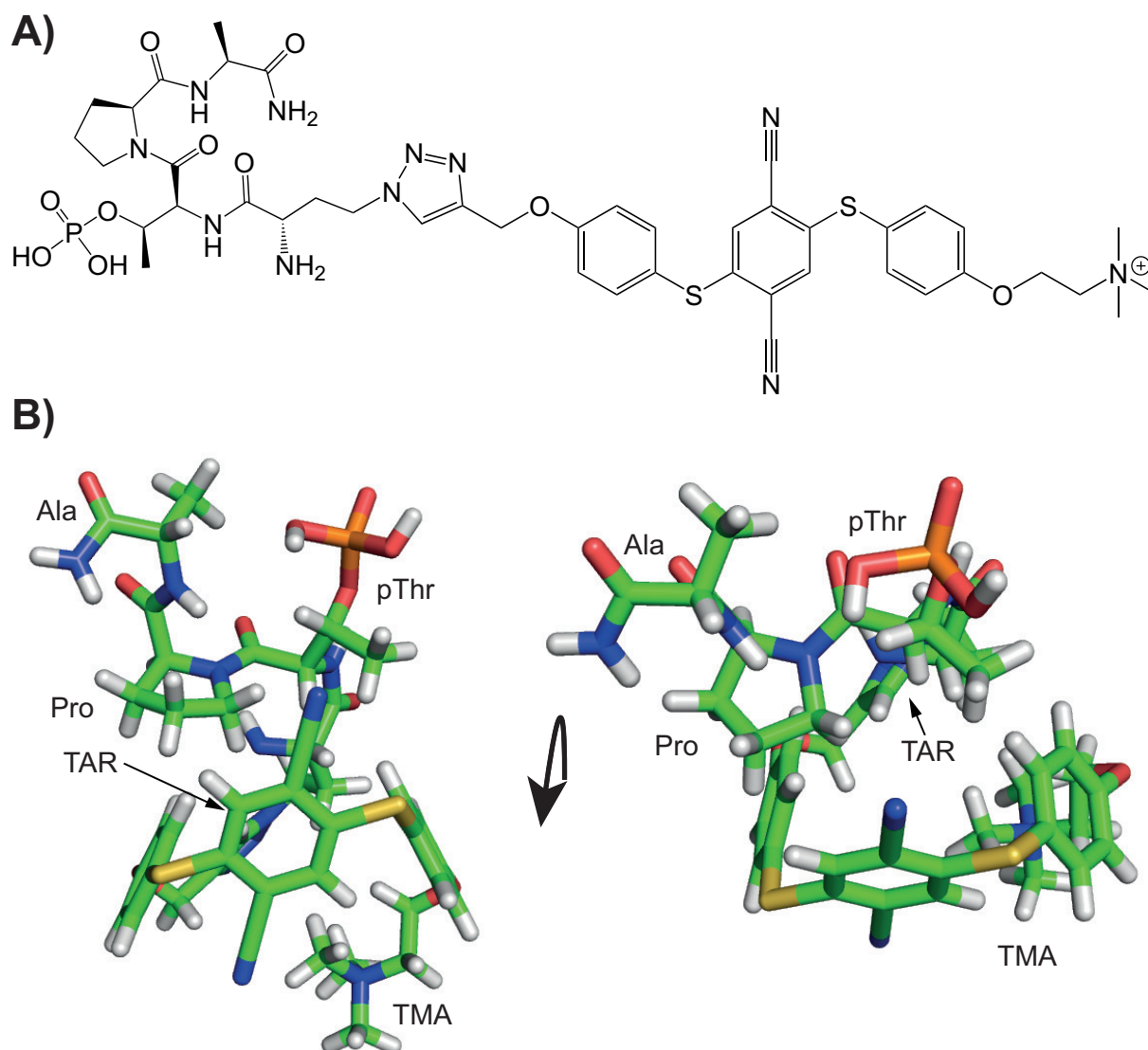


Figure 27: Structure of the isolated fluorophore F10. (A) Chemical structure of the fluorophore F10. **(B)** The structure of F10 is shown from the side (left) and rotated vertically (right). TAR: Triazole ring, TMA: Trimethylamine.

Superposition of the 30 best structures showed a relatively rigid structure with rotations of the outer phenylene rings around the ether-thioether axes and movement of the triazole ring. Figure 28 B displays the two conformational states with the largest differences in rotation and movement. Considering the ring symmetry, the 90° angle between the two structures displays that the outer phenylene rings can rotate freely. As a result, the triazole ring moves up to avoid steric hindrance which also changes

the position of proline slightly. While the outer phenylene rings are flexible in rotation, the middle ring is shown to be rigid and does not rotate.

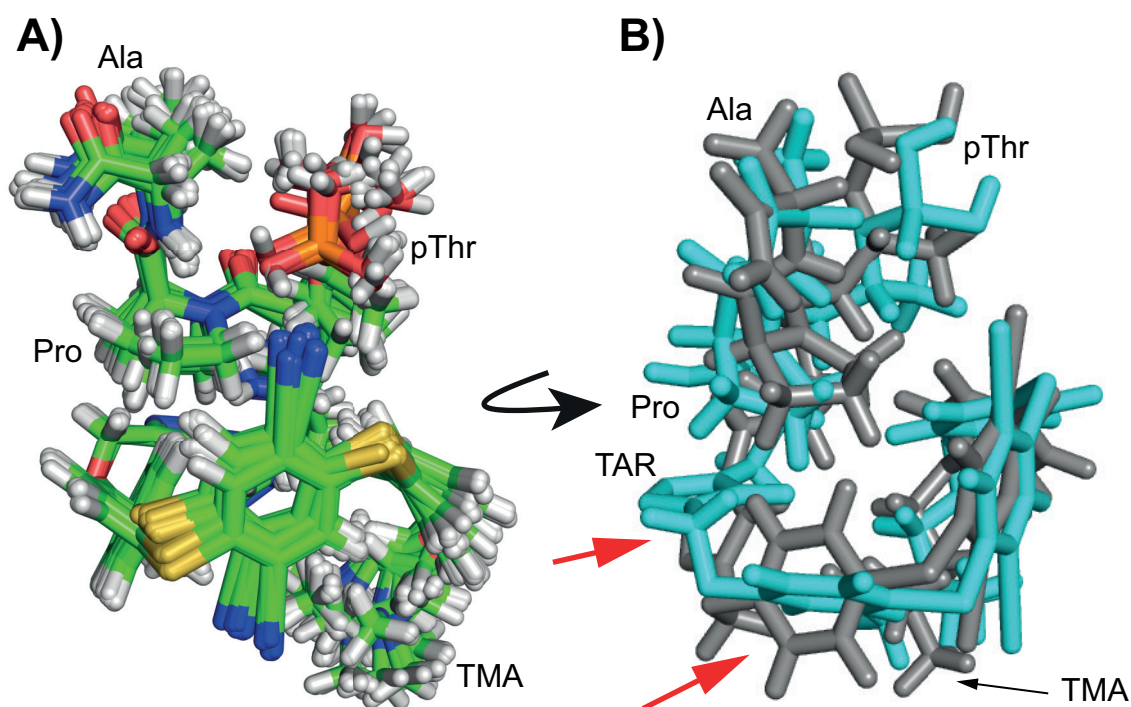


Figure 28: Rotations of the AIE-core in the F10 structure. (A) The best 30 structures from NMR structure calculation shown in stick representation. (B) Two different states from the NMR structure calculation with CYANA. Marked (red arrows) are the two regions which varied the most. The outer phenylene rings were shown to be rotatable, which also moved the triazole ring. TMA: Trimethylamine, TAR: Triazole ring.

5.7 Analysis of the complex structure of *hPin1*-WW with fluorophore F10

After solving the structure of the isolated fluorophore F10, which revealed a cage-like AIE-core, an additional structure of F10 in complex with the *hPin1*-WW domain was calculated. In addition to the fluorescence data, the binding can be seen on a structural level and provided insight into the binding interface and rigidity of the bound AIE-core, completing the study of specific protein binding. For this the *hPin1*-WW domain was expressed and purified doubly labelled (^{15}N and ^{13}C), while the binding partner F10 was synthesized without isotopic labeling. Isotope labeling of one binding partner allows observation of the individual partners in binary complexes and thus discriminates between intra- and intermolecular contacts with the help of filter-edited and double-filtered NOESY spectra. The complex of the *hPin1*-WW domain and F10 was mixed in an equimolar ratio and acquisition parameters were summarized in table A1.

5.7.1 Assignment of intermolecular and intramolecular contacts

Intermolecular contacts between F10 and the *hPin1*-WW domain were detected by aromatic and aliphatic F1(^{13}C -filtered)-F2(^{13}C -edited) 3D-NOESY spectra. With the isotope labeling of the *hPin1*-WW domain, protons were selected or filtered based on the coupled atom. Isotope filtering in the first dimension suppressed protons directly bound to an NMR active heteronucleus (^{13}C - ^1H) and protons bound to inactive nuclei (^{12}C - ^1H) were detected. In contrast, isotope editing in the second dimension selected protons directly bound to an NMR active nucleus [24]. Combining isotope filtering and editing resulted in cross-peaks of fluorophore F10 and the *hPin1*-WW domain (^{12}C - ^1H to ^{13}C - ^1H). The chemical shifts list was imported from an *hPin1*-WW domain apo structure (BMRB: 19528) and adjusted to the secondary and tertiary dimension F2 and F3 (^1H and ^{13}C) of the complex structure using the unfiltered ^{13}C -NOESY spectra. The ^1H dimension, recorded for the fluorophore F10, and shifts were assigned manually with the help of the intramolecular fluorophore cross-peaks obtained from 2D-double filtered NOESY and TOCSY spectra.

Chemical shifts for F10 and distance information of the intramolecular fluorophore contacts were gained by a F1(^{13}C -filtered)-F2(^{13}C -filtered) NOESY (2D-x2NOESY) spectrum. For the assignment of fluorophore protons a F1(^{13}C -filtered)-F2(^{13}C -filtered) TOCSY (2D-x2TOCSY) spectrum was also used. The double filtered spectra suppressed protons bound to NMR-active heteronuclei (^{13}C -H or ^{15}N -H) in both dimensions and resulted in 2D spectra with protons bound to inactive NMR nuclei (^{12}C - ^1H to ^{12}C - ^1H). The superimposed x2NOESY and x2TOCSY in figure 29 show similar peak patterns for the bound fluorophore compared to the isolated fluorophore. The right expansion displays the typical TOCSY pattern for proline, which is shifted upfield by 0.6-1.6 ppm compared to the isolated fluorophore. Due to the peak pattern the chemical shifts were assigned in a similar order as for the isolated fluorophore. The lower expansion shows the aromatic area at 6.6-7.8 ppm with cross-peaks between the AIE-core and H₃, H₂₄, H₂₅ and TMA. Also, here the pattern is similar to the isolated fluorophore and ring protons could be distinguished and assigned manually.

The third set of spectra used, showing both intra-protein and protein-fluorophore NOEs, were the aromatic and aliphatic unfiltered ^{13}C 3D-NOESY, which were picked and assigned automatically by the program UNIO.

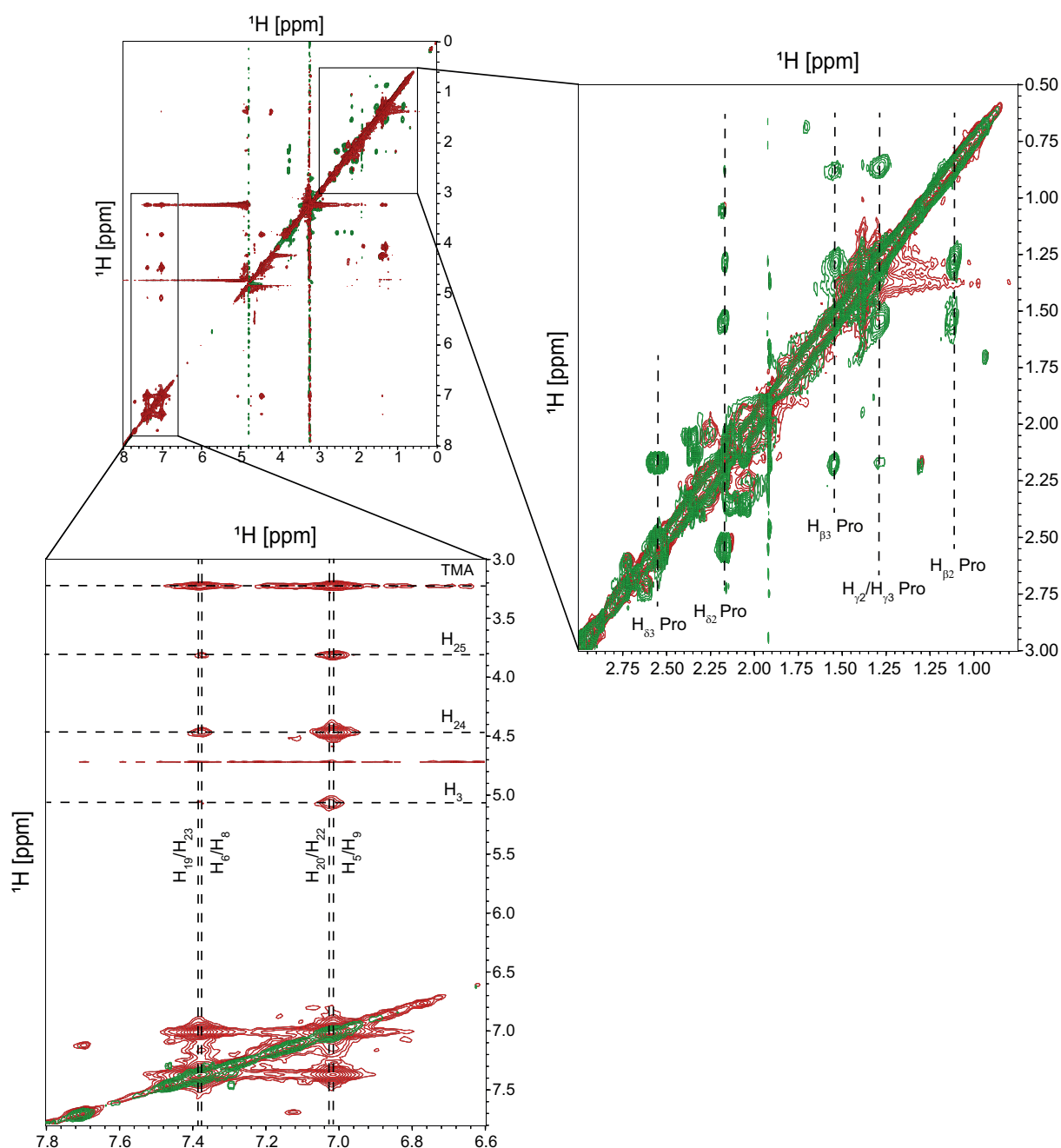


Figure 29: Superposition of the 2D-x2NOESY (red) and 2D-x2TOCSY (green) spectra. The superimposed total spectra are shown at the top left. The right expansion shows the assignment for the proline protons highlighted in the 2D-x2TOCSY. The lower expansion shows the assignment for the aromatic AIE-core highlighted in the 2D-x2NOESY spectra.

5.7.2 Calculation of the NMR complex structure of *hPin1*-WW and F10

The complex structure of the *hPin1*-WW domain and the fluorophore F10 was calculated in cooperation with Dr. Torsten Herrman using the UNIO program. To obtain the WW-domain core structure, known hydrogen bonds for the three antiparallel β -sheets were added from the apo structure (PDB: 2M8I). For the final calculation, intermolecular distance information (35) and intramolecular distances information of the ligand

(22) were given as upper distance limits (.upl). The intramolecular distance information of the protein, however, were given as aromatic and aliphatic ^{13}C 3D-NOESY spectra and were automatically assigned by UNIO (ATNOS/CANDID NOE cross-peak assignment [100, 101]). After 7 cycles of calculation, a total number of 377 upper distance restraints and 10 lower distance restraints were used in combination with 80 dihedral restraints for the final structure. In each cycle 40 structures were calculated. For each structure, the CYANA target function (equation 3) was calculated and the structures sorted in ascending order. The top 20 structures with the lowest target function were selected and output as final ensemble (figure 30). The final ensemble shows an average target function of $2.70 \pm 0.29 \text{ \AA}^2$ and an average backbone RMSD of $0.52 \pm 0.10 \text{ \AA}$. The statistics for the 20 best structures are summarized in table 20.

Table 20: Statistics of the NMR complex structure calculated by UNIO

Parameter	
All upper distance restraints	377
intraresidual ($ i-j = 0$)	86 (22.81%)
sequential ($ i-j = 1$)	57 (15.12%)
medium range ($1 < i-j \leq 4$)	33 (8.75%)
long range ($ i-j \geq 5$)	201 (53.32%)
-intermolecular	35 (9.28%)
Torsion angle restrictions	
ψ -angles	40
ϕ -angles	40
Ramachandran statistics	
favorable	78.64%
additional	19.24%
generously	1.82%
disallowed	0.3%
Average target function value	$2.70 \pm 0.29 \text{ \AA}^2$ (1.99 - 3.14 \AA^2)
Root mean square deviation (RMSD)	
Average backbone RMSD (residues 6-54)	$0.52 \pm 0.10 \text{ \AA}$
Average heavy atom RMSD (residues 6-54)	$1.01 \pm 0.10 \text{ \AA}$

The structures display the typical three antiparallel β -sheets of the *hPin1*-WW domain and the fluorophore is stretched over the top of the β -sheet (figure 30). The pThr-Pro binding motif is recognized as expected by the amino acids S¹⁶, R¹⁷, Y²³ and W³⁴.

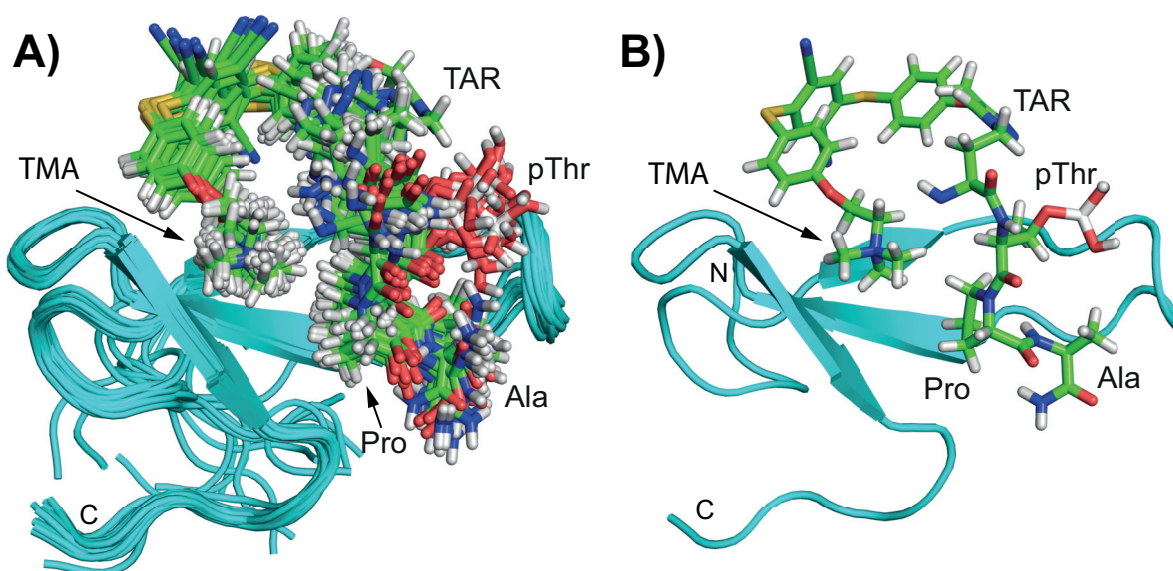


Figure 30: NMR solution structure of *hPin1* in complex with fluorophore F10. (A) The best 20 structures with the lowest target function are shown as cartoon (WW-domain) and sticks representation (fluorophore). **(B)** The best single structure (target function: 1.99 \AA^2) with labeled termini. TMA: Trimethylamine, TAR: Triazole ring.

The fluorophore shows the aromatic rings forming a C-shaped cage-like AIE-core, as it was shown for the isolated fluorophore (figure 27). The TMA and conjugated peptide are directed straight towards the binding site without the helical twist observed in the free fluorophore. The AIE-core shows different motions for the three aromatic rings (figure 30). While the left ring (TMA side) shows no rotation or movement, the other two rings do. The middle ring displays two different states rotated by 180° and visualized by the switching nitrile group. The right ring (peptide side) however, shows multiple rotational states around the ether-thioether axis. The largest movements, however, are shown by the triazole ring. Influenced by the outer ring rotation and resulting steric hindrance, the triazole ring rotates and moves up.

In figure 31 A the coordination of the proline is shown. Here the proline is sandwiched between the amino acids Y^{23} and W^{34} , forming π - π interactions. The phosphoryl group of the neighboring threonine points towards the loop between $\beta 1$ and $\beta 2$, which contains the amino acids S^{16} and R^{17} that were described to bind the phosphoryl group [233]. In this structure, both amino acids were calculated with flexible side chains, due to missing signals.

A detailed view of the AIE-core of the fluorophore reveals another possible face-to-edge π - π interaction between two aromatic rings of the fluorophore and the *hPin1*-WW domain (figure 31 B). The sphere representation displays the side chain of F^{25} being oriented orthogonal to the middle ring and the outer phenylene ring of the fluorophore, forming a face-to-edge π - π interaction and stabilizing the fluorophore binding.

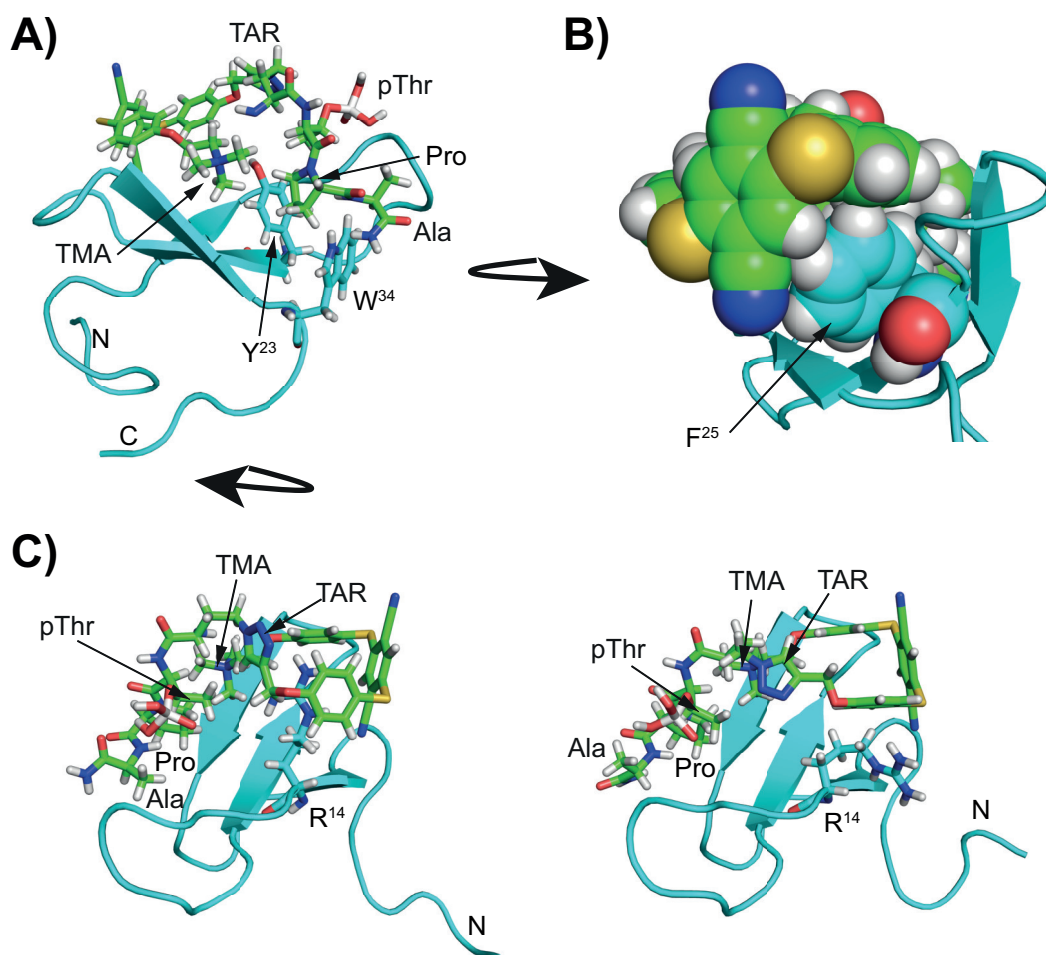


Figure 31: Contacts between the fluorophore F10 and *hPin1*-WW domain. (A) Shown in cartoon representation is the WW-domain with the bound fluorophore in stick representation and the interacting amino acids Y²³ and W³⁴ also as sticks. Additionally labeled are both termini. (B) Close up of the stacking of the phenylene rings with the amino acid F²⁵. The fluorophore and the amino acid F²⁵ are represented as spheres. (C) Interaction of the side chain of amino acid R¹⁴ with the fluorophore F10. The guanidine group of R¹⁴ contacts either all three rings (left) or the fluorophore at a single outer ring (right) by cation- π interaction.

In addition to the ring stabilizing face-to-face π - π interactions by F²⁵, the protein is contacting the aromatic AIE-core by cation- π interaction with amino acid R¹⁴. With rotation of the left outer ring (peptide side) the side chain of R¹⁴ switches between the two conformation states shown in figure 31, C.

In summary, the AIE-core with the aromatic ring structure did not interfere with the binding site of the *hPin1*-WW domain and the peptide arm of the fluorophore was recognized by the protein. With the stretched fluorophore conformation, bound on top of the β -sheet, the fluorophore F10 displays multiple contacts to the protein. The contacts to the aromatic rings will help to understand and explain the molecular restrictions caused by protein binding.

6 Discussion

Since the first mention of aggregation-induced emission (AIE) by the group of B. Z. Tang in 2001, the phenomenon of AIE has become increasingly popular. Multiple molecules featuring the AIE effect (AIEgens) were synthesized for the specific recognition of a wide range of targets including small biomolecules, macromolecules such as proteins and even complete cells.

The focus of this work was the design, synthesis and characterization of new protein specific AIEgens to build up a model system for the specific recognition of the *hPin1*-WW domain and the quantitative analysis of the binding on the basis of new aromatic thioterephthalonitrile (TPN) fluorophores.

6.1 Synthesis of peptide-coupled TPN derivatives

The peptides in this work were successfully synthesized by the fast and efficient solid phase peptide synthesis (SPPS) using Fmoc chemistry [16, 64, 184]. The use of an automated SPPS made it possible to synthesize multiple peptide sequences automatically and simultaneously in a short time without the need for manual purification between coupling steps. High yields of 93-98% were achieved for short peptides up to six amino acids. However, peptides with a longer linker sequence of alternating alanines and glycines exhibited lower coupling efficiency for glycine and consequently reduced yields. Double coupling of each amino acid finally resulted in yields of 88% (P4) or 87% (P5), respectively.

With the exchange of proline to the larger phenylalanine, the yield of peptide P9 decreased to 35%. However, no by-products were identified to account for the loss and also first purification step by ether precipitation did not cause a significant loss of peptide P9, so no reason for the low yields could be identified. Nevertheless, the amount of P9 was sufficient for further synthesis, so no adjustments were made.

The following and final synthesis step for protein specific AIEgens by CuAAC is a well described mechanism to couple molecules by the reaction of alkynes and azides [149]. The reaction works with multiple copper catalysts and in a wide range of solvents, yielding high amounts of product without the need a complicated and time-consuming purification. The most commonly used protocols include CuSO₄ in an aqueous solution and a similar condition was used in this work [201]. The azide-bearing peptides were perfectly soluble in water, but the hydrophobic alkyne-bearing AIE-core was insoluble in H₂O and barely soluble in organic solvents such as THF and DMF. The final mix of H₂O and THF was a necessary compromise to get sufficient yields of fluorophores for the following fluorescence and NMR experiments. Starting the click reaction with concentrations of 2 mg/ml, the alkyne-bearing AIE-core compounds A1 and A2 were poorly dissolved, resulting in low yields of 5-10%. By the simple dilution of reactants, the yields were increased to 50% and could possibly be improved further if needed

by even lower concentrations, optimized solvents and catalysts and higher reaction temperature of 40-70 °C [200,201].

6.2 The new *hPin1*-WW specific fluorophores form a well-defined structure with enhanced solubility and good AIEE properties

In total, five of the six *hPin1*-WW specific fluorophores (F1-F4 and F10) exhibited high solubility and enhanced salt tolerance in an aqueous solution up to the tested concentration of 20 mM and potentially even higher. The NMR solution structure of fluorophore F10 showed that the peptide covered the hydrophobic AIE-core by ring stacking interactions of proline and the aromatic rings (see section 5.6.3, figure 27). As the proline interacts with the aromatic AIE-core, the phosphoryl group is directed outwards where it can interact with the solvent and adds the required hydrophilicity. These were tremendous improvements in solubility and salt tolerance over thioterephthalonitrile (TPN) derivatives such as the disulfonate (DSA) from the group of J. Voskuhl [97].

In contrast to the elongated conformation of the crystal structure of DSA, the peptide-conjugated fluorophore is presented as a partially helically twisted solution structure. As the aromatic substituents of the central ring rotate to face the same side, forming a C-shaped binding groove, the proline interacts with the aromatic rings from above. Proline motifs and proline-rich regions such as the pThr-Pro motif are known to be recognized and bound in aromatic grooves of proteins [308]. Specific proline recognition domains are WW domains [248,250], SRC homology 3 (SH3) domains [202] and Ena/Vasp homology 1 (EVH1) domains [179], which were found as interacting modules for signaling proteins [143]. Induced by the intramolecular contacts the fluorophore forms such a binding groove and binds its own peptide on top of the AIE-core. The fluorophores exhibit only low autofluorescence at working concentration and therefore exhibit good AIEE properties for protein recognition.

The only insoluble *hPin1* specific TPN derivative was fluorophore F5 and it contained the largest non-polar peptide linker. Therefore, the maximum peptide length for TPN derivatives containing non-polar amino acids was considered to be four or five amino acids. When longer linker sequences are present the peptides potentially form a loop or hydrophobic patch that promotes hydrophobic interactions of adjacent fluorophores resulting in insoluble aggregates. However, the maximum peptide length could possibly be prolonged with polar amino acids such as asparagine, glutamine etc., which should be able to interrupt possible hydrophobic stretches and increase the solubility of larger fluorophores.

Control fluorophores containing peptides lacking the pThr-Pro binding motif were either insoluble (F0, F6 and F9) or had poor autofluorescence properties, making them unusable.

How does the structure of the symmetric fluorophore F1 look?

The molecular structure of fluorophore F10 was the first ever solved structure of an AIEgen solved by NMR spectroscopy. However, the calculations for fluorophore F1 were not possible due to the high symmetry of the molecule, which causes ambiguity for almost all NOE restraints.

A detailed analysis of the 2D-NOESY spectra of the fluorophores F1 and F10 revealed a similar peak pattern, suggesting a similar core structure (figure 32 A, B). In contrast to fluorophore F10, the fluorophore F1 contains two identical *hPin1*-WW specific peptides, which led to a highly symmetric molecule with chemically equivalent hydrogens for both the peptides and the aromatic AIE-core. In fact, the signals of all equivalent hydrogens overlapped perfectly and added up to a single peak with double intensity, which caused problems during structure calculation. Even with locked and manually double picked and assigned cross peaks the CYANA program was not capable of calculating a structure. Therefore a model for fluorophore F1, based on the structure of F10, was manually build with the program Pymol (figure 32 C).

Using the calculated structure of the isolated fluorophore F10 as a starting model, the functional TMA group was replaced by a second identical peptide fused to a triazole ring. Using the center of the middle ring as mirror point, the peptide was built below the aromatic ring system. Building the fluorophore as a point symmetric molecule, the second peptide exhibited the opposite conformation (R-conformation) of the first peptide. However, the model is just a proposal based on the NMR peak pattern and is intended to give only a visual overview of a possible symmetric fluorophore structure and help to understand fluorescence properties.

In contrast to fluorophore F10, the aromatic hydrogen signals of the left and right phenylene ring were no longer distinguishable. Assuming a similar C-shaped core, the peptide arms would be in close proximity, not forming a symmetric molecule and in addition causing steric hindrance. As a result, the aromatic rings probably no longer form a C-shaped AIE-core, but an S-shaped AIE-core. From the fluorescence and NMR titration experiments it was shown that the fluorophores F1-F4 can bind one WW domain on each of the two peptide arms and with the S-shaped ring conformation the AIE-core would act as the needed spacer between the two *hPin1*-WW domains.

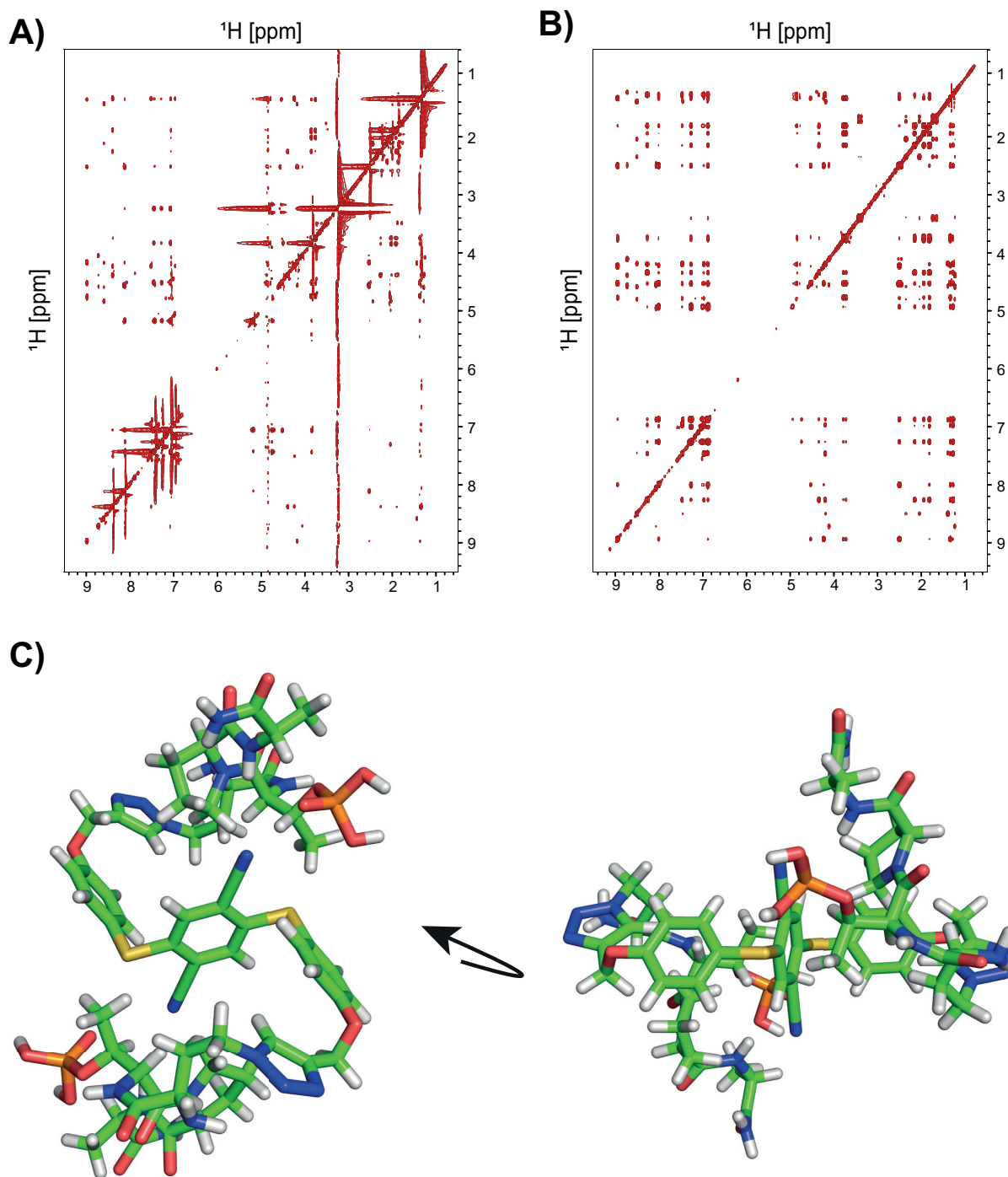


Figure 32: Model of the fluorophore F1. (A) Peak pattern of the 2D-NOESY spectrum from fluorophore F10. (B) Peak pattern of the 2D-NOESY spectrum from fluorophore F1 reveals a similar pattern of cross-peaks. (C) Model of the molecular structure from fluorophore F1, built with Pymol.

6.3 The newly designed AIEgens bind specifically to the *hPin1*-WW domain

The main goal of this work was the design and synthesis of protein specific AIEgens based on thioterephthalonitriles and the implementation of a fluorescence assay with direct read-out to detect and analyze binding to the *hPin1*-WW domain. The specific recognition of the peptide arm of the fluorophores was successfully demonstrated with an NMR titration experiment.

In NMR titration experiments the chemical shift perturbations of the *hPin1*-WW domain upon fluorophore binding were similar for all tested fluorophores (F1-F4 and F10) and analysis of the resulting binding curves resulted in binding constants in a low μM range, which were comparable to published peptides and peptide-covered nanoparticles [224, 269]. Small differences were only found in the maximum shift perturbation of selected amino acids in the first loop (K¹³ and R¹⁴) and the middle strand of the β -sheet (V²² and Y²³), indicating no major differences in ligand binding, but potentially additional contacts to the WW domain (discussed in section 6.4 and shown in figure 33, 34 C).

In addition to the NMR titrations, the fluorescence titration experiments also displayed specific binding curves for all fluorophores. However, after reaching saturation the fluorescence intensity increased again at higher protein concentrations, indicating further unidentified molecular restriction of the fluorophores. Along with a hypsochromic shift of the emission maximum (section 5.4.2, figure 19), the additional increase of fluorescence intensity could result from additional unspecific protein-protein or protein-fluorophore contacts. As seen for the fluorescence of tryptophan, the emission wavelength can be sensitive to changes in the close environment. [188, 270]. For the TPN derivatives, undefined and unknown contacts such as hydrophobic interactions and higher aggregation are possible explanations for the phenomenon of shifting maximum and additional fluorescence increase.

In comparison to the NMR spectroscopy, the fluorescence titration experiments can be performed at lower concentrations, making the K_D calculation more precise. With the relatively high concentration in NMR experiments needed for sufficient signal intensity, the fluorophore concentration is significantly higher than the binding constant of the *hPin1*-WW domain. Moreover, in fluorescence titration experiments twice the number of data points were recorded, making the binding curves and K_D calculations more accurate.

Overall, all designed fluorophores bound via the coupled peptides to the *hPin1*-WW domain as intended, resulting in good low μM K_D values and proving the assumed binding models of 2 proteins binding a single fluorophore molecule carrying two peptides (2:1 for F1-F4) and a single protein binding the fluorophore F10 with a single peptide.

6.3.1 A short peptide exhibits better binding properties

As described in the previous part, the increase of linker length did not affect the protein binding or maximum fluorescence intensity at low fluorophore concentrations ($\leq 25 \mu\text{M}$). However, it affected the binding stoichiometry at higher fluorophore concentrations ($\geq 100 \mu\text{M}$). At the same fluorophore concentrations, the autofluorescence intensity also increased drastically with linker length, indicating a possible correlation. At low concentrations, the fluorophore molecules are assumed to be perfectly dissolved and to form just few intermolecular contacts. At higher concentrations however, the fluorophore interacts with other adjacent fluorophore molecules and possibly forms water-soluble aggregates. The soluble aggregates are only visible at concentrations above $600 \mu\text{M}$ and in combination with UV-light (17 B). Here the fluorescence was concentrated at the bottom of the cuvettes, showing a heterogeneous distribution of fluorophore molecules. The interacting fluorophore molecules and possible soluble aggregates are blocking protein binding sites and therefore influencing the established 2:1 binding model.

Interestingly, the effect of changing stoichiometry was not observed in NMR titrations, where the fluorophore concentration was even higher, up to 1 mM. However, in fluorescence titration experiments the protein is titrated to a defined fluorophore concentration ($10\text{-}200 \mu\text{M}$) and in NMR titrations the fluorophore is titrated to the protein ($400 \mu\text{M}$). Since the fluorophore is at an equilibrium between fully dissolved and soluble-aggregated molecules, the excess of the *hPin1*-WW domain removes the fully dissolved fluorophores from equilibrium, thus shifting the equilibrium toward the fully dissolved fluorophores. As a result, the fluorophore molecules can bind the protein with the expected stoichiometry.

In summary, the TPN fluorophore in combination with a relatively short peptide such as the peptide P1 showed the best results for protein binding, resulting in a soluble fluorophore with low autofluorescence, a large working concentration range up to $50 \mu\text{M}$ and a significant increase of fluorescence upon protein binding.

6.3.2 The asymmetric and single peptide-conjugated fluorophore F10 is less emissive upon protein binding

In the next step the influence of a single protein binding event on the fluorophore was investigated with the asymmetric fluorophore F10. However, the induced fluorescence signal was significantly lower than for the symmetric fluorophores F1-F4 and could barely be used for the quantitative analysis of protein binding. F10 displayed similar binding properties to F1-F4 and could be used in a similar concentration range, but only with a total fluorescence increase of $\approx 50\%$ compared to the other fluorophores. Assuming an elongated fluorophore molecule the *hPin1*-WW domain was expected to restrict just a single rotational thioether bond, with the other bond reaching out and

being completely unrestricted. However, the complex structure demonstrated a completely different C-shaped fluorophore conformation and two restricted rotary bonds (discussed in the next section). Therefore, it is expected that the fluorophore is almost completely restricted upon protein binding. As discovered later, the general quantum yield for the TMA-conjugated AIEgen A2 was lower compared to A1 (figure 11, oral communication from J. Voskuhl), making F10 not comparable to F1-F4.

However, a detailed look into the binding curves of the symmetric fluorophores F1-F4 showed a linear initial increase of fluorescence, indicating a consistent restriction without differences between the first and second protein bound to the fluorophore. Therefore, the fluorescence signal was assumed to be induced equally for every protein bound to a fluorophore molecule. As a result, a similar quantum yield for F10 should result in a fluorescence signal with 50% intensity compared to the tested fluorophores F1-F4.

6.4 The fluorophore F10 binds on top of the *hPin1*-WW domain

In this work the structure of the *hPin1*-WW domain in complex with an AIEgen was solved, which represents the first structure of an AIEgen in complex with its target protein. In recent years multiple structures of the *hPin1*-WW domain as apo structure and in complex with target peptides were solved and characterized by both crystallography and NMR spectroscopy [167, 249, 287], and allow a comparison of the ligand binding mode.

The peptide arm interacted as expected with the amino acids S¹⁶, R¹⁷, Y²³ and W³⁴ and the asymmetric TPN-based fluorophore F10 binds on top of the *hPin1*-WW domain. Small peptide sequences of known biological target proteins are all bound in a similar area as the F10 peptide, but the AIE-core of F10 contributes additional interactions (figure 33). The tau peptide (figure 33 C) and the CDC25 peptide (figure 33, D) barely contact the *hPin1*-WW domain except for the binding area around amino acids R¹⁷ and W³⁴ and are therefore quite flexible [287]. In contrast, fluorophore F10 is bound more rigidly (figure 33 A), and similar to the Smad3 peptide (figure 33 B) [8], with additional contacts to the side chains of amino acids R¹⁴ and F²⁵.

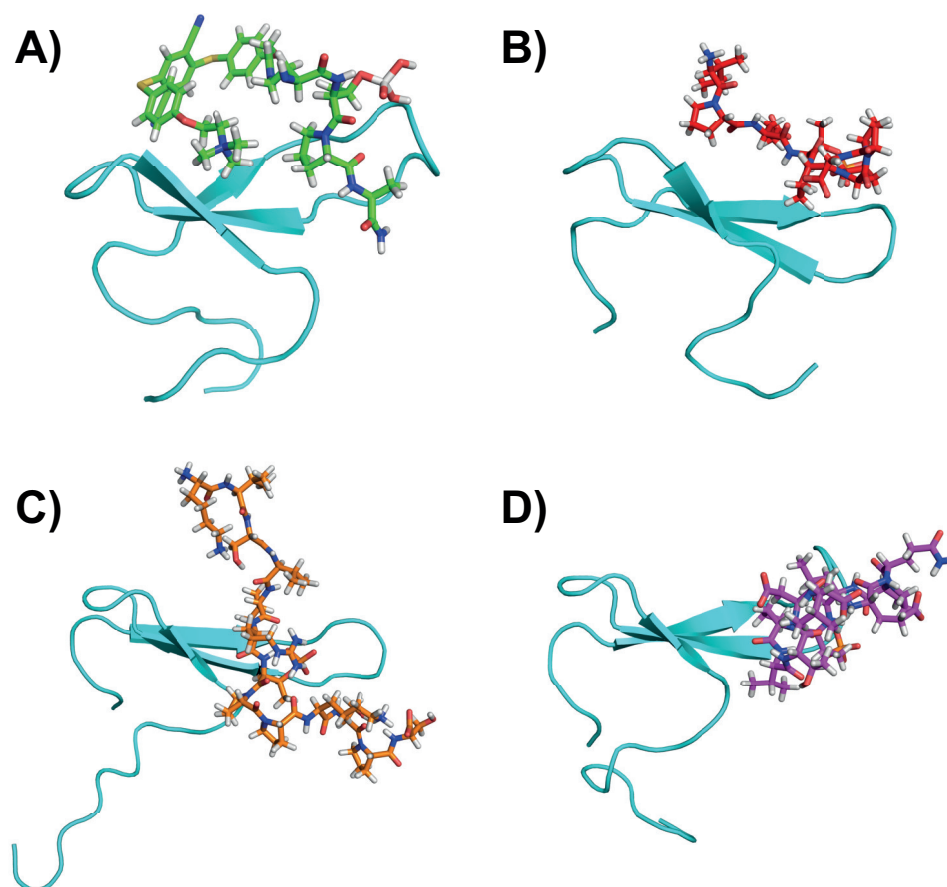


Figure 33: Comparison of *hPin1*-WW complex structures and ligand binding. NMR solution structure of the *hPin1*-WW domain in complex with the (A) fluorophore F10, (B) Smad3 peptide (IPEpTPPPG, PDB: 2LB3) [8], (C) tau peptide (KVSVVRpTPPKSPS, PDB:118H) [287] and (D) CDC25 peptide (EQPLpTPVTDL, PDB: 118G) [287]. The AIE coupled peptide with the pThr-Pro binding motif is recognized by the *hPin1* WW domain and the AIE core is bound from above with additional contacts to the WW domain.

A detailed analysis of the contacts between fluorophore F10 and the *hPin1*-WW domain (figure 34) revealed both minor and major conformational changes of amino acid side chains compared to the *hPin1*-WW apo structure (PDB: 2M8I). Residues Y²³ and W³⁴ form the typical XXX-Pro binding groove of WW domains, which is often flanked by loops giving the WW domain its specificity for defined proline motifs [308]. Residue Y²³ is in the same conformation in all but a single structure [287]. With small adjustments of around 1 Å the tyrosine adapts to the proline of the ligand forming a ring stacking interaction. The side chain of amino acid W³⁴ was oriented differently in all structures and the side chain shifted up to 7.8 Å compared to the apo structure of Luh *et al.* (figure 34 A) [167]. With the highly flexible W³⁴ the protein can adapt to different substrate sequences around the pT-P binding motif and avoid steric hindrance.

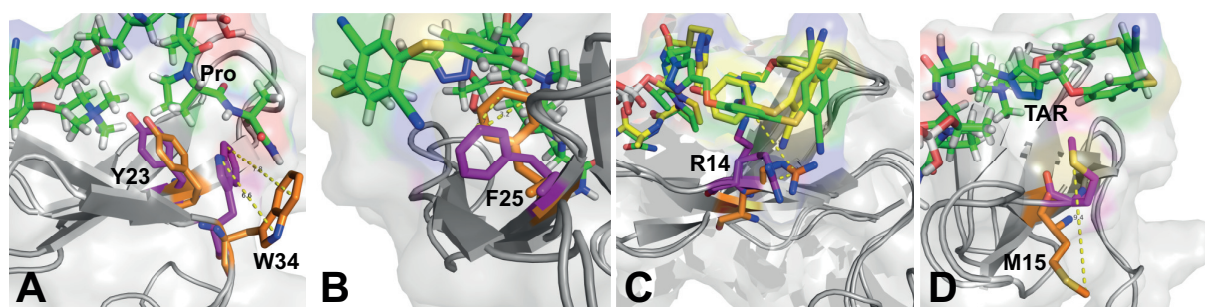


Figure 34: Protein changes upon fluorophore binding. Comparison of the complex structure and the *hPin1*-WW apo structure (PDB: 2M8I). The structures with the lowest target function are aligned and shown as cartoon representations. The fluorophore F10 (green) and selected amino acids of *hPin1*-WW (complex: purple and 2M8I: orange) are shown as sticks. **(A)** Binding of the proline by the side chains of amino acids Y²³ and W³⁴. **(B)** Binding of the aromatic AIE ring system by the phenyl ring of amino acid F²⁵. **(C)** Different orientations of the amino acid R¹⁴ upon fluorophore (green and yellow) binding. The guanidine group of R¹⁴ binds the fluorophore by cation- π interactions with the aromatic ring system. **(D)** Flip of the amino acid M¹⁵ towards the fluorophore F10. TAR: Triazole ring.

As expected, amino acids located in the unstructured loop regions such as W³⁴ are more flexible and changed more upon fluorophore binding than the side chain of e.g. Y²³ within the β -sheet. The side chain of residue R¹⁷ is described as the additional recognition residue for phosphorylated substrates [216]. The arginine residue is not assigned in the NMR spectra, because its signal is absent in the ¹⁵N-HSQC. Therefore, its position is not well defined in the structure.

In addition to the recognition site, consisting of residues S¹⁶, R¹⁷, Y²³ and W³⁴, the fluorophore contacts the *hPin1*-WW domain with the aromatic ring system causing small structural changes in the side chains of the protein at residues F²⁵ and R¹⁴ (figure 34 B, C). The phenylalanine F²⁵ rotated down 2-3 Å into the cleft formed by the middle ring and the right (TMA side) phenylene ring of the AIE-core. Here F²⁵ formed face-to-edge π - π interactions with both rings and restricted molecular rotations of the AIE-core. A similar stabilizing effect of F²⁵ was only seen for the complex structure containing the Smad3 peptide (IPEpTPPPG), in which the phenyl ring forms a face-to-edge ring stacking interaction with the first proline of the peptide [8].

Due to similar binding on top of the WW domain, both the Smad3 peptide and fluorophore F10 made contact with residue R¹⁴. For the Smad3 peptide, the guanidine group of R¹⁴ of the *hPin1*-WW domain forms a salt bridge with the glutamic acid of the Smad3 peptide. In contrast, the calculated complex structure in this work exhibited two possible conformations for R¹⁴, both forming a cation- π interface with the phenylene rings of F10. In this work the structure with the lowest target function (1.99 Å²) displayed the arginine, similar to the structure with the Smad3 peptide, pointing to the outside and contacting just the left outer phenylene ring (peptide side) of fluorophore F10. Other conformational states exhibited the guanidine group in the middle of the

phenylene rings, possibly forming equal interactions with all three aromatic rings (figure 34 C).

Unique for the new complex structure is the conformation of M¹⁵ (figure 34 D). In all known structures (apo and complex structures) the side chain is pointed downwards, but here the amino acid exhibited a flipped conformation, pointing up to the triazole ring of the fluorophore (figure 34 D). Methionine-aromatic interactions were first mentioned by bioinformatics studies [189, 190] and were shown to stabilize protein folding [266]. With the upwards flip the side chain, sulfur is in close proximity to the triazole ring and the left outer phenylene ring (peptide side) displaying the potential of a similar interaction and an additional contact of the protein-fluorophore interface. This contact is supported by several intermolecular NOEs between the M¹⁵ methyl group and the aromatic protons and the connected methylene group of F10 (Q3, see figure 25).

Summing up the calculated complex structure, the fluorophore is bound on top of the *hPin1*-WW domain covering almost the complete upper protein surface. The peptide arm was recognized as expected with the aromatic ring system making additional contacts to the β -sheet. The additional contacts explain the molecular restrictions of the AIE-core that finally induce the AIEE effect and result in the fluorescence signal. With the additional π - π interactions of F²⁵, the right (TMA side) phenylene ring and middle aromatic ring are bound in two different states, rotated by 180°. The missing intermediate states indicates a strictly bound fluorophore without rotations during protein binding. However, rotations can happen between the bound and unbound conformations, resulting in the chemically equal hydrogens in NMR spectroscopy. In contrast, the left outer (peptide side) phenylene ring is bound to the protein in multiple conformations, indicating a partly rotatable phenylene ring and resulting in less molecular restriction of the aromatic AIE-core.

Overall, the TPN-based fluorophore cores (A1 and A2) were successfully modified with *hPin1* specific peptides, resulting in AIEgens with excellent solubility and good AIEE properties upon protein binding. The specific recognition of the *hPin1*-WW domain as a model system for protein binding was demonstrated by both NMR- and fluorescence titration experiments and proved the usability of TPN-based fluorophores for specific protein recognition. At low fluorophore concentrations the fluorophores perfectly recognized the *hPin1*-WW domain and binding induced a significant increase in fluorescence. In general, the symmetric fluorophore F1 with two peptide arms and no additional linker sequence showed the best binding properties with good AIEE properties and a wide concentration range for the recognition of proteins. In addition to the fluorescence data, the specific recognition of the F10-coupled peptide was shown on a structural level and compared to other *hPin1*-WW complex structures. The NMR solution structure is the first structure of an AIEgen in complex with its target protein and showed the AIE-core bound on top *hPin1*-WW domain, making additional contacts.

7 Outlook

New and unique thioterephthalonitrile AIEgens were successfully modified and tested for specific recognition of the *hPin1*-WW domain, shown by a fluorescence assay with direct read-out. With the proven applicability of the fluorophores for protein detection and quantitative binding analysis, the TPN fluorophores can be adapted for further target proteins and other macromolecules. By varying the new peptide-coupled TPN fluorophores and coupling other peptide sequences or supramolecular ligands such as the GCP motif [237] or molecular tweezers [18], the fluorophores can be used to detect and characterize numerous proteins with known binding motifs.

Since the quantum yield of A2 was lower compared to A1 and the AIEE properties of F10 were worse than those of F1, a two-arm fluorophore is preferred. However, the group of J. Voskuhl increased the quantum yield of single-arm fluorophores by replacing the functional TMA group with another aromatic ring (not published, oral communication from J. Voskuhl). With similar quantum yields the single-arm fluorophore could offer steric advantages for the binding of larger proteins and proteins with deeper binding sites.

In addition, the cellular uptake of TPN-based fluorophores could be optimized by adding small peptide sequences containing cellular target sequences such as nuclear localization signals (NLS) or mitochondria target signals (MTS). This would lead to improved and regulated cellular uptake that would no longer depend on the substitution pattern [221]. One group of classic NLS is the monopartite (MP) class [22], which consists of small sequences of four to eight mainly basic amino acids. A typical MP NLS is the sequence K(K/R)X(K/R) [203] with X being any amino acid or PKKKRKV [2]. The signal sequences could be used as a linker between the binding motif and the AIE-core or replace one peptide completely, making the fluorophore a dual targeting AIEgen.

Finally, during the process of structure calculation of the *hPin1*-WW domain in complex with fluorophore F10, the UNIO program was updated by Dr. Torsten Herrmann. The program can now be used for complex structures exhibiting non-natural amino acids, e.g. proteins in complex with their small natural or non-natural inhibitors.

8 Appendix

8.1 NMR spectroscopy

8.1.1 Acquisition parameter of NMR spectra

Table A1: Acquisition parameter of NMR spectra. NS: number of scans, SW: spectral width, TD: data acquisition size (size of fid), MT: mixing time.

Spectrum Pulse program	NS	SW [ppm]			TD		
		F3	F2	F1	F3	F2	F1
¹H-1D zgesgp	256			16			32768
¹H,¹H-COSY cosygpprqf	64		16	16		2048	512
¹H,¹H-TOCSY dipsi2etgpsi19 (MT: 150 ms)	64		16	16		2048	512
¹H,¹H-NOESY dipsi2etgpsi19 (MT: 200 ms)	160		16	16		2048	512
¹H,¹⁵N-HSQC hsqcetf3gpsi2	4		16	28		2048	256
¹H,¹³C-Ali-NOESY c13noesy_ks_600MHz (MT: 100 ms)	24	14	40	14	2048	64	128
¹H,¹³C-Aro-NOESY aronsyhsqc_ks (MT: 100 ms)	8	14	14	40	2048	200	90
¹H,¹³C filtered-edited Ali-NOESY noesyhsqcgpwgx13d (MT: 100 ms)	32	14	40	14	2048	64	128
¹H,¹³C filtered-edited Aro-NOESY noesyhsqcgpwgx13d (MT: 100 ms)	32	14	35	14	2048	64	128
¹H,¹H double filtered TOCSY dipsigpphwx13d (MT: 150 ms)	128		14	14		4016	512
¹H,¹H double filtered NOESY dipsigpphwx13d (MT: 100 ms)	128		15	15		2048	512

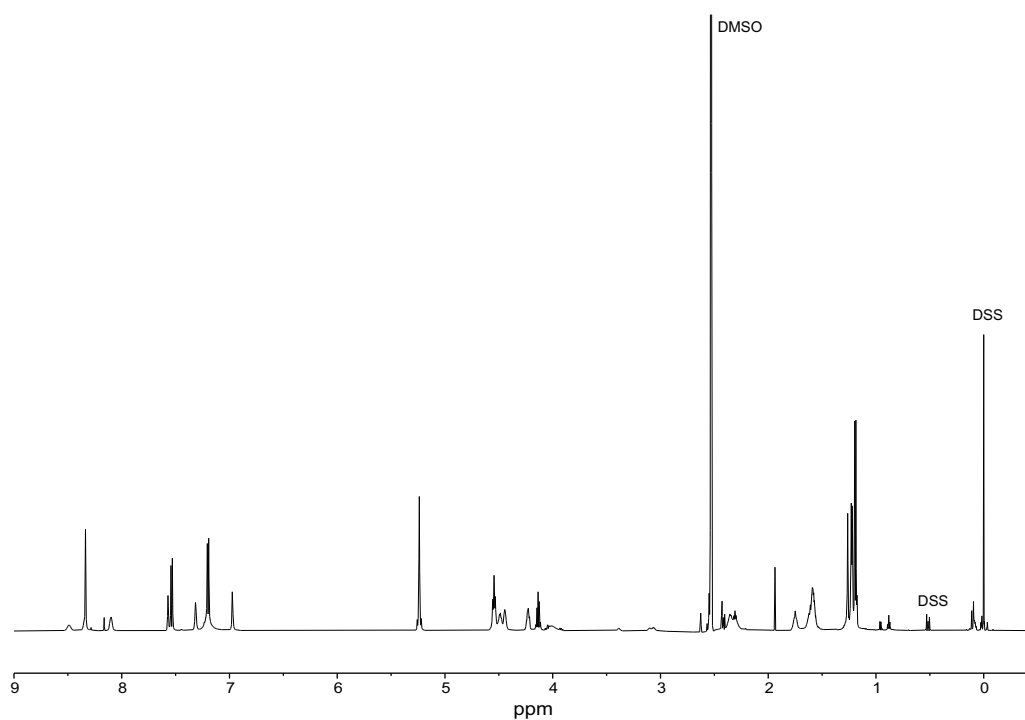
8.1.2 $^1\text{H-NMR}$ spectra

Figure A1: $^1\text{H-NMR}$ spectra of fluorophore F0 (700 MHz, 10 % $\text{D}_2\text{O}/\text{H}_2\text{O}$).

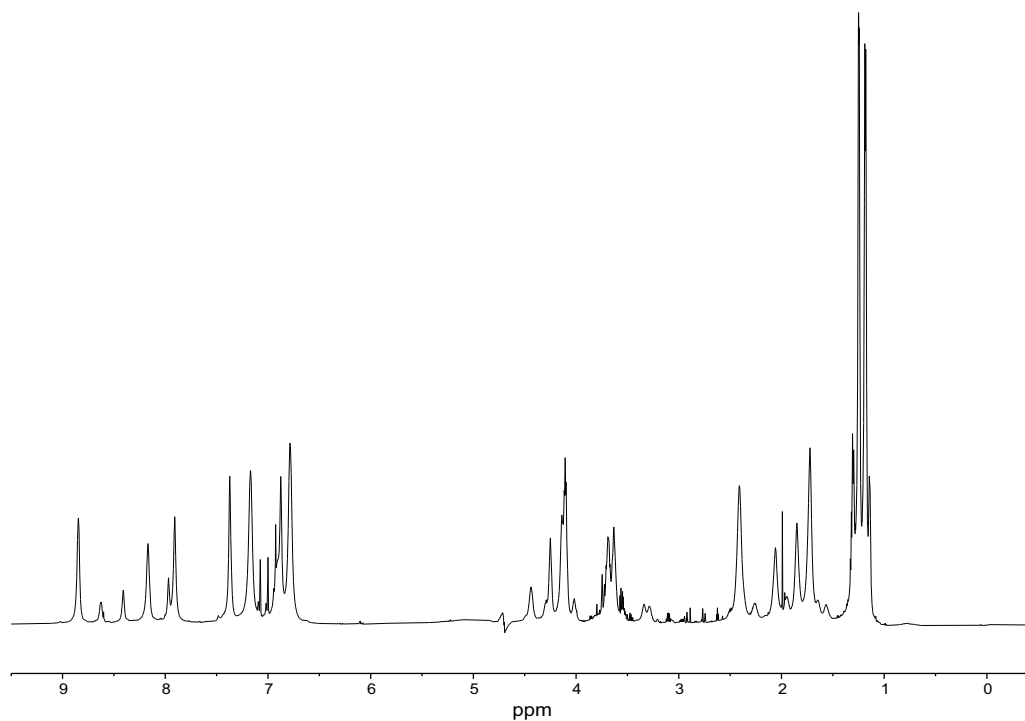


Figure A2: $^1\text{H-NMR}$ spectra of fluorophore F1 (700 MHz, 10 % $\text{D}_2\text{O}/\text{H}_2\text{O}$).

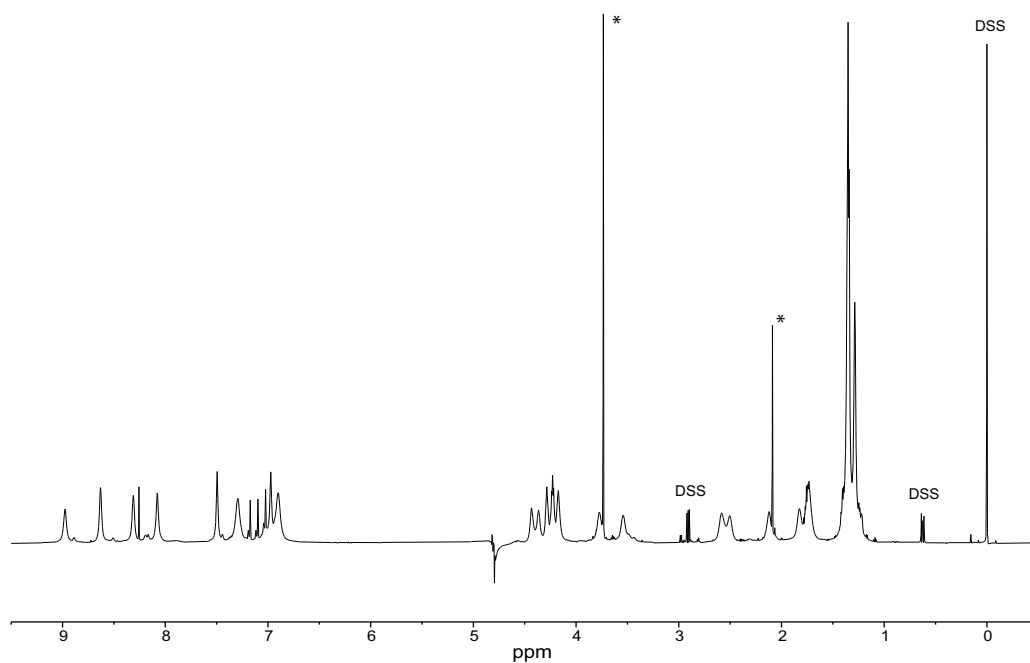


Figure A3: $^1\text{H-NMR}$ spectra of fluorophore F2 (700 MHz, 10% $\text{D}_2\text{O}/\text{H}_2\text{O}$). (*) Unknown contamination.

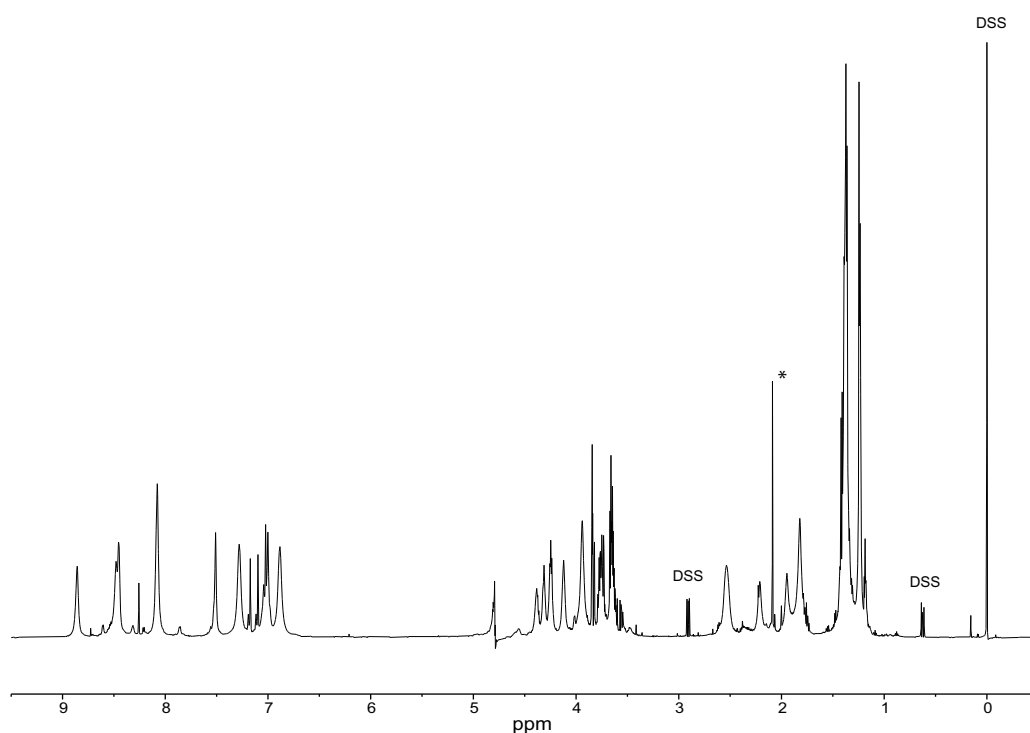


Figure A4: $^1\text{H-NMR}$ spectra of fluorophore F3 (700 MHz, 10% $\text{D}_2\text{O}/\text{H}_2\text{O}$). (*) Unknown contamination.

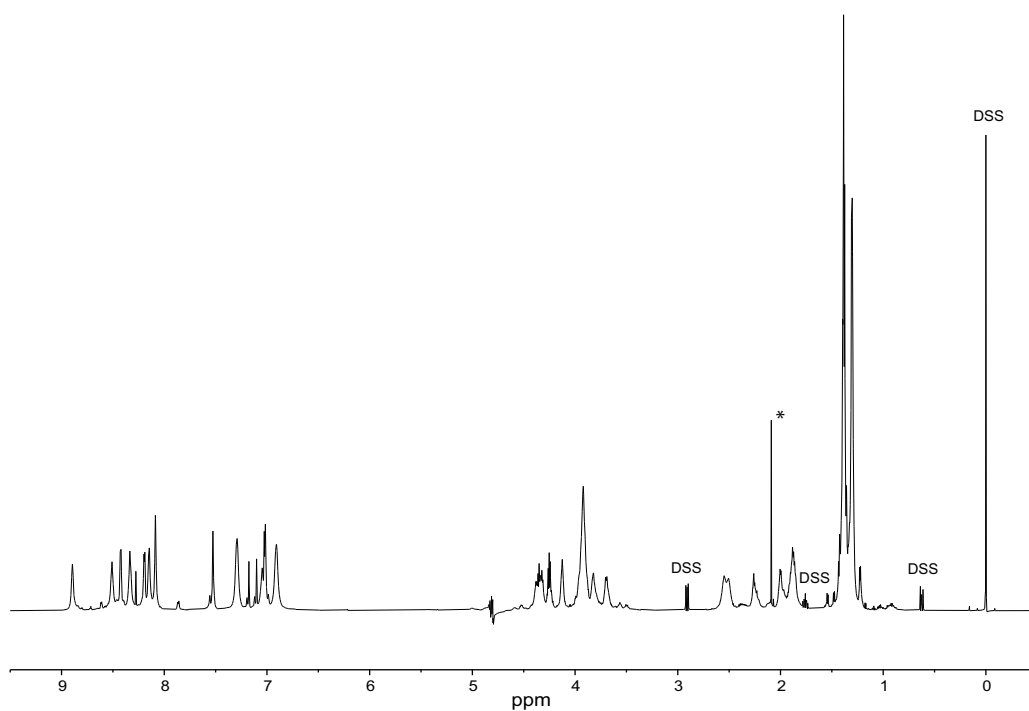


Figure A5: ¹H-NMR spectra of fluorophore F4 (700 MHz, 10 % D₂O/H₂O).(*) Unknown contamination.

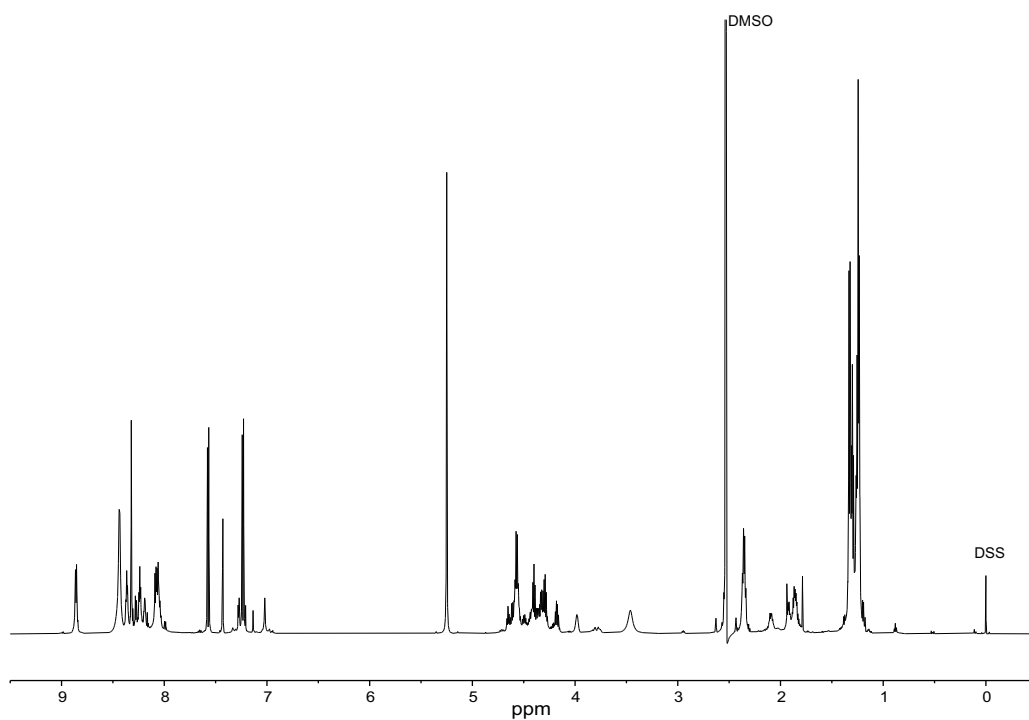


Figure A6: ¹H-NMR spectra of fluorophore F5 (700 MHz, DMSO).

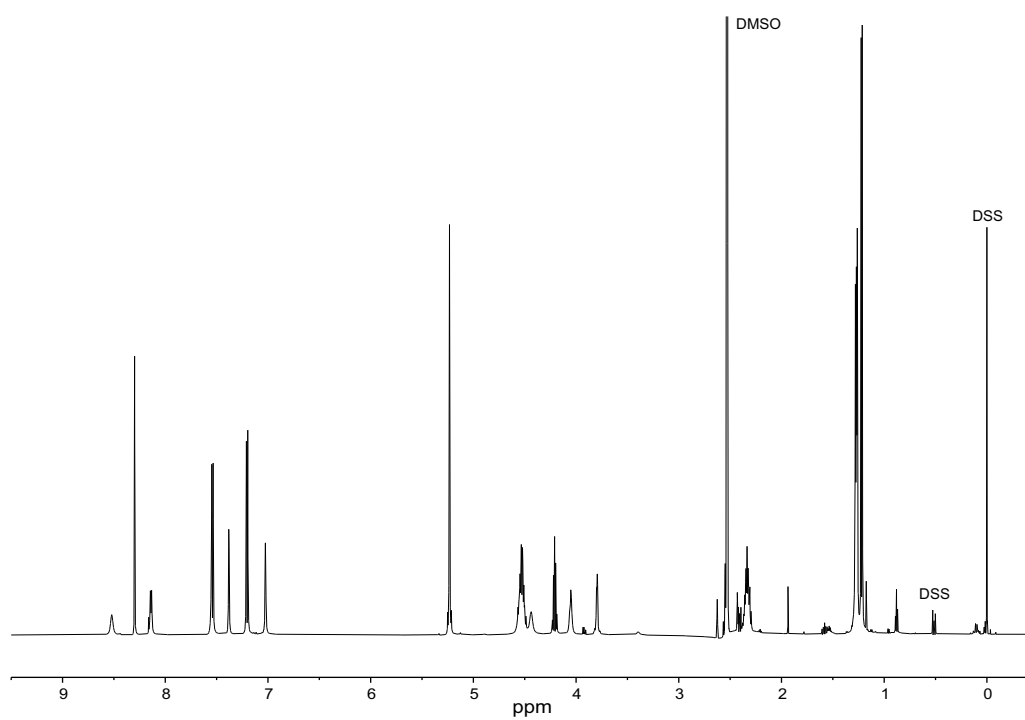


Figure A7: $^1\text{H-NMR}$ spectra of fluorophore F6 (700 MHz, DMSO).

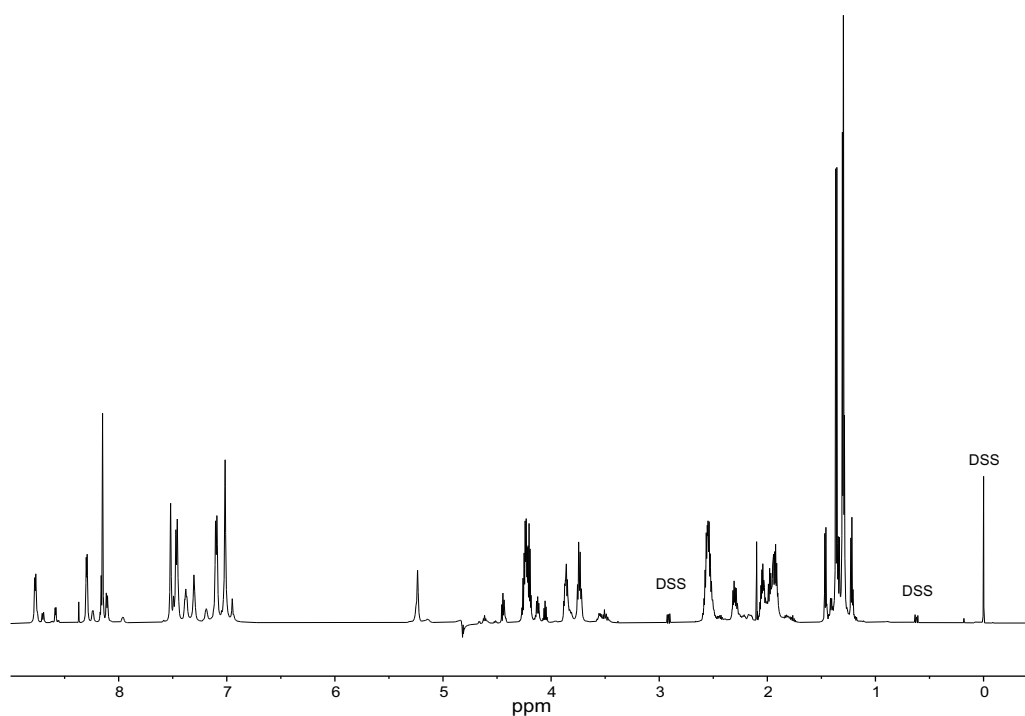


Figure A8: $^1\text{H-NMR}$ spectra of fluorophore F7 (700 MHz, 10% $\text{D}_2\text{O}/\text{H}_2\text{O}$).

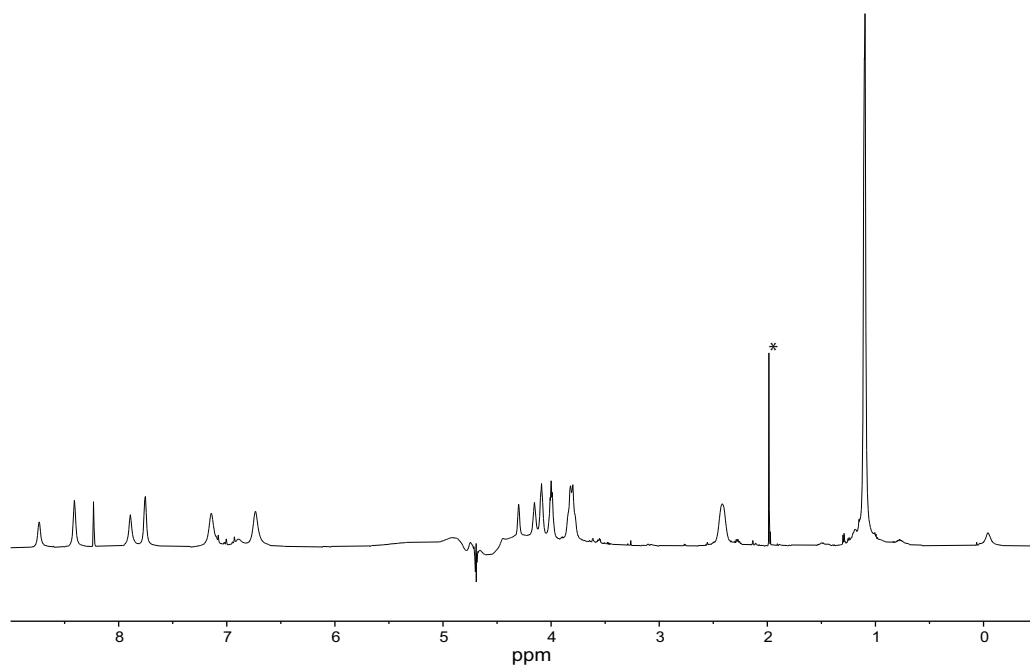


Figure A9: ¹H-NMR spectra of fluorophore F8 (700 MHz, 10% D₂O/H₂O).(*) Unknown contamination.

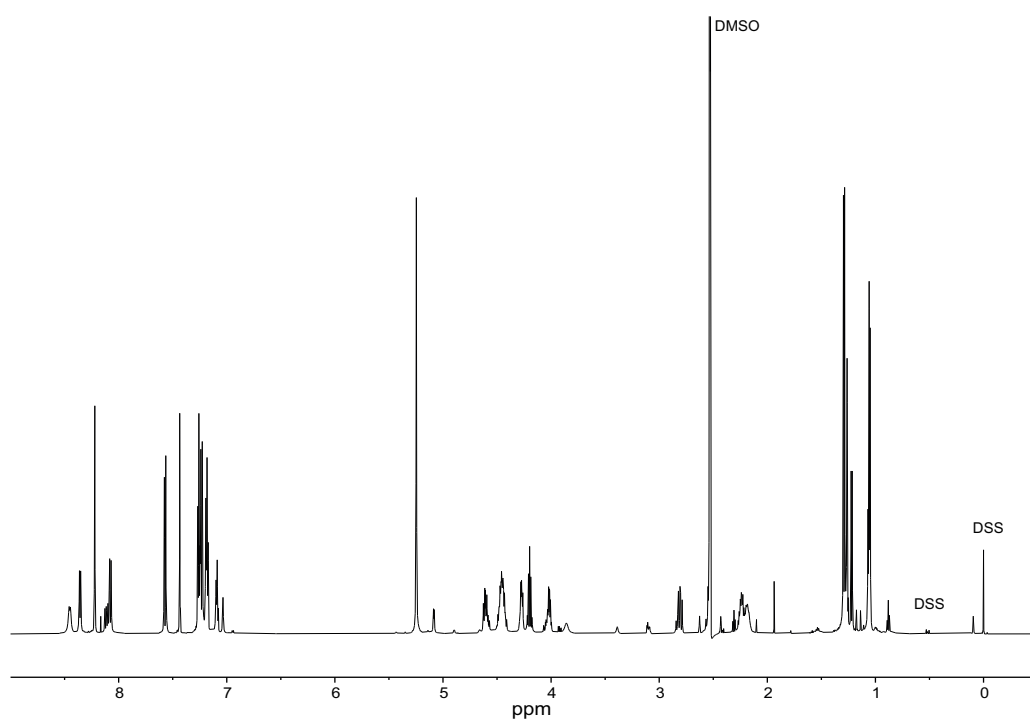


Figure A10: ¹H-NMR spectra of fluorophore F9 (700 MHz, DMSO).

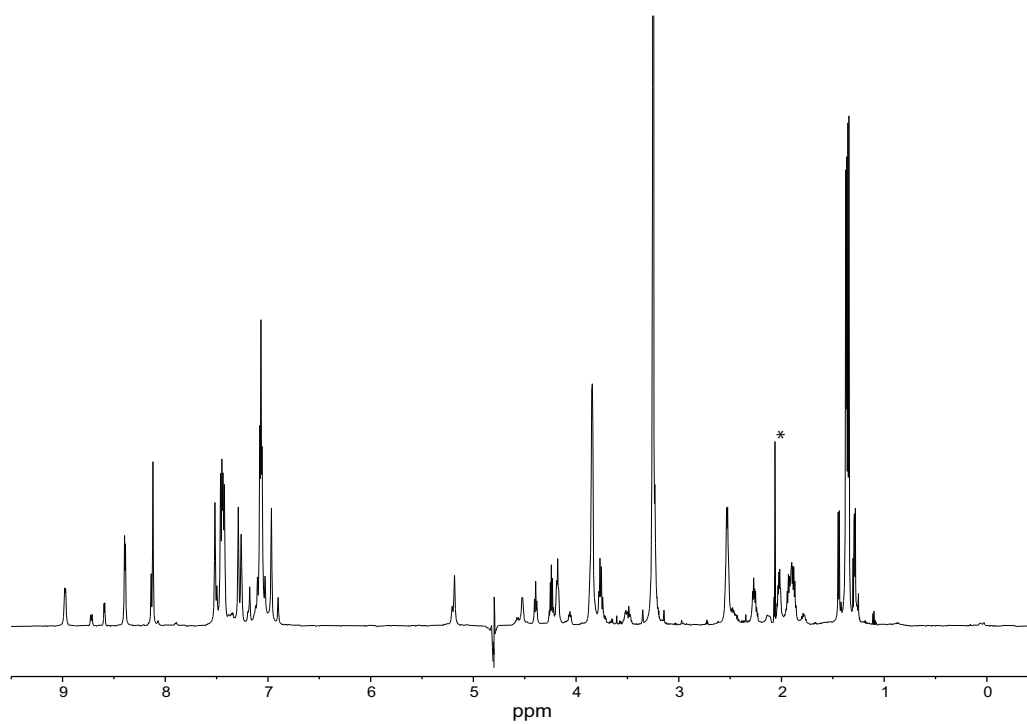


Figure A11: ¹H-NMR spectra of fluorophore F10 (700 MHz, 10 % D₂O/H₂O).(*) Unknown contamination.

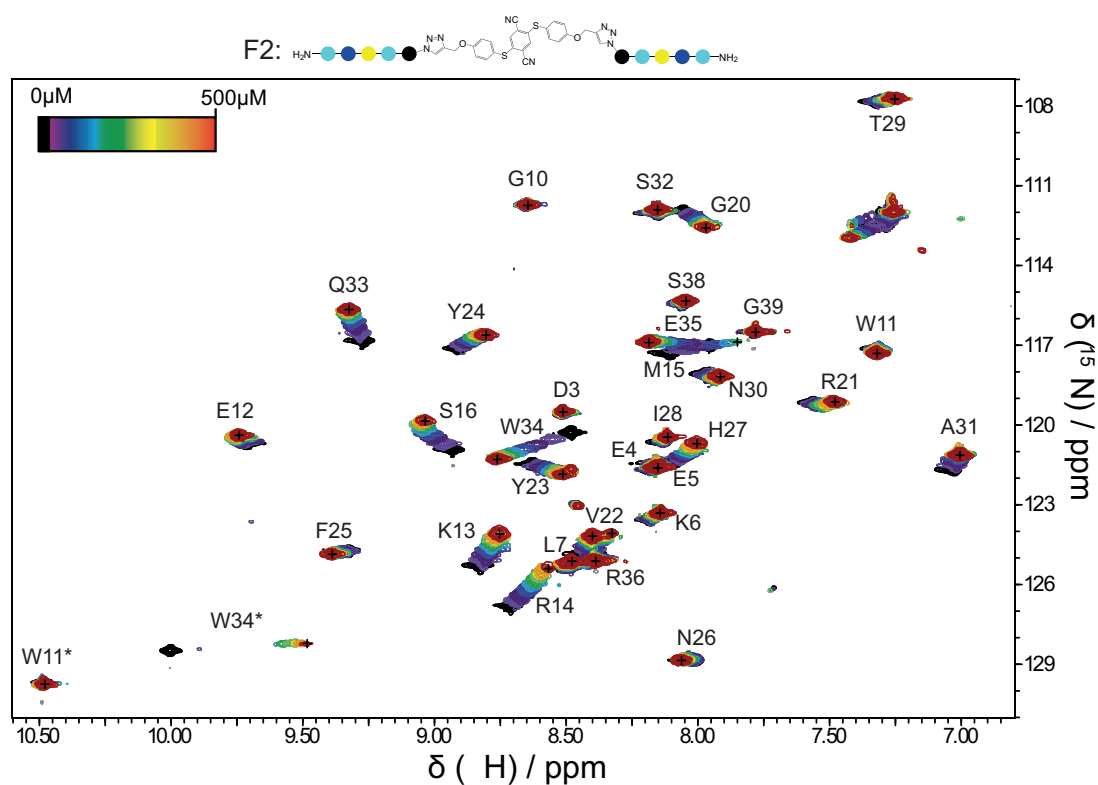
8.1.3 $^1\text{H}, ^{15}\text{N}$ -HSQC titration experiments

Figure A12: $^1\text{H}, ^{15}\text{N}$ -HSQC titration spectra of *hPin1*-WW domain with fluorophore F2. Shown are the $^1\text{H}, ^{15}\text{N}$ -HSQC spectra from the *hPin1*-WW domain with increasing concentration (0-500 μM) of fluorophore F2. In addition to the backbone amides, the side chain amides of W¹¹ and W³⁴ are labelled with an additional star (*).

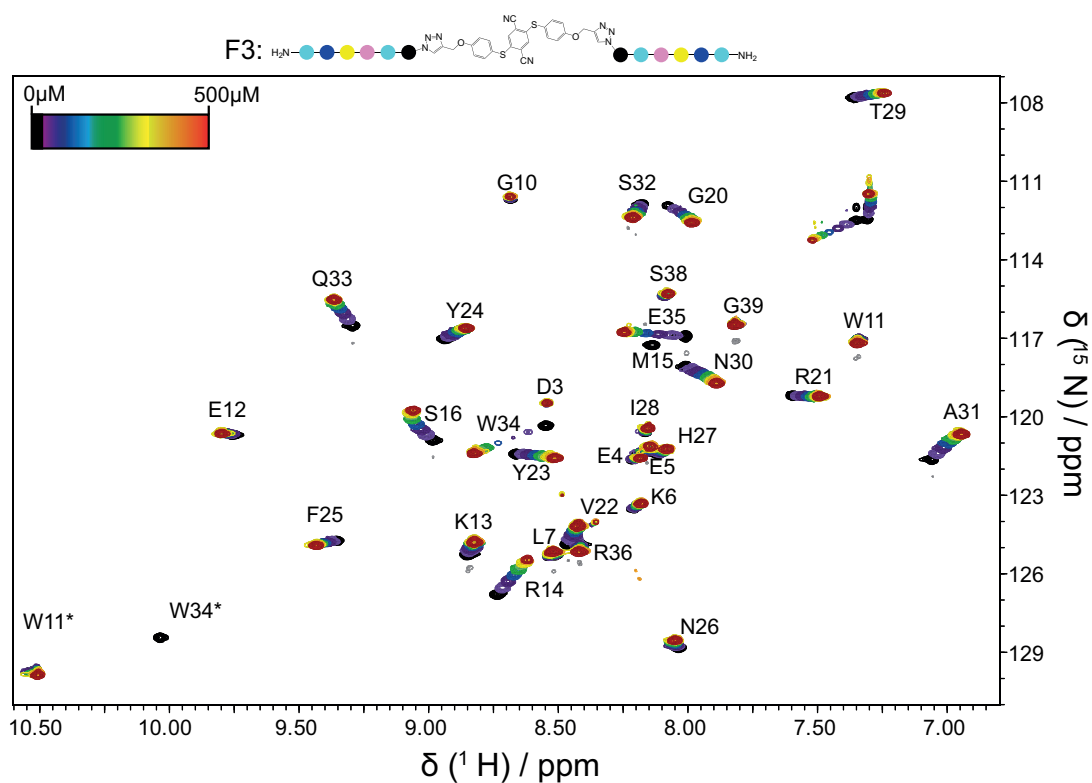


Figure A13: $^1\text{H}, ^{15}\text{N}$ -HSQC titration spectra of *hPin1*-WW domain with fluorophore **F3**. Shown are the $^1\text{H}, ^{15}\text{N}$ -HSQC spectra from the *hPin1*-WW domain with increasing concentration (0-500 μM) of fluorophore **F3**. In addition to the backbone amides, the side chain amides of W^{11} and W^{34} are labelled with an additional star (*).

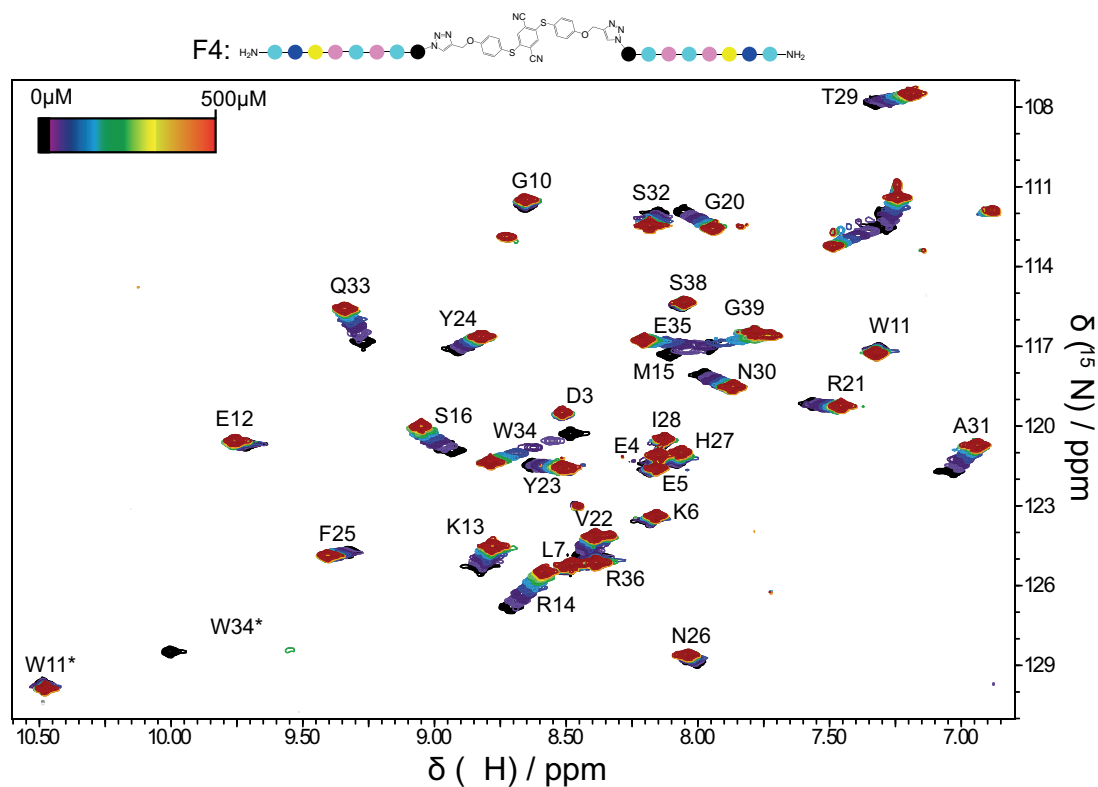


Figure A14: ^1H , ^{15}N -HSQC titration spectra of *hPin1*-WW domain with fluorophore F4. Shown are the ^1H , ^{15}N -HSQC spectra from the *hPin1*-WW domain with increasing concentration (0-500 μM) of fluorophore F4. In addition to the backbone amides, the side chain amides of W¹¹ and W³⁴ are labelled with an additional star (*).

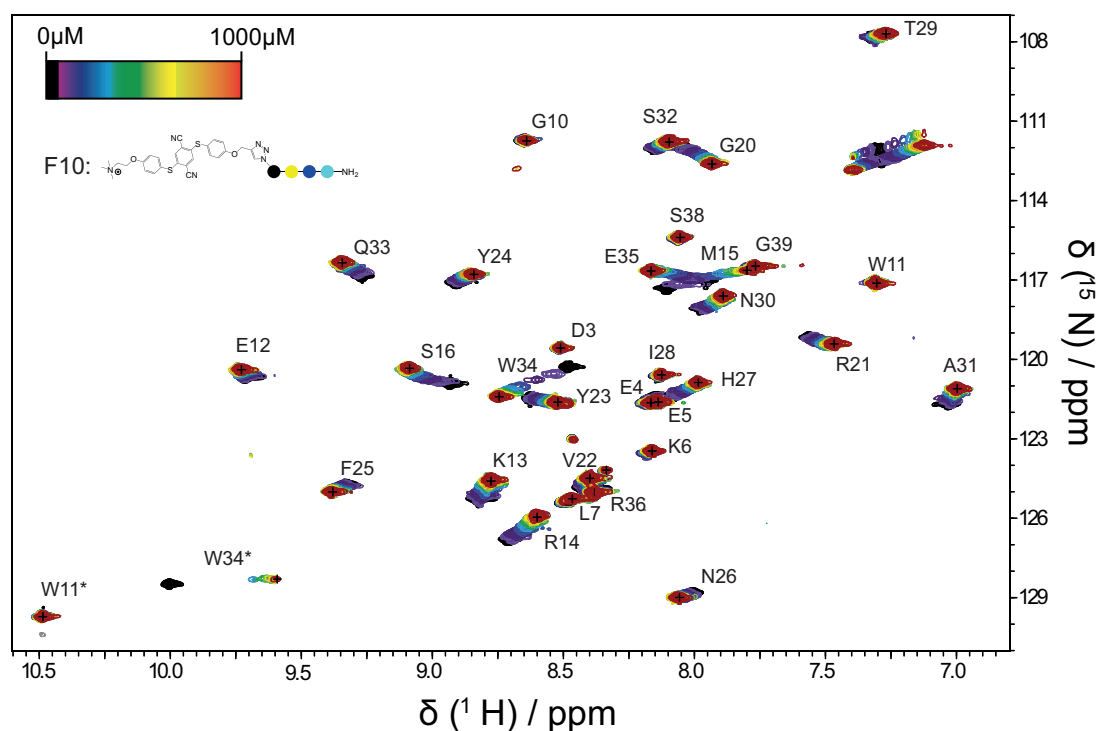


Figure A15: ^1H , ^{15}N -HSQC titration spectra of *hPin1*-WW domain with fluorophore F10. Shown are the ^1H , ^{15}N -HSQC spectra from the *hPin1*-WW domain with increasing concentration (0-1000 μM) of fluorophore F10. In addition to the backbone amides, the side chain amides of W¹¹ and W³⁴ are labelled with an additional star (*).

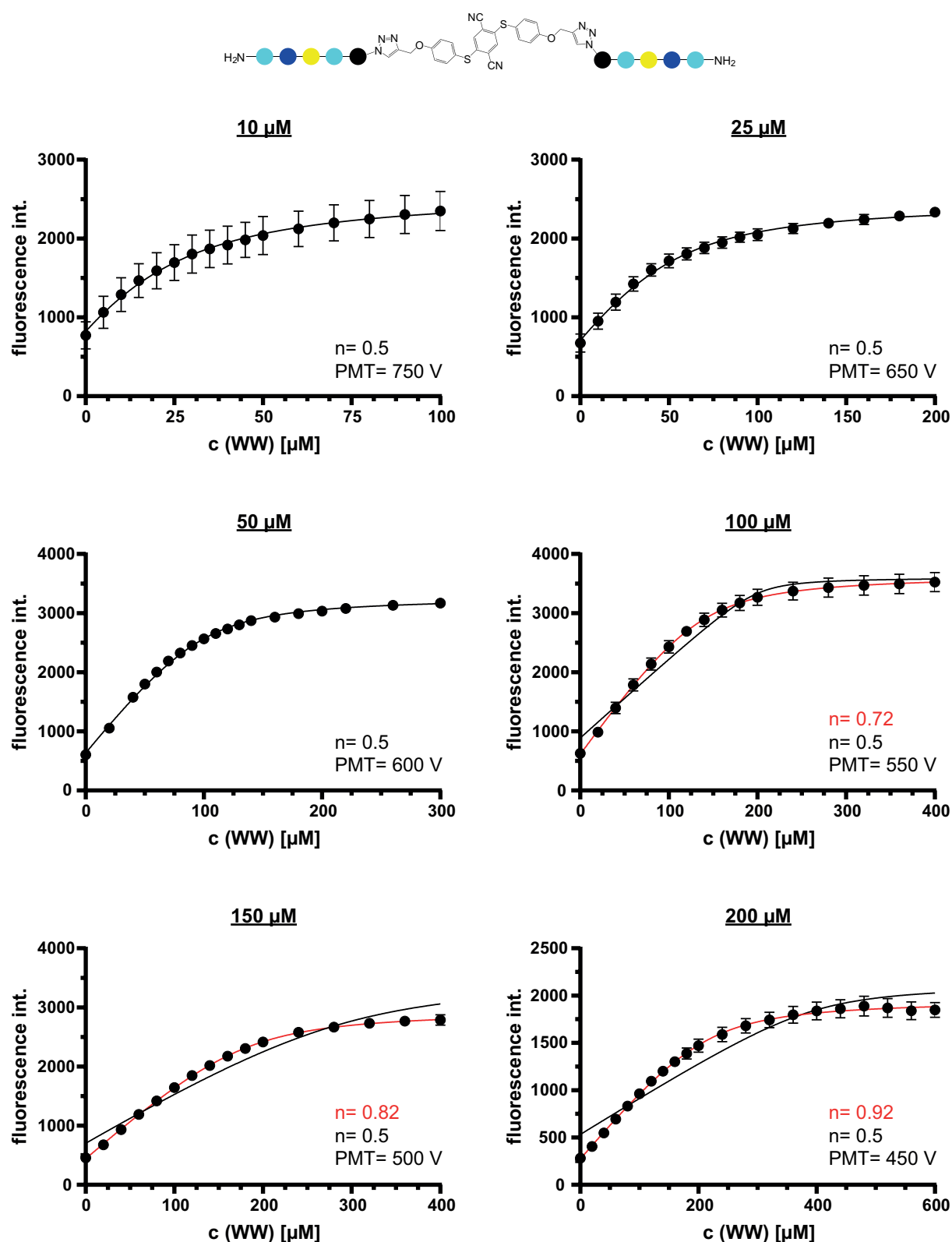
8.2 Fluorescence titrations of fluorophores F2-4 with *hPin1*-WW

Figure A16: Concentration dependency of fluorophore F2. Fluorescence titrations with various concentrations of F2 (10–200 μM). Shown are non-linear fits with a fixed stoichiometry factor n of 0.5 (black) and a variable factor (red).

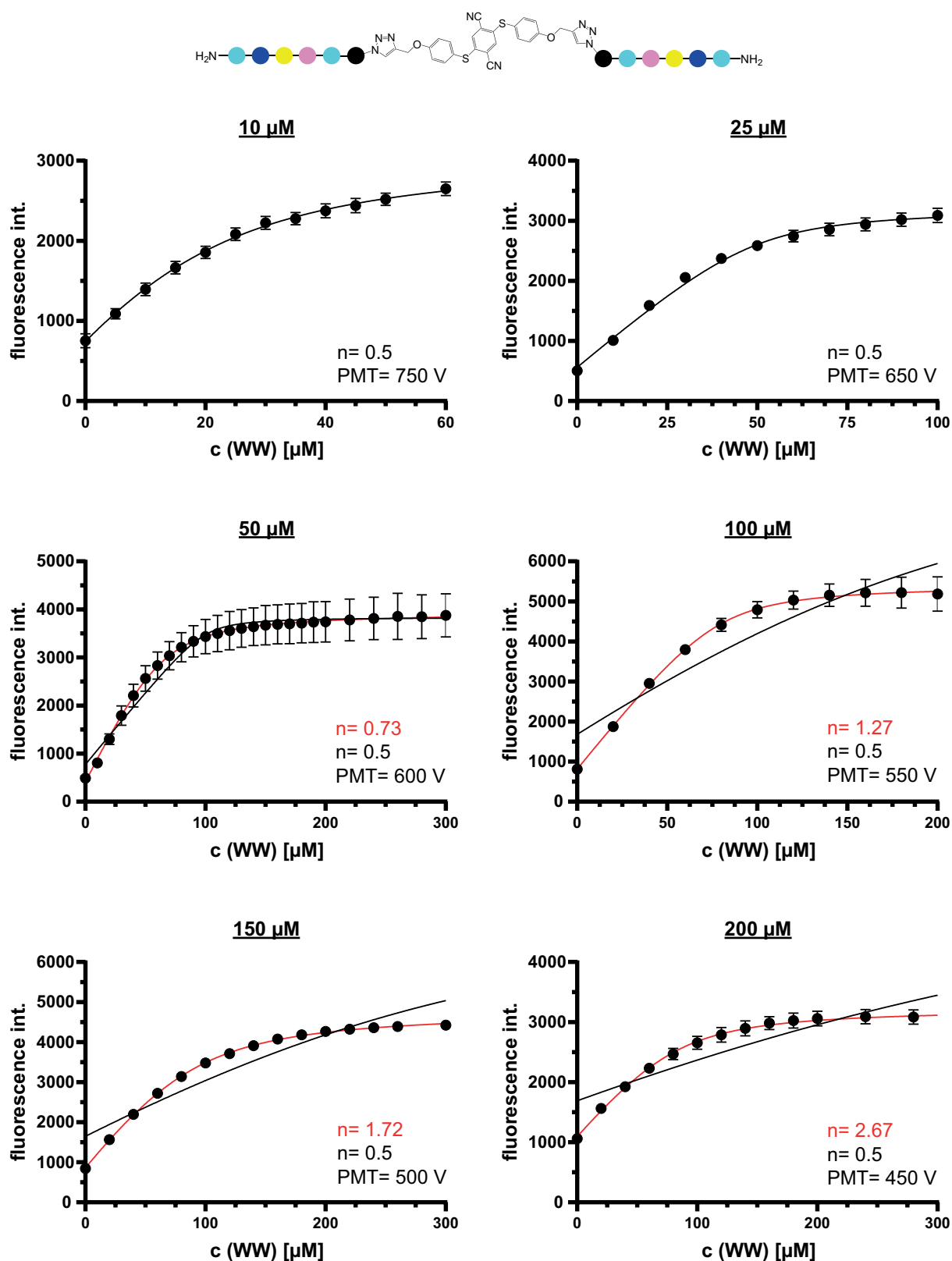


Figure A17: Concentration dependency of fluorophore F3. Fluorescence titrations with various concentrations of F3 (10-200 μM). Shown are non-linear fits with a fixed stoichiometry factor n of 0.5 (black) and a variable factor (red).

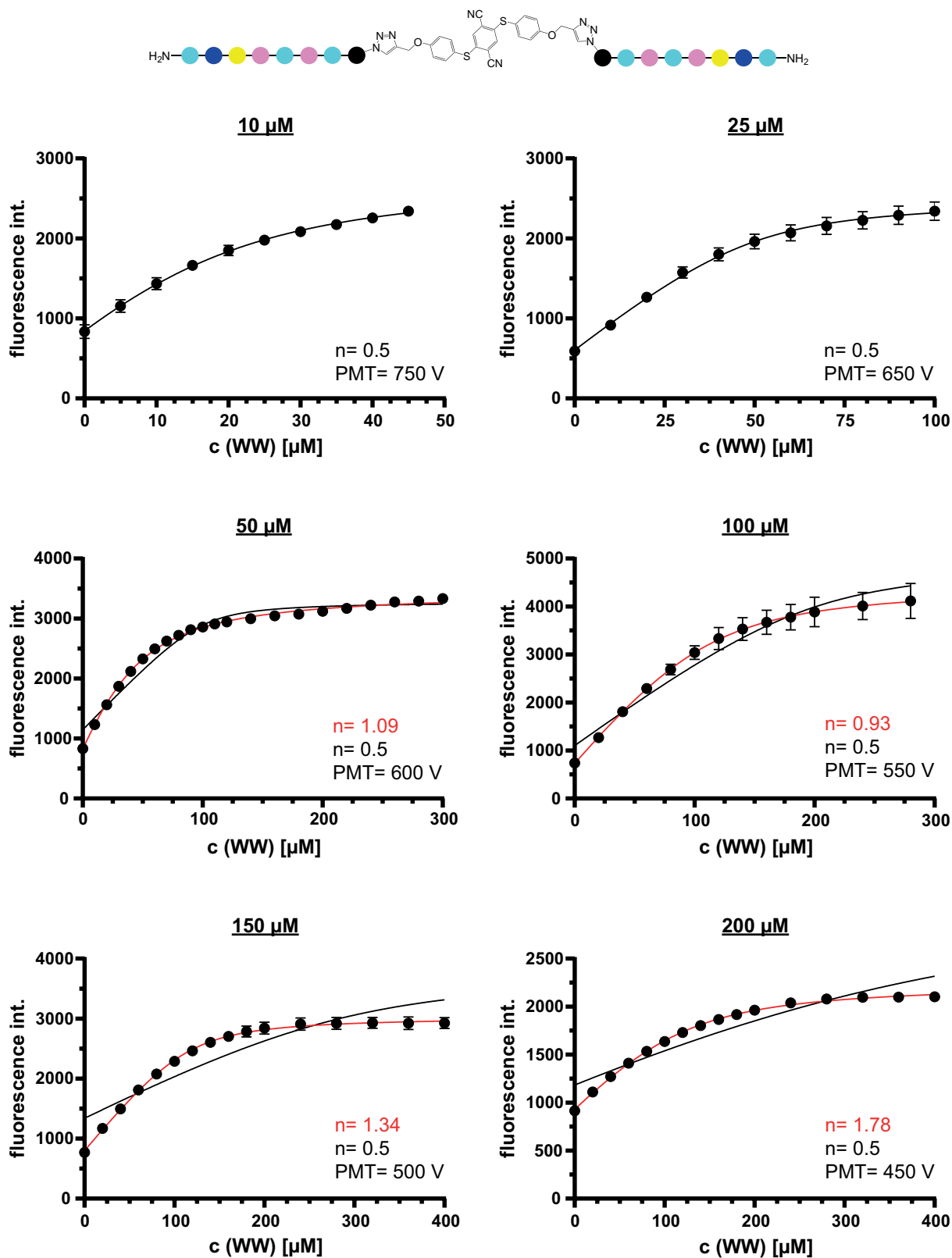


Figure A18: Concentration dependency of fluorophore F4. Fluorescence titrations with various concentrations of F4 (10-200 μM). Shown are non-linear fits with a fixed stoichiometry factor n of 0.5 (black) and a variable factor (red).

8.3 Liquid chromatography-mass spectroscopy (LC-MS)

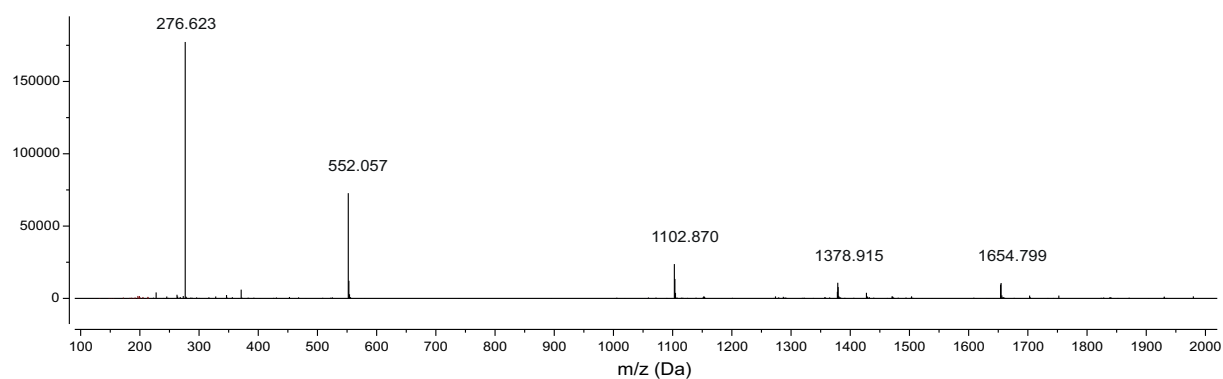


Figure A19: LC-MS spectra of peptide P0.

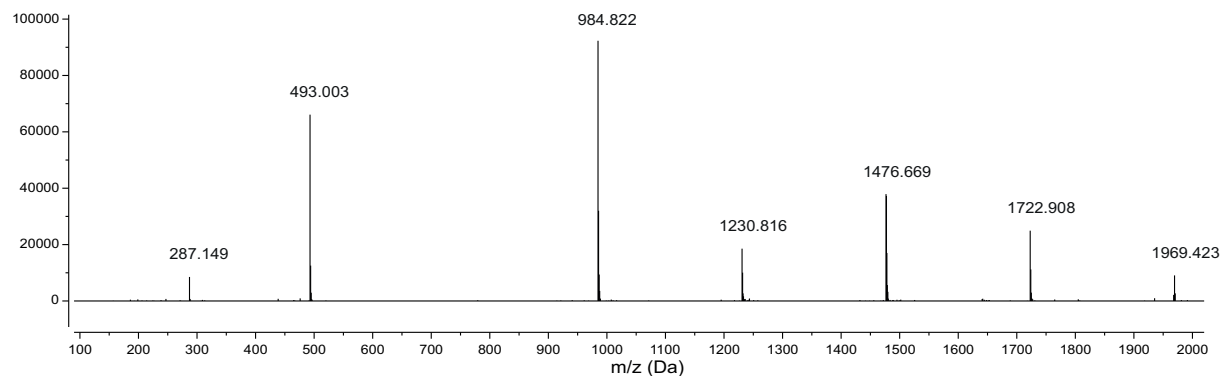


Figure A20: LC-MS spectra of peptide P1.

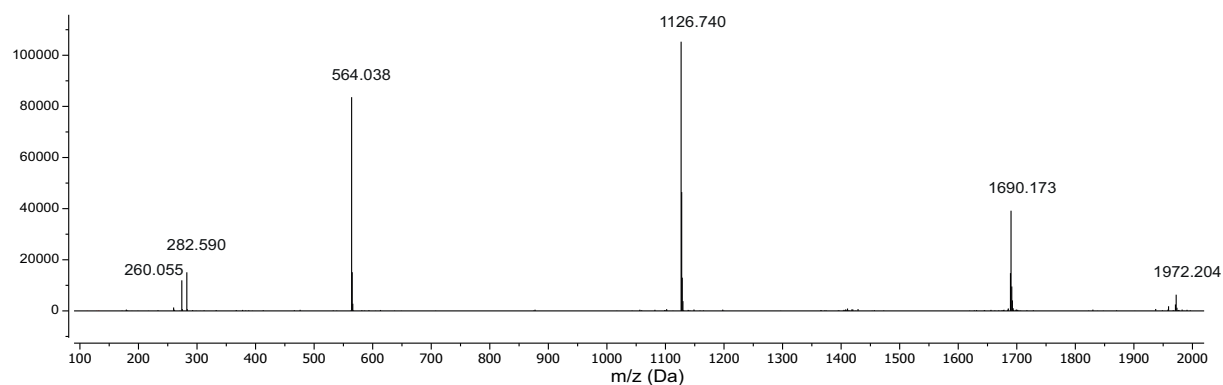


Figure A21: LC-MS spectra of peptide P2.

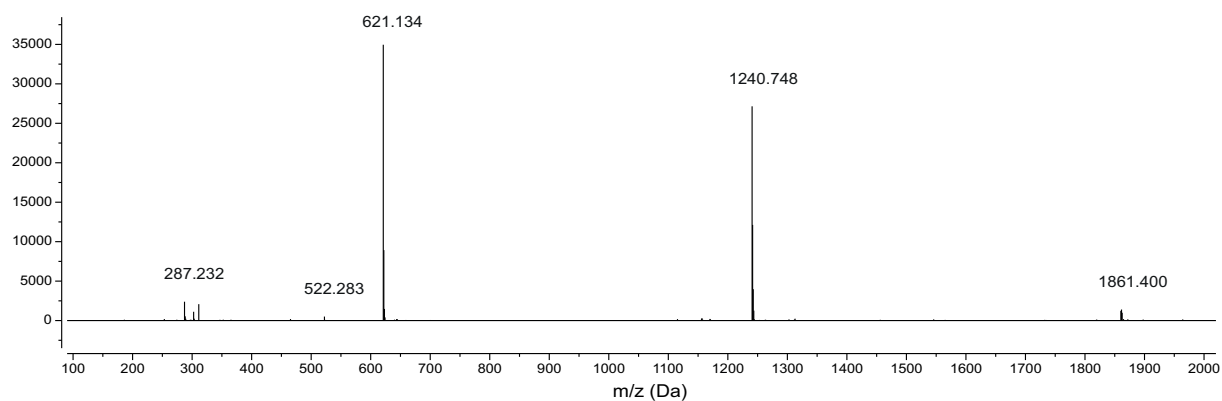


Figure A22: LC-MS spectra of peptide P3.

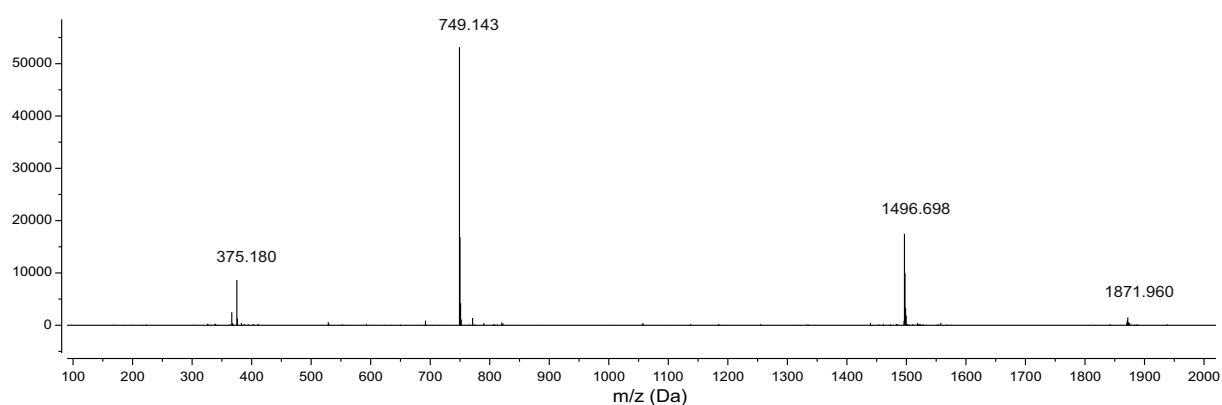


Figure A23: LC-MS spectra of peptide P4.

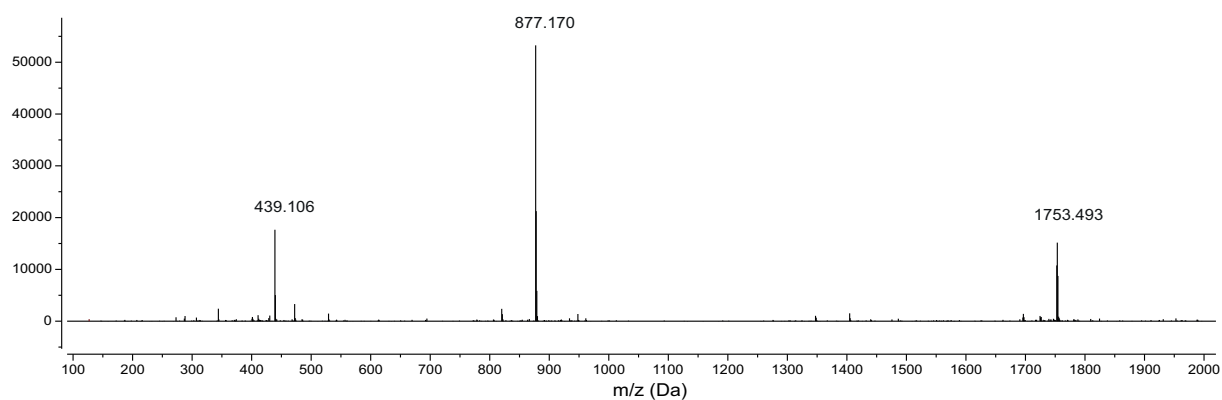


Figure A24: LC-MS spectra of peptide P5.

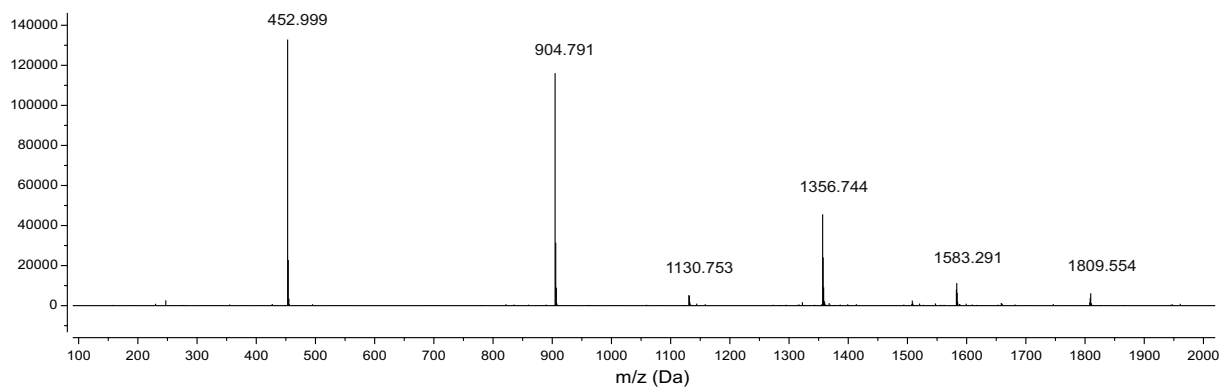


Figure A25: LC-MS spectra of peptide P6.

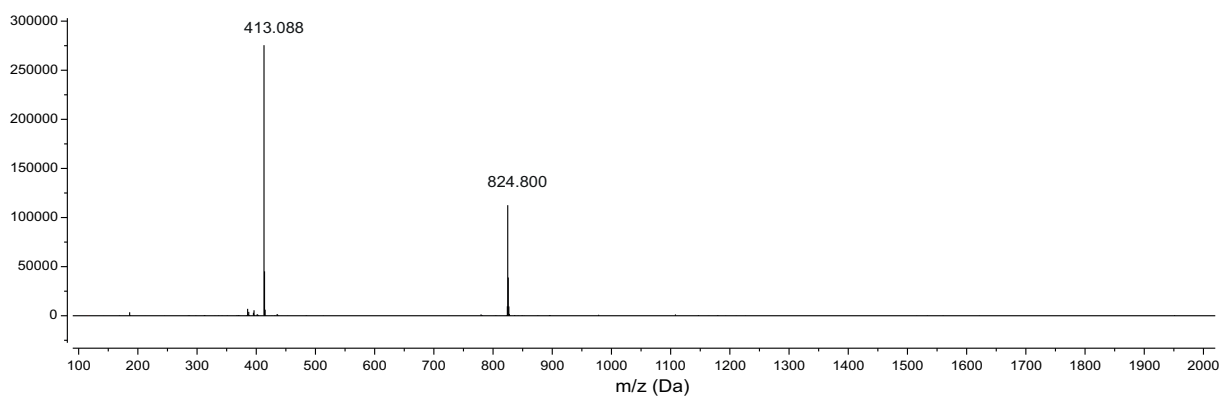


Figure A26: LC-MS spectra of peptide P7.

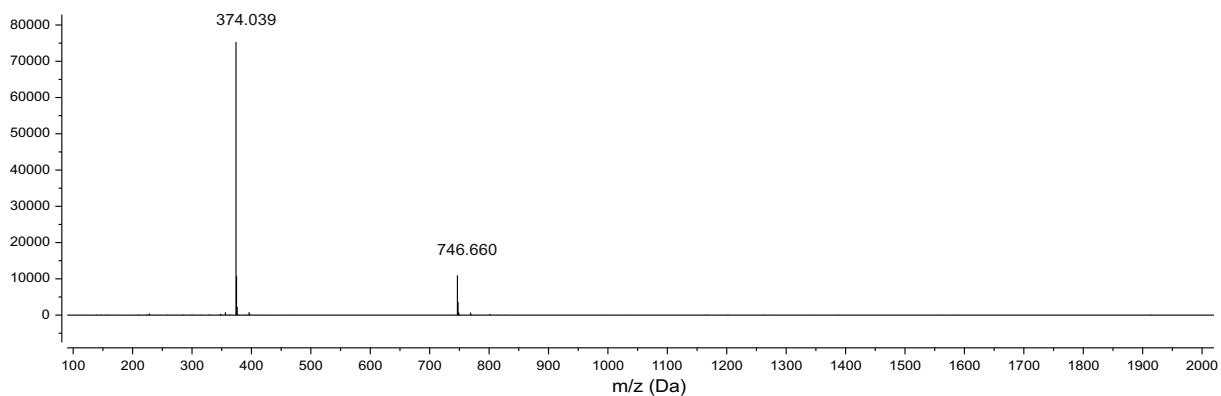


Figure A27: LC-MS spectra of peptide P8.

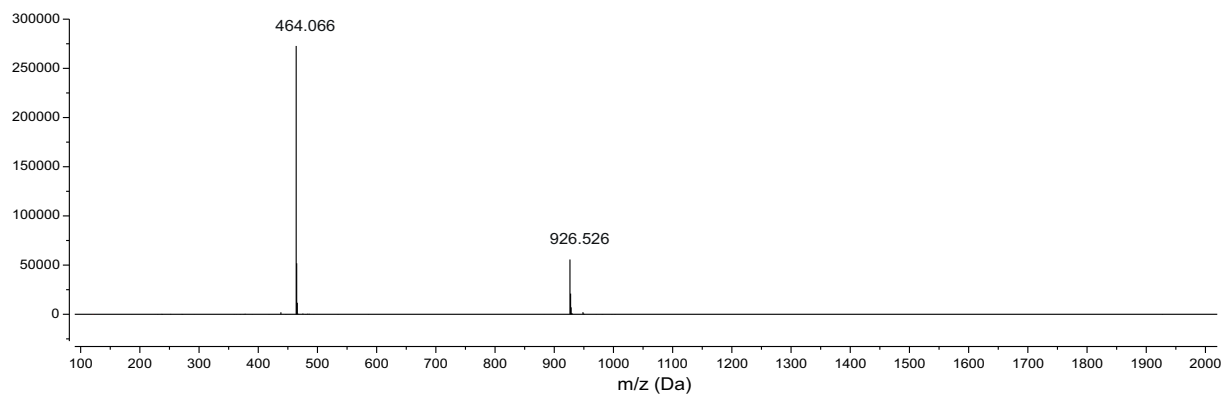


Figure A28: LC-MS spectra of peptide P9.

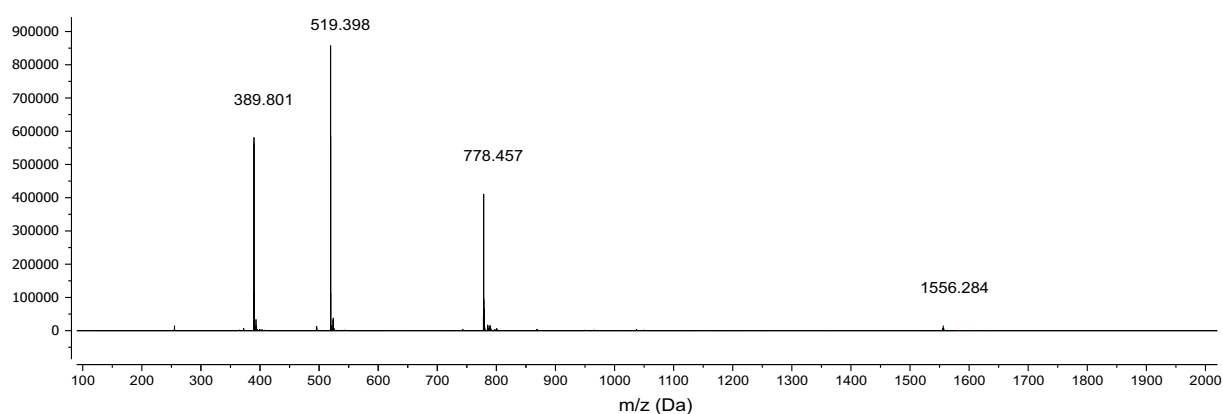


Figure A29: LC-MS spectra of fluorophore F0.

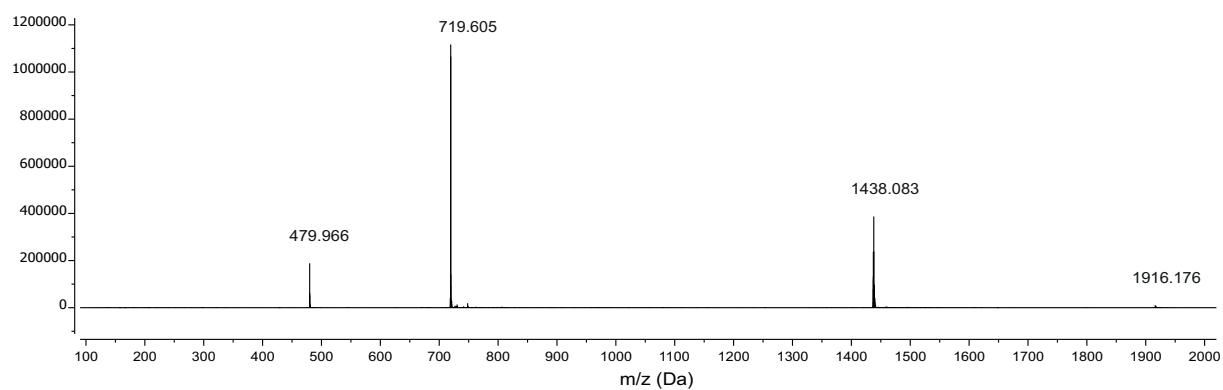


Figure A30: LC-MS spectra of fluorophore F1.

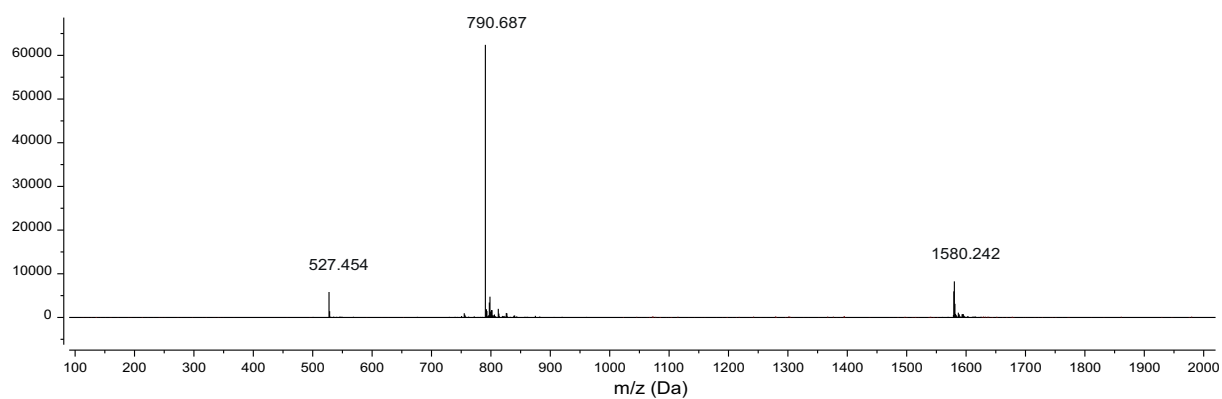


Figure A31: LC-MS spectra of fluorophore F2.

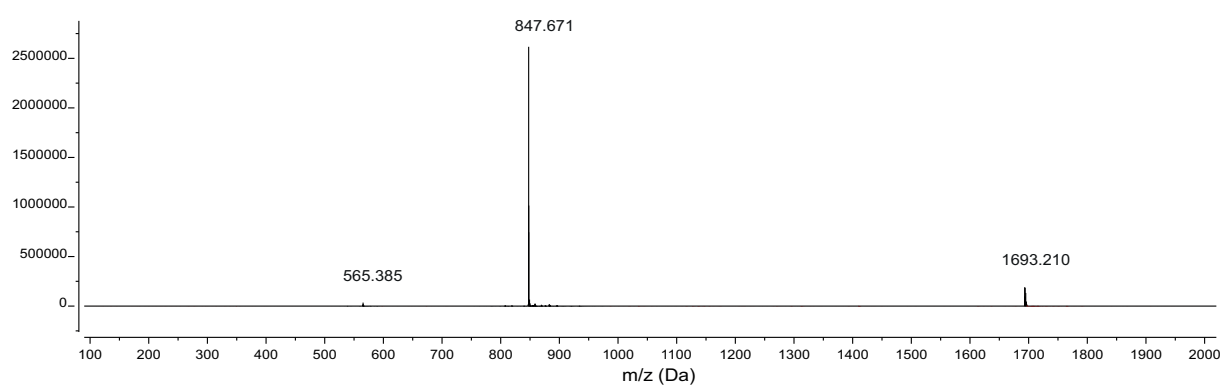


Figure A32: LC-MS spectra of fluorophore F3.

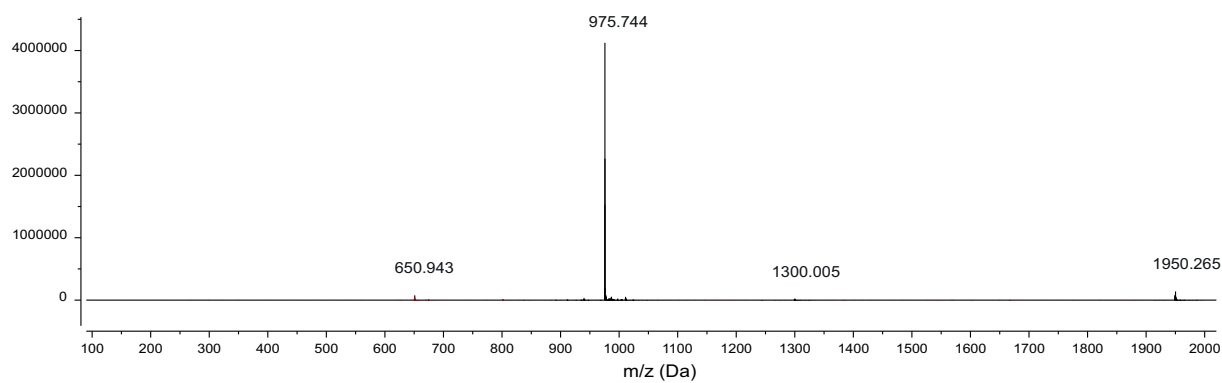


Figure A33: LC-MS spectra of fluorophore F4.

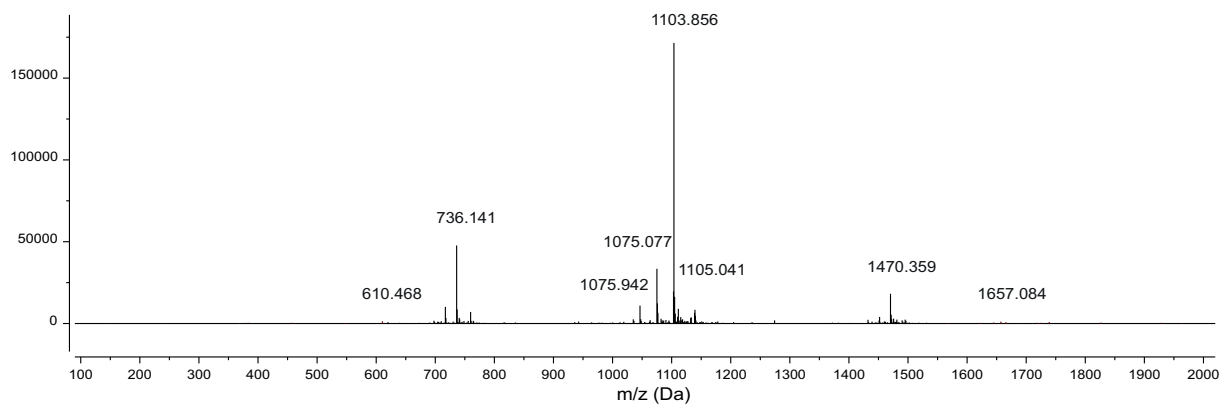


Figure A34: LC-MS spectra of fluorophore F5.

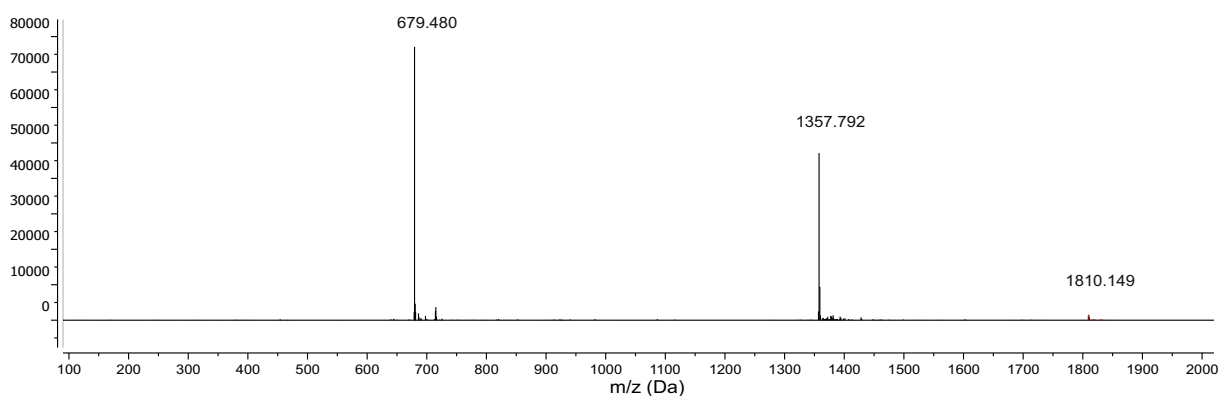


Figure A35: LC-MS spectra of fluorophore F6.

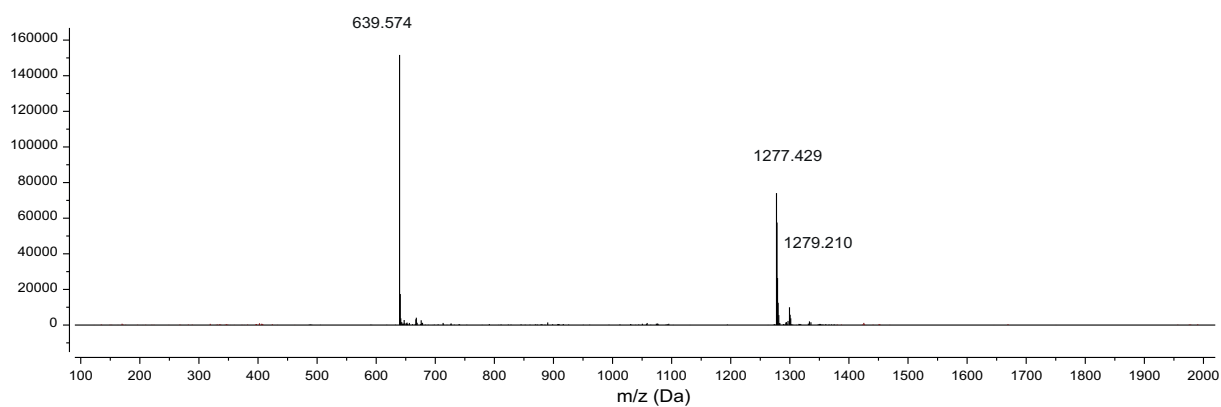


Figure A36: LC-MS spectra of fluorophore F7.

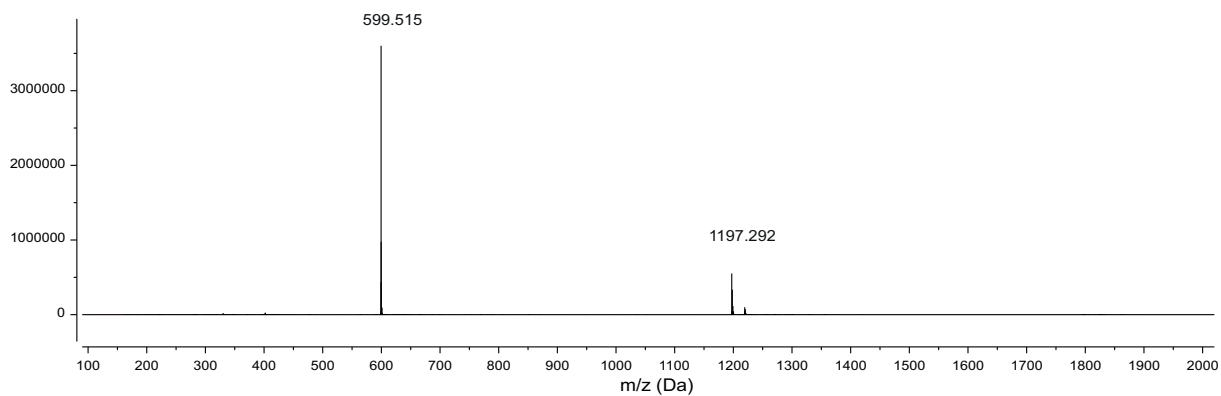


Figure A37: LC-MS spectra of fluorophore F8.

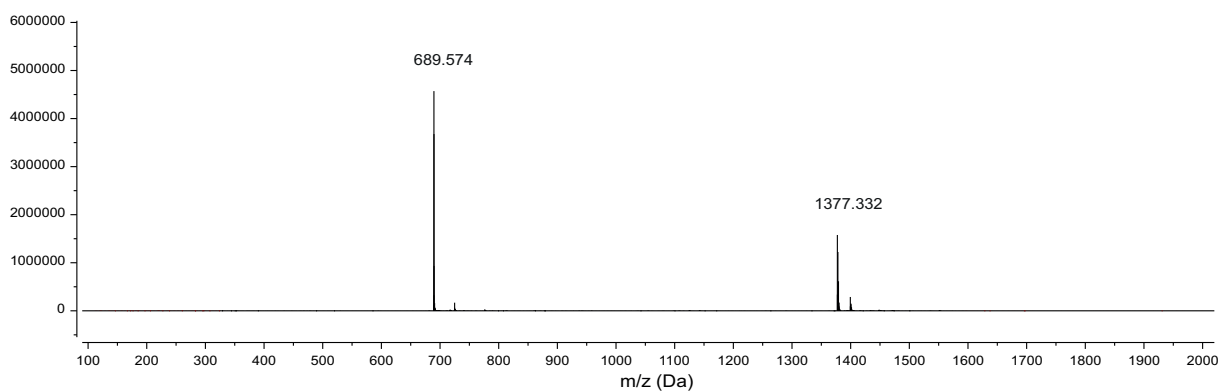


Figure A38: LC-MS spectra of fluorophore F9.

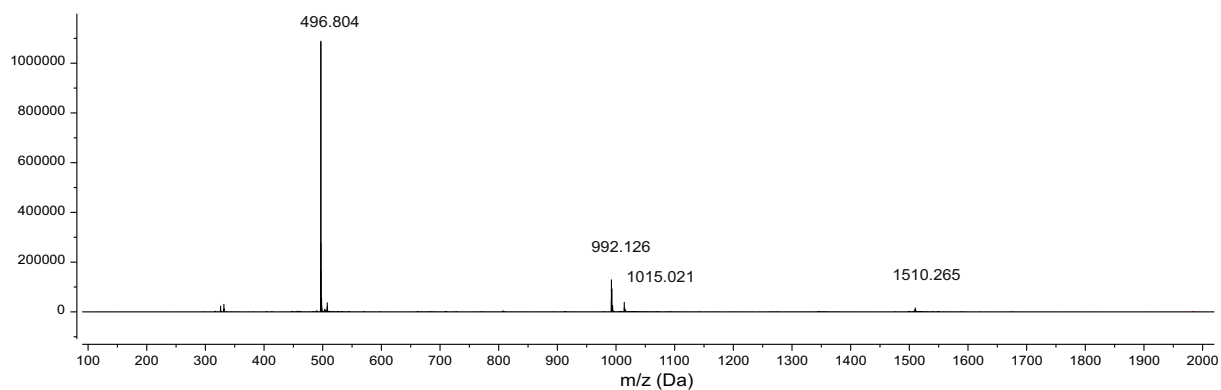


Figure A39: LC-MS spectra of fluorophore F10.

References

- [1] S. E. Acuner Ozbabacan, H. B. Engin, A. Gursoy, and O. Keskin. Transient protein-protein interactions. 24(9):635–648, 2011. Journal Article Research Support, Non-U.S. Gov't Review.
- [2] S. A. Adam, T. J. Lobl, M. A. Mitchell, and L. Gerace. Identification of specific binding proteins for a nuclear location sequence. 337(6204):276–279, 1989. Journal Article Research Support, Non-U.S. Gov't Journal Article Research Support, Non-U.S. Gov't.
- [3] V. Aggarwal, H. S. Tuli, A. Varol, F. Thakral, M. B. Yerer, K. Sak, M. Varol, A. Jain, M. A. Khan, and G. Sethi. Role of Reactive Oxygen Species in Cancer Progression: Molecular Mechanisms and Recent Advancements. 9(11), 2019. Journal Article Review.
- [4] H. Akiyama, R.-W. Shin, C. Uchida, T. Kitamoto, and T. Uchida. Pin1 promotes production of Alzheimer's amyloid beta from beta-cleaved amyloid precursor protein. 336(2):521–529, 2005. Journal Article Research Support, Non-U.S. Gov't.
- [5] A. Albert, S. Lavoie, and M. Vincent. A hyperphosphorylated form of RNA polymerase II is the major interphase antigen of the phosphoprotein antibody MPM-2 and interacts with the peptidyl-prolyl isomerase Pin1. 112 (Pt 15):2493–2500, 1999. Journal Article Research Support, Non-U.S. Gov't.
- [6] M. P. Aldred, G.-F. Zhang, C. Li, G. Chen, T. Chen, and M.-Q. Zhu. Optical properties and red to near infrared piezo-responsive fluorescence of a tetraphenylethene–perylenebisimide–tetraphenylethene triad. 1(40):6709, 2013.
- [7] A. H. Andreotti. Native state proline isomerization: an intrinsic molecular switch. 42(32):9515–9524, 2003. Journal Article Research Support, Non-U.S. Gov't Research Support, U.S. Gov't, P.H.S. Review.
- [8] E. Aragón, N. Goerner, A.-I. Zaromytidou, Q. Xi, A. Escobedo, J. Massagué, and M. J. Macias. A Smad action turnover switch operated by WW domain readers of a phosphoserine code. 25(12):1275–1288, 2011. Journal Article Research Support, N.I.H., Extramural Research Support, Non-U.S. Gov't.
- [9] N. Armaroli and V. Balzani. Solar Electricity and Solar Fuels: Status and Perspectives in the Context of the Energy Transition. 22(1):32–57, 2016. Journal Article Research Support, Non-U.S. Gov't Review.
- [10] A. Ayed, F. A. Mulder, G. S. Yi, Y. Lu, L. E. Kay, and C. H. Arrowsmith. Latent and active p53 are identical in conformation. 8(9):756–760, 2001. Journal Article Research Support, Non-U.S. Gov't.

-
- [11] S. Barghorn, P. Davies, and E. Mandelkow. Tau paired helical filaments from Alzheimer's disease brain and assembled in vitro are based on beta-structure in the core domain. 43(6):1694–1703, 2004. Journal Article Research Support, Non-U.S. Gov't.
- [12] E. Bayer, S. Goetsch, J. W. Mueller, B. Griewel, E. Guiberman, L. M. Mayr, and P. Bayer. Structural analysis of the mitotic regulator hPin1 in solution: insights into domain architecture and substrate binding. 278(28):26183–26193, 2003. Journal Article Research Support, Non-U.S. Gov't.
- [13] E. Bayer, M. Thutewohl, C. Christner, T. Tradler, F. Osterkamp, H. Waldmann, and P. Bayer. Identification of hPin1 inhibitors that induce apoptosis in a mammalian Ras transformed cell line. (4):516–518, 2005. Journal Article Research Support, Non-U.S. Gov't.
- [14] E. B. E. Becker and A. Bonni. Pin1 in neuronal apoptosis. 6(11):1332–1335, 2007. Journal Article Research Support, N.I.H., Extramural.
- [15] W. Bedewy, H. Liao, N. A. Abou-Taleb, S. F. Hammad, T. Nasr, and D. Pei. Generation of a cell-permeable cycloheptapeptidyl inhibitor against the peptidyl-prolyl isomerase Pin1. 15(21):4540–4543, 2017. Journal Article.
- [16] R. Behrendt, P. White, and J. Offer. Advances in Fmoc solid-phase peptide synthesis. 22(1):4–27, 2016. Journal Article Review.
- [17] V. Bhalla, A. Gupta, and M. Kumar. A pentacenequinone derivative with aggregation-induced emission enhancement characteristics for the picogram detection of Fe(3+) ions in mixed aqueous media. 42(13):4464–4469, 2013. Journal Article Research Support, Non-U.S. Gov't.
- [18] D. Bier, S. Mittal, K. Bravo-Rodriguez, A. Sowislok, X. Guillory, J. Briels, C. Heid, M. Bartel, B. Wettig, L. Brunsveld, E. Sanchez-Garcia, T. Schrader, and C. Ottmann. The Molecular Tweezer CLR01 Stabilizes a Disordered Protein-Protein Interface. 139(45):16256–16263, 2017. Journal Article Research Support, Non-U.S. Gov't Journal Article Research Support, Non-U.S. Gov't.
- [19] L. I. Binder, A. L. Guillozet-Bongaarts, F. Garcia-Sierra, and R. W. Berry. Tau, tangles, and Alzheimer's disease. 1739(2-3):216–223, 2005. Journal Article Research Support, U.S. Gov't, P.H.S. Review.
- [20] R. S. Boston, P. V. Viitanen, and E. Vierling. Molecular chaperones and protein folding in plants. 32(1-2):191–222, 1996. Journal Article Research Support, Non-U.S. Gov't Research Support, U.S. Gov't, Non-P.H.S. Research Support, U.S. Gov't, P.H.S. Review.

- [21] M. M. Bradford. A rapid and sensitive method for the quantitation of microgram quantities of protein utilizing the principle of protein-dye binding. 72(1-2):248–254, 1976. PII: 0003269776905273.
- [22] K. J. Bradley, M. R. Bowl, S. E. Williams, B. N. Ahmad, C. J. Partridge, A. L. Patmanidi, A. M. Kennedy, N. Y. Loh, and R. V. Thakker. Parafibromin is a nuclear protein with a functional monopartite nuclear localization signal. 26(8):1213–1221, 2007. Journal Article Research Support, Non-U.S. Gov't Journal Article Research Support, Non-U.S. Gov't.
- [23] J. F. Brandts, M. Brennan, and L. Lung-Nan. Unfolding and refolding occur much faster for a proline-free proteins than for most proline-containing proteins. 74(10):4178–4181, 1977. Journal Article.
- [24] A. L. Breeze. Isotope-filtered NMR methods for the study of biomolecular structure and interactions. 36(4):323–372, 2000. PII: S0079656500000200.
- [25] A. Breiman, T. W. Fawcett, M. L. Ghirardi, and A. K. Mattoo. Plant organelles contain distinct peptidylprolyl cis,trans-isomerases. 267(30):21293–21296, 1992. PII: S0021925819366050.
- [26] D. A. Butterfield, H. M. Abdul, W. Opii, S. F. Newman, G. Joshi, M. A. Ansari, and R. Sultana. Pin1 in Alzheimer's disease. 98(6):1697–1706, 2006. Journal Article Research Support, N.I.H., Extramural Review.
- [27] X. Cai and B. Liu. Aggregation-Induced Emission: Recent Advances in Materials and Biomedical Applications. 59(25):9868–9886, 2020. Journal Article Research Support, Non-U.S. Gov't Review.
- [28] Y. Cai, L. Li, Z. Wang, J. Z. Sun, A. Qin, and B. Z. Tang. A sensitivity tuneable tetraphenylethene-based fluorescent probe for directly indicating the concentration of hydrogen sulfide. 50(64):8892–8895, 2014. Journal Article Research Support, Non-U.S. Gov't.
- [29] E. Campaner, A. Rustighi, A. Zannini, A. Cristiani, S. Piazza, Y. Ciani, O. Kalid, G. Golan, E. Baloglu, S. Shacham, B. Valsasina, U. Cucchi, A. C. Pippione, M. L. Lolli, B. Giabbai, P. Storici, P. Carloni, G. Rossetti, F. Benvenuti, E. Bello, M. D'Incalci, E. Cappuzzello, A. Rosato, and G. Del Sal. A covalent PIN1 inhibitor selectively targets cancer cells by a dual mechanism of action. 8:15772, 2017. Journal Article Research Support, Non-U.S. Gov't.
- [30] S. H. Chao, A. L. Greenleaf, and D. H. Price. Juglone, an inhibitor of the peptidylprolyl isomerase Pin1, also directly blocks transcription. 29(3):767–773, 2001. Journal Article Research Support, U.S. Gov't, P.H.S.

- [31] S. Cheek, H. Zhang, and N. V. Grishin. Sequence and Structure Classification of Kinases. 320(4):855–881, 2002.
- [32] C.-H. Chen, C.-C. Chang, T. H. Lee, M. Luo, P. Huang, P.-H. Liao, S. Wei, F.-A. Li, R.-H. Chen, X. Z. Zhou, H.-M. Shih, and K. P. Lu. SENP1 deSUMOylates and regulates Pin1 protein activity and cellular function. 73(13):3951–3962, 2013. Journal Article Research Support, N.I.H., Extramural Research Support, Non-U.S. Gov't Research Support, U.S. Gov't, Non-P.H.S.
- [33] C.-H. Chen, W. Li, R. Sultana, M.-H. You, A. Kondo, K. Shahpasand, B. M. Kim, M.-L. Luo, M. Nechama, Y.-M. Lin, Y. Yao, T. H. Lee, X. Z. Zhou, A. M. Swomley, D. A. Butterfield, Y. Zhang, and K. P. Lu. Pin1 cysteine-113 oxidation inhibits its catalytic activity and cellular function in Alzheimer's disease. 76:13–23, 2015. Journal Article Research Support, N.I.H., Extramural Research Support, U.S. Gov't, Non-P.H.S.
- [34] D. Chen, L. Wang, and T. H. Lee. Post-translational Modifications of the Peptidyl-Prolyl Isomerase Pin1. 8, 2020. Journal Article Review.
- [35] J. Chen, C. C. W. Law, J. W. Y. Lam, Y. Dong, S. M. F. Lo, I. D. Williams, D. Zhu, and B. Z. Tang. Synthesis, Light Emission, Nanoaggregation, and Restricted Intramolecular Rotation of 1,1-Substituted 2,3,4,5-Tetraphenylsiloles. 15(7):1535–1546, 2003.
- [36] L. Chen, J. Liu, X. Tao, G. Wang, Q. Wang, and X. Liu. The role of Pin1 protein in aging of human tendon stem/progenitor cells. 464(2):487–492, 2015. Journal Article Research Support, Non-U.S. Gov't.
- [37] S. Chen and X.-L. Ni. Development of an AIE based fluorescent probe for the detection of nitrate anions in aqueous solution over a wide pH range. 6(9):6997–7001, 2016.
- [38] W. Chen, Y. Zhao, T. Seefeldt, and X. Guan. Determination of thiols and disulfides via HPLC quantification of 5-thio-2-nitrobenzoic acid. 48(5):1375–1380, 2008. Journal Article Research Support, N.I.H., Extramural Research Support, Non-U.S. Gov't.
- [39] Y. Chen, Y.-R. Wu, H.-Y. Yang, X.-Z. Li, M.-M. Jie, C.-J. Hu, Y.-Y. Wu, S.-M. Yang, and Y.-B. Yang. Prolyl isomerase Pin1: a promoter of cancer and a target for therapy. 9(9):883, 2018. Journal Article Research Support, Non-U.S. Gov't Review.
- [40] Y. S. Cho, S. Y. Park, D. J. Kim, S.-H. Lee, K.-M. Woo, K.-A. Lee, Y.-J. Lee, Y.-Y. Cho, and J.-H. Shim. TPA-induced cell transformation provokes a complex

- formation between Pin1 and 90 kDa ribosomal protein S6 kinase 2. 367(1-2):85–92, 2012. Journal Article Research Support, Non-U.S. Gov't.
- [41] C. Corbi-Verge and P. M. Kim. Motif mediated protein-protein interactions as drug targets. 14:8, 2016. Journal Article Research Support, Non-U.S. Gov't Review.
- [42] G. Cornilescu, F. Delaglio, and A. Bax. Protein backbone angle restraints from searching a database for chemical shift and sequence homology. 13(3):289–302, 1999. Journal Article.
- [43] S. Costantino, F. Paneni, T. F. Lüscher, and F. Cosentino. Pin1 inhibitor Juglone prevents diabetic vascular dysfunction. 203:702–707, 2016. Journal Article Research Support, Non-U.S. Gov't.
- [44] M. P. Coughlan. Cyanide in Biology. B. Vennesland , E. E. Conn , C. J. Knowles , J. Westley , F. Wissing. 58(1):143, 1983.
- [45] D. G. Crenshaw, J. Yang, A. R. Means, and S. Kornbluth. The mitotic peptidyl-prolyl isomerase, Pin1, interacts with Cdc25 and Plx1. 17(5):1315–1327, 1998. Journal Article.
- [46] C. Dartigalongue and S. Raina. A new heat-shock gene, ppiD, encodes a peptidyl-prolyl isomerase required for folding of outer membrane proteins in *Escherichia coli*. 17(14):3968–3980, 1998. Journal Article Research Support, Non-U.S. Gov't.
- [47] A. Drazic, L. M. Myklebust, R. Ree, and T. Arnesen. The world of protein acetylation. 1864(10):1372–1401, 2016. Journal Article Research Support, Non-U.S. Gov't Review.
- [48] S. Drouault, J. Anba, S. Bonneau, A. Bolotin, S. D. Ehrlich, and P. Renault. The peptidyl-prolyl isomerase motif is lacking in PmpA, the PrsA-like protein involved in the secretion machinery of *Lactococcus lactis*. 68(8):3932–3942, 2002. Journal Article Research Support, Non-U.S. Gov't.
- [49] D. Durocher, J. Henckel, A. R. Fersht, and S. P. Jackson. The FHA Domain Is a Modular Phosphopeptide Recognition Motif. 4(3):387–394, 1999. PII: S1097276500803408.
- [50] D. Durocher, I. A. Taylor, D. Sarbassova, L. F. Haire, S. L. Westcott, S. P. Jackson, S. J. Smerdon, and M. B. Yaffe. The Molecular Basis of FHA Domain:Phosphopeptide Binding Specificity and Implications for Phospho-Dependent Signaling Mechanisms. 6(5):1169–1182, 2000. PII: S1097276500001143.

- [51] F. Eckerdt, J. Yuan, K. Saxena, B. Martin, S. Kappel, C. Lindenau, A. Kramer, S. Naumann, S. Daum, G. Fischer, I. Dikic, M. Kaufmann, and K. Strebhardt. Polo-like kinase 1-mediated phosphorylation stabilizes Pin1 by inhibiting its ubiquitination in human cells. 280(44):36575–36583, 2005. Journal Article Research Support, Non-U.S. Gov't.
- [52] J. O. Egekeze and F. W. Oehme. Cyanides and their toxicity: A literature review. 2(2):104–114, 1980. Journal Article.
- [53] L. Eichinger, J. A. Pachebat, G. Glöckner, M.-A. Rajandream, R. Sucgang, and M. e. a. Berriman. The genome of the social amoeba *Dictyostelium discoideum*. 435(7038):43–57, 2005. Journal Article Research Support, Non-U.S. Gov't Research Support, U.S. Gov't, P.H.S.
- [54] E. D. Erben, E. Valguarnera, S. Nardelli, J. Chung, S. Daum, M. Potenza, S. Schenkman, and M. T. Téllez-Iñón. Identification of an atypical peptidyl-prolyl cis/trans isomerase from trypanosomatids. 1803(9):1028–1037, 2010. Journal Article Research Support, Non-U.S. Gov't.
- [55] S. Esnault, R. K. Braun, Z.-J. Shen, Z. Xiang, E. Heninger, R. B. Love, M. Sandor, and J. S. Malter. Pin1 modulates the type 1 immune response. 2(2):e226, 2007. Journal Article Research Support, N.I.H., Extramural Research Support, Non-U.S. Gov't.
- [56] S. Esnault, Z.-J. Shen, and J. S. Malter. Pinning down signaling in the immune system: the role of the peptidyl-prolyl isomerase Pin1 in immune cell function. 28(1):45–60, 2008. Journal Article Research Support, N.I.H., Extramural Review.
- [57] F. Fagiani, S. Govoni, M. Racchi, and C. Lanni. The Peptidyl-prolyl Isomerase Pin1 in Neuronal Signaling: from Neurodevelopment to Neurodegeneration. 58(3):1062–1073, 2021. Journal Article Review.
- [58] G. Fan, Y. Fan, N. Gupta, I. Matsuura, F. Liu, X. Z. Zhou, K. P. Lu, and C. Gélinas. Peptidyl-prolyl isomerase Pin1 markedly enhances the oncogenic activity of the rel proteins in the nuclear factor-kappaB family. 69(11):4589–4597, 2009. Journal Article Research Support, N.I.H., Extramural.
- [59] J. Fanghänel. Enzymatic catalysis of the peptidyl-prolyl bond rotation: are transition state formation and enzyme dynamics directly linked? 42(5):490–492, 2003. Journal Article.
- [60] J. Fanghänel, H. Akiyama, C. Uchida, and T. Uchida. Comparative analysis of enzyme activities and mRNA levels of peptidyl prolyl cis/trans isomerases in

- various organs of wild type and Pin1^{-/-} mice. 580(13):3237–3245, 2006. Journal Article Research Support, Non-U.S. Gov't.
- [61] G. Feng, R. T. K. Kwok, B. Z. Tang, and B. Liu. Functionality and versatility of aggregation-induced emission luminogens. 4(2):021307, 2017.
- [62] P. N. Fernando, M. A. McLean, I. N. Egwu, E. deGuzman, and C. Weyker. Analysis of residual trifluoroacetic acid in a phosphate-buffered saline matrix by ion chromatography with suppressed conductivity detection. 920(1-2):155–162, 2001.
- [63] E. Ferri, B. Arosio, C. D'Addario, D. Galimberti, C. Gussago, M. Pucci, M. Casati, C. Fenoglio, C. Abbate, P. D. Rossi, E. Scarpini, M. Maccarrone, and D. Mari. Gene promoter methylation and expression of Pin1 differ between patients with frontotemporal dementia and Alzheimer's disease. 362:283–286, 2016. Journal Article.
- [64] G. B. Fields and R. L. Noble. Solid phase peptide synthesis utilizing 9-fluorenylmethoxycarbonyl amino acids. 35(3):161–214, 1990. Comparative Study Journal Article Review Comparative Study Journal Article Review.
- [65] G. Fischer. Chemical aspects of peptide bond isomerisation. 29(2):119–127, 2000.
- [66] G. Fischer, H. Bang, E. Berger, and A. Schellenberger. Conformational specificity of chymotrypsin toward proline-containing substrates. 791(1):87–97, 1984. PII: 0167483884902851.
- [67] G. Fischer, T. Tradler, and T. Zarnt. The mode of action of peptidyl prolyl cis/trans isomerases in vivo: binding vs. catalysis. 426(1):17–20, 1998.
- [68] G. FORLONI, L. TERRENI, I. BERTANI, S. FOGLIARINO, R. INVERNIZZI, A. ASSINI, G. RIBIZZI, A. NEGRO, E. CALABRESE, and M. VOLONTE. Protein misfolding in Alzheimer's and Parkinson's disease: genetics and molecular mechanisms. 23(5):957–976, 2002.
- [69] T. Förster and K. Kasper. Ein Konzentrationsumschlag der Fluoreszenz. 1(5_6):275–277, 1954.
- [70] S. Fujiyama, M. Yanagida, T. Hayano, Y. Miura, T. Isobe, F. Fujimori, T. Uchida, and N. Takahashi. Isolation and proteomic characterization of human Parvulin-associated preribosomal ribonucleoprotein complexes. 277(26):23773–23780, 2002. Journal Article Research Support, Non-U.S. Gov't.
- [71] S. Fujiyama-Nakamura, H. Yoshikawa, K. Homma, T. Hayano, T. Tsujimura-Takahashi, K. Izumikawa, H. Ishikawa, N. Miyazawa, M. Yanagida, Y. Miura,

- T. Shinkawa, Y. Yamauchi, T. Isobe, and N. Takahashi. Parvulin (Par14), a peptidyl-prolyl cis-trans isomerase, is a novel rRNA processing factor that evolved in the metazoan lineage. 8(7):1552–1565, 2009. Journal Article Research Support, Non-U.S. Gov't.
- [72] M.-C. Galas, P. Dourlen, S. Bégard, K. Ando, D. Blum, M. Hamdane, and L. Buée. The peptidylprolyl cis/trans-isomerase Pin1 modulates stress-induced dephosphorylation of Tau in neurons. Implication in a pathological mechanism related to Alzheimer disease. 281(28):19296–19304, 2006. Journal Article Research Support, Non-U.S. Gov't.
- [73] J. Gandhi, A. C. Antonelli, A. Afridi, S. Vatsia, G. Joshi, V. Romanov, I. V. J. Murray, and S. A. Khan. Protein misfolding and aggregation in neurodegenerative diseases: a review of pathogeneses, novel detection strategies, and potential therapeutics. 30(4):339–358, 2019. Journal Article Review.
- [74] Y.-L. Gao, N. Wang, F.-R. Sun, X.-P. Cao, W. Zhang, and J.-T. Yu. Tau in neurodegenerative disease. 6(10):175, 2018. Journal Article Review Conflicts of Interest: The authors have no conflicts of interest to declare.
- [75] T. R. Gemmill, X. Wu, and S. D. Hanes. Vanishingly low levels of Ess1 prolyl-isomerase activity are sufficient for growth in *Saccharomyces cerevisiae*. 280(16):15510–15517, 2005. Journal Article Research Support, N.I.H., Extramural Research Support, U.S. Gov't, P.H.S.
- [76] George Gabriel Stokes. On the change of refrangibility of light. - No. II. 6:333–335, 1854.
- [77] A. Ghosh, H. Saminathan, A. Kanthasamy, V. Anantharam, H. Jin, G. Sondarva, D. S. Harischandra, Z. Qian, A. Rana, and A. G. Kanthasamy. The Peptidyl-prolyl Isomerase Pin1 Up-regulation and Proapoptotic Function in Dopaminergic Neurons: RELEVANCE TO THE PATHOGENESIS OF PARKINSON DISEASE*. 288(30):21955–21971, 2013. Journal Article.
- [78] A. Goehring, I. Michin, T. Gerdes, N. Schulze, M. Blueggel, E. Rehic, F. Kaschani, M. Kaiser, and P. Bayer. Targeting of parvulin interactors by diazirine mediated cross-linking discloses a cellular role of human Par14/17 in actin polymerization. 401(8):955–968, 2020. Journal Article.
- [79] J. Y. Goh, C.-Y. Lai, L. C. Tan, D. Yang, C. Y. He, and Y.-C. Liou. Functional characterization of two novel parvulins in *Trypanosoma brucei*. 584(13):2901–2908, 2010. Journal Article Research Support, Non-U.S. Gov't.

- [80] S. F. Göthel and M. A. Marahiel. Peptidyl-prolyl cis-trans isomerases, a superfamily of ubiquitous folding catalysts. 55(3):423–436, 1999. Journal Article Research Support, Non-U.S. Gov't Review.
- [81] G. K. Gouras, T. T. Olsson, and O. Hansson. β -Amyloid peptides and amyloid plaques in Alzheimer's disease. 12(1):3–11, 2015. Journal Article Research Support, Non-U.S. Gov't Review.
- [82] D. Guan and H.-Y. Kao. The function, regulation and therapeutic implications of the tumor suppressor protein, PML. 5:60, 2015. Journal Article Review.
- [83] P. Güntert. Automated NMR structure calculation with CYANA. 278:353–378, 2004. Journal Article.
- [84] P. Güntert, W. Braun, and K. Wüthrich. Efficient computation of three-dimensional protein structures in solution from nuclear magnetic resonance data using the program DIANA and the supporting programs CALIBA, HABAS and GLOMSA. 217(3):517–530, 1991. PII: 002228369190754T.
- [85] P. Güntert and L. Buchner. Combined automated NOE assignment and structure calculation with CYANA. 62(4):453–471, 2015. Journal Article Research Support, Non-U.S. Gov't.
- [86] P. Güntert, C. Mumenthaler, and K. Wüthrich. Torsion angle dynamics for NMR structure calculation with the new program DYANA. 273(1):283–298, 1997. Journal Article Research Support, Non-U.S. Gov't.
- [87] D. Gupta and N. Tuteja. Chaperones and foldases in endoplasmic reticulum stress signaling in plants. 6(2):232–236, 2011. Journal Article Research Support, Non-U.S. Gov't Review.
- [88] S. Halder, S. Samanta, and G. Das. Exploring the potential of a urea derivative: an AIE-luminogen and its interaction with human serum albumin in aqueous medium. 2019. Journal Article.
- [89] I. W. Hamley. The amyloid beta peptide: a chemist's perspective. Role in Alzheimer's and fibrillization. 112(10):5147–5192, 2012. Journal Article Research Support, Non-U.S. Gov't Review.
- [90] Y. Han, S. H. Lee, M. Bahn, C.-Y. Yeo, and K. Y. Lee. Pin1 enhances adipocyte differentiation by positively regulating the transcriptional activity of PPAR γ . 436:150–158, 2016. Journal Article Research Support, Non-U.S. Gov't.
- [91] S. D. Hanes. The Ess1 prolyl isomerase: traffic cop of the RNA polymerase II transcription cycle. 1839(4):316–333, 2014. Journal Article Research Support, N.I.H., Extramural Research Support, U.S. Gov't, Non-P.H.S. Review.

- [92] S. D. Hanes, P. R. Shank, and K. A. Bostian. Sequence and mutational analysis of ESS1, a gene essential for growth in *Saccharomyces cerevisiae*. 5(1):55–72, 1989. Journal Article Research Support, Non-U.S. Gov't Research Support, U.S. Gov't, P.H.S.
- [93] J. Hani, G. Stumpf, and H. Domdey. PTF1 encodes an essential protein in *Saccharomyces cerevisiae*, which shows strong homology with a new putative family of PPlases. 365(2-3):198–202, 1995.
- [94] M. W. Harding, A. Galat, D. E. Uehling, and S. L. Schreiber. A receptor for the immunosuppressant FK506 is a cis-trans peptidyl-prolyl isomerase. 341(6244):758–760, 1989. Journal Article Research Support, U.S. Gov't, P.H.S.
- [95] M. Hashimoto, E. Rockenstein, L. Crews, and E. Masliah. Role of Protein Aggregation in Mitochondrial Dysfunction and Neurodegeneration in Alzheimer's and Parkinson's Diseases. 4(1-2):21–36, 2003.
- [96] D. M. Hatters. Protein misfolding inside cells: the case of huntingtin and Huntington's disease. 60(11):724–728, 2008. Journal Article Review.
- [97] M. Hayduk, S. Riebe, K. Rudolph, S. Schwarze, F. van der Vight, C. G. Daniluc, G. Jansen, and J. Voskuhl. Molecular Recognition of Spermine using Aggregation-Induced Emission. 58(8):927–931, 2018.
- [98] Z. He, L. Shan, J. Mei, H. Wang, J. W. Y. Lam, H. H. Y. Sung, I. D. Williams, X. Gu, Q. Miao, and B. Z. Tang. Aggregation-induced emission and aggregation-promoted photochromism of bis(diphenylmethylene)dihydroacenes. 6(6):3538–3543, 2015. Journal Article.
- [99] L. Hennig, C. Christner, M. Kipping, B. Schelbert, K. P. Rücknagel, S. Grabley, G. Küllertz, and G. Fischer. Selective inactivation of parvulin-like peptidyl-prolyl cis/trans isomerases by juglone. 37(17):5953–5960, 1998. Journal Article Research Support, Non-U.S. Gov't.
- [100] T. Herrmann, P. Güntert, and K. Wüthrich. Protein NMR Structure Determination with Automated NOE Assignment Using the New Software CANDID and the Torsion Angle Dynamics Algorithm DYANA. 319(1):209–227, 2002. PII: S0022283602002413.
- [101] T. Herrmann, P. Güntert, and K. Wüthrich. Protein NMR structure determination with automated NOE-identification in the NOESY spectra using the new software ATNOS. 24(3):171–189, 2002. Comparative Study Journal Article Research Support, Non-U.S. Gov't Validation Study.
- [102] I. Hoffmann. The role of Cdc25 phosphatases in cell cycle checkpoints. 211(1-2):8–11, 2000. PII: BF01279894.

- [103] Y. Hong, J. W. Y. Lam, and B. Z. Tang. Aggregation-induced emission. 40(11):5361–5388, 2011. Journal Article Research Support, Non-U.S. Gov't Review.
- [104] Y. Hong, L. Meng, S. Chen, C. W. T. Leung, L.-T. Da, M. Faisal, D.-A. Silva, J. Liu, J. W. Y. Lam, X. Huang, and B. Z. Tang. Monitoring and inhibition of insulin fibrillation by a small organic fluorogen with aggregation-induced emission characteristics. 134(3):1680–1689, 2012. Journal Article Research Support, Non-U.S. Gov't.
- [105] H. Hou, J.-Z. Wang, B.-G. Liu, and T. Zhang. Pin1 liberates the human immunodeficiency virus type-1 (HIV-1): Must we stop it? 565(1):9–14, 2015. Journal Article Research Support, Non-U.S. Gov't Review.
- [106] F. Hu, Y. Huang, G. Zhang, R. Zhao, and D. Zhang. A highly selective fluorescence turn-on detection of hydrogen peroxide and d-glucose based on the aggregation/deaggregation of a modified tetraphenylethylene. 55(8):1471–1474, 2014. PII: S0040403914000902.
- [107] Y.-G. Hu, Y.-F. Shen, and Y. Li. Effect of Pin1 inhibitor juglone on proliferation, migration and angiogenic ability of breast cancer cell line MCF7Adr. 35(4):531–534, 2015. Journal Article.
- [108] H. Huang, F. Ullah, D.-X. Zhou, M. Yi, and Y. Zhao. Mechanisms of ROS Regulation of Plant Development and Stress Responses. 10:800, 2019. Journal Article Review.
- [109] Y. Huang, F. Hu, R. Zhao, G. Zhang, H. Yang, and D. Zhang. Tetraphenylethylene Conjugated with a Specific Peptide as a Fluorescence Turn-On Bioprobe for the Highly Specific Detection and Tracing of Tumor Markers in Live Cancer Cells. 20(1):158–164, 2014.
- [110] B. T. Innes, M. L. Bailey, C. J. Brandl, B. H. Shilton, and D. W. Litchfield. Non-catalytic participation of the Pin1 peptidyl-prolyl isomerase domain in target binding. 4:18, 2013. Journal Article.
- [111] G. B. Irvine, O. M. El-Agnaf, G. M. Shankar, and D. M. Walsh. Protein aggregation in the brain: the molecular basis for Alzheimer's and Parkinson's diseases. 14(7-8):451–464, 2008. Journal Article Research Support, Non-U.S. Gov't Review.
- [112] R. Islam, W.-J. Yoon, and H.-M. Ryoo. Pin1, the Master Orchestrator of Bone Cell Differentiation. 232(9):2339–2347, 2017. Journal Article Review.
- [113] A. Jabłoński. Über den Mechanismus der Photolumineszenz von Farbstoffphosphoren. 94(1-2):38–46, 1935. PII: BF01330795.

- [114] A. Jabs, M. S. Weiss, and R. Hilgenfeld. Non-proline cis peptide bonds in proteins. 286(1):291–304, 1999. Journal Article Research Support, Non-U.S. Gov't.
- [115] D. M. Jacobs, K. Saxena, M. Vogtherr, P. Bernado, M. Pons, and K. M. Fiebig. Peptide binding induces large scale changes in inter-domain mobility in human Pin1. 278(28):26174–26182, 2003. Journal Article Research Support, Non-U.S. Gov't.
- [116] M. R. Jacobson, V. L. Cash, M. C. Weiss, N. F. Laird, W. E. Newton, and D. R. Dean. Biochemical and genetic analysis of the nifUSVWZM cluster from *Azotobacter vinelandii*. 219(1-2):49–57, 1989. Journal Article Research Support, U.S. Gov't, Non-P.H.S. Research Support, U.S. Gov't, P.H.S.
- [117] J. Janin, R. P. Bahadur, and P. Chakrabarti. Protein-protein interaction and quaternary structure. 41(2):133–180, 2008. Journal Article Research Support, Non-U.S. Gov't Review.
- [118] M. Jouanne, S. Rault, and A.-S. Voisin-Chiret. Tau protein aggregation in Alzheimer's disease: An attractive target for the development of novel therapeutic agents. 139:153–167, 2017. Journal Article Review.
- [119] D. Kamiyama, S. Sekine, B. Barsi-Rhyne, J. Hu, B. Chen, L. A. Gilbert, H. Ishikawa, M. D. Leonetti, W. F. Marshall, J. S. Weissman, and B. Huang. Versatile protein tagging in cells with split fluorescent protein. 7:11046, 2016. Journal Article Research Support, N.I.H., Extramural Research Support, Non-U.S. Gov't.
- [120] R. Kanaoka, A. Kushiya, Y. Seno, Y. Nakatsu, Y. Matsunaga, T. Fukushima, Y. Tsuchiya, H. Sakoda, M. Fujishiro, T. Yamamotoya, H. Kamata, A. Matsubara, and T. Asano. Pin1 Inhibitor Juglone Exerts Anti-Oncogenic Effects on LNCaP and DU145 Cells despite the Patterns of Gene Regulation by Pin1 Differing between These Cell Lines. 10(6):e0127467, 2015. Journal Article Research Support, Non-U.S. Gov't.
- [121] C. Karlsson, S. Katich, A. Hagting, I. Hoffmann, and J. Pines. Cdc25b and Cdc25c Differ Markedly in Their Properties as Initiators of Mitosis. 146(3):573–584, 1999. Journal Article.
- [122] T. Kato, A. Kawaguchi, K. Nagata, and K. Hatanaka. Development of tetraphenylethylene-based fluorescent oligosaccharide probes for detection of influenza virus. 394(1):200–204, 2010. Journal Article Research Support, Non-U.S. Gov't.
- [123] R. Keller. *The computer aided resonance assignment tutorial*. Cantina Verl., 1. ed. edition, 2004. Keller, Rochus (Verfasser).

- [124] D. Kessler, P. Papatheodorou, T. Stratmann, E. A. Dian, C. Hartmann-Fatu, J. Rassow, P. Bayer, and J. W. Mueller. The DNA binding parvulin Par17 is targeted to the mitochondrial matrix by a recently evolved prepeptide uniquely present in Hominidae. 5:37, 2007. Journal Article Research Support, Non-U.S. Gov't.
- [125] G. A. Houry, R. C. Baliban, and C. A. Floudas. Proteome-wide post-translational modification statistics: frequency analysis and curation of the swiss-prot database. 1, 2011. Journal Article.
- [126] G. Kim, P. Khanal, J. Y. Kim, H.-J. Yun, S.-C. Lim, J.-H. Shim, and H. S. Choi. COT phosphorylates prolyl-isomerase Pin1 to promote tumorigenesis in breast cancer. 54(6):440–448, 2015. Journal Article Research Support, Non-U.S. Gov't.
- [127] J. Kim, S. Cho, and B.-K. Cho. An unusual stacking transformation in liquid-crystalline columnar assemblies of clicked molecular propellers with tunable light emissions. 20(40):12734–12739, 2014. Journal Article.
- [128] Y. Kim, S. O. Ho, N. R. Gassman, Y. Korlann, E. V. Landorf, F. R. Collart, and S. Weiss. Efficient site-specific labeling of proteins via cysteines. 19(3):786–791, 2008. Journal Article Research Support, N.I.H., Extramural Research Support, U.S. Gov't, Non-P.H.S.
- [129] T. Kimura, K. Tsutsumi, M. Taoka, T. Saito, M. Masuda-Suzukake, K. Ishiguro, F. Plattner, T. Uchida, T. Isobe, M. Hasegawa, and S.-i. Hisanaga. Isomerase Pin1 stimulates dephosphorylation of tau protein at cyclin-dependent kinase (Cdk5)-dependent Alzheimer phosphorylation sites. 288(11):7968–7977, 2013. Journal Article Research Support, Non-U.S. Gov't.
- [130] V. P. Kontinen, P. Saris, and M. Sarvas. A gene (*prsA*) of *Bacillus subtilis* involved in a novel, late stage of protein export. 5(5):1273–1283, 1991. Comparative Study Journal Article Research Support, Non-U.S. Gov't.
- [131] L. Kovačič and R. Boelens. Protein-DNA Interactions. In G. Parigi, I. Bertini, and K. S. McGreevy, editors, *NMR of biomolecules*, pages 238–252. Wiley-VCH, 2012.
- [132] J. R. Lakowicz. *Principles of fluorescence spectroscopy*. Springer, third edition, corrected at 4. printing edition, 2010. Lakowicz, Joseph R. (VerfasserIn).
- [133] I. Landrieu, L. de Veylder, J. S. Fruchart, B. Odaert, P. Casteels, D. Portetelle, M. van Montagu, D. Inzé, and G. Lippens. The *Arabidopsis thaliana* PIN1At gene encodes a single-domain phosphorylation-dependent peptidyl prolyl cis/trans isomerase. 275(14):10577–10581, 2000. Journal Article Research Support, Non-U.S. Gov't.

- [134] S. W. Lazar and R. Kolter. SurA assists the folding of Escherichia coli outer membrane proteins. 178(6):1770–1773, 1996. Journal Article Research Support, U.S. Gov't, Non-P.H.S. Research Support, U.S. Gov't, P.H.S.
- [135] D. Y. Lee, C. Teyssier, B. D. Strahl, and M. R. Stallcup. Role of protein methylation in regulation of transcription. 26(2):147–170, 2005. Journal Article Research Support, N.I.H., Extramural Research Support, U.S. Gov't, P.H.S. Review.
- [136] K.-H. Lee, F.-C. Lin, T.-I. Hsu, J.-T. Lin, J.-H. Guo, C.-H. Tsai, Y.-C. Lee, Y.-C. Lee, C.-L. Chen, M. Hsiao, and P.-J. Lu. MicroRNA-296-5p (miR-296-5p) functions as a tumor suppressor in prostate cancer by directly targeting Pin1. 1843(9):2055–2066, 2014. Journal Article Research Support, Non-U.S. Gov't.
- [137] T. H. Lee, C.-H. Chen, F. Suizu, P. Huang, C. Schiene-Fischer, S. Daum, Y. J. Zhang, A. Goate, R.-H. Chen, X. Z. Zhou, and K. P. Lu. Death Associated Protein Kinase 1 Phosphorylates Pin1 and Inhibits its Prolyl Isomerase Activity and Cellular Function. 42(2):147–159, 2011. Journal Article.
- [138] W. Lee, M. J. Revington, C. Arrowsmith, and L. E. Kay. A pulsed field gradient isotope-filtered 3D ^{13}C HMQC-NOESY experiment for extracting intermolecular NOE contacts in molecular complexes. 350(1):87–90, 1994.
- [139] Y.-C. Lee, J. Que, Y.-C. Chen, J.-T. Lin, Y.-C. Liou, P.-C. Liao, Y.-P. Liu, K.-H. Lee, L.-C. Lin, M. Hsiao, L.-Y. Hung, C.-Y. Huang, and P.-J. Lu. Pin1 acts as a negative regulator of the G2/M transition by interacting with the Aurora-A-Bora complex. 126(Pt 21):4862–4872, 2013. Journal Article Research Support, Non-U.S. Gov't.
- [140] K.-W. Leong, C.-W. Cheng, C.-M. Wong, I. O.-L. Ng, Y.-L. Kwong, and E. Tse. miR-874-3p is down-regulated in hepatocellular carcinoma and negatively regulates PIN1 expression. 8(7):11343–11355, 2017. Journal Article.
- [141] N. L. C. Leung, N. Xie, W. Yuan, Y. Liu, Q. Wu, Q. Peng, Q. Miao, J. W. Y. Lam, and B. Z. Tang. Restriction of intramolecular motions: the general mechanism behind aggregation-induced emission. 20(47):15349–15353, 2014. Journal Article.
- [142] H. Li, S. Wang, T. Zhu, J. Zhou, Q. Xu, Y. Lu, and D. Ma. Pin1 contributes to cervical tumorigenesis by regulating cyclin D1 expression. 16(3):491–496, 2006. Journal Article Research Support, Non-U.S. Gov't.
- [143] S. S.-C. Li. Specificity and versatility of SH3 and other proline-recognition domains: structural basis and implications for cellular signal transduction. 390(Pt 3):641–653, 2005. Journal Article Research Support, Non-U.S. Gov't Review.

- [144] Y. Li, Z. Li, Y. Wang, A. Compaan, T. Ren, and W.-J. Dong. Increasing the power output of a CdTe solar cell via luminescent down shifting molecules with intramolecular charge transfer and aggregation-induced emission characteristics. 6(10):2907, 2013.
- [145] Y. Li, K. Xu, Y. Si, C. Yang, Q. Peng, J. He, Q. Hu, and K. Li. An aggregation-induced emission (AIE) fluorescent chemosensor for the detection of Al(III) in aqueous solution. 171:107682, 2019. PII: S014372081931112X.
- [146] Y. Li, Z. Xu, X. Zhu, B. Chen, Z. Wang, B. Xiao, J. W. Y. Lam, Z. Zhao, D. Ma, and B. Z. Tang. Creation of Efficient Blue Aggregation-Induced Emission Lumino-gens for High-Performance Nondoped Blue OLEDs and Hybrid White OLEDs. 11(19):17592–17601, 2019. Journal Article.
- [147] Z. Li and P. Srivastava. Heat-shock proteins. Appendix 1:Appendix 1T, 2004. Journal Article Review.
- [148] J. Liang, R. T. K. Kwok, H. Shi, B. Z. Tang, and B. Liu. Fluorescent light-up probe with aggregation-induced emission characteristics for alkaline phosphatase sensing and activity study. 5(17):8784–8789, 2013. Journal Article Research Support, Non-U.S. Gov't.
- [149] L. Liang and D. Astruc. The copper(I)-catalyzed alkyne-azide cycloaddition (CuAAC) “click” reaction and its applications. An overview. 255(23-24):2933–2945, 2011. PII: S0010854511001809.
- [150] J. H. Lim, Y. Liu, E. Reineke, and H.-Y. Kao. Mitogen-activated protein kinase extracellular signal-regulated kinase 2 phosphorylates and promotes Pin1 protein-dependent promyelocytic leukemia protein turnover. 286(52):44403–44411, 2011. Journal Article Research Support, N.I.H., Extramural Research Support, Non-U.S. Gov't.
- [151] Y.-S. Lim, H. T. L. Tran, S.-J. Park, S.-A. Yim, and S. B. Hwang. Peptidyl-prolyl isomerase Pin1 is a cellular factor required for hepatitis C virus propagation. 85(17):8777–8788, 2011. Journal Article Research Support, Non-U.S. Gov't.
- [152] J. Lin, X. Zeng, Y. Xiao, L. Tang, J. Nong, Y. Liu, H. Zhou, B. Ding, F. Xu, H. Tong, Z. Deng, and X. Hong. Novel near-infrared II aggregation-induced emission dots for in vivo bioimaging. 10(4):1219–1226, 2019. Journal Article.
- [153] S. I. Liochev. Reactive oxygen species and the free radical theory of aging. 60:1–4, 2013. Journal Article Review.
- [154] G. Lippens, A. Sillen, I. Landrieu, L. Amniai, N. Sibille, P. Barbier, A. Leroy, X. Hanoulle, and J.-M. Wieruszeski. Tau aggregation in Alzheimer's disease:

- what role for phosphorylation? 1(1):21–25, 2007. Comparative Study Journal Article Research Support, Non-U.S. Gov't Review.
- [155] H. Liu, L.-H. Xiong, R. T. K. Kwok, X. He, J. W. Y. Lam, and B. Z. Tang. AIE Bioconjugates for Biomedical Applications. 8(14):2000162, 2020.
- [156] K. Liu, H. Shang, X. Kong, M. Ren, J.-Y. Wang, Y. Liu, and W. Lin. A novel near-infrared fluorescent probe for H₂O₂ in alkaline environment and the application for H₂O₂ imaging in vitro and in vivo. 100:162–171, 2016. Journal Article Research Support, Non-U.S. Gov't.
- [157] T. Liu, Y. Liu, H.-Y. Kao, and D. Pei. Membrane permeable cyclic peptidyl inhibitors against human Peptidylprolyl Isomerase Pin1. 53(6):2494–2501, 2010. Journal Article Research Support, N.I.H., Extramural Research Support, Non-U.S. Gov't.
- [158] Y. Liu, C. Deng, L. Tang, A. Qin, R. Hu, J. Z. Sun, and B. Z. Tang. Specific detection of D-glucose by a tetraphenylethene-based fluorescent sensor. 133(4):660–663, 2011. Journal Article Research Support, Non-U.S. Gov't.
- [159] Y. Liu, Y. Guo, and Y. Liu. High-Mobility Organic Light-Emitting Semiconductors and Its Optoelectronic Devices. 2(1):2000083, 2021.
- [160] Y. Liu, Y. Yu, J. W. Y. Lam, Y. Hong, M. Faisal, W. Z. Yuan, and B. Z. Tang. Simple biosensor with high selectivity and sensitivity: thiol-specific biomolecular probing and intracellular imaging by AIE fluorogen on a TLC plate through a thiol-ene click mechanism. 16(28):8433–8438, 2010. Journal Article Research Support, Non-U.S. Gov't.
- [161] X. Lou, Y. Hong, S. Chen, C. W. T. Leung, N. Zhao, B. Situ, J. W. Y. Lam, and B. Z. Tang. A selective glutathione probe based on AIE fluorogen and its application in enzymatic activity assay. 4:4272, 2014. Journal Article Research Support, Non-U.S. Gov't.
- [162] X. Lou, C. W. T. Leung, C. Dong, Y. Hong, S. Chen, E. Zhao, J. W. Y. Lam, and B. Z. Tang. Detection of adenine-rich ssDNA based on thymine-substituted tetraphenylethene with aggregation-induced emission characteristics. 4(63):33307, 2014.
- [163] K. P. Lu, S. D. Hanes, and T. Hunter. A human peptidyl-prolyl isomerase essential for regulation of mitosis. 380(6574):544–547, 1996. Journal Article Research Support, Non-U.S. Gov't Research Support, U.S. Gov't, P.H.S.
- [164] P. J. Lu, G. Wulf, X. Z. Zhou, P. Davies, and K. P. Lu. The prolyl isomerase Pin1 restores the function of Alzheimer-associated phosphorylated tau protein.

- 399(6738):784–788, 1999. Journal Article Research Support, Non-U.S. Gov't Research Support, U.S. Gov't, P.H.S.
- [165] P.-J. Lu, X. Z. Zhou, Y.-C. Liou, J. P. Noel, and K. P. Lu. Critical role of WW domain phosphorylation in regulating phosphoserine binding activity and Pin1 function. 277(4):2381–2384, 2002. Journal Article Research Support, Non-U.S. Gov't Research Support, U.S. Gov't, P.H.S.
- [166] Z. Lu, Y. Liu, S. Lu, Y. Li, X. Liu, Y. Qin, and L. Zheng. A highly selective TPE-based AIE fluorescent probe is developed for the detection of Ag⁺. 8(35):19701–19706, 2018.
- [167] L. M. Luh, R. Hänsel, F. Löhr, D. K. Kirchner, K. Krauskopf, S. Pitzius, B. Schäfer, P. Tufar, I. Corbeski, P. Güntert, and V. Dötsch. Molecular crowding drives active Pin1 into nonspecific complexes with endogenous proteins prior to substrate recognition. 135(37):13796–13803, 2013. Journal Article Research Support, Non-U.S. Gov't Journal Article Research Support, Non-U.S. Gov't.
- [168] L. M. Luh, D. K. Kirchner, F. Loehr, R. Haensel, and V. Doetsch. Pin1 WW domain, 2014.
- [169] L. M. Luh, D. K. Kirchner, F. Loehr, R. Haensel, and V. Doetsch. *Structure of Pin1 WW domain*. 2014.
- [170] J. Luo, K. Song, F. I. Gu, and Q. Miao. Switching of non-helical overcrowded tetrabenzoheptafulvalene derivatives. 2(10):2029, 2011.
- [171] J. Luo, Z. Xie, J. W. Y. Lam, L. Cheng, B. Z. Tang, H. Chen, C. Qiu, H. S. Kwok, X. Zhan, Y. Liu, and D. Zhu. Aggregation-induced emission of 1-methyl-1,2,3,4,5-pentaphenylsilole. (18):1740–1741, 2001.
- [172] M.-L. Luo, C. Gong, C.-H. Chen, D. Y. Lee, H. Hu, P. Huang, Y. Yao, W. Guo, F. Reinhardt, G. Wulf, J. Lieberman, X. Z. Zhou, E. Song, and K. P. Lu. Prolyl isomerase Pin1 acts downstream of miR200c to promote cancer stem-like cell traits in breast cancer. 74(13):3603–3616, 2014. Journal Article Research Support, N.I.H., Extramural Research Support, Non-U.S. Gov't.
- [173] L. Lv, J. Zhang, L. Zhang, G. Xue, P. Wang, Q. Meng, and W. Liang. Essential role of Pin1 via STAT3 signalling and mitochondria-dependent pathways in restenosis in type 2 diabetes. 17(8):989–1005, 2013. Journal Article Research Support, Non-U.S. Gov't.
- [174] K. Ma, F. Zhang, N. Sayyadi, W. Chen, A. G. Anwer, A. Care, B. Xu, W. Tian, E. M. Goldys, and G. Liu. "Turn-on" Fluorescent Aptasensor Based on AIEgen Labeling for the Localization of IFN- γ in Live Cells. 3(2):320–326, 2018. Journal Article.

- [175] Y. Ma, M. Cametti, Z. Džolić, and S. Jiang. Selective Cu(ii) sensing by a versatile AIE cyanostilbene-based gel system. 15(30):6145–6150, 2019. Journal Article.
- [176] Z. Ma, D. Atencio, C. Barnes, H. Defiglio, and S. D. Hanes. Multiple roles for the Ess1 prolyl isomerase in the RNA polymerase II transcription cycle. 32(17):3594–3607, 2012. Journal Article Research Support, American Recovery and Reinvestment Act Research Support, N.I.H., Extramural Research Support, Non-U.S. Gov't Research Support, U.S. Gov't, Non-P.H.S.
- [177] S. Maity, R. K. Gundampati, and T. K. Suresh Kumar. NMR Methods to Characterize Protein-Ligand Interactions. 14(5):1934578X1984929, 2019.
- [178] E. Mandelkow, M. von Bergen, J. Biernat, and E.-M. Mandelkow. Structural principles of tau and the paired helical filaments of Alzheimer's disease. 17(1):83–90, 2007. Journal Article Research Support, Non-U.S. Gov't Review.
- [179] B. J. Mayer. SH3 domains: complexity in moderation. 114(7):1253–1263, 2001.
- [180] J. Mei, Y. Hong, J. W. Y. Lam, A. Qin, Y. Tang, and B. Z. Tang. Aggregation-induced emission: the whole is more brilliant than the parts. 26(31):5429–5479, 2014. Journal Article Research Support, Non-U.S. Gov't Review.
- [181] J. Mei, N. L. C. Leung, R. T. K. Kwok, J. W. Y. Lam, and B. Z. Tang. Aggregation-Induced Emission: Together We Shine, United We Soar! 115(21):11718–11940, 2015. Journal Article Research Support, Non-U.S. Gov't Review.
- [182] M. Meldal and C. W. Tornøe. Cu-catalyzed azide-alkyne cycloaddition. 108(8):2952–3015, 2008. Journal Article Review Journal Article Review.
- [183] F. Meng, C. Luo, Y. Hu, M. Yin, M. Lin, G. Lou, and R. Zhou. Overexpression of LAPTM4B-35 in cervical carcinoma: a clinicopathologic study. 29(6):587–593, 2010. Journal Article.
- [184] R. B. Merrifield. Solid Phase Peptide Synthesis. I. The Synthesis of a Tetrapeptide. 85(14):2149–2154, 1963.
- [185] Y. Miao, W. Yang, and J. Lv. Fluorescence detection of fluorine ions in biological fluids based on aggregation-induced emission. 10(47):28205–28212, 2020.
- [186] J. B. Millar, J. Blevitt, L. Gerace, K. Sadhu, C. Featherstone, and P. Russell. p55CDC25 is a nuclear protein required for the initiation of mitosis in human cells. 88(23):10500–10504, 1991. Journal Article Research Support, Non-U.S. Gov't Research Support, U.S. Gov't, P.H.S.
- [187] H. Misonou, M. Morishima-Kawashima, and Y. Ihara. Oxidative stress induces intracellular accumulation of amyloid beta-protein (Abeta) in human neuroblastoma cells. 39(23):6951–6959, 2000. Journal Article.

- [188] M. Möller and A. Denicola. Study of protein-ligand binding by fluorescence. 30(5):309–312, 2002.
- [189] R. S. Morgan and J. M. McAdon. Predictor for sulfur-aromatic interactions in globular proteins. 15(2):177–180, 1980. Journal Article.
- [190] R. S. Morgan, C. E. Tatsch, R. H. Gushard, J. McAdon, and P. K. Warne. Chains of alternating sulfur and pi-bonded atoms in eight small proteins. 11(3):209–217, 1978. Journal Article.
- [191] D. P. Morris, H. P. Phatnani, and A. L. Greenleaf. Phospho-carboxyl-terminal domain binding and the role of a prolyl isomerase in pre-mRNA 3'-End formation. 274(44):31583–31587, 1999. Journal Article.
- [192] M. Mücke and F. X. Schmid. Enzymatic catalysis of prolyl isomerization in an unfolding protein. 31(34):7848–7854, 1992. Journal Article Research Support, Non-U.S. Gov't.
- [193] J. W. Mueller and P. Bayer. Small family with key contacts: par14 and par17 parvulin proteins, relatives of pin1, now emerge in biomedical research. 2:11–20, 2008. Journal Article.
- [194] J. W. Mueller, D. Kessler, D. Neumann, T. Stratmann, P. Papatheodorou, C. Hartmann-Fatu, and P. Bayer. Characterization of novel elongated Parvulin isoforms that are ubiquitously expressed in human tissues and originate from alternative transcription initiation. 7:9, 2006. Journal Article.
- [195] J. W. Mueller, N. M. Link, A. Matena, L. Hoppstock, A. Rüppel, P. Bayer, and W. Blankenfeldt. Crystallographic proof for an extended hydrogen-bonding network in small prolyl isomerases. 133(50):20096–20099, 2011. Journal Article Research Support, Non-U.S. Gov't.
- [196] M. P. Murphy and H. LeVine. Alzheimer's disease and the amyloid-beta peptide. 19(1):311–323, 2010. Journal Article Research Support, N.I.H., Extramural Review.
- [197] K. Nakamura, I. Kosugi, D. Y. Lee, A. Hafner, D. A. Sinclair, A. Ryo, and K. P. Lu. Prolyl isomerase Pin1 regulates neuronal differentiation via β -catenin. 32(15):2966–2978, 2012. Journal Article Research Support, N.I.H., Extramural.
- [198] Y. Nakatsu, Y. Matsunaga, T. Yamamotoya, K. Ueda, Y. Inoue, K. Mori, H. Sakoda, M. Fujishiro, H. Ono, A. Kushiyama, and T. Asano. Physiological and Pathogenic Roles of Prolyl Isomerase Pin1 in Metabolic Regulations via Multiple Signal Transduction Pathway Modulations. 17(9), 2016. Journal Article Review The authors declare no conflict of interest.

- [199] Y. Narita, T. Murata, A. Ryo, D. Kawashima, A. Sugimoto, T. Kanda, H. Kimura, and T. Tsurumi. Pin1 interacts with the Epstein-Barr virus DNA polymerase catalytic subunit and regulates viral DNA replication. 87(4):2120–2127, 2013. Journal Article Research Support, Non-U.S. Gov't.
- [200] N. Nebra and J. García-Álvarez. Recent Progress of Cu-Catalyzed Azide-Alkyne Cycloaddition Reactions (CuAAC) in Sustainable Solvents: Glycerol, Deep Eutectic Solvents, and Aqueous Media. 25(9):2015, 2020. PII: molecules25092015.
- [201] S. Neumann, M. Biewend, S. Rana, and W. H. Binder. The CuAAC: Principles, Homogeneous and Heterogeneous Catalysts, and Novel Developments and Applications. 41(1):e1900359, 2020. Journal Article Review Journal Article Review.
- [202] J. T. Nguyen, C. W. Turck, F. E. Cohen, R. N. Zuckermann, and W. A. Lim. Exploiting the basis of proline recognition by SH3 and WW domains: design of N-substituted inhibitors. 282(5396):2088–2092, 1998. Journal Article Research Support, Non-U.S. Gov't Research Support, U.S. Gov't, P.H.S. Journal Article Research Support, Non-U.S. Gov't Research Support, U.S. Gov't, P.H.S.
- [203] A. N. Nguyen Ba, A. Pogoutse, N. Provar, and A. M. Moses. NLStradamus: a simple Hidden Markov Model for nuclear localization signal prediction. 10:202, 2009. Journal Article Research Support, Non-U.S. Gov't Journal Article Research Support, Non-U.S. Gov't.
- [204] A. H. Osmani, S. L. McGuire, and S. A. Osmani. Parallel activation of the NIMA and p34cdc2 cell cycle-regulated protein kinases is required to initiate mitosis in *A. nidulans*. 67(2):283–291, 1991.
- [205] W. K. Paik, D. C. Paik, and S. Kim. Historical review: the field of protein methylation. 32(3):146–152, 2007. Historical Article Journal Article Research Support, Non-U.S. Gov't Review.
- [206] L. Pastorino, A. Sun, P.-J. Lu, X. Z. Zhou, M. Balastik, G. Finn, G. Wulf, J. Lim, S.-H. Li, X. Li, W. Xia, L. K. Nicholson, and K. P. Lu. The prolyl isomerase Pin1 regulates amyloid precursor protein processing and amyloid-beta production. 440(7083):528–534, 2006. Journal Article Research Support, N.I.H., Extramural Research Support, Non-U.S. Gov't Research Support, U.S. Gov't, Non-P.H.S.
- [207] L. Peng, M. Wang, G. Zhang, D. Zhang, and D. Zhu. A fluorescence turn-on detection of cyanide in aqueous solution based on the aggregation-induced emission. 11(9):1943–1946, 2009. Journal Article Research Support, Non-U.S. Gov't.

- [208] J. R. Perkins, I. Diboun, B. H. Dessailly, J. G. Lees, and C. Orengo. Transient protein-protein interactions: structural, functional, and network properties. 18(10):1233–1243, 2010. Journal Article Review.
- [209] P. Pinton, A. Rimessi, S. Marchi, F. Orsini, E. Migliaccio, M. Giorgio, C. Contursi, S. Minucci, F. Mantovani, M. R. Wieckowski, G. Del Sal, P. G. Pelicci, and R. Rizzuto. Protein kinase C beta and prolyl isomerase 1 regulate mitochondrial effects of the life-span determinant p66Shc. 315(5812):659–663, 2007. Journal Article Research Support, Non-U.S. Gov't.
- [210] S. Prabakaran, G. Lippens, H. Steen, and J. Gunawardena. Post-translational modification: nature's escape from genetic imprisonment and the basis for dynamic information encoding. 4(6):565–583, 2012. Journal Article Research Support, N.I.H., Extramural Research Support, Non-U.S. Gov't Review.
- [211] S. Pramanik, V. Bhalla, and M. Kumar. Hexaphenylbenzene-based fluorescent aggregates for ratiometric detection of cyanide ions at nanomolar level: set-reset memorized sequential logic device. 6(8):5930–5939, 2014. Journal Article Research Support, Non-U.S. Gov't.
- [212] S. Prasad, S. C. Gupta, and A. K. Tyagi. Reactive oxygen species (ROS) and cancer: Role of antioxidative nutraceuticals. 387:95–105, 2017. Journal Article Review.
- [213] A. Preiß, J. Kruppa, J. Buschmann, and C. Mügge. The determination of trifluoroacetic acid in rat milk samples by ¹⁹F-NMR spectroscopy and capillary gas chromatography. 16(8):1381–1385, 1998.
- [214] J.-U. Rahfeld, K. P. Rücknagel, B. Schelbert, B. Ludwig, J. Hacker, K. Mann, and G. Fischer. Confirmation of the existence of a third family among peptidyl-prolyl cis/trans isomerases Amino acid sequence and recombinant production of parvulin. 352(2):180–184, 1994.
- [215] J.-U. Rahfeld, A. Schierhorn, K. Mann, and G. Fischer. A novel peptidyl-prolyl cis/trans isomerase from *Escherichia coli*. 343(1):65–69, 1994.
- [216] R. Ranganathan, K. P. Lu, T. Hunter, and J. P. Noel. Structural and Functional Analysis of the Mitotic Rotamase Pin1 Suggests Substrate Recognition Is Phosphorylation Dependent. 89(6):875–886, 1997. PII: S0092867400802731.
- [217] V. Rangasamy, R. Mishra, G. Sondarva, S. Das, T. H. Lee, J. C. Bakowska, G. Tzivion, J. S. Malter, B. Rana, K. P. Lu, A. Kanthasamy, and A. Rana. Mixed-lineage kinase 3 phosphorylates prolyl-isomerase Pin1 to regulate its nuclear translocation and cellular function. 109(21):8149–8154, 2012. Journal Article Research Support, N.I.H., Extramural Research Support, U.S. Gov't, Non-P.H.S.

- [218] H. Refsum, P. M. Ueland, O. Nygård, and S. E. Vollset. Homocysteine and cardiovascular disease. 49:31–62, 1998. Journal Article Review.
- [219] T. Reimer, M. Weiwad, A. Schierhorn, P.-K. Ruecknagel, J.-U. Rahfeld, P. Bayer, and G. Fischer. Phosphorylation of the N-terminal Domain Regulates Subcellular Localization and DNA Binding Properties of the Peptidyl-prolyl cis/trans Isomerase hPar14. 330(5):955–966, 2003.
- [220] S. Riebe, M. Saccone, J. Stelzer, A. Sowa, C. Wölper, K. Soloviova, C. A. Strassert, M. Giese, and J. Voskuhl. Alkylated Aromatic Thioethers with Aggregation-Induced Emission Properties-Assembly and Photophysics. 2018. Journal Article.
- [221] S. Riebe, C. Vallet, F. van der Vight, D. Gonzalez-Abradelo, C. Wölper, C. A. Strassert, G. Jansen, S. Knauer, and J. Voskuhl. Aromatic Thioethers as Novel Luminophores with Aggregation-Induced Fluorescence and Phosphorescence. 23(55):13660–13668, 2017. Journal Article.
- [222] J. F. Rippmann, S. Hobbie, C. Daiber, B. Guilliard, M. Bauer, J. Birk, H. Nar, P. Garin-Chesa, W. J. Rettig, and A. Schnapp. Phosphorylation-dependent proline isomerization catalyzed by Pin1 is essential for tumor cell survival and entry into mitosis. 11(7):409–416, 2000. Journal Article.
- [223] F. Rizzolio, C. Lucchetti, I. Caligiuri, I. Marchesi, M. Caputo, A. J. Klein-Szanto, L. Bagella, M. Castronovo, and A. Giordano. Retinoblastoma tumor-suppressor protein phosphorylation and inactivation depend on direct interaction with Pin1. 19(7):1152–1161, 2012. Journal Article Research Support, Non-U.S. Gov't.
- [224] T. Ruks, K. Loza, M. Heggen, O. Prymak, A. L. Sehnem, C. L. P. Oliveira, P. Bayer, C. Beuck, and M. Epple. Peptide-Conjugated Ultrasmall Gold Nanoparticles (2 nm) for Selective Protein Targeting. 4(1):945–965, 2021.
- [225] A. Rustighi, L. Tiberi, A. Soldano, M. Napoli, P. Nuciforo, A. Rosato, F. Kaplan, A. Capobianco, S. Pece, P. P. Di Fiore, and G. Del Sal. The prolyl-isomerase Pin1 is a Notch1 target that enhances Notch1 activation in cancer. 11(2):133–142, 2009. Journal Article Research Support, N.I.H., Extramural Research Support, Non-U.S. Gov't.
- [226] A. Rustighi, A. Zannini, E. Campaner, Y. Ciani, S. Piazza, and G. Del Sal. PIN1 in breast development and cancer: a clinical perspective. 24(2):200–211, 2017. Journal Article Review Research Support, Non-U.S. Gov't The authors declare no conflict of interest.
- [227] A. Ryo, Y.-C. Liou, G. Wulf, M. Nakamura, S. W. Lee, and K. P. Lu. PIN1 is an E2F target gene essential for Neu/Ras-induced transformation of mammary epithelial

- cells. 22(15):5281–5295, 2002. Journal Article Research Support, Non-U.S. Gov't Research Support, U.S. Gov't, P.H.S.
- [228] A. Ryo, F. Suizu, Y. Yoshida, K. Perrem, Y.-C. Liou, G. Wulf, R. Rottapel, S. Yamaoka, and K. P. Lu. Regulation of NF- κ B Signaling by Pin1-Dependent Prolyl Isomerization and Ubiquitin-Mediated Proteolysis of p65/RelA. 12(6):1413–1426, 2003.
- [229] A. Ryo, T. Togo, T. Nakai, A. Hirai, M. Nishi, A. Yamaguchi, K. Suzuki, Y. Hirayasu, H. Kobayashi, K. Perrem, Y.-C. Liou, and I. Aoki. Prolyl-isomerase Pin1 accumulates in lewy bodies of parkinson disease and facilitates formation of alpha-synuclein inclusions. 281(7):4117–4125, 2006. Journal Article Research Support, Non-U.S. Gov't.
- [230] N. Sachini, P. Arampatzi, A. Klonizakis, C. Nikolaou, T. Makatounakis, E. W.-F. Lam, A. Kretsovali, and J. Papamatheakis. Promyelocytic leukemia protein (PML) controls breast cancer cell proliferation by modulating Forkhead transcription factors. 13(6):1369–1387, 2019. Journal Article Research Support, Non-U.S. Gov't.
- [231] M. Saegusa, M. Hashimura, and T. Kuwata. Pin1 acts as a modulator of cell proliferation through alteration in NF- κ B but not β -catenin/TCF4 signalling in a subset of endometrial carcinoma cells. 222(4):410–420, 2010. Journal Article Research Support, Non-U.S. Gov't.
- [232] A. D. Saningong and P. Bayer. Human DNA-binding peptidyl-prolyl cis/trans isomerase Par14 is cell cycle dependently expressed and associates with chromatin in vivo. 16:4, 2015. Journal Article Research Support, Non-U.S. Gov't.
- [233] C. Schelhorn, P. Martín-Malpartida, D. Suñol, and M. J. Macias. Structural Analysis of the Pin1-CPEB1 interaction and its potential role in CPEB1 degradation. 5:14990, 2015. Journal Article Research Support, Non-U.S. Gov't.
- [234] G. Scherer, M. L. Kramer, M. Schutkowski, U. Reimer, and G. Fischer. Barriers to Rotation of Secondary Amide Peptide Bonds. 120(22):5568–5574, 1998.
- [235] M. Schieber and N. S. Chandel. ROS function in redox signaling and oxidative stress. 24(10):R453–62, 2014. Journal Article Research Support, N.I.H., Extramural Review.
- [236] E. Schmidt and P. Güntert. A new algorithm for reliable and general NMR resonance assignment. 134(30):12817–12829, 2012. Journal Article Research Support, Non-U.S. Gov't.

- [237] C. Schmuck. Carboxylate Binding by 2-(Guanidiniocarbonyl)pyrrole Receptors in Aqueous Solvents: Improving the Binding Properties of Guanidinium Cations through Additional Hydrogen Bonds. 6(4):709–718, 2000.
- [238] E. Sekerina, J. U. Rahfeld, J. Müller, J. Fanghänel, C. Rascher, G. Fischer, and P. Bayer. NMR solution structure of hPar14 reveals similarity to the peptidyl prolyl cis/trans isomerase domain of the mitotic regulator hPin1 but indicates a different functionality of the protein. 301(4):1003–1017, 2000. Journal Article Research Support, Non-U.S. Gov't.
- [239] N. Sewald and H.-D. Jakubke. *Peptides: chemistry and biology*. Wiley-VCH, 2., rev. and updated ed. edition, 2009.
- [240] G.-Z. Shao, R.-L. Zhou, Q.-Y. Zhang, Y. Zhang, J.-J. Liu, J.-A. Rui, X. Wei, and D.-X. Ye. Molecular cloning and characterization of LAPTM4B, a novel gene up-regulated in hepatocellular carcinoma. 22(32):5060–5069, 2003. Journal Article Research Support, Non-U.S. Gov't.
- [241] M. Shen, P. T. Stukenberg, M. W. Kirschner, and K. P. Lu. The essential mitotic peptidyl-prolyl isomerase Pin1 binds and regulates mitosis-specific phosphoproteins. 12(5):706–720, 1998. Journal Article Research Support, Non-U.S. Gov't Research Support, U.S. Gov't, P.H.S.
- [242] Y. Shen, F. Delaglio, G. Cornilescu, and A. Bax. TALOS+: a hybrid method for predicting protein backbone torsion angles from NMR chemical shifts. 44(4):213–223, 2009. Journal Article Research Support, N.I.H., Extramural Research Support, N.I.H., Intramural.
- [243] J. Shi, N. Chang, C. Li, J. Mei, C. Deng, X. Luo, Z. Liu, Z. Bo, Y. Q. Dong, and B. Z. Tang. Locking the phenyl rings of tetraphenylethene step by step: understanding the mechanism of aggregation-induced emission. 48(86):10675–10677, 2012. Journal Article Research Support, Non-U.S. Gov't.
- [244] O. SHIMOMURA, F. H. JOHNSON, and Y. SAIGA. Extraction, purification and properties of aequorin, a bioluminescent protein from the luminous hydromedusa, *Aequorea*. 59:223–239, 1962. Journal Article.
- [245] J. J. Siekierka, S. H. Hung, M. Poe, C. S. Lin, and N. H. Sigal. A cytosolic binding protein for the immunosuppressant FK506 has peptidyl-prolyl isomerase activity but is distinct from cyclophilin. 341(6244):755–757, 1989. Journal Article.
- [246] N. Singh, Z. Ma, T. Gemmill, X. Wu, H. Defiglio, A. Rossettini, C. Rabeler, O. Beane, R. H. Morse, M. J. Palumbo, and S. D. Hanes. The Ess1 prolyl isomerase is required for transcription termination of small noncoding RNAs via the

- Nrd1 pathway. 36(2):255–266, 2009. Journal Article Research Support, N.I.H., Extramural Research Support, Non-U.S. Gov't.
- [247] S. Song, H.-F. Zheng, D.-M. Li, J.-H. Wang, H.-T. Feng, Z.-H. Zhu, Y.-C. Chen, and Y.-S. Zheng. Monomer emission and aggregate emission of TPE derivatives in the presence of γ -cyclodextrin. 16(8):2170–2173, 2014. Journal Article Research Support, Non-U.S. Gov't.
- [248] O. Staub and D. Rotin. WW domains. 4(5):495–499, 1996. PII: S0969212696000548.
- [249] D. Strotz, J. Orts, H. Kadavath, M. Friedmann, D. Ghosh, S. Olsson, C. N. Chi, A. Pokharna, P. Güntert, B. Vögeli, and R. Riek. Protein Allostery at Atomic Resolution. 59(49):22132–22139, 2020. Journal Article Research Support, U.S. Gov't, Non-P.H.S. Journal Article Research Support, U.S. Gov't, Non-P.H.S.
- [250] M. Sudol, H. I. Chen, C. Bougeret, A. Einbond, and P. Bork. Characterization of a novel protein-binding module - the WW domain. 369(1):67–71, 1995.
- [251] R. Sultana, D. Boyd-Kimball, H. F. Poon, J. Cai, W. M. Pierce, J. B. Klein, W. R. Markesbery, X. Z. Zhou, K. P. Lu, and D. A. Butterfield. Oxidative modification and down-regulation of Pin1 in Alzheimer's disease hippocampus: A redox proteomics analysis. 27(7):918–925, 2006. Journal Article Research Support, N.I.H., Extramural.
- [252] B. Sun, X. Yang, L. Ma, C. Niu, F. Wang, N. Na, J. Wen, and J. Ouyang. Design and application of anthracene derivative with aggregation-induced emission characteristics for visualization and monitoring of erythropoietin unfolding. 29(6):1956–1962, 2013. Journal Article Research Support, Non-U.S. Gov't.
- [253] H. Sung, J. Ferlay, R. L. Siegel, M. Laversanne, I. Soerjomataram, A. Jemal, and F. Bray. Global cancer statistics 2020: GLOBOCAN estimates of incidence and mortality worldwide for 36 cancers in 185 countries. 2021. Journal Article.
- [254] T. A. Surmacz, E. Bayer, J.-U. Rahfeld, G. Fischer, and P. Bayer. The N-terminal Basic Domain of Human Parvulin hPar14 is Responsible for the Entry to the Nucleus and High-affinity DNA-binding. 321(2):235–247, 2002.
- [255] T. D. Goddard and D. G. Kneller. SPARKY 3.
- [256] B. Z. Tang, X. Zhan, G. Yu, P. P. Sze Lee, Y. Liu, and D. Zhu. 11(12):2974–2978, 2001.
- [257] Y. Tatara, Y.-C. Lin, Y. Bamba, T. Mori, and T. Uchida. Dipentamethylene thiuram monosulfide is a novel inhibitor of Pin1. 384(3):394–398, 2009. Journal Article Research Support, Non-U.S. Gov't.

- [258] A. Thiele, K. Krentzlin, F. Erdmann, D. Rauh, G. Hause, J. Zerweck, S. Kilka, S. Pösel, G. Fischer, M. Schutkowski, and M. Weiwad. Parvulin 17 promotes microtubule assembly by its peptidyl-prolyl cis/trans isomerase activity. 411(4):896–909, 2011. Journal Article Research Support, Non-U.S. Gov't.
- [259] T. Tian, X. Chen, H. Li, Y. Wang, L. Guo, and L. Jiang. Amidine-based fluorescent chemosensor with high applicability for detection of CO₂: a facile way to "see" CO₂. 138(4):991–994, 2013. Journal Article Research Support, Non-U.S. Gov't.
- [260] H. Toko, N. Hariharan, M. H. Konstandin, L. Ormachea, M. McGregor, N. A. Gude, B. Sundararaman, E. Joyo, A. Y. Joyo, B. Collins, S. Din, S. Mohsin, T. Uchida, and M. A. Sussman. Differential regulation of cellular senescence and differentiation by prolyl isomerase Pin1 in cardiac progenitor cells. 289(9):5348–5356, 2014. Journal Article Research Support, N.I.H., Extramural Research Support, Non-U.S. Gov't.
- [261] A. Tormo, M. Almirón, and R. Kolter. *surA*, an *Escherichia coli* gene essential for survival in stationary phase. 172(8):4339–4347, 1990. Journal Article Research Support, Non-U.S. Gov't Research Support, U.S. Gov't, Non-P.H.S. Research Support, U.S. Gov't, P.H.S.
- [262] T. Uchida, F. Fujimori, T. Tradler, G. Fischer, and J.-U. Rahfeld. Identification and characterization of a 14 kDa human protein as a novel parvulin-like peptidyl prolyl cis / trans isomerase. 446(2-3):278–282, 1999.
- [263] T. Uchida, M. Takamiya, M. Takahashi, H. Miyashita, H. Ikeda, T. Terada, Y. Matsuo, M. Shirouzu, S. Yokoyama, F. Fujimori, and T. Hunter. Pin1 and Par14 Peptidyl Prolyl Isomerase Inhibitors Block Cell Proliferation. 10(1):15–24, 2003. PII: S1074552102003101.
- [264] K. Ulrich and U. Jakob. The role of thiols in antioxidant systems. 140:14–27, 2019. Journal Article Research Support, N.I.H., Extramural Research Support, Non-U.S. Gov't Review.
- [265] D. V. Urusova, J.-H. Shim, D. J. Kim, S. K. Jung, T. A. Zykova, A. Carper, A. M. Bode, and Z. Dong. Epigallocatechin-gallate suppresses tumorigenesis by directly targeting Pin1. 4(9):1366–1377, 2011. Journal Article Research Support, N.I.H., Extramural Research Support, Non-U.S. Gov't.
- [266] C. C. Valley, A. Cembran, J. D. Perlmutter, A. K. Lewis, N. P. Labello, J. Gao, and J. N. Sachs. The methionine-aromatic motif plays a unique role in stabilizing protein structure. 287(42):34979–34991, 2012. Journal Article.
- [267] O. Vallon. Chlamydomonas Immunophilins and Parvulins: Survey and Critical Assessment of Gene Models†. 4(2):230–241, 2005. Journal Article Review.

- [268] R. Vélez-Cruz and D. G. Johnson. The Retinoblastoma (RB) Tumor Suppressor: Pushing Back against Genome Instability on Multiple Fronts. 18(8), 2017. Journal Article Review The authors declare no conflict of interest.
- [269] M. A. Verdecia, M. E. Bowman, K. P. Lu, T. Hunter, and J. P. Noel. Structural basis for phosphoserine-proline recognition by group IV WW domains. 7(8):639–643, 2000. Journal Article Research Support, Non-U.S. Gov't Research Support, U.S. Gov't, Non-P.H.S. Research Support, U.S. Gov't, P.H.S.
- [270] J. T. Vivian and P. R. Callis. Mechanisms of Tryptophan Fluorescence Shifts in Proteins. 80(5):2093–2109, 2001. PII: S0006349501761838.
- [271] C. T. Walsh, S. Garneau-Tsodikova, and G. J. Gatto. Protein posttranslational modifications: the chemistry of proteome diversifications. 44(45):7342–7372, 2005. Journal Article Review.
- [272] H. Wang, Y. He, Y. Li, C. Zhang, P. Zhang, J. Cui, Y. Long, S. Chen, R. Zeng, and J. Chen. Selective ratiometric fluorescence detection of hypochlorite by using aggregation-induced emission dots. 2019. Journal Article.
- [273] H. Wang, Y. Huang, X. Zhao, W. Gong, Y. Wang, and Y. Cheng. A novel aggregation-induced emission based fluorescent probe for an angiotensin converting enzyme (ACE) assay and inhibitor screening. 50(95):15075–15078, 2014. Journal Article Research Support, Non-U.S. Gov't.
- [274] J. Wang, L. Lu, C. Wang, M. Wang, J. Ju, J. Zhu, and T. Sun. An AIE and PET fluorescent probe for effective Zn(ii) detection and imaging in living cells. 44(36):15426–15431, 2020.
- [275] K. Wang, J. Li, S. Ji, L. Li, Z. Qiu, C. Pan, J. Zhang, and Y. Huo. Fluorescence probes based on AIE luminogen: application for sensing Hg 2+ in aqueous media and cellular imaging. 42(16):13836–13846, 2018.
- [276] L. Wang, Y. Zhou, D. Chen, and T. H. Lee. Peptidyl-Prolyl Cis/Trans Isomerase Pin1 and Alzheimer's Disease. 8:355, 2020. Journal Article Review.
- [277] M. Wang, D. Zhang, G. Zhang, Y. Tang, S. Wang, and D. Zhu. Fluorescence turn-on detection of DNA and label-free fluorescence nuclease assay based on the aggregation-induced emission of silole. 80(16):6443–6448, 2008. Journal Article Research Support, Non-U.S. Gov't.
- [278] M. Wang, G. Zhang, and D. Zhang. New Chemo-/Biosensors with Silole and Tetraphenylethene Molecules Based on the Aggregation and Deaggregation Mechanism. In A. Qin and B. Z. Tang, editors, *Aggregation-induced emission*, pages 165–188. John Wiley & Sons Inc, 2014.

- [279] M. Wang, G. Zhang, D. Zhang, D. Zhu, and B. Z. Tang. Fluorescent bio/chemosensors based on silole and tetraphenylethene luminogens with aggregation-induced emission feature. 20(10):1858, 2010.
- [280] W. Wang, L. Li, S. Liu, C. Ma, and S. Zhang. Determination of physiological thiols by electrochemical detection with piaszelenole and its application in rat breast cancer cells 4T-1. 130(33):10846–10847, 2008. Journal Article Research Support, Non-U.S. Gov't.
- [281] X. Wang, H. Wang, Y. Niu, Y. Wang, and L. Feng. A facile AIE fluorescent probe for broad range of pH detection. 226:117650, 2020. Journal Article.
- [282] X. J. Wang, B. Xu, A. B. Mullins, F. K. Neiler, and F. A. Etzkorn. Conformationally locked isostere of phosphoSer-cis-Pro inhibits Pin1 23-fold better than phosphoSer-trans-Pro isostere. 126(47):15533–15542, 2004. Journal Article Research Support, U.S. Gov't, P.H.S.
- [283] X. Wen, Q. Wang, and Z. Fan. Highly selective turn-on fluorogenic chemosensor for Zn(II) detection based on aggregation-induced emission. 194:366–373, 2018. PII: S0022231317307883.
- [284] G. Wider, C. Weber, R. Traber, H. Widmer, and K. Wuethrich. Use of a double half-filter in two-dimensional proton NMR studies of receptor-bound cyclosporin. 112(24):9015–9016, 1990.
- [285] D. Wildemann, F. Erdmann, B. H. Alvarez, G. Stoller, X. Z. Zhou, J. Fanghänel, M. Schutkowski, K. P. Lu, and G. Fischer. Nanomolar inhibitors of the peptidyl prolyl cis/trans isomerase Pin1 from combinatorial peptide libraries. 49(7):2147–2150, 2006. Journal Article Research Support, N.I.H., Extramural.
- [286] A. Windelberg, O. Arseth, G. Kvalheim, and P. M. Ueland. Automated assay for the determination of methylmalonic acid, total homocysteine, and related amino acids in human serum or plasma by means of methylchloroformate derivatization and gas chromatography-mass spectrometry. 51(11):2103–2109, 2005. Journal Article Research Support, Non-U.S. Gov't.
- [287] R. Wintjens, J. M. Wieruszkeski, H. Drobecq, P. Rousselot-Pailley, L. Buée, G. Lipens, and I. Landrieu. ¹H NMR study on the binding of Pin1 Trp-Trp domain with phosphothreonine peptides. 276(27):25150–25156, 2001. Journal Article Research Support, Non-U.S. Gov't.
- [288] B. T. Worrell, J. A. Malik, and V. V. Fokin. Direct evidence of a dinuclear copper intermediate in Cu(I)-catalyzed azide-alkyne cycloadditions. 340(6131):457–460, 2013. Journal Article Research Support, N.I.H., Extramural Research Support, U.S. Gov't, Non-P.H.S.

- [289] G. M. Wulf, A. Ryo, G. G. Wulf, S. W. Lee, T. Niu, V. Petkova, and K. P. Lu. Pin1 is overexpressed in breast cancer and cooperates with Ras signaling in increasing the transcriptional activity of c-Jun towards cyclin D1. 20(13):3459–3472, 2001. Journal Article Research Support, Non-U.S. Gov't Research Support, U.S. Gov't, P.H.S.
- [290] L. Xi, Y. Wang, Q. He, Q. Zhang, and L. Du. Interaction between Pin1 and its natural product inhibitor epigallocatechin-3-gallate by spectroscopy and molecular dynamics simulations. 169:134–143, 2016. Journal Article.
- [291] C. Xia, Y. Tao, M. Li, T. Che, and J. Qu. Protein acetylation and deacetylation: An important regulatory modification in gene transcription (Review). 20(4):2923–2940, 2020. Journal Article Review.
- [292] M. Xiao, S. Jia, H. Wang, J. Wang, Y. Huang, and Z. Li. Overexpression of LAPTM4B: an independent prognostic marker in breast cancer. 139(4):661–667, 2013. Journal Article Research Support, Non-U.S. Gov't.
- [293] S. Xie, A. Y. H. Wong, R. T. K. Kwok, Y. Li, H. Su, J. W. Y. Lam, S. Chen, and B. Z. Tang. Fluorogenic Ag⁺-Tetrazolate Aggregation Enables Efficient Fluorescent Biological Silver Staining. 57(20):5750–5753, 2018. Journal Article.
- [294] Y. Xie, L. Yan, Y. Tang, M. Tang, S. Wang, L. Bi, W. Sun, and J. Li. A Smart Fluorescent Probe Based on Salicylaldehyde Schiff's Base with AIE and ESIPT Characteristics for the Detections of N₂H₄ and ClO. 2019. Journal Article.
- [295] G. G. Xu and F. A. Etzkorn. Pin1 as an anticancer drug target. 22(7):399–407, 2009. Journal Article Research Support, N.I.H., Extramural Review.
- [296] G. G. Xu, Y. Zhang, A. Y. Mercedes-Camacho, and F. A. Etzkorn. A reduced-amide inhibitor of Pin1 binds in a conformation resembling a twisted-amide transition state. 50(44):9545–9550, 2011. Journal Article Research Support, N.I.H., Extramural Research Support, Non-U.S. Gov't.
- [297] P. Xu, Z. Bao, C. Yu, Q. Qiu, M. Wei, W. Xi, Z. Qian, and H. Feng. A water-soluble molecular probe with aggregation-induced emission for discriminative detection of Al³⁺ and Pb²⁺ and imaging in seedling root of Arabidopsis. 223:117335, 2019. Journal Article.
- [298] Y.-X. Xu, Y. Hirose, X. Z. Zhou, K. P. Lu, and J. L. Manley. Pin1 modulates the structure and function of human RNA polymerase II. 17(22):2765–2776, 2003. Journal Article Research Support, U.S. Gov't, P.H.S.
- [299] Y.-X. Xu and J. L. Manley. Pin1 modulates RNA polymerase II activity during the transcription cycle. 21(22):2950–2962, 2007. Journal Article Research Support, N.I.H., Extramural.

- [300] M. B. Yaffe, M. Schutkowski, M. Shen, X. Z. Zhou, P. T. Stukenberg, J. U. Rahfeld, J. Xu, J. Kuang, M. W. Kirschner, G. Fischer, L. C. Cantley, and K. P. Lu. Sequence-specific and phosphorylation-dependent proline isomerization: a potential mitotic regulatory mechanism. 278(5345):1957–1960, 1997. Journal Article Research Support, Non-U.S. Gov't Research Support, U.S. Gov't, P.H.S.
- [301] X. Yan, Z. Zhu, S. Xu, L.-N. Yang, X.-H. Liao, M. Zheng, D. Yang, J. Wang, D. Chen, L. Wang, X. Liu, J. Liu, R.-H. Chen, X. Z. Zhou, K. P. Lu, and H. Liu. MicroRNA-140-5p inhibits hepatocellular carcinoma by directly targeting the unique isomerase Pin1 to block multiple cancer-driving pathways. 7:45915, 2017. Journal Article Research Support, N.I.H., Extramural Research Support, Non-U.S. Gov't.
- [302] H. Yang, F. Xiong, R. Qi, Z. Liu, M. Lin, J. Rui, J. Su, and R. Zhou. LAPTM4B-35 is a novel prognostic factor of hepatocellular carcinoma. 101(5):363–369, 2010. Journal Article Research Support, Non-U.S. Gov't.
- [303] J. L. Yao, O. Kops, P. J. Lu, and K. P. Lu. Functional conservation of phosphorylation-specific prolyl isomerases in plants. 276(17):13517–13523, 2001. Journal Article Research Support, Non-U.S. Gov't Research Support, U.S. Gov't, P.H.S.
- [304] E. S. Yeh and A. R. Means. PIN1, the cell cycle and cancer. 7(5):381–388, 2007. Research Support, N.I.H., Extramural Review.
- [305] M. Yin, C. Li, X. Li, G. Lou, B. Miao, X. Liu, F. Meng, H. Zhang, X. Chen, M. Sun, Q. Ling, and R. Zhou. Over-expression of LAPTM4B is associated with poor prognosis and chemotherapy resistance in stages III and IV epithelial ovarian cancer. 104(1):29–36, 2011. Journal Article.
- [306] J. H. Yu, C. Y. Im, and S.-H. Min. Function of PIN1 in Cancer Development and Its Inhibitors as Cancer Therapeutics. 8:120, 2020. Journal Article Review.
- [307] Y. Yu, A. Qin, C. Feng, P. Lu, K. M. Ng, K. Q. Luo, and B. Z. Tang. An amine-reactive tetraphenylethylene derivative for protein detection in SDS-PAGE. 137(23):5592–5596, 2012. Comparative Study Journal Article Research Support, Non-U.S. Gov't.
- [308] A. Zarrinpar, R. P. Bhattacharyya, and W. A. Lim. The structure and function of proline recognition domains. 2003(179):RE8, 2003. Journal Article Review Journal Article Review.
- [309] Q. Zeng, Z. Li, Y. Dong, C. Di, A. Qin, Y. Hong, L. Ji, Z. Zhu, C. K. W. Jim, G. Yu, Q. Li, Z. Li, Y. Liu, J. Qin, and B. Z. Tang. Fluorescence enhancements of

- benzene-cored luminophors by restricted intramolecular rotations: AIE and AIEE effects. (1):70–72, 2007. Journal Article Research Support, Non-U.S. Gov't.
- [310] J. Zhang and M. W. Germann. Characterization of secondary amide peptide bond isomerization: thermodynamics and kinetics from 2D NMR spectroscopy. 95(11):755–762, 2011. Journal Article Research Support, N.I.H., Extramural Research Support, Non-U.S. Gov't.
- [311] R. Zhang, Y. Yuan, J. Liang, R. T. K. Kwok, Q. Zhu, G. Feng, J. Geng, B. Z. Tang, and B. Liu. Fluorogen-peptide conjugates with tunable aggregation-induced emission characteristics for bioprobe design. 6(16):14302–14310, 2014. Journal Article Research Support, Non-U.S. Gov't.
- [312] X. Zhang, B. Zhang, J. Gao, X. Wang, and Z. Liu. Regulation of the microRNA 200b (miRNA-200b) by transcriptional regulators PEA3 and ELK-1 protein affects expression of Pin1 protein to control anoikis. 288(45):32742–32752, 2013. Journal Article Research Support, Non-U.S. Gov't.
- [313] Y. Zhang, S. Daum, D. Wildemann, X. Z. Zhou, M. A. Verdecia, M. E. Bowman, C. Lücke, T. Hunter, K.-P. Lu, G. Fischer, and J. P. Noel. Structural basis for high-affinity peptide inhibition of human Pin1. 2(5):320–328, 2007. Journal Article Research Support, N.I.H., Extramural Research Support, Non-U.S. Gov't.
- [314] M. Zhao, M. Wang, H. Liu, D. Liu, G. Zhang, D. Zhang, and D. Zhu. Continuous on-site label-free ATP fluorometric assay based on aggregation-induced emission of silole. 25(2):676–678, 2009. Journal Article.
- [315] Z. Zhao, S. Chen, X. Shen, F. Mahtab, Y. Yu, P. Lu, J. W. Y. Lam, H. S. Kwok, and B. Z. Tang. Aggregation-induced emission, self-assembly, and electroluminescence of 4,4'-bis(1,2,2-triphenylvinyl)biphenyl. 46(5):686–688, 2010. Journal Article Research Support, Non-U.S. Gov't.
- [316] Z. Zhao, B. He, and B. Z. Tang. Aggregation-induced emission of siloles. 6(10):5347–5365, 2015. Journal Article Review.
- [317] Z. Zhao, J. W. Y. Lam, and B. Z. Tang. Tetraphenylethene: a versatile AIE building block for the construction of efficient luminescent materials for organic light-emitting diodes. 22(45):23726, 2012.
- [318] J. Zhou, P. Jangili, S. Son, M. S. Ji, M. Won, and J. S. Kim. Fluorescent Diagnostic Probes in Neurodegenerative Diseases. 32(51):e2001945, 2020. Journal Article Review.
- [319] X. Z. Zhou, O. Kops, A. Werner, P.-J. Lu, M. Shen, G. Stoller, G. Küllertz, M. Stark, G. Fischer, and K. P. Lu. Pin1-Dependent Prolyl Isomerization Regulates Dephosphorylation of Cdc25C and Tau Proteins. 6(4):873–883, 2000.

- [320] L. Zhu, J. Zhou, G. Xu, C. Li, P. Ling, B. Liu, H. Ju, and J. Lei. DNA quadruplexes as molecular scaffolds for controlled assembly of fluorogens with aggregation-induced emission. 9(9):2559–2566, 2018. Journal Article.
- [321] Z. Zhu, H. Zhang, F. Lang, G. Liu, D. Gao, B. Li, and Y. Liu. Pin1 promotes prostate cancer cell proliferation and migration through activation of Wnt/ β -catenin signaling. 18(8):792–797, 2016. Journal Article.
- [322] C. Zwahlen, P. Legault, S. J. F. Vincent, J. Greenblatt, R. Konrat, and L. E. Kay. Methods for Measurement of Intermolecular NOEs by Multinuclear NMR Spectroscopy: Application to a Bacteriophage λ N-Peptide/ boxB RNA Complex. 119(29):6711–6721, 1997.

Danksagung

Es gibt so viele Personen, denen ich auf diesem Wege danken möchte. In erster Linie bedanke ich mich bei Prof. Dr. Peter Bayer, der es mir ermöglicht hat diese spannende Arbeit in seiner Arbeitsgruppe anzufertigen. Vielen Dank für die angeregten Diskussionen und die schnelle Entwicklung eines neuen Projektes nach dem Rückschlag mit der Paraoxonase.

Anschließend möchte ich mich bei Prof. Dr. Jens Voskuhl bedanken, dass wir so schnell ein interessantes und vielversprechendes Projekt auf die Beine gestellt haben. Außerdem danke ich für die Übernahme des Koreferats, die super Kooperation über fast 3 Jahre und die jederzeit offene Tür bei jeglichen Fragen.

Ebenso gilt mein Dank Prof. Dr. Markus Kaiser für die Unterstützung der Peptidsynthese und die Möglichkeit frei in seinem Labor zu arbeiten.

Dem Sonderforschungsbereich 1093 danke ich für die Unterstützung und die Aufnahme als assoziiertes Mitglied. Danke Lydia, dass ich an allem Teil haben durfte und so viel Unterstützung erfahren habe.

Ein ganz besonderes großer Dank geht an Christine. Dafür, dass du mir ein ständiger Ansprechpartner warst (besonders in der schwierigen Schreibphase), immer ein offenes Ohr und so viel Geduld mit mir am NMR hattest. Danke auch für die mentalen Pausen und das Neuordnen von Gedanken in meinem Kopf.

Zusätzlich ein großes Danke an Dr. Torsten Herrmann für die Kooperation zur Berechnung der Proteinkomplexstruktur und die Unterstützung bei Programmfragen.

Bei den aktuellen und ehemaligen Mitgliedern der AG Voskuhl möchte ich mich für die tolle Kooperation und die gegenseitige Hilfe bedanken. Besonders bei Matthias, für die Fluorophorgrundgerüste, die Unterstützung bei der Klickchemie und die Bierrunden.

Dann gilt mein Dank den aktuellen und ehemaligen Mitarbeitern der AG Kaiser, danke, dass Ihr mich so freundlich aufgenommen habt und mich als Gruppenmitglied integriert habt. Vielen Dank für die stetige Unterstützung und auch für die Einladungen zu Weihnachtsfeiern. Ein besonderen Dank geht an Dr. Steffen Köcher, der mir stets chemische Unterstützung gab und auch sonst immer ein toller Gesprächspartner war.

Danke an alle Mitglieder der AG Bayer. Ich bin wirklich gerne ein Teil von euch gewesen und hatte mit euch so viele schöne Momente und kann sagen, dass die Atmosphäre und Hilfsbereitschaft wirklich super sind und ich die Arbeit mit euch vermissen werde.

Mein Promotionsbuddy Anna, danke für all die wunderbaren Jahre zusammen. Du bist mir eine wirklich gute Freundin geworden und weißt immer wie man mich wieder aufbauen kann (Schokolade).

Danke auch dir Mike, für all die schönen und witzigen Momente als Labornachbar (Merke: Immer eine Sporthose dabei haben) und die super Comics an unserer Tür. Wir hatten wirklich gute Diskussionen und du wirst es noch weit bringen Professor.

Meiner langjährigen Sitznachbarin Dana möchte ich für den guten Anschluss an die Gruppe und viele schöne Erinnerungen danken.

Eddo, danke, dass du mich sofort aufgenommen hast, wir über alles sprechen konnten und du immer einen guten Rat hattest.

Bianca, danke für viele schöne Momente und Diskussionen, unsere gemeinsame Anfangszeit im SFB und einige Feierabendbier mit "Halt mal kurz".

Jenni, danke für die vielen Stunden, die du für mich investiert hast und die zahlreichen Englischlektionen. I hope you are no longer offended.

Liebe Anja, danke für die ganze Organisation der verschiedenen Praktika. Die Bochum-connection hat es mir einfach gemacht mich einzufinden. Danke Tina für die stetige Hilfe, die Bestellungen und den Spaß bei unseren Unterhaltungen. Mina, danke für die Laborhilfen und dass du uns immer so viel Arbeit abgenommen hast. Alma, danke für deine Unterstützung im Labor und der Proteinreinigung. Peter, danke für die Organisation der Retreats, die Arbeit am NMR und die vielen Fotos. Elke, du hast immer ein offenes Ohr und danke für deine Hilfe bei organisatorischen Dingen. Du hast mir das Leben damit so viel einfacher gemacht.

Ein besonderer Dank gilt meiner Familie, die mich in allen Phasen voll unterstützt hat und immer wieder Verständnis für meine Stimmungsschwankungen hatten.

Danke Oma und Opa, dass Ihr immer an mich geglaubt habt. Ich hätte gerne mit euch gefeiert.

Danke auch an alle Ronsdorfer, neu Ronsorfer und alle meine Freunde. Ihr wart und seid mein mentaler Ausgleich, ich kann mich immer auf euch verlassen und Ihr gebt mir seit teilweise 20 Jahren das Gefühl von Heimat.

Lebenslauf

Der Lebenslauf ist in der Online-Version aus Gründen des Datenschutzes nicht enthalten.

Eidesstattliche Erklärungen:

Erklärung:

Hiermit erkläre ich, gem. § Abs. (2) d) + f) der Promotionsordnung der Fakultät für Biologie zur Erlangung des Dr. rer. nat., dass ich die vorliegende Dissertation selbstständig verfasst und mich keiner anderen als der angegebenen Hilfsmittel bedient, bei der Abfassung der Dissertation nur die angegebenen Hilfsmittel benutzt und alle wörtlich oder inhaltlich übernommenen Stellen als solche gekennzeichnet habe.

Essen, den _____

Unterschrift des/r Doktoranden/in

Erklärung:

Hiermit erkläre ich, gem. § 7 Abs. (2) e) + g) der Promotionsordnung der Fakultät für Biologie zur Erlangung des Dr. rer. nat., dass ich keine anderen Promotionen bzw. Promotionsversuche in der Vergangenheit durchgeführt habe und dass diese Arbeit von keiner anderen Fakultät/Fachbereich abgelehnt worden ist.

Essen, den _____

Unterschrift des/r Doktoranden/in

Erklärung:

Hiermit erkläre ich, gem. § 6 Abs. (2) g) der Promotionsordnung der Fakultät für Biologie zur Erlangung der Dr. rer. nat., dass ich das Arbeitsgebiet, dem das Thema „Peptide-conjugated fluorophores with aggregation-induced emission properties for specific protein recognition“ zuzuordnen ist, in Forschung und Lehre vertrete und den Antrag von Daniel Seifert befürworte und die Betreuung auch im Falle eines Weggangs, wenn nicht wichtige Gründe dem entgegenstehen, weiterführen werde.

Name des Mitglieds der Universität Duisburg-Essen in
Druckbuchstaben

Essen, den _____

Unterschrift eines Mitglieds der Universität Duisburg-Essen